Uniwersytet Mikołaja Kopernika w Toruniu
Wydział Chemii UMK w Toruniu

mgr Adrian Gołębiowski

Układy koloidalne oraz ich oddziaływania z wybranymi metalami ciężkimi

Rozprawa doktorska na stopień doktora w dziedzinie nauk ścisłych i przyrodniczych w dyscyplinie nauki chemiczne

Wykonana pod kierunkiem promotora prof. zw. dr hab. Bogusława Buszewskiego

Toruń 2023

UNIWERSYTET
MIKOŁAJA KOPERNIKA
W TORUNIU
Wydział Chemii

Nicolaus Copernicus University in Torun
Faculty of Chemistry, NCU in Torun

MSc Adrian Gołębiowski

Colloidal systems and their interactions with selected heavy metals

Thesis for the PhD degree
in the field of natural sciences in the discipline of chemistry

under supervision prof. zw. dr hab. Bogusław Buszewski

Torun 2023

UNIWERSYTET
MIKOŁAJA KOPERNIKA
W TORUNIU
Wydział Chemii

Podziękowania:

Niniejsza rozprawa doktorska została przygotowana na podstawie prac badawczych finansowanych z puli środków Narodowego Centrum Nauki, z grantu numer 2017/27/B/ST4/02628, pt. *Synteza kompleksowych związków srebra i cynku na bazie kazein i białek serwatki oraz nanocząstek srebra i tlenku cynku przez probiotyczne bakterie kwasu mlekowego*.

Niektóre zadania badawcze były finansowane z puli Grantu Młodych Naukowców Wydziału Chemii UMK w Toruniu.

Uzyskałem wsparcie finansowe na wyjazd na zagraniczną konferencje z grantu PROM NAWA.

Osobiście chciałbym podziękować promotorowi, profesorowi Buszewskiemu za pomoc, rady i udzielane wsparcie oraz za rolę w moim rozwoju jako naukowca, jak również człowieka.

Pracę dedykuje mojej najbliżej Rodzinie, szczególnie żonie Karolinie oraz córeczce Dianie oraz Rodzicom.

Spis Treści

Wykaz skrótów

AF4, frakcjonowanie przepływowe w asymetrycznym polu sił przepływu, asymmetric flow field flow fractionation

CE, elektroforeza kapilarna, capillary electrophoresis

Da, Dalton, Dalton

DHB, kwas 2,5-dihydroksybenzoesowy, 2,5-Dihydroxybenzoic acid

DLS, dynamiczne rozpraszanie światła, dynamic light scattering

EDX, spektroskopia rentgenowska z dyspersją energii, energy dispersive X-ray spectroscopy

FFF, frakcjonowanie w polu sił przepływu, field flow fractionation

FT IR, spektroskopia w podczerwieni z transformatą Fouriera, Fourier-transform infrared spectroscopy

HCCA, kwas α-cyjano-4-hydroksycynamonowy, α-Cyano-4-hydroxycinnamic acid

ICP/MS, spektrometria mas z indukcyjnie sprzężoną plazmą, inductively coupled plasma mass spectrometry

MALDI, desorpcja/jonizacja laserem wspomagana matrycą, matrix-assisted laser desorption/ionization

MALS, wielokątowe rozpraszanie światła, multi angle light scattering

MS, spektrometria mas, mass spectrometry

Pdi, wskaźnik polidyspersyjności, polydispersity index

SA, kwas synapinowy, sinapic acid

SEC, chromatografia wykluczania, size-exclusion chromatography

SEM, skaningowa mikroskopia elektronowa, scanning electron microscopy

SLS, statyczne rozproszenie światła, static light scattering

SP ICP/MS, spektrometria mas z indukcyjnie sprzężoną plazmą pojedynczych cząstek, single particle inductively coupled plasma mass spectrometry

TEM, transmisyjna mikroskopia elektronowa, transmission electron microscopy

TOF, czas przelotu, time of flight

UV, ultraviolet, ultraviolet

Wstęp

Poznawanie mechanizmów i znaczenia odziaływaniami pomiędzy koloidami stanowi punkt wyjścia w interpretacji zjawisk przejść fazowych jak również ocenę i charakterystykę produktów wdrażanych w licznych gałęziach przemysłu [1].

Układ koloidalny to pojęcie odnoszące się do mieszaniny co najmniej dwóch składników. Pierwszym składnikiem jest cząstka fazy rozproszonej a drugim cząstki/cząsteczki fazy rozpraszającej. Wskaźnikiem determinującym charakter koloidalny cząstek fazy rozproszonej jest ich rozmiar; w zakresie od 1 nm do 1000 nm (rozmiar wyrażony dla co najmniej jednego z kierunków) [2]. Cząsteczki fazy rozpraszającej stanowią fazę ciągłą. Stan skupienia cząstek fazy rozpraszającej oraz rozproszonej jest dowolny; może być stały, ciekły lub gazowy. Poszczególne kompozycje obydwu faz noszą odrębne nazwy. Dla przykładu, cząstki fazy rozproszonej o stanie skupienia stałym rozproszone w cieczy noszą nazwę zolu, natomiast nazwa układu stanowiącego cząstki w stanie ciekłym rozproszone w cieczy to emulsja. W zależności od stopnia powinowactwa fazy rozproszonej do wody, koloidy można sklasyfikować jako hydrofilowe (przeważają siły przyciągające pomiędzy cząstkami a cząsteczkami wody) lub hydrofobowe (przeważają siły odpychające). Przykładami cząstek o cechach hydrofilowych są niektóre białka oraz polisacharydy [3].

Cząstki koloidalne wykazują kilka specyficznych właściwości i cech, które pozwalają na ich charakterystykę, jak również odróżnienie cząstek koloidalnych od cząsteczek tworzących roztwory rzeczywiste. Cząstki koloidalne wykazują specyficzne ruchy cząstek w fazie rozpraszającej płynnej (np. ciecz lub gaz) nazywane ruchami Browna [4]. Pierwsze z postulowanych przyczyn występowania tego zjawiska są podawane w pionierskich pracach Einsteina [5] oraz Smoluchowskiego [6]. Cząstki koloidalne wykazywały spontaniczny i chaotyczny ruch makroskopowy w płynie wynikający z ciągłych zderzeń cząstek koloidu z cząsteczkami płynu. Z kolei przemieszczanie się cząstek w systemie względem gradientu stężenia, nazywane dyfuzją, może być rozpatrywane jako makroskopowy obraz ruchów Browna [7].

Rozproszenie światła zachodzące na cząstkach koloidalnych jest kolejną z cech charakterystycznych i stanowi wraz z ruchami Browna oraz dyfuzją podstawowe

założenia technik instrumentalnych dynamicznego (DLS) [8] i statycznego (SLS) [9] rozproszenia światła, jak również technik separacyjnych z rodziny frakcjonowania w polu sił przepływu (FFF) [10–12]. Występowanie przepływu laminarnego jest również warunkiem zachodzenia separacji cząstek podczas analiz wykonywanych za pomocą frakcjonowania przepływowego w asymetrycznym polu sił przepływu (AF4).

Cząstki koloidu wykazują w medium również tendencje do zachodzenia reakcji kwasowo-zasadowych w wyniku między innymi dysocjacji grup funkcyjnych zdolnych do jonizacji. Prowadzi to w efekcie to powstawania naładowanej elektrycznie cząstki koloidalnej w medium [13]. Ładunek elektryczny może być rozpatrywany jako rozproszony na powierzchni cząstki. W medium ciekłym, powoduje to przepływ jonów (kationów oraz anionów) w kierunku naładowanej elektrycznie cząstki koloidalnej oraz specyficzną dystrybucje tych jonów względem cząstki; powstająca podwójna warstwa dyfuzyjna złożona z ściśle związanych jonów o przeciwnym znaku ładunku elektrycznego do cząstki tworzy warstwę Sterna, z kolei do tej warstwy przyłączają się oraz oddziałują jony o przeciwnym znaku (warstwa dyfuzyjna), aż do ustalenia się równowagi [14]. Wartość ładunku elektrycznego wyznaczona w miejscu pomiędzy warstwą Sterna a dyfuzyjną nazywana jest potencjałem zeta [14]. Parametr ten jest jednym z kluczowych stosowanych do charakterystyki koloidów oraz opisu odziaływań koloid-koloid oraz koloid-jony, jak również opisu zjawiska stabilności układu koloidalnego.

Występowanie ładunku elektrycznego na powierzchni cząstki koloidalnej stanowi przyczynek do zapewnienia stabilności układu koloidalnego. Cząstki, które posiadają wystarczająco wysoki ładunek elektryczny (przyjęto ± 30 mV) [15] wykazują zdolność do elektrostatycznego odpychania się cząstek. Zgodnie z teorią DLVO, akronim pochodzi od nazwisk twórców (Boris **D**erjaguin, Lev **L**andau, Evert **V**erwey, Theodoor **O**verbeek), postulującą występowanie sił elektrostatycznego przyciągania oraz odpychania, które wskazują na kierunek oraz szybkość zachodzenia procesu aglomeracji cząstek [16]. Aglomeracja jak również procesy jednostkowe oligomeryzacji polegają na łączeniu się pojedynczych cząstek (monomerów) w bardziej liczne kompleksy cząstek, co w końcowym efekcie może powodować utworzenie cząstki

o bardzo dużej masie cząsteczkowej i gęstości, której wartość będzie wyższa od gęstości rozpuszczalnika, czego efektem będzie sedymentacja cząstek w cieczy. Przyjęto stosować termin *stabilności koloidalnej* odnoszącej się do zachodzącego w wolnym stopniu procesu aglomeracji cząstek [17]. Wartości potencjału zeta oraz zależności od zmiennych eksperymentalnych (takich jak pH czy siła jonowa) mogą być wyznaczane poprzez odpowiednią aparaturę analityczną [18,19]. Użycie aparatury służącej do wyznaczania potencjału zeta, oprócz występowania dystrybucji ładunku elektrycznego zlokalizowanego na cząstkach, zakłada występowanie ruchów Browna i dyfuzji (innymi słowy analizowana cząstka powinna być w stanie koloidalnym). Ruch naładowanych cząstek w zewnętrznym polu elektrycznym jest nazywany zjawiskiem elektroforetycznym. Zjawisko stanowi podstawę technik elektromigracyjnych takich jak elektroforeza: żelowa, kapilarna CE czy izotachoforeza jak również elektrochromatografia [20,21].

Koloidy wykazują silne efekty solwatacyjne mające wpływ na szereg wspomnianych już właściwości (wielkość cząstek, potencjał elektrokinetyczny) [22]. Niektóre z polimerów hydrofilowych posiadają właściwości do tworzenia trójwymiarowej struktury w wyniku indukowanego chemicznie lub fizycznie sieciowania, a typowym związkiem ulegającym temu procesowi są pektyny, który stanowi przykład polisacharydu hydrofilowego [23] oraz „żelatyna”.

Wymienione już wcześniej niektóre z technik separacyjnych stosowanych do analizowania koloidów mają szczególnie ważne zastosowania dla tego układu. Wynika to z faktu, że koloidy naturalnie najczęściej występują w stanie silnie heterogenicznym. Heterogeniczność występuje pod wieloma właściwościami: od budowy strukturalnej, masy molowej, wielkości cząstek czy przyjmowanych konformacjach koloidu w fazie rozpraszającej lub może być skutkiem prowadzonych procesów syntez czy też izolowania koloidów z próbek rzeczywistych. Rozpatrując dogłębniej koloidy, można zauważyć wpływ, jaki wywierają odpowiednie modyfikacje post translacyjne na właściwości białek czy dystrybucje ładunku elektrycznego na cząstkach, co później ma przełożenie na właściwości aplikacyjne oraz użytkowe [24].

Selekcja technik separacyjnych wykorzystywanej do danego zastosowania jest uzależniona od kilku czynników, takich jak nominalny zakres wielkości cząstek, ładunek elektryczny czy stopień rozgałęzienia polimerów. Wykazano, że zastosowanie AF4 w kontekście analizy silnie rozgałęzionych polimerów jest szczególnie optymalnym wyborem, ze względu na panujące stosunkowo łagodne warunki podczas separacji rozumiane jako występujące niskich ciśnień wewnątrz kanału oraz potencjalnie niewielka powierzchnia kontaktu cząstek analitu z powierzchnią stałą membrany półprzepuszczalnej (porównując do SEC fazą stacjonarna). Zauważono, że notowane wyższe wartości parametrów podczas analizy wykonywanej przez SEC mogą sprzyjać występowaniu: dysocjacji kompleksów powstałych na drodze słabszych od wiązania kowalencyjnego elektrostatycznego przyciągania, znaczącego efektu adsorpcji cząstek do fazy stacjonarnej, niewytłumaczalnych zmian konformacji jak również tworzenia się produktów częściowej degradacji struktury pierwotnej dla kompleksów niestabilnych [25]. Dodatkowo, techniki przepływowe cechują się szerokim zakresem warunków separacji, rozumianej jako skali pH, siły jonowej, dodatku substancji organicznych czy temperatury. Natomiast charakteryzowanie cząstek za pomocą MALS pozwala na bezpośrednie wyznaczenie rozkładu wielkości promieni bezwładności oraz mas molowych. Należy również dodać, że zaletą jest również charakteryzowanie w warunkach odpowiadających składu fazy cieczy nośnej, a przez to implementacje tych warunków jako na przykład fizjologicznych. Wyznaczanie masy molowej substancji, wielkości cząstek, konformacji oraz śledzenie zmian tych wartości powstałych w wyniku różnego typu reakcji (syntezy nowych substancji, odziaływania liganda ze substratem, śledzenie produktów degradacji itp.) może być wykorzystywane w badaniach nad oddziaływaniami pomiędzy polimerami, jak zostało zaprezentowane na przykładzie charakteryzacji reakcji syntezy przeprowadzonej pomiędzy polimerami PVP a PAMPS [26], pomiędzy białkami [27], kropek kwantowych z białkiem [28], cząsteczek DNA z chitozanem [29], badaniami nad indukowanymi foto katalitycznie zmianami w (nano)cząstkach srebra [30] jak również charakteryzowaniu koniugacji oligonukleotydu z (nano)cząstkami złota, stosując przy tym detekcje *on-line* ICP/MS [31].

Niektóre metale można sklasyfikować jako tzw. metale ciężkie. Pojęcie odnosi się do charakteryzowania i klasyfikacji metali w świecie nauk biologicznych czy środowiskowych. Trudno wskazać precyzyjne kryteria pozwalające na klasyfikacje metali zaliczanych do grupy „ciężkich", jednakże często definiowanie terminu odnosi się do parametru gęstości metalu. Wartość graniczna gęstości również jest przedmiotem dyskusji, jednakże najniższa wartość gęstości, którą autorzy proponują wynosi powyżej 3.5 g/cm^3 [32]. W naukach biologicznych często odnosi się ten termin do parametru toksyczności, którą metal może wywierać na środowisko czy organizmy żywe.

Typowymi przykładami metali wykazującymi potencjalnie toksyczny charakter na środowisko są As, Cd, Cr, Cu, Pb, Hg, Ni, Se, Zn [33]. Przykładowo, r**tęć** występuje naturalnie w środowisku i nawet przy niskich stężeniach może powodować poważne zagrożenie dla zdrowia czy życia, szczególnie dla dzieci [34]. W kontekście oceny charakteru toksyczności metalu ważnym aspektem jest dawka, stężenie, które będzie wywierało toksyczny efekt na środowisko. **Cynk** przy wyższych stężeniach może powodować skurcze żołądka, podrażnienia skóry, wymioty, nudności i anemię, jednocześnie jest uznawany za niezbędny mikroelement do prawidłowego funkcjonowania wielu orgazmów żywych, ponieważ między innymi wspiera prawidłowe funkcjonowanie układu odpornościowego, gojenie się ran, krzepnięcie krwi, czynność tarczycy oraz zmysły smaku i węchu [35]. **Srebro** znane jest z wykazywania właściwości przeciwdrobnoustrojowych, jednakże chroniczne i wysokie narażenie może skutkować uszkodzeniem nerek, wątroby, podrażnieniem skóry i oczów oraz niekorzystnych zmian w drogach oddechowych i jelitach oraz w komórkach krwi [36]. **Kadm** wykazuje wiele toksycznych działań na różnorakie narządy, między innymi przy chronicznym narażeniu powoduje demineralizacje kości oraz naraża nerki na występowanie dysfunkcji kanalikowej [37]. Przez wiele lat zastosowanie miedzi w różnych gałęziach przemysłu i gospodarki było szerokie: od zastosowania związków zawierających **miedź** w środkach przeznaczonych do dezynfekcji poprzez środki przeciwdrobnoustrojowe, a skończywszy na przemyśle oraz metalurgii [38]. Dodatkowo, miedź jest jednym z niezbędnych pierwiastków do przeprowadzania metabolizmu w roślinach i zwierzętach. Jednakże cząstki miedzi potrafią uszkadzać

komórki na wiele sposobów, między innymi poprzez współudział w procesach utlenianiu tłuszczów i białek [39].

Ważnym zagadnieniem w kontekście charakteryzowania toksyczności metali ciężkich na środowisko czy też efektów działania jest wyznaczanie form występowania danego pierwiastka, ponieważ występuje silne rozróżnienie względem toksyczności czy działania wobec form, czyli tak zwanej specjacji pierwiastka, takich jak różne stopnie utlenienia, wpływ liganda czy też obecność specyficznych ugrupowań chemicznych obecnych związanych z metalem [40]. Na podstawie tego opracowywane są nowe kompozytowe materiały łączące w sobie część metaliczną wraz z odpowiednio dobranym związkiem, najczęściej charakteru makrocyklicznej cząstki, na przykład koloidu (białka, polisacharydu, cyklitoli) [41,42]. Takie podejście ma na celu otrzymanie nowego typu materiału o pozytywnych właściwościach (również synergicznych) dyktowanych przede wszystkim poprzez obecność jonów metali oraz wykorzystanie liganda w celu zapewnienia optymalnych właściwości biologicznych kompleksu oraz przede wszystkim redukowanie toksyczności preparatu poprzez utworzoną modyfikacje organiczną, która zmienia, często poprawia, właściwości, np. biodostępność, szybkość uwalniania jonów metali jak również ma wpływ na stabilność oraz miejsca uwalniania jonów w trakcie przewodu pokarmowego człowieka [43].

Odziaływania pomiędzy koloidami oraz koloidami a jonami metali mogą być różnej natury. Można zakładać, że ze względu na obecność grup funkcyjnych obecnych w strukturze koloidów zdolnych do jonizacji, odziaływania elektrostatyczne (równowaga pomiędzy elektrostatycznym przyciąganiem oraz odpychaniem) będą pełniły kluczową rolę w powstawaniu związków typu koloid-metal w odpowiednich warunkach środowiska; pH, siła jonowa, temperatura itd. [44,45]. Odziaływania prowadzące do oligomeryzacji (oprócz elektrostatycznych) mogą zawierać również odziaływania hydrofobowe, wiązania wodorowe [46] czy mostki dwusiarczkowe w przypadku białek [47]. Na rysunku 1 przedstawiono różne odmiany odziaływań ze wskazaniem na najczęściej spotykane grupy funkcyjne odpowiedzialne za ich występowanie.

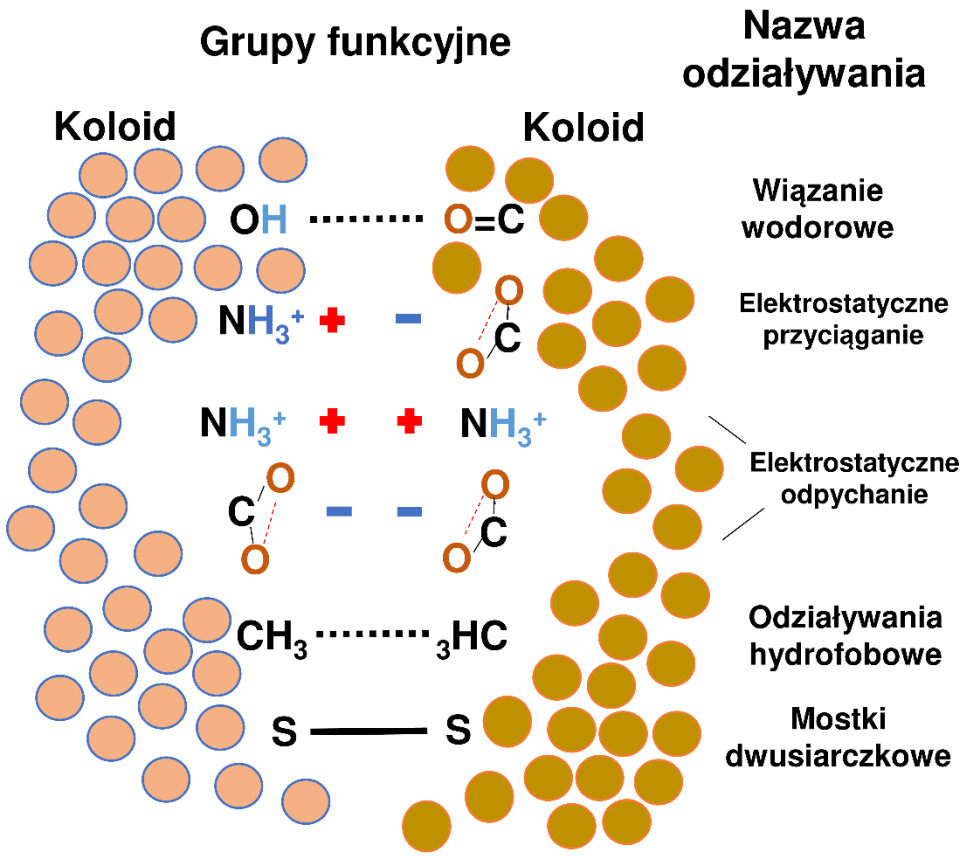

Rys. 1 Przedstawienie wybranych typów oddziaływań występujących pomiędzy koloidami.

W ramach przedstawionej dysertacji pt. „*Układy koloidalne oraz ich odziaływania z wybranymi metalami ciężkimi*” poruszono wyżej wymienione tematy, które zostały zawarte w serii pięciu [**P1-P5]** spójnie tematycznie publikacji naukowych opublikowanych w czasopismach z listy JCR.

[P1] **Golebiowski, Adrian** & Buszewski, Bogusław. (2023). Characterization of colloidal particles of a biological and metallic nature, *Microchemical Journal*, 108864, https://doi.org/10.1016/j.microc.2023.108864.

[P2] **Golebiowski, Adrian** & Kowalkowski, Tomasz & Buszewski, Bogusław. (2020). Molecular parameters of low methoxylated pectin affected by gelation with copper and cadmium cations. *Bioactive Carbohydrates and Dietary Fibre*. **21**. 100211. 10.1016/j.bcdf.2020.100211.

[P3] **Golebiowski, Adrian** & Pomastowski, Paweł & Rodzik, Agnieszka & Król-Górniak, Anna & Kowalkowski, Tomasz & Górecki, Marcin & Buszewski, Bogusław. (2020). Isolation and Self-Association Studies of Beta-Lactoglobulin. *International Journal of Molecular Sciences*. **21**. 10.3390/ijms21249711.

[P4] **Golebiowski, Adrian** & Pomastowski, Paweł & Rafińska, Katarzyna & Žuvela, Petar & Wong, Ming & Pryshchepa, Oleksandra & Madajski, Piotr & Buszewski, Bogusław. (2022). Functionalization of Alpha-Lactalbumin by Zinc Ions. *ACS Omega*. **7**, 43, 10.1021/acsomega.2c03674.

[P5] **Golebiowski, Adrian** & Pomastowski, Paweł & Rafińska, Katarzyna & Žuvela, Petar & Wong, M.W. & Madajski, P. & Buszewski, Bogusław. (2022). Binding of silver ions to alpha-lactalbumin. *Journal of Molecular Structure*. **1270**. 133940. 10.1016/j.molstruc.2022.133940.

Wymienione publikacje zamieszczono w całości na końcu dysertacji. Praca [P1] to artykuł przeglądowy, który wraz z przedstawionym *Wstępem* stanowi część teoretyczną do niniejszej dysertacji. Oryginalne publikacje zawarte w pozycjach [P2-P5] ukazują obecny stan wiedzy o tematyce badawczej.

Cele badawcze pracy

Nadrzędnym celem pracy było badanie odziaływań pomiędzy wybranymi koloidami oraz jonami metali.

Cel ten realizowano na grupie wyselekcjonowanych związków: pektynach, beta-laktoglobulinie, alfa-laktoalbuminie oraz jonów metali, szczególnie z grupy metali ciężkich: miedzi, kadmie, cynku oraz srebrze.

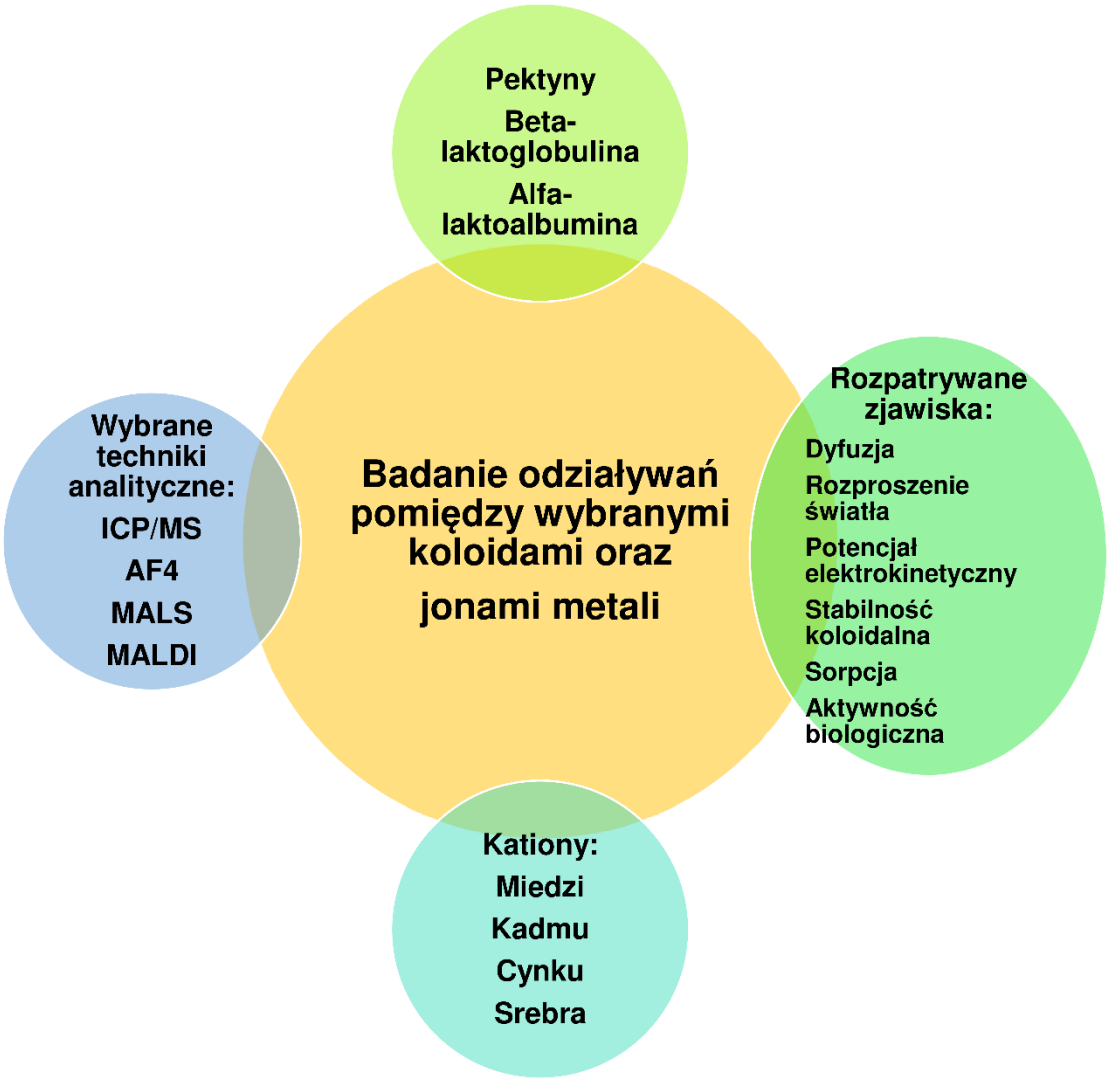

Rys. 2 Zarys podejmowanej tematyki.

Celami szczegółowymi były:

1. Opracowanie nowych metod analitycznych AF4 służących do separowania i charakteryzowania cząstek pektyn oraz beta-laktoglobuliny.

- Charakteryzowanie procesu żelowania pektyn indukowanymi przez kationy miedzi oraz kadmu poprzez monitorowanie zmian w wielkości cząstek, rozmiarów fraktalnych, dystrybucji cząstek oraz zawartości kadmu w cząstkach w funkcji czasu trwania syntezy.
- Charakteryzowanie form oligomerycznych oraz procesu aglomeracji beta-laktoglobuliny przy pH 3.0, 5.0 oraz 7.0 oraz wyznaczenie dodatkowych czynników warunkujących równowagę form białka w mieszaninie.

2. Charakteryzowanie stabilności koloidalnej pektyn, beta-laktoglobuliny oraz alfa-laktoalbuminy.
3. Izolowanie beta-laktoglobuliny z mieszaniny izolatu białek serwatkowych oraz wykonanie fizykochemicznej charakterystyki białka.
4. Opracowanie protokołów syntezy kompleksów alfa-laktoalbuminy z kationami cynku oraz srebra.
5. Charakteryzacja przebiegu reakcji syntezy kompleksów alfa-laktoalbuminy z kationami cynku oraz srebra, fizykochemiczne charakteryzowanie produktu ze szczególnym nastawieniem na poznawanie chemizmu (odnoszenie się do pojęcia sorpcji, wyznaczaniu grup funkcyjnych uczestniczących w odziaływaniu itp.)
6. Wyznaczanie parametrów: stabilności kompleksów w syntetycznych płynach pokarmowych, badania nad aktywnością biologiczną kompleksów w układzie *in vitro* przeprowadzonych w kontekście aplikacyjności kompleksów alfa-laktoalbuminy z kationami cynku oraz srebra.

Na rysunku 2 przedstawiono w sposób graficzny kwestie dyskutowane w pracy.

Przedmiot badań oraz komentarz

[P1] Characterization of colloidal particles of a biological and metallic nature

Microchemical Journal

W pracy podjęto dyskusję nad charakteryzowaniem cząstek koloidalnych o biologicznym oraz metalicznym pochodzeniu. Dokonano przeglądu 130 prac źródłowych, na podstawie których został przedstawiony temat badawczy. Praca składa się z pięciu zasadniczych części. Za cel pierwszej części postanowiono przedstawienie zaplecza teoretycznego popularnie stosowanych technik służących do charakteryzowania rozkładu wielkości i mas molowych cząstek. Dokonywano porównania pomiędzy technikami, uwzględniając parametry, takie jak zakres stosowalności technik oraz ich zalety oraz ograniczenia. Wykazano, że istnieją techniki analityczne pozwalające na charakteryzowanie koloidów w szerokim zakresie wielkości cząstek oraz specyficznej natury, które są wzajemnie komplementarne.

Jednym z głównych problemów spotykanych podczas analizy próbek koloidów jest ich bardzo duża polidyspersyjność mierzona poprzez indeks polidyspersyjności. Techniki analityczne oparte na rozproszeniu światła (dynamicznym oraz statycznym), pomimo bezpośredniego pomiaru masy oraz wielkości cząstek (intensywność rozproszonego statycznie światła na cząstce bezpośrednio koreluje z wielkością cząstki), dużej precyzji oraz uniwersalności zastosowań, często zawodzą (pomiary prowadzone wskazują na błędne wartości) podczas analizy próbek w stanie polidyspersyjnym w wielkości cząstek, która jest często spotykana dla próbek w stanie natywnym (pomiar bezpośrednio po procesie przygotowania próbka na sposób rozpuszczenia/zawieszenia koloidu w fazie rozpraszającej). W tym kontekście dyskutowano i przedstawiano różne możliwości rozwiązywania tego problemu. Wskazano, że jednym z tych rozwiązań może być zastosowanie technik separacyjnych w celu charakteryzowania w trybie *on-line* poszczególnych frakcji cząstek. Jednakże to podejście niestety niesie za sobą pewne trudności w postaci często niezadawalających odzysków substancji po procesie separacji. Jednymi z przyczyn utraty substancji podczas separacji mogą być odziaływania (elektrostatycznie przyciągające lub wodorowe itp.) analizowanych cząstek koloidu

z wypełnieniem fazy stacjonarnej (w przypadku SEC) lub membrany półprzepuszczalnej (dla AF4). Jednakże dzięki przeprowadzonej optymalizacji metod analitycznych możliwa jest znacząca poprawa wartości odzysku. Dyskutowano również nad krytyczną cechą koloidów, jaką jest kształt cząstek oraz znaczenie tego parametru dla niektórych typów stosowanych technik. Ze względu na to, że część stosowanych technik odnosi się często wprost do założenia sferycznego kształtu podczas kalkulacji wyników, dyskutowano nad możliwymi dokonaniami transformacji uzyskiwanych dystrybucji wielkości cząstek.

W drugiej części poruszono temat terminu potencjału zeta jak również metodologii wyznaczania jego wartości. Przedstawiono założenia teoretyczne oraz konsekwencje wynikające z doboru parametrów zmiennych eksperymentalnych (iloczyn promienia jonu oraz długość Debye'a) w kontekście relacji faza-rozproszona (cząstka koloidu) - faza rozpraszająca (ciecz). Przedstawiono znaczenie terminu stabilności dla koloidu oraz wyszczególniono dwa z potencjalnych mechanizmów stabilizowania mieszaniny (elektrostatyczny oraz steryczny) oraz zależność obu procesów z wartością potencjału zeta. Dyskutowano również nad parametrami mającymi wpływ na wartość potencjału zeta, takimi jak pH, siła jonowa, adsorpcja drugiego koloidu oraz debatowano nad efektami, jakie wywierają różnego rodzaju kationy oraz aniony na wartość potencjału zeta oraz stabilność koloidalną.

W kolejnej, trzeciej części artykułu przedstawiano potencjalne mechanizmy oddziaływania koloidów z jonami metali. Wskazywano, jaką rolę pełnią poszczególne grupy funkcyjne cząstek koloidów w procesach ogólnie pojętych sorpcji jonów metali na koloidach. Przedstawiano poszczególne techniki analityczne, które mogą być stosowane w charakteryzowaniu mechanizmów oddziaływania.

W czwartym rozdziale przedstawiano metody przygotowania próbki do analizy pierwiastkowej oraz wyznaczania rozmiaru cząstek za pomocą techniki SP ICP/MS. W kolejnym rozdziale przedstawiano możliwe zastosowania wybranych technik separacyjnych do analizowania próbek w kontekście badań nad specjacją pierwiastków, ustalania mechanizmów odziaływań koloidów z jonami metali w obszarze nauk biologicznych oraz gałęziach inżynierii.

[P2] Molecular parameters of low methoxylated pectin affected by gelation with copper and cadmium cations

Bioactive Carbohydrates and Dietary

Celem pracy była charakterystyka pektyn (promieni bezwładności jako miary wielkości cząstek, mas molowych, rozmiarów fraktalnych, indeksu polidyspersyjności oraz wartości potencjału zeta) oraz procesu żelowania z udziałem jonów metali kadmu oraz miedzi. Eksperymenty przeprowadzano w specyficznych warunkach fazy rozproszonej, jaką była woda podwójnie destylowana. Wybrano ten układ ze względu na potrzebę minimalizowania efektów elektrostatycznego przesłaniania grup funkcyjnych pektyn przez jony pochodzące z rozpuszczalnika, które prowadziłyby do konkurencyjnej reakcji pomiędzy jonami sieciującymi pektyny w badaniach prowadzonymi nad żelowaniem. Kolejnym zagadnieniem było wyznaczenie zmian w dystrybucji wielkości cząstek oraz konformacji żeli pektyn wraz z upływem czasu trwania procesu żelowania. Powiązane z tym kolejne pytanie odnosiło się do wyznaczenia dystrybucji zawartości metali w cząstkach żeli pektyn wraz z czasem trwania procesu. Podjęto próbę utworzenia metod analitycznych służących do ilościowego oznaczania zawartości metali w frakcjach.

Pektyny to przykład polisacharydu o właściwościach hydrofilowych. Zgodnie z definicją pektyny to substancja zawierająca co najmniej 65% masy kwasu galakturonowego [48]. Pektyny przyjmują nieustrukturalizowaną budowę przestrzenną, jednakże można wyróżnić regiony zbudowane z silnie rozgałęzionych i heterogenicznych bloków przede wszystkim ramnogalakturonanu I oraz ramnogalakturonanu II (ang. *hairy region*) oraz liniowo połączonego homogalakturonanu (ang. *smooth region*). Na rysunku 3 przedstawiono fragment ze struktury pektyn, na którym wyróżnić można dwa główne łańcuchy budujące pektyny: Ramnogalakturonan I oraz homogalakturonan. Pierwszy z nich zbudowany jest z powtarzających się jednostek reszt kwasu galakturonowego i ramnozy, rozgałęzienia łańcucha powstają poprzez przyłączenie reszt galaktozy lub arabinozy oraz ich pochodnych do reszty ramnozy. Parametrami charakteryzującymi pektyny są stopnie: estryfikacji (wyrażający procent estryfikowanych grup karboksylowych kwasu galakturonowego); acetylacji oraz amidacji (wyrażające z kolei stopnie podstawienia grupami odpowiednio

acetylowymi czy amidowymi) [49,50]. Modyfikacje te występują naturalnie za wyjątkiem amidacji.

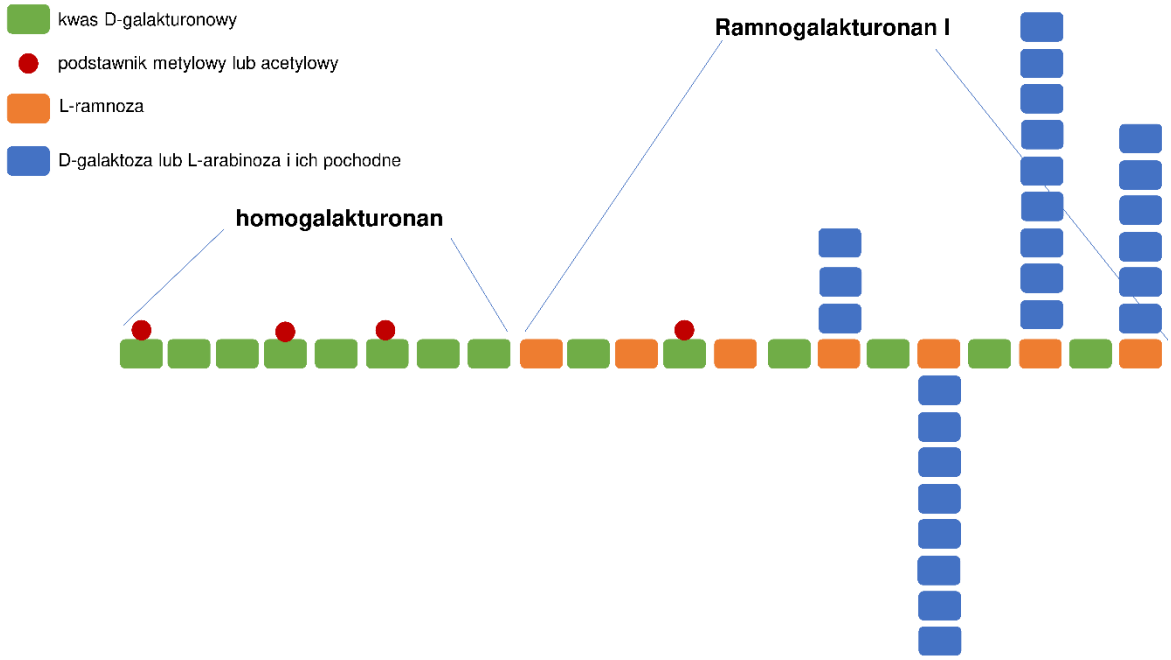

Rys. 3 Fragment z cząsteczki pektyn przedstawiający dwie główne łańcuchy budujące strukturę: ramnogalakturonan I oraz homogalakturonan.

Mają decydujący wpływ na chemiczny i fizyczny charakter pektyn, w tym warunkują zdolność oraz mechanizm żelowania [51] czy też parametry hydrodynamiczne [52]. Najszerzej opisanym mechanizmem żelowania dla pektyn jest model z ang. *egg-box* [53] Odnosi się on do utworzenia struktury typu *sandwich* zbudowanej z dwóch łańcuchów pektyn oraz jonu sieciującego zlokalizowanego pomiędzy nimi poprzez elektrostatyczne przyciąganie. Uczestniczącą grupą funkcyjną jest wolna i zjonizowana grupa karboksylowa. Wpływ siły jonowej na wartość oddziaływania pomiędzy kwasem galakturonowym a kationami metali jest znaczący i wynika z efektu przesłaniania ujemnego ładunku elektrycznego grupy karboksylowej przez kationy soli obecne w roztworze, co w efekcie skutkuje zmniejszeniem efektywnej siły przyciągania elektrostatycznego pomiędzy centrum aktywnym a jonami sieciującymi [54].

Proces żelowania stanowi podstawę wytwarzania wielu produktów spożywczych na bazie galaretek. Odnotowano także, że charakteryzowanie pektyn, parametrów strukturalnych takich jak: stopień podstawienia, masy molowej, struktury przestrzennej

[55,56] jest ważne ze względu na odmienny charakter oraz mechanizm zachodzenia procesu dla odmiennych struktur. Dogłębna charakterystyka zawiera się również w określaniu zmiennych eksperymentalnych, takich jak stężenia pektyn w mieszaninie oraz kationów sieciujących, pH, siły jonowej oraz temperatury [53].

Najszerzej opisanym i wykorzystywanym kationem sieciującym jest wapń, a wskazywany jako równowagowy stosunek molowy jonów wapnia do wolnych jonów karboksylowych wynosi 2 [53].

Pektyny mogą ulegać przejściu z zolu w żel w wyniku sieciowania z innymi jonami metali takimi jak: Cu, Al oraz La [57]. Jednakże wskazano, że badania reologii nad tego typu nowymi połączeniami nie były dotąd dostatecznie dobrze poznane. Wykazano za pomocą izoterm wiązania różnych jonów metali do pektyn, występowanie selektywności w sile odziaływania pomiędzy kationami a pektynami według szeregu:

Pb^{2+}-$Cu^{2'}$>Zn^{2+}>Cd^{2+} \Ni^{2+}>Ca^{2+}, oraz wskazano na trend, że siła wiązania wzrastała wraz z zmniejszeniem siły jonowej roztworu [58]. Różnice w selektywności, można interpretować poprzez wykazanie różnic w zdolności i właściwościami jonów do interakcji z wodą. Kationy silnie wiążące wodę wykazywały niższe powinowactwa do odziaływania z jonami kwasu karboksylowego pektyn, tworząc te dwie możliwe drogi odziaływania za konkurencyjne.

Pektyny wykazują silnią polidyspersyjność, gdy występują w układzie koloidalnym. Wyznaczona przez autorów masa molowa pektyn mieściła się w granicach $8 \times 10^3 - 1 \times 10^6$ g/mol w zależności od źródła pochodzenia [59]. Pektyny izolowane z owoców kiwi za pomocą różnych metodologii czy w różnym czasie sezonu wegetacyjnego wykazywały heterogeniczny charakter, przy współczynniku polidyspersyjności sięgającym nawet 12,6 oraz promieniach bezwładności od 96 nm do 183 nm [60]. Parametry mas molowych oraz konformacji pektyn zostały wskazane jako wywierające największy wpływ na właściwości funkcjonalne dla tego związku [61].

Na podstawie przytoczonych informacji postanowiono opracować nową metodę analityczną obejmującą zastosowanie techniki asymetrycznego frakcjonowania w polu sił przepływu (AF4) wraz z detekcją wielokątowego rozpraszania światła (MALS)

oraz spektrometrii mas z indukcyjnie sprzężoną plazmą (ICP/MS). Próbki pektyn po zakończeniu procesu rozpuszczania oraz uwodnienia analizowano za pomocą wspomnianych technik. Proces żelowania indukowano solami miedzi lub kadmu o odpowiednich stężeniach. Po wyszczególnionych czasach prowadzenia syntez badano homogenne porcje próbek.

Wyznaczona wartość potencjału zeta pektyn nisko metylowanych w warunkach eksperymentalnych wynosiła 0,25±0,49 mV, co wskazuje na elektro neutralność cząstek pektyn w tych warunkach. Jednakże może to być również spowodowane niską zawartością jonów obecnych w roztworze, które są nośnikiem ładunku elektrycznego podczas pomiaru oraz transportu naładowanych elektrycznie cząstek w polu elektrycznym. Postulowano, że prawdopodobnym źródłem jonów w warunkach eksperymentalnych mogą być jony pochodzące z procesów kwasowo-zasadowych grup funkcyjnych, jak również uwalnianie się zanieczyszczeń rozpuszczalnych w wodzie z materiału pektyn. Jednakże, obok efektu pH, który jest z pewnością kluczowy w kontekście wartości potencjału zeta oraz stabilności, ważną sprawą jest również wpływ stężenia pektyn w analizowanej próbce. Zastosowanie techniki AF4 w tym kontekście oznacza uzyskanie efektywnie niskiego stężenia próbki w warunkach separacji w kanale do frakcjonowania AF4 oraz dodatkowo w warunkach dynamicznie oczyszczania próbki z substancji o rozmiarach niższych niż wartość nominalna średnicy porów membrany półprzepuszczalnej. Można dzięki temu sformułować, że efektywne pH oraz siła jonowa są determinowane poprzez skład cieczy nośnej podczas separacji. Dzięki temu można dalej założyć, że przy pH powyżej 6 grupy funkcyjne (szczególnie karboksylowa kwasu galakturonowego, dla którego pK_a dla wolnego kwasu wynosi około 3,6 [62]) pektyn będą wysoce zjonizowane w warunkach eksperymentalnych oraz będą wykazywały znaczącą stabilność wskazywaną poprzez efekty elektrostatycznego odpychania się łańcuchów pektyn w warunkach eksperymentalnych w odniesieniu do skali wewnątrzcząsteczkowej jak również międzycząsteczkowej. Wewnątrzcząsteczkowe odpychanie się grup funkcyjnych będzie miało przełożenie na konformacje pektyn (silnie wyprostowaną) oraz wielkość cząstek.

Wyniki eksperymentalne analizy pektyn przed procesem żelowania wskazywały na ich polidyspersyjność. Odnotowano dwie frakcje cząstek pektyn w zakresie promieni

bezwładności od 593 nm do 671 nm. Wielkość cząstek w ciągu kolejnych trzech dni badania stabilności nie ulegały znaczącej zmianie, a szczególnie rozmiary nie zwiększały się, co może świadczyć o stabilności pektyn w układzie.

Analiza cząstek po indukowanym przez kationy kadmu oraz miedzi procesie żelowania pektyn dostarczyła kilku interesujących informacji na temat potencjalnie występujących struktur. Obserwacja promieni bezwładności cząstek pokazała, że zakres wielkości poszerzył się oraz nastąpiła inwersja mechanizmu elucji podczas separacji z normalnego na mechanizm steryczny, co może sugerować znaczące zmiany konformacyjne cząstek po procesie wiązania z jonami metali. Populacja cząstek po procesie wiązania wykazywała większe rozmiary niż wykrywane w samych pektynach (co może świadczyć o posuniętej aglomeracji – sieciowaniu struktury) oraz mniejsze rozmiary (co może wskazywać na efekty relaksacji konformacji cząstek pektyn z jonami w kontekście redukowania wewnątrzcząsteczkowego elektrostatycznego odpychania w porównaniu do pektyn w wodzie). Zwiększenie stężenia wyjściowego miedzi i kadmu oraz czasu trwania syntezy prowadziło do nieznacznego wzrostu promieni bezwładności cząstek. Na rysunku 4 przedstawiono graficznie proponowany schemat zachodzących przemian w wyniku procesu żelowania.

Cząstki żeli pektyn z kadmem oraz miedzią wykazywały znacząco większe rozmiary fraktalne dla cząstek największych, co może świadczyć o tworzących bardzo gęsto upakowanych, rozgałęzionych sieci żeli w porównaniu do kontroli (pektyny przed procesem). Rozmiary fraktalne są wskaźnikiem przedstawiającymi liczbowo zależność masy cząstki od promienia bezwładności. W wyniku bardzo wysoko posuniętego sieciowania cząstek uzyskano w efekcie wysokie wartości masy molowej w obrębie promienia bezwładności cząstki. Wartości współczynnika dla cząstek mniejszych nie zmieniały się znacząco po procesie wiązania.

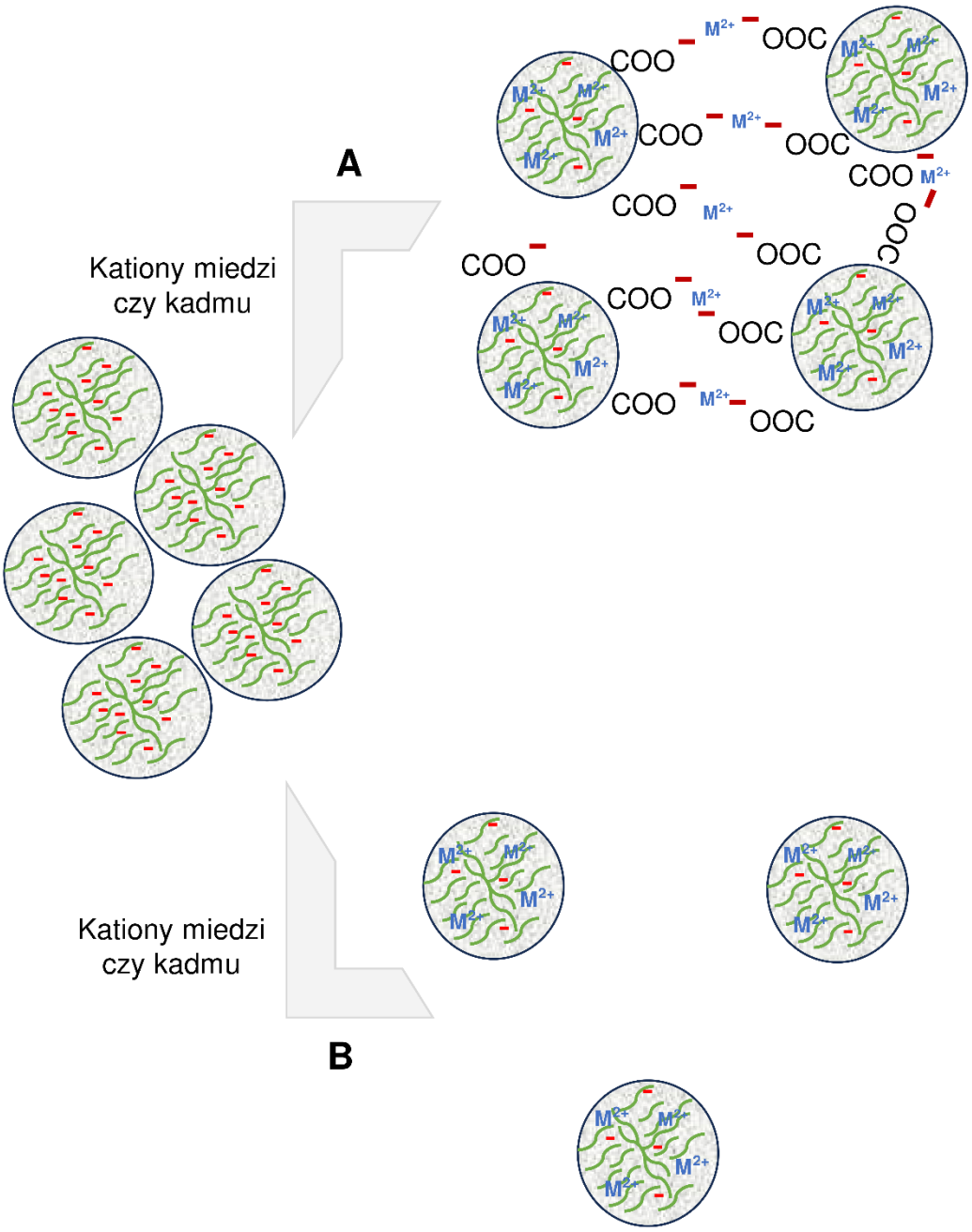

Rys. 4 Schemat przedstawiający cząstki pektyn, które oddziałują z kationami miedzi lub kadmu. W wyniku procesu odziaływania zaobserwowano doświadczalnie zwiększenie wielkości cząstek oraz rozmiarów fraktalnych dla populacji co może być interpretowane zachodzącym sieciowaniem łańcuchów pektyn z kationami metali (A). Ścieżka B reprezentuje interpretacje efektu zmniejszenia rozmiarów cząstek przy praktycznie nie zmieniającej się wartości rozmiarów fraktalnych, co może być odzwierciedleniem efektu redukowania elektrostatycznego wewnątrz cząsteczkowego odpychania się łańcuchów pektyn.

W kolejnym kroku wykazano, że sprzężenie technik AF4-MALS-ICP/MS może być wykorzystane do oznaczania kadmu w cząstkach żeli oraz mogłyby być implementowane do badań nad kinetyką odziaływań/wiązania metali przez pektyny. Wykazano, że zastosowane podejście kalibracji oznaczania metali wykazuje akceptowalną liniowość oraz może być stosowane w badanym zakresie stężeń metalu (w przeliczeniu na masę kadmu w zakresie 0-20 μg). Wraz z postępem procesu żelowania następuje heterogenna dystrybucja kadmu względem cząstek. Wraz z zwiększaniem czasu trwania syntezy zawartość kadmu zwiększała się szczególnie znacząco dla największych cząstkach, co może potwierdzać, że jony kadmu aktywnie uczestniczyły w sieciowaniu oraz wzrost wielkości cząstek koreluje proporcjonalnie z zawartością kadmu. Odnotowano obecność „kadmu" dla próbki pektyn analizowanej bez dodatku kadmu, przed procesem żelowania. Mogło to być spowodowane efektem matrycy lub pamięci (trudno znaleźć odniesienie literaturowe odnoszące się do efektu pamięci dla kadmu, szczególnie dla techniki AF4), zanieczyszczeniem samych pektyn lub skażeniem powstałym na drodze wykonywanych wcześniej analiz.

Podsumowując pracę [P2] dotyczącą pektyn oraz procesu żelowania indukowanego jonami miedzi i kadmu, można wypunktować:

- Pektyny wykazują polidyspersyjność w wielkości cząstek.
- Jony miedzi i kadmu uczestniczą w sieciowaniu pektyn.
- Sieciowanie pektyn z jonami kadmu i miedzi może być charakteryzowane poprzez zmiany parametrów wielkości cząstek i rozmiarów fraktalnych
- Sprzężenie *on-line* technik AF4-MALS-ICP/MS może być stosowana do charakteryzowania właściwości przypisywanych koloidom jak również w ciągu jednej analizy możliwe jest oznaczanie zawartości i dystrybucji jonów kadmu.

[P3] Isolation and Self-Association Studies of Beta-Lactoglobulin

International Journal of Molecular Sciences

Beta-laktoglobulina to białko globularne występujące naturalnie i w przeważających ilościach w mleku krowim. W procesach przetwórstwa serwatki mleka producenci wytwarzają produkty uboczne (izolat, hydrolizat lub koncentrat białek serwatkowych), które są bardzo bogatym źródłem białka. Dlatego ze względu na wysoką dostępność i niską cenę tych produktów mogą stanowić atrakcyjne źródło do pozyskania beta-laktoglobuliny w zadawalającej ilości oraz potencjalnie wysokiej czystości. Pierwszym celem pracy była izolacja białka z roztworu izolatu białek serwatkowych oraz charakterystyka uzyskanego białka, w szczególności czystości, potwierdzenia tożsamości oraz fizykochemiczna charakterystyka (masa molowa, stabilność w roztworach o różnym składzie jakościowym-wpływ jakościowy jonów na stabilność) oraz wyznaczanie potencjalnych izoform białka.

Interesującym zagadnieniem podjętym w pracy była charakterystyka procesu oligomeryzacji – spontanicznej samo-asocjacji białka. Na podstawie badań źródłowych wiadomo, że proces przebiega dzięki mechanizmowi, w którym uczestniczą wiązania wodorowe, łączące kolejne łańcuchy białka. Badacze wyznaczyli, że zmiany w formach występowania białka w roztworze przyjmują przede wszystkim zależność od pH środowiska. W środowisku kwasowym, przy pH 2-3 autorzy wyznaczyli zachodzącą równowagę pomiędzy monomerami a dimerami, która jest również zależna od stężenia soli w roztworze, przy pH w okolicach punktu izoelektrycznego (pI około 5.3) autorzy wyznaczyli równowagę form dimer-oktamer, skupiając się również na efekcie, jaki wywiera temperatura [63]. Z kolei, Mercadante i inni, poszerzyli zakres badań i wskazali, że w środowisku zasadowym białko przyjmują formę dimeru [64]. Na rysunku 5 przedstawiono strukturę dimeru beta-laktoglobuliny w modelu powierzchniowym.

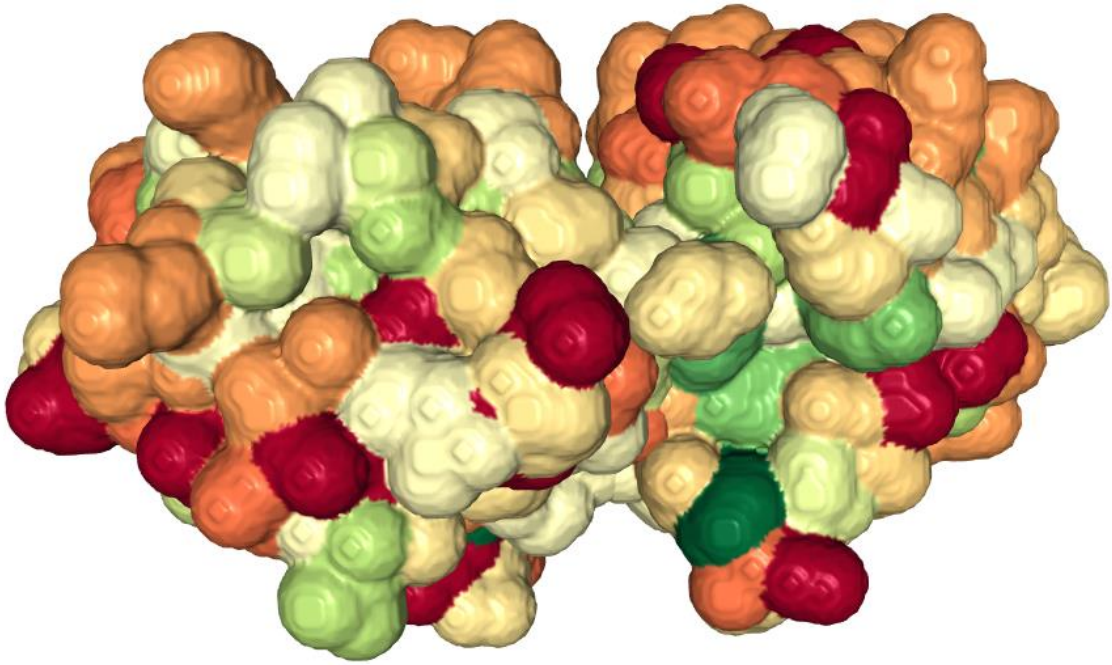

Rys. 5. Struktura dimeru beta-laktoglobuliny w formie natywnej. Za styl prezentacji struktury wybrano powierzchniowy. Gradacja kolorów występuje względem hydrofobowości regionów strukturalnych; od intensywnie czerwonego oznaczającego wysoce hydrofilowe do intensywnie zielonego oznaczających silnie hydrofobowe. [Vijayalakshmi, L., Krishna, R., Sankaranarayanan, R. and Vijayan, M. (2008), An asymmetric dimer of β-lactoglobulin in a low humidity crystal form—Structural changes that accompany partial dehydration and protein action. Proteins, 71: 241-249. https://doi.org/10.1002/prot.21695][AS Rose et al. (2018) NGL viewer: web-based molecular graphics for large complexes. Bioinformatics doi:10.1093/bioinformatics/bty419]

W swoich badaniach zaproponowałem oryginalne wykorzystanie technik: AF4-UV-MALS oraz CE w kontekście badań nad charakteryzowaniem form oligomerycznymi białka przy pH 3.0 5.0 oraz 7.0. Ortogonalne dwa mechanizmy separacji były jednym z innowacyjnych podejść w tego typu badaniach. W kolejnym etapie za cele postawiono wyznaczenie struktur drugorzędowych białka przy tożsamych wartościach pH.

Do przeprowadzenia izolacji beta-laktoglobuliny z roztworu izolatu białek serwatkowych wykorzystano chromatografię kolumnową z silnie kwasowym wypełnieniem (SP Sephadex C-25). Dokonano doboru parametrów objętości złoża i przepływu fazy ruchomej. Fazą ruchomą był roztwór cytrynianu sodu o stężeniu 0,2 M. Separacje prowadzono względem roztworów o wzrastającym pH od 3.0 do 6.5. Zebrane frakcje analizowano techniką elektroforezy żelowej pod kątem wstępnej oceny składu

poszczególnych frakcji w porównaniu do substancji wzorcowych. Wykazano, że jedna zebrana frakcja przy pH=4.8 jest elektroforetycznie jednorodną mieszaniną złożoną z substancji o masie molowej bliskiej teoretycznej masie monomeru beta-laktoglobuliny (18 kDa). W celu przeprowadzonej identyfikacji oraz charakteryzacji przebadano również inne frakcje stosując podejście trawienia enzymatycznego (trypsyną) substancji zawartych w żelu do charakterystycznych peptydów oraz ich spektrometrycznej analizy techniką MALDI-TOF/MS/MS oraz ich identyfikacja poprzez zastosowanie narzędzi bibliotek bioinformatycznych. Potwierdzono z dużym prawdopodobieństwem na podstawie porównania sekwencji peptydów teoretycznych oraz identyfikowanych, że izolowane białko przy pH=4.8 to beta-laktoglobulina. Dodatkowo, wyznaczono eksperymentalnie masy molowe białek: beta laktoglobuliny oraz alfa-laktoalbuminy (izolowana przy pH=4.2), które były porównywalne w wartościach z podawanymi w literaturze dla monomerów.

Wykazano, że dobierając matrycę stosowaną w pomiarach MALDI (szczególnie poprzez właściwości hydrofilowości związku matrycy), można analizować z jednej strony dystrybucje izoform białka (wykryto formy A i B beta-laktoglobuliny) (dzięki zastosowaniu kwasu synapinowego oraz DHB), z kolei wybierając matrycę HCCA można skupić się na analizie formy monomeru białka.

Badania nad wyznaczaniem stabilności koloidalnej białka przeprowadzono w czterech różnych składach jakościowych roztworu: chlorku sodu, chlorku potasu, siarczanie amonu oraz buforze cytrynianowym. Wykazano, że skład jakościowy roztworu ma również znaczący wpływ na wartości potencjału zeta oprócz kluczowej zależności od pH środowiska. Punkt izoelektryczny białka zmieniał się w zależności od składu jakościowego roztworu, co można rozpatrywać pod względem wartościowości poszczególnych przeciw-jonów w odniesieniu do ładunku elektrycznego zlokalizowanego na białku oraz specyficznych efektów jakościowych wykazywanych przez poszczególne jony. Przez to informacja na temat składu całego systemu powinna być raportowana podczas raportowania wartości stabilności czy punktów izoelektrycznych. Wyznaczony z modelu wartości punktu izoelektrycznego była najbliższa wartościom podawanym w literaturze dla roztworu cytrynianu sodu (pI=5.3). Jony obdarzone większym ładunkiem elektrycznym wykazywały większe zdolności efektywnego odziaływania (zmieniały zeta potencjał

znacząco) z białkiem. Postulowano, że bufor cytrynianowy stabilizuje białko najlepiej w badanym zakresie pH, szczególnie w środowisku kwaśnym. Dodatkowo, jony mogą wykazywać selektywność w odziaływaniu z białkiem, czego efektem są odmienne wartości potencjału zeta przy niezmiennych parametrach pH, stężenia jonu oraz białka, a także parametrów temperatury oraz lepkości roztworu, co może być interpretowane korzystając z szeregu Hofmeistera.

Bufor cytrynianowy ze względu na najwyższe właściwości do stabilizowania białka w środowisku kwaśnym został wybrany do dalszych badań nad oligomeryzacją, która obejmowała szeroki zakres pH (3.0 5.0 oraz 7.0). Wykorzystano dwie techniki: CE-UV oraz AF4-UV-MALS. Wyniki uzyskane techniką CE wykazały przy pH 3 obecność jednej głównej frakcji- tj. jednej formy białka, przy pH 7 trzech frakcji, przy pH 5- blisko punktu izoelektrycznego, w sumie 8 frakcji. Jednakże ze względu na brak detektora umożliwiającego bezpośrednie wyznaczanie masy molowej nie udało się charakteryzować (wyznaczyć masy molowej formy białka w sposób bezpośredni) w poszczególnych frakcjach. Potencjalne zastosowanie kalibracji zewnętrznej, tj. porównywania czasów migracji substancji względem wzorcowych o znanych masach molowych, jest trudna do zastosowania w tych badaniach ze względu na potencjalne rozbieżności w przyjmowanych konformacjach pomiędzy beta-laktoglobuliną a wzorcami i stąd potencjalnie rozbieżnościami w ruchliwości elektroforetycznej pomiędzy substancją a wzorcem.

Dokonano komplementarnych analiz korzystając z techniki AF4 oraz wykorzystaniu detektora MALS w celu bezpośredniego pomiaru masy molowej cząstek w tych warunkach. Utworzono i optymalizowano metody dla trzech różnych warunków eksperymentalnych. Porównując wyznaczone masy molowe z teoretycznymi, wyznaczono, że dominującą formą białka przy pH 3 jest monomer, przy pH 7 główną frakcje stanowią dimery białka oraz pewna zawartość cząstek o wysokich masach molowych (zapewne aglomeratów). Przy pH równym 5 wykryto mieszaninę kilku form (co potwierdzało wyniki otrzymane po CE), jednakże udało się scharakteryzować formy jako pochodzące od dimeru poprzez kolejne formy aż do oktameru. Przy tym pH odnotowano również formy wysokocząsteczkowe aglomeratów. Co ciekawe, zauważono, że wyższe stężenie białka w analizowanych

warunkach koreluje z przesunięciem równowagi oligomerycznych form w kierunku oktameru.

Badania dichroizmu kołowego pozwoliły na wyznaczenie równowagi i dystrybucji form drugorzędowych białka (alfa-helisa, beta-kartka oraz „kłębka statystycznego") względem trzech pH 3, 5 oraz 7. Wyznaczono, że w środowisku kwaśnym białko przyjmuje równowagową konformacje złożoną z form: beta-kartki oraz kłębka statystycznego (o podobnej zawartości) oraz niewielkiej zawartości alfa-helisy. Przy pH 5 zawartość alfa-helisy była około dwukrotnie wyższa (25 %), która wraz z beta-kartką były dominujące. Przy pH 7 wyznaczono, że trzy formy stanowią praktycznie równo cenne w zawartości formy białka (każda w zawartości około 30%).

W pracy [P3] dotyczącej beta-laktoglobuliny skupiono się na izolowaniu w skali (pół)preparatywnej białka z popularnego i łatwo dostępnego surowca dzięki wykorzystaniu chromatografii kolumnowej oraz wieloaspektowej charakterystyce białka. Pracę można podsumować w kilku punktach:

- Dobierając matrycę stosowaną do MALDI można uzyskiwać informacje na temat form izomerycznych beta-laktoglobuliny lub form oligomerycznych.
- Skład jakościowy roztworu fazy rozpraszającej ma wpływ na stabilność beta-laktoglobuliny w roztworze i dlatego należy raportować wszystkie zmienne eksperymentalne w kontekście podawania danych, np. dotyczących punktu izoelektrycznego.
- Beta; laktoglobulina wykazuje zależne od pH formy oligomeryczne, które w warunkach pH bliskich punktowi izoelektrycznemu wykazywały również zależność od stężenia białka w środowisku (wyższe stężenie prowadzi do formy oktameru).
- Technika AF4 może być wykorzystywana do separowania form oligomerycznych beta-laktoglobuliny a detekcja UV-MALS daje możliwość bezpośredniego pomiaru mas molowych cząstek.

[P4] Functionalization of Alpha-Lactalbumin by Zinc Ions

ACS Omega

Alfa-laktoalbumina to drugie pod względem zawartości białko spotykane w serwatce. Jednakże w mleku ludzkim jest najbardziej rozpowszechnione. W odróżnieniu do beta-laktoglobuliny spożycie nie wywołuje znaczącej reakcji immunologicznej dla niektórych ludzi, stąd białko stanowi ważny produkt dla przemysłu spożywczego oraz przemysłu farmaceutycznego pod względem opracowywania produktów spożywczych/leczniczych (suplementacja) opracowywanych dla niemowląt czy seniorów. Stanowi również bazę do przygotowywanych produktów sfunkcjonalizowanych. Ze względu na niską masę cząsteczkową monomeru (około 14 kDa), szczególnie wysoką stabilność białka w środowisku kwaśnym (które jest obecne w części przewodu pokarmowego człowieka) oraz udowodnione właściwości do wiązania substancji biologicznie aktywnych szerokiego spektrum od hydrofilowych jonów metali [65,66] poprzez hydrofobowe substancje takie jak kwasy oleinowy i palmitynowy, których synteza jest efektywna dla formy *apo* białka [67,68] badania nad tym białkiem są obecnie często przeprowadzane. Kompleksy tych substancji posiadają wyjątkowo ciekawe właściwości, ponieważ możliwa jest kontrola biodostępności jonów metali wiązanych w strukturach cząstek oraz modyfikowana jest toksyczność dla niektórych z nich. Z kolei kompleksy z kwasami tłuszczowymi są obecnie szeroko i intensywnie badane pod kątem właściwości, jakie wywierają na apoptozę komórek rakowych [69–72]. Na rysunku 6 przedstawiono strukturę alfa-laktoalbuminy w modelu powierzchniowym.

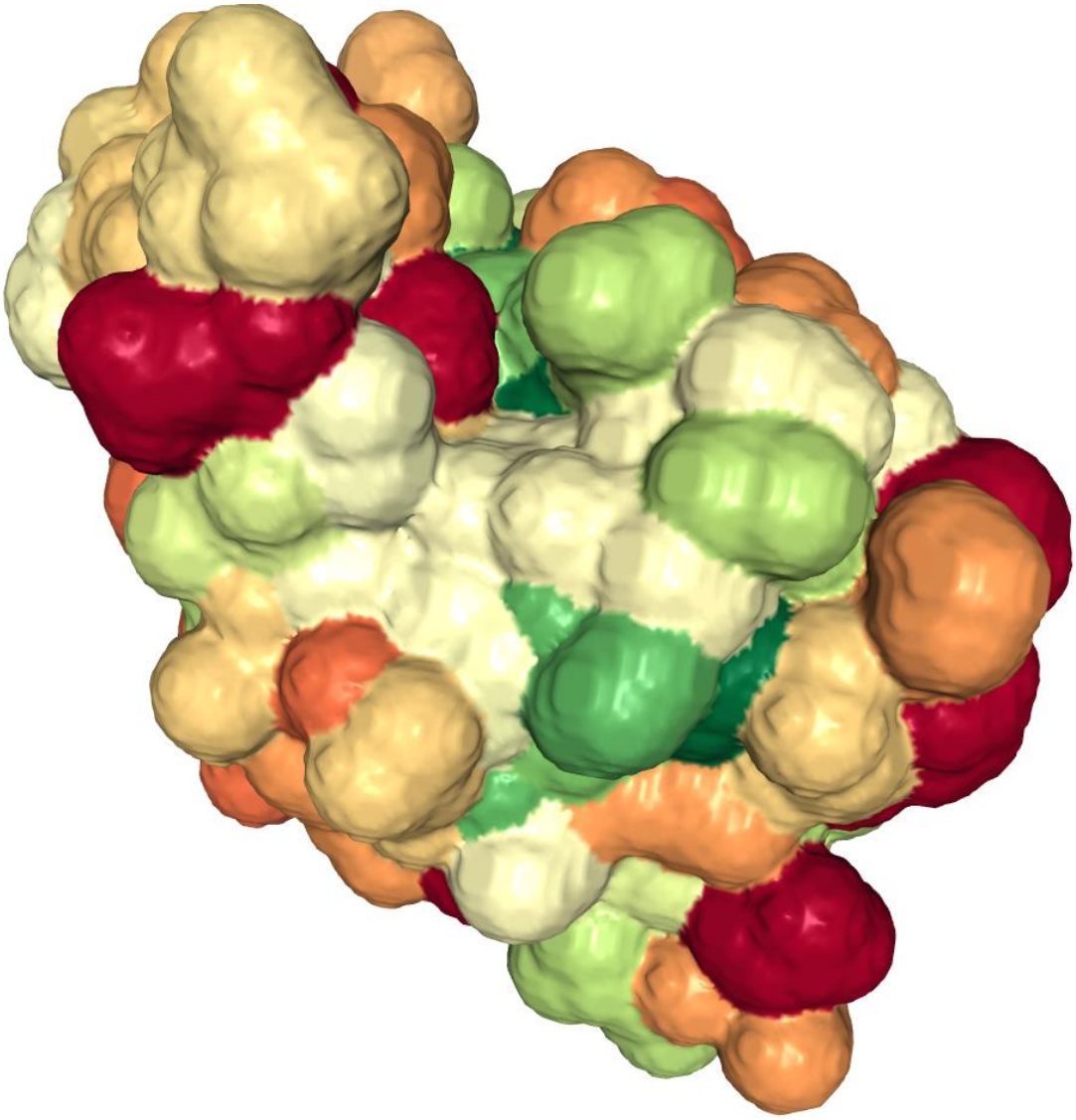

Rys.6. Struktura alfa-laktoalbuminy. Za styl prezentacji struktury wybrano powierzchniowy. Gradacja kolorów występuje względem hydrofobowości regionów strukturalnych; od intensywnie czerwonego oznaczającego wysoce hydrofilowe do intensywnie zielonego oznaczających silnie hydrofobowe. [Chandra N, Brew K, Acharya KR. Structural evidence for the presence of a secondary calcium binding site in human alpha-lactalbumin. Biochemistry. 1998 Apr 7;37(14):4767-72. doi: 10.1021/bi973000t][AS Rose et al. (2018) NGL viewer: web-based molecular graphics for large complexes. Bioinformatics doi:10.1093/bioinformatics/bty419]

Celem tej pracy była fizykochemiczna charakterystyka białka alfa-laktoalbuminy pod kątem wyznaczenia ruchliwości elektroforetycznej (w badaniach nad czystością), potwierdzenia tożsamości, masy molowej, stabilności koloidalnej w roztworze soli fizjologicznej. Zebrane informacje posłużyły również do optymalizacji oraz sporządzenia

protokołu procesu syntezy kompleksów na bazie alfa-laktoalbuminy z jonami cynku. Przeprowadzono charakterystykę kinetyki procesu oraz wyznaczenia miejsc wiążących oraz zmian w strukturze grup funkcyjnych białka po procesie wiązania, jak również wyznaczenia miejsc wiążących cynk przez białko. Dokonano charakterystyki morfologii oraz topografii uzyskanych cząstek, których badania mogłyby prowadzić do wyznaczenia formy cynku zlokalizowanego w kompleksie. Jako badania aplikacyjne pod kątem stosowania tego typu kompleksu w celach spożywczych, jako suplement diety, wykonano testy stabilności kompleksów w płynach fizjologicznych, indukowanego trypsyną trawienia enzymatycznego oraz biologicznej aktywności kompleksów względem linii komórkowych Caco-2 oraz L929.

Białko migrowało w warunkach przeprowadzonej analizy elektroforezy żelowej pomiędzy substancjami wzorcowymi o masach 14 kDa a 17 kDa, w postaci jednego wąskiego prążka, co może potwierdzać, że białko występuje w postaci czystej oraz jest elektroforetycznie stabilne. Przeprowadzono dogłębną identyfikację opartą na charakteryzowaniu sekwencji peptydów po degradacji enzymatycznej (trypsyną) białka za pomocą techniki MALDI-TOF/MS/MS. Z dużym prawdopodobieństwem potwierdzono tożsamość izolowanego białka jako alfa-laktoalbuminy. Wyznaczono również masy molowe monomerów białka, które były wysoce zgodne z literaturowymi. Wykazano obecność trzech różnych form białka, które mogą być wynikiem obecności występowania modyfikacji post translacyjnych, źródła białka lub zanieczyszczeń.

Wykonując pomiary potencjału zeta w funkcji pH, wyznaczono punkt izoelektryczny białka na występujący przy 4.5 w roztworze 0,09% NaCl, który zgadza się z danymi literaturowymi w badaniach wykonanych w podobnych warunkach pomiarowych. Przy tej wartości pH, białko wykazuje między innymi najniższą rozpuszczalność oraz konformację wykazującą najwyższą dostępność grup funkcyjnych, przy której wykonywano syntezę kompleksu metal-białko.

W pierwszym etapie charakteryzowano kinetykę reakcji syntezy, stosując technikę ICP/MS w celu oznaczania stężenia niezwiązanej porcji jonów cynku po procesie syntezy. Wyznaczono, że proces wiązania można rozpatrywać jako dwuetapowy. W pierwszym z nich, szybkim etapie trwającym niecałe 5 minut, następuje efektywny proces wiązania jonów cynku przez białko (rozumiany jako ubytek stężenia jonów cynku w roztworze

pozostałym po procesie). Wyznaczona z modelu stała szybkości reakcji wynosiła $7{,}3\text{x}10^{-5}\, mg\, min/L$. Po tym czasie następuje etap, który można określić jako równowagowy, w którym zmiany stężeń cynku są mało znaczące w kontekście przedłużonego czasu trwania syntezy. Wyznaczoną doświadczalnie pojemność sorpcyjna cynku na białku wynosiła 1.58 mg/g. Wyliczona entalpia swobodną reakcji wynosiła 9,45 kJ/mol, co wskazuje, że proces wiązania cynku przez białko był spontaniczny.

Badania kompleksów komplementarnymi technikami spektroskopii w podczerwieni (FT-IR oraz Raman) pozwoliły na szacowanie oraz wykrywanie zmian w obrębie grup funkcyjnych, a przez to wskazywały na potencjalne grupy funkcyjne, które mogą być odpowiedzialne za odziaływania z cynkiem. Odnotowano subtelne zmiany w intensywnościach oraz położeniu poszczególnych drgań przypisywanych do drgań Amidu II oraz Amidu III oraz zmian w zakresie drgań, które mogą wskazywać na zmiany konformacyjne.

Badania technikami mikroskopowymi (SEM oraz TEM wraz z różnymi detektorami) wskazywały na utworzenia depozytu metalicznego na powierzchni ciała amorficznego, jaką stanowiła próbka białka. Na powiększeniach skali obrazów widoczne są cząstki o kształtach, które można opisać jako sferyczne, które były ściśle powiązane z powierzchnią struktury białka. Z kolei badania TEM wykluczyły obecność strątów czy form cynku w postaci nanocząsteczek (znikoma zawartość tlenu w analizowanych punktach pomiarowych, w których wykrywany był cynk) (typu ZnO), co poprzez drogę eliminacji może sugerować zachodzenie mechanizmów elektrostatycznego przyciągania między jonami cynku a grupami funkcyjnymi białka prowadzącymi do uzyskania kompleksów.

Badania prowadzone technikami dynamiki molekularnej nad potencjalnymi typami odziaływania oraz nad grupami funkcjonalnymi białko odpowiedzialnymi za wiązanie wskazały na dominujący udział aminokwasów kwasowych (kwasu asparaginowego oraz glutaminowego) oraz mniejszego, lecz wartego odnotowania wpływu lizyny, w procesie elektrostatycznego przyciągania jonów cynku przez białko. Wskazano na grupę karboksylową aminokwasów, a ściślej na ujemny ładunek elektryczny zlokalizowany w strukturze grupy COO^- za potencjalne dominujące miejsce wiążące jony cynku.

Badane kompleksy okazały się być stabilne pod względem działania syntetycznych oraz syntetyzowanych płynów: żołądkowego oraz jelitowego, gdzie działanie tych płynów powodowało uwolnienie cynku nie przekraczające 10 % ilości pierwotnie związanej. Jednakże działanie syntetycznego płynu jelitowego z dodatkiem enzymu doprowadziło do znaczącego poziomu uwolnienia cynku z kompleksu (ponad 41 %), co oznacza, że w przypadku potencjalnego zastosowania produktu, dominującym miejscem uwalniania cynku będzie jelita. Prawdopodobnym mechanizmem powodującym uwolnienie cynku w środowisku zasadowym wraz z użyciem enzymów charakterystycznych dla jelita mogłoby być spowodowane enzymatycznym (specyficznym) trawieniem struktury białka do peptydów w połączeniu z uwolnieniem jonów cynku w postaci wolnej lub cynku wraz z peptydami o masie cząsteczkowej poniżej 3 kDa (taka membrana została wykorzystana podczas badań).

Białko oraz jego kompleksy wykazywały również stabilność względem działania trypsyny. Jeśli chodzi o badania nad cytotoksycznością kompleksów, wykazano, że kompleksy nie zmniejszały przeżywalności komórek L929 w badanym zakresie stężeń. Uszkodzenie ciągłości membran odnotowano dla najwyższego badanego stężenia cynku – 200 μM dla linii komórkowej L929. Z kolei dla komórek Caco-2 odnotowano ten trend przy niższych stężeniach (od 6,25 μM do 200 μM). Badania przyswajalności cynku przez komórki L929 potwierdziły dwukrotne niższą ilość akumulowaną pobieraną z kompleksów alfa-laktoalbuminy w odniesieniu do prostej formy jonowej cynku pochodzącej od soli nieorganicznej azotanu cynku.

Praca [P4] odnosi się do charakterystyki alfa-laktoalbuminy oraz kompleksu z jonami cynku wraz z przeprowadzonymi badaniami nad potencjalnymi aplikacjami do stosowania jako np. suplementu diety. Można konkludować tezy zawarte w pracy w poniższych punktach:

- Analiza kinetyki wiązania cynku przez alfa-laktoalbuminę wskazuje na proces uzyskujący równowagę w ciągu 5 minut trwania procesu; ilość wiązanego cynku wynosi 1,58 mg na gram białka.

- Grupa karboksylowa kwasów asparaginowego oraz glutaminowego mają dominujący udział w wiązaniu jonów cynku na drodze elektrostatycznego przyciągania; odziaływanie z lizyną wpływa również na odziaływanie.
- Kompleksy wykazywały zadowalającą stabilność na degradacje enzymatyczną (trypsyna) jak również w syntetycznych płynach fizjologicznych.

[P5] Binding of silver ions to alpha-lactalbumin

Journal of Molecular Structure

Jon srebra, ze względu na przeciwny potencjał redox formy jonowej, wskazuje na potencjalnie odmienny charakter zachodzenia procesu oraz mechanizm zachodzącej syntezy z alfa-laktoalbuminą w porównaniu do przedstawionej w pracy [P4] procesu wiązania białka z cynkiem. Kompleksy z srebrem kierują uwagę nad aplikacyjnym charakterem badań w kierunku zastosowania tego typu kompleksów jako środków przeciwdrobnoustrojowych, w tym stosowanych na trudno gojące się rany. Korzystając z danych otrzymanych w pracy P4 dotyczących charakteryzacji alfa-laktoalbuminy, proces syntezy kompleksu przeprowadzono w identycznych warunkach. Do charakteryzacji wykorzystano analogiczne techniki oraz podejścia (nie uwzględniając badań nad indukowaną trypsyną stabilnością kompleksu).

Badania kinetyki wiązania jonów srebra przez białko wskazywały na zachodzenie procesu, który można podzielić na dwa etapy jednostkowe. W pierwszym etapie procesu wiązania, trwającym dwie minuty, następował praktycznie całkowity ubytek jonów srebra w pozostającym po procesie roztworze, co mogło oznaczać, że ta ilość jonów srebra uległa związaniu na/przez białko. Wyznaczona stała szybkości reakcji wynosząca 13,75 mg min/L wskazuje na zachodzący bardzo szybko proces wiązania. Kolejne punkty pomiarowe wskazywały na ustalenie się drugiego etapu procesu - równowagowego. W tym etapie zmiany stężeń srebra były mało znaczące. Entalpia swobodna reakcji wynosząca -25,85 kJ/mol świadczy o (silnej) samorzutnej tendencji do procesu wiązania srebra przez białko.

Wyznaczono, że aminokwasy o charakterze kwasowym (asparaginowy oraz glutaminowy) determinowanymi poprzez grupę funkcyjną karboksylową odpowiedzialne są za ponad 90% całości odziaływania białka z jonami srebra. Jednakże uzyskane dane wskazują na warte odnotowania udziały aminokwasów tyrozyny oraz lizyny w wiązaniu srebra przez alfa-laktoalbuminę, które były większe niż w porównaniu do procesu z cynkiem [P4].

Badania nad kompleksami przeprowadzonymi technikami spektroskopii FT-IR oraz Ramana wskazywały na rolę, jaką odgrywało ugrupowanie Amidu II oraz mostków dwusiarczkowych S-S, obecnych w białku i wykazujących silne powinowactwo do jonów srebra.

Wykonane badania mikroskopowe dostarczyły informacji na temat sferycznego kształtu cząstek na powierzchni amorficznych cząstek białka. Badania techniką TEM z detekcją elementarną EDX wykazały, że klastry cząstek (zebrane w większe skupiska formacje cząstek srebra na powierzchni) nie zawierają znaczącej zawartości tlenu, co poprzez dedukcje oraz na podstawie dokonanego przeglądu literatury nad potencjalnymi formami srebra w kompleksach może prowadzić do wniosku, że srebro zlokalizowane na powierzchni kompleksu występuje zredukowane do postaci elementarnej Ag^0. Redukcja srebra z formy kationu, przed syntezą Ag^+, do formy elementarnej była już zauważana w przypadkach badań prowadzonych z innymi białkami, np. kazeinami. Mechanizm tworzenia się tych struktur opierał się na transferze elektronów z ujemnie nakładowych grup karboksylowych do kationów srebra (redukcja) [73].

Badania nad stabilnością kompleksów w syntetycznych płynach fizjologicznych (żołądkowym oraz jelitowym) wykazały, że dodatek enzymu żołądkowego - *pepsyny* wpływa na zwiększenie uwalnianej ilości srebra z kompleksów z niespełna 1% do niespełna 30% ilości pierwotnie związanej. Z kolei w płynach syntetycznych jelitowych oznaczana ilość nie przekraczała 5% wartości początkowej. Może to być tłumaczone zjawiskiem wytrącania się srebra po uwolnieniu się z struktury kompleksu w wyniku strącania się do trudno rozpuszczalnego w wodzie tlenku srebra (I) w warunkach zasadowych (pH 7.4), cząstek srebra, które były zatrzymywane podczas filtrowania roztworów na etapie przygotowania próbek.

Badania nad cytotoksycznością podobnie jak ciągłością membran oraz zawartości wewnątrzkomórkowych reaktywnych form tlenu, dla kompleksów w odniesieniu do kontroli w postaci soli azotanu srebra wykazały podobny i znaczący wpływ na żywotność komórek L929 w stężeniach wyższych niż 0.88 μM, przy czym linia Caco-2 okazała się wykazywać wyższą żywotność komórek. Apoptoza komórek L929 była rejestrowana dla komórek po traktowaniu kompleksami o stężeniu wyższym niż 0,05 mM. Badania nad przyswajalnością srebra przez komórki wskazywały na podwojenie akumulowanej ilości srebra przez komórki z postaci kompleksów w porównaniu do kontroli w stężeniu niższym niż 0.05 mM. Biodostępność dla stężeń wyjściowych wyższych niż 0.5 mM była już porównywalne dla komórek. Podsumowując, preparat mógł być stosowany przy niższej efektywnie dawce w celu zamierzonego efektu działania terapeutycznego.

Artykuł [P5] przedstawia charakterystykę procesu oraz produktu syntezy alfa-laktoalbuminy z jonami srebra. Postuluje się:

- Proces wiązania srebra przez białko wykazuje ustalenie się równowagi w ilości wiązanego srebra przez białko po upływie 2 minutach procesu; pojemość sorpcyjna wynosi 11,2 mg/g.
- Grupa karboksylowa (pochodząca od kwasów asparaginowego oraz glutaminowego) są odpowiedzialne za ponad 90 % wartości odziaływania prowadzącego do łączenia się alfa-laktoalbuminy z srebrem, znaczący udział mają tyrozyna oraz lizyna.
- Stosowanie produktu mogłoby się wiązać z uwalnianiem jonów srebra w środowisku syntetycznego płynu żołądkowego.
- Biologiczna aktywność kompleksów wykazuje interesujące własności polegające na poprawionej aktywności biologicznej (względem przeprowadzonych badań) dla stężeń niższych 0,05 mM względem kontroli.

Podsumowanie

Charakteryzowanie grupy związków: pektyn, beta-laktoglobuliny oraz alfa-laktoalbuminy pozwoliła na wykazanie kilku zjawisk, w których współuczestniczyły jony miedzi, kadmu, cynku oraz srebra. Do charakteryzowania przebiegu i skutków procesów zastosowano kilka technik analitycznych bazujących na procesach jednostkowych takich jak rozproszenie światła, dyfuzja, ruchy Browna, szybkość elektromigracji jak również innych typów odziaływania promieniowania elektromagnetycznego z próbką (układem koloidalnym), technik spektrometrii mas, narzędzi bioinformatycznych oraz obliczeń kwantowo mechanicznych. Zastosowanie szerokiego wachlarza podejść analitycznych pozwoliło na ukazanie procesów zachodzących na powierzchni cząstek koloidalnych, jak również w skali wewnątrz- oraz zewnątrz- cząsteczkowych odziaływań.

Najważniejsze osiągniecia pracy można przedstawić następująco:

- ✓ Opracowano i zaproponowano nowe metody analityczne AF4 wraz z detekcją UV, MALS i ICP/MS służące do charakteryzowania odziaływań pomiędzy pektynami oraz kationami miedzi oraz kadmu jak również do badań nad beta-laktoglobuliną
- ✓ Oznaczono formy występowania beta-laktoglobuliny przy pH 3.0, 5.0, oraz 7.0, wykazano, że pH środowiska wywiera kluczowy wpływ na przyjmowane formy oraz wykazano, że wyższe stężenie białka przy pH 5.0 prowadzi do dominującej formy oktamerycznej
- ✓ Można wyróżnić dwie konsekwencje odziaływania kationów kadmu oraz miedzi na pektyny; pierwszy to zachodzące sieciowanie struktury pektyn prowadzące do żelu oraz drugi to zmniejszenie elektrostatycznego wewnątrzcząsteczkowego odpychania się populacji cząstek w warunkach badania
- ✓ Wyizolowano beta-laktoglobulinę w formie elektroforetycznie czystej z mieszaniny białek oraz dokonano identyfikacji oraz charakteryzacji białka; wskazano, na obecność dwóch izoform białka

- ✓ Wykazano, że skład jakościowy roztworu wpływa na stabilność koloidalną beta-laktoglobuliny poprzez zmiany przebiegu krzywej zależności potencjału zeta od pH jak również punktu izoelektrycznego
- ✓ Opracowano nowe protokoły syntezy kompleksów alfa-laktoalbuminy z kationami cynku oraz srebra
- ✓ Wyznaczono kinetykę reakcji syntezy kompleksów z uwzględnieniem modelowania według modeli kinetycznych oraz wyznaczono parametry sorpcji takie jak pojemność sorpcji, wyliczono entalpie swobodną reakcji
- ✓ Określono aktywne grupy funkcyjne alfa-laktoalbuminy mające szczególny wpływ na wiązanie kationów srebra oraz cynku
- ✓ Wykazano kilka właściwości biologicznych, które można określić jako obiecujące w kontekście potencjalnych zastosowań aplikacyjnych

Nowością osiągniętą w pracy [P2] było opracowanie metody analitycznej bazującej na AF4-MALS i połączeniu *on-line* z ICP/MS w kontekście charakteryzowania pektyn oraz kinetyki procesu żelowania. Również badane jony sieciujące: miedzi i kadmu nie były wcześniej dogłębnie charakteryzowane pod tym kątem. Przedstawione wnioski mogą stanowić podstawę do rozpoczęcia badań nad zastosowaniem zaproponowanego sprzężenia technik w kontekście badań nad kinetyką wiązania przeprowadzoną na szerszej grupie przykładów. Zauważony efekt zwiększenia rozmiarów cząstek może być wzięty pod uwagę np. w optymalizowaniu aspektów technologicznych (np. doborze wielkości filtrów itp.) podczas przeprowadzania procesów sorpcji (np. oczyszczania cieczy z pozostałości jonów metali ciężkich).

Innowacją w pracy [P3] było zastosowanie techniki AF4-MALS do charakteryzowania procesu oligomeryzacji. W tym celu opracowano trzy metody analityczne dla warunków pH 3, 5 oraz 7. Poznawanie procesu oligomeryzacji oraz warunków, w których przebiega proces, jest kluczowe w kontekście poznawania właściwości funkcji biologicznych białka, dyfuzji jak również transportu substancji biologicznie aktywnych.

Prace [P4-P5] poszerzają dotychczasowy stan wiedzy o dogłębnie przeprowadzoną fizykochemiczną charakterystykę produktu oraz procesu syntezy w oparciu o chemizm: mechanizm oraz badania kinetyczne. Na podstawie prac (opracowanych metodyk syntezy oraz dokonanych badań aplikacyjnych) widoczne są dalsze kierunki badań szczególnie prowadzonych nad aplikacjami, w tym w systemach *in vivo.*

Bibliografia:

[1] J. Wu, D. Bratko, J.M. Prausnitz, Interaction Between Like-Charged Colloidal Spheres In Electrolyte Solutions, Proceedings Of The National Academy Of Sciences. 95 (1998) 15169–15172. Https://Doi.Org/10.1073/Pnas.95.26.15169.

[2] V. Gold, Ed., The Iupac Compendium Of Chemical Terminology, International Union Of Pure And Applied Chemistry (Iupac), Research Triangle Park, Nc, 2019. Https://Doi.Org/10.1351/Goldbook.

[3] J. Loeb, Hydrophilic And Hydrophobic Colloids And The Influence Of Electrolytes On Membrane Potentials And Cataphoretic Potentials, Journal Of General Physiology. 6 (1924) 307–328. Https://Doi.Org/10.1085/Jgp.6.3.307.

[4] A. Torres-Carbajal, S. Herrera-Velarde, R. Castañeda-Priego, Brownian Motion Of A Nano-Colloidal Particle: The Role Of The Solvent, Physical Chemistry Chemical Physics. 17 (2015) 19557–19568. Https://Doi.Org/10.1039/C5cp02777b.

[5] A. Einstein, Zur Theorie Der Brownschen Bewegung, Ann Phys. 324 (1906) 371–381. Https://Doi.Org/10.1002/Andp.19063240208.

[6] M. (1872-1917) Smoluchowski, Zur Kinetischen Theorie Der Brownschen Molekularbewegung Und Der Suspensionen, Ann Phys. Bd (1906) 756–780. Http://Jbc.Bj.Uj.Edu.Pl/Dlibra/Publication/Edition/386520.

[7] P.G. Saffman, M. Delbrück, Brownian Motion In Biological Membranes., Proceedings Of The National Academy Of Sciences. 72 (1975) 3111–3113. Https://Doi.Org/10.1073/Pnas.72.8.3111.

[8] P.A. Hassan, S. Rana, G. Verma, Making Sense Of Brownian Motion: Colloid Characterization By Dynamic Light Scattering, Langmuir. 31 (2015) 3–12. Https://Doi.Org/10.1021/La501789z.

[9] N.A. Clark, J.H. Lunacek, A Study Of Brownian Motion Using Light Scattering, Am J Phys. 37 (1969) 853–854. Https://Doi.Org/10.1119/1.1975897.

[10] G.B. Adkins, E. Sun, R. Coreas, W. Zhong, Asymmetrical Flow Field Flow Fractionation Coupled To Nanoparticle Tracking Analysis For Rapid Online Characterization Of Nanomaterials, Anal Chem. 92 (2020) 7071–7078. Https://Doi.Org/10.1021/Acs.Analchem.0c00406.

[11] J.C. Giddings, F.J.F. Yang, M.N. Myers, Flow-Field-Flow Fractionation: A Versatile New Separation Method, Science (1979). 193 (1976) 1244–1245. Https://Doi.Org/10.1126/Science.959835.

[12] T. Kowalkowski, B. Buszewski, C. Cantado, F. Dondi, Field-Flow Fractionation: Theory, Techniques, Applications And The Challenges, Crit Rev Anal Chem. 36 (2006) 129–135. Https://Doi.Org/10.1080/10408340600713702.

[13] G.M.C. Ong, A. Gallegos, J. Wu, Modeling Surface Charge Regulation Of Colloidal Particles In Aqueous Solutions, Langmuir. 36 (2020) 11918–11928. Https://Doi.Org/10.1021/Acs.Langmuir.0c02000.

[14] B. Buszewski, S. Bocian, E. Dziubakiewicz, Zeta Potential Determination As A New Way Of Stationary Phases Characterization For Liquid Chromatography, J Sep Sci. 33 (2010) 1529–1537. Https://Doi.Org/10.1002/Jssc.200900466.

[15] A. Król-Górniak, K. Rafińska, F. Monedeiro, P. Pomastowski, B. Buszewski, Comparison Study Of Cytotoxicity Of Bare And Functionalized Zinc Oxide Nanoparticles, Int J Mol Sci. 22 (2021). Https://Doi.Org/10.3390/Ijms22179529.

[16] T. Missana, A. Adell, On The Applicability Of Dlvo Theory To The Prediction Of Clay Colloids Stability, J Colloid Interface Sci. 230 (2000) 150–156. Https://Doi.Org/10.1006/Jcis.2000.7003.

[17] V. Gold, Ed., The Iupac Compendium Of Chemical Terminology, International Union Of Pure And Applied Chemistry (Iupac), Research Triangle Park, Nc, 2019. Https://Doi.Org/10.1351/Goldbook.

[18] G. Midekessa, K. Godakumara, J. Ord, J. Viil, F. Lättekivi, K. Dissanayake, S. Kopanchuk, A. Rinken, A. Andronowska, S. Bhattacharjee, T. Rinken, A. Fazeli, Zeta Potential Of Extracellular Vesicles: Toward Understanding The Attributes That Determine Colloidal Stability, Acs Omega. 5 (2020) 16701–16710. Https://Doi.Org/10.1021/Acsomega.0c01582.

[19] G.A. Schumacher, T.G.M. Van De Ven, Brownian Motion Of Charged Colloidal Particles Surrounded By Electric Double Layers, Faraday Discuss Chem Soc. 83 (1987) 75. Https://Doi.Org/10.1039/Dc9878300075.

[20] B. Buszewski, M. Szumski, E. Kłodzińska, H. Dahm, Separation Of Bacteria By Capillary Electrophoresis, J Sep Sci. 26 (2003) 1045–1049. Https://Doi.Org/10.1002/Jssc.200301442.

[21] E. Dziubakiewicz, B. Buszewski, Principles Of Electromigration Techniques, In: 2013: Pp. 5–26. Https://Doi.Org/10.1007/978-3-642-35043-6_2.

[22] J. Eisermann, L. Prager, D. Hinderberger, Solvent And Concentration Effects On Highly Defined, Colloid-Like Ionic Clusters In Solution, Physical Chemistry Chemical Physics. 20 (2018) 1421–1430. Https://Doi.Org/10.1039/C7cp06501a.

[23] M.A.K. Williams, Pectin Gelation And Its Assembly Into Functional Materials, In: Pectin: Technological And Physiological Properties, Springer International Publishing, Cham, 2020: Pp. 125–148. Https://Doi.Org/10.1007/978-3-030-53421-9_7.

[24] A. Schönichen, B.A. Webb, M.P. Jacobson, D.L. Barber, Considering Protonation As A Posttranslational Modification Regulating Protein Structure And Function, Annu Rev Biophys. 42 (2013) 289–314. Https://Doi.Org/10.1146/Annurev-Biophys-050511-102349.

[25] I.K. Ventouri, S. Loeber, G.W. Somsen, P.J. Schoenmakers, A. Astefanei, Field-Flow Fractionation For Molecular-Interaction Studies Of Labile And Complex Systems: A Critical Review, Anal Chim Acta. 1193 (2022) 339396. Https://Doi.Org/10.1016/J.Aca.2021.339396.

[26] C. Fuentes, J. Castillo, J. Vila, L. Nilsson, Application Of Asymmetric Flow Field-Flow Fractionation (Af4) And Multiangle Light Scattering (Mals) For The Evaluation Of Changes In The Product Molar Mass During Pvp-B-Pamps Synthesis, Anal Bioanal Chem. 410 (2018) 3757–3767. Https://Doi.Org/10.1007/S00216-018-1039-1.

[27] P.-O. Wahlund, N. Lorenzen, C. Rischel, Screening For Protein–Protein Interactions With Asymmetrical Flow Field-Flow Fractionation, J Pharm Sci. 110 (2021) 2336–2339. Https://Doi.Org/10.1016/J.Xphs.2021.02.026.

[28] U. Nagarajan, S. Chandra, T. Yamazaki, N. Shirahata, F.M. Winnik, Analysis Of Silicon Quantum Dots And Serum Proteins Interactions Using Asymmetrical Flow Field-Flow Fractionation, Langmuir. 39 (2023) 7557–7565. Https://Doi.Org/10.1021/Acs.Langmuir.3c00109.

[29] P.L. Ma, M.D. Buschmann, F.M. Winnik, Complete Physicochemical Characterization Of Dna/Chitosan Complexes By Multiple Detection Using Asymmetrical Flow Field-Flow Fractionation, Anal Chem. 82 (2010) 9636–9643. Https://Doi.Org/10.1021/Ac100711j.

[30] S. Motellier, N. Pélissier, J.-G. Mattei, Aging Of Silver Nanocolloids In Sunlight: Particle Size Has A Major Influence, Environmental Chemistry. 15 (2018) 450. Https://Doi.Org/10.1071/En18056.

[31] B. Moreira-Alvarez, A.L. Larraga-Urdaz, A. Fuentes-Cervantes, M.L. Fernandez-Sánchez, J.M. Costa-Fernández, J.R. Encinar, Af4-Uv/Vis-Mals-Icpms/Ms For The Characterization Of The Different Nanoparticulated Species Present In Oligonucleotide-Gold Nanoparticle Conjugates, Talanta. 256 (2023) 124309. Https://Doi.Org/10.1016/J.Talanta.2023.124309.

[32] J.H. Duffus, “Heavy Metals”-A Meaningless Term? (Iupac Technical Report), W. A. Temple, 2002.

[33] J.S. Scott, P.G. Smith, Dictionary Of Waste And Water Treatment, Butterworths, 1981. Https://Books.Google.Pl/Books?Id=3rwbtaeacaaj.

[34] E. Ha, N. Basu, S. Bose-O’reilly, J.G. Dórea, E. Mcsorley, M. Sakamoto, H.M. Chan, Current Progress On Understanding The Impact Of Mercury On Human Health, Environ Res. 152 (2017) 419–433. Https://Doi.Org/10.1016/J.Envres.2016.06.042.

[35] N. Roohani, R. Hurrell, R. Kelishadi, R. Schulin, Zinc And Its Importance For Human Health: An Integrative Review, 2013.

[36] S. Prabhu, E.K. Poulose, Silver Nanoparticles: Mechanism Of Antimicrobial Action, Synthesis, Medical Applications, And Toxicity Effects, Int Nano Lett. 2 (2012) 32. Https://Doi.Org/10.1186/2228-5326-2-32.

[37] V. Hiatt, J.E. Huff, The Environmental Impact Of Cadmium: An Overview, International Journal Of Environmental Studies. 7 (1975) 277–285. Https://Doi.Org/10.1080/00207237508709704.

[38] M. Vincent, R.E. Duval, P. Hartemann, M. Engels-Deutsch, Contact Killing And Antimicrobial Properties Of Copper, J Appl Microbiol. 124 (2018) 1032–1046. Https://Doi.Org/10.1111/Jam.13681.

[39] T. Ameh, C.M. Sayes, The Potential Exposure And Hazards Of Copper Nanoparticles: A Review, Environ Toxicol Pharmacol. 71 (2019) 103220. Https://Doi.Org/10.1016/J.Etap.2019.103220.

[40] D.M. Templeton, H. Fujishiro, Terminology Of Elemental Speciation – An Iupac Perspective, Coord Chem Rev. 352 (2017) 424–431. Https://Doi.Org/10.1016/J.Ccr.2017.02.002.

[41] R. Viorica, P. Pawel, T. Płociński, M. Gloc, R. Dobrucka, K.J. Kurzydłowski, B. Boguslaw, Consideration Of A New Approach To Clarify The Mechanism Formation Of Agnps, Agncl And Agnps@Agncl Synthesized By Biological Method, Discover Nano. 18 (2023) 2. Https://Doi.Org/10.1186/S11671-023-03777-W.

[42] L.B. Lahuta, J. Szablińska-Piernik, K. Stałanowska, M. Horbowicz, R.J. Górecki, V. Railean, P. Pomastowski, B. Buszewski, Exogenously Applied Cyclitols And Biosynthesized Silver Nanoparticles Affect The Soluble Carbohydrate Profiles Of Wheat (Triticum Aestivum L.) Seedling, Plants. 12 (2023) 1627. Https://Doi.Org/10.3390/Plants12081627.

[43] A. Rogowska, K. Rafińska, P. Pomastowski, J. Walczak, V. Railean-Plugaru, M. Buszewska-Forajta, B. Buszewski, Silver Nanoparticles Functionalized With Ampicillin, Electrophoresis. 38 (2017) 2757–2764. Https://Doi.Org/10.1002/Elps.201700093.

[44] A. Rodzik, P. Pomastowski, G.N. Sagandykova, B. Buszewski, Interactions Of Whey Proteins With Metal Ions, Int J Mol Sci. 21 (2020) 2156. Https://Doi.Org/10.3390/Ijms21062156.

[45] A. Totosaus, J.G. Montejano, J.A. Salazar, I. Guerrero, A Review Of Physical And Chemical Protein-Gel Induction, Int J Food Sci Technol. 37 (2002) 589–601. Https://Doi.Org/10.1046/J.1365-2621.2002.00623.X.

[46] G. Gotte, M. Libonati, Protein Oligomerization, In: Oligomerization Of Chemical And Biological Compounds, Intech, 2014. Https://Doi.Org/10.5772/57489.

[47] S. Nirwan, R. Kakkar, Rhinovirus Rna Polymerase, In: Viral Polymerases, Elsevier, 2019: Pp. 301–331. Https://Doi.Org/10.1016/B978-0-12-815422-9.00011-5.

[48] J. Müller-Maatsch, M. Bencivenni, A. Caligiani, T. Tedeschi, G. Bruggeman, M. Bosch, J. Petrusan, B. Van Droogenbroeck, K. Elst, S. Sforza, Pectin Content And Composition From Different Food Waste Streams, Food Chem. 201 (2016) 37–45. Https://Doi.Org/10.1016/J.Foodchem.2016.01.012.

[49] J. Du, C.T. Anderson, C. Xiao, Dynamics Of Pectic Homogalacturonan In Cellular Morphogenesis And Adhesion, Wall Integrity Sensing And Plant Development, Nat Plants. 8 (2022) 332–340. Https://Doi.Org/10.1038/S41477-022-01120-2.

[50] S.E. Guillotin, E.J. Bakx, P. Boulenguer, H.A. Schols, A.G.J. Voragen, Determination Of The Degree Of Substitution, Degree Of Amidation And Degree Of Blockiness Of Commercial Pectins By Using Capillary Electrophoresis, Food Hydrocoll. 21 (2007) 444–451. Https://Doi.Org/10.1016/J.Foodhyd.2006.05.003.

[51] C. Lara-Espinoza, E. Carvajal-Millán, R. Balandrán-Quintana, Y. López-Franco, A. Rascón-Chu, Pectin And Pectin-Based Composite Materials: Beyond Food Texture, Molecules. 23 (2018) 942. Https://Doi.Org/10.3390/Molecules23040942.

[52] G. Morris, The Effect Of The Degree Of Esterification On The Hydrodynamic Properties Of Citrus Pectin, Food Hydrocoll. 14 (2000) 227–235. Https://Doi.Org/10.1016/S0268-005x(00)00007-2.

[53] L. Cao, W. Lu, A. Mata, K. Nishinari, Y. Fang, Egg-Box Model-Based Gelation Of Alginate And Pectin: A Review, Carbohydr Polym. 242 (2020) 116389. Https://Doi.Org/10.1016/J.Carbpol.2020.116389.

[54] B.L.H.M. Sperber, H.A. Schols, M.A. Cohen Stuart, W. Norde, A.G.J. Voragen, Influence Of The Overall Charge And Local Charge Density Of Pectin On The Complex Formation Between Pectin And B-Lactoglobulin, Food Hydrocoll. 23 (2009) 765–772. Https://Doi.Org/10.1016/J.Foodhyd.2008.04.008.

[55] H.S. Owens, H.A. Swenson, T.H. Schultz, Factors Influencing Gelation With Pectin, In: 1954: Pp. 10–15. Https://Doi.Org/10.1021/Ba-1954-0011.Ch003.

[56] M. Celus, C. Kyomugasho, Z.J. Kermani, K. Roggen, A.M. Van Loey, T. Grauwet, M.E. Hendrickx, Fe 2+ Adsorption On Citrus Pectin Is Influenced By The Degree And Pattern Of Methylesterification, Food Hydrocoll. 73 (2017) 101–109. Https://Doi.Org/10.1016/J.Foodhyd.2017.06.021.

[57] B.A. Mckenna, T.M. Nicholson, J.B. Wehr, N.W. Menzies, Effects Of Ca, Cu, Al And La On Pectin Gel Strength: Implications For Plant Cell Walls, Carbohydr Res. 345 (2010) 1174–1179. Https://Doi.Org/10.1016/J.Carres.2010.03.044.

[58] V. Dronnet, Characterisation And Selectivity Of Divalent Metal Ions Binding By Citrus And Sugar-Beet Pectins, Carbohydr Polym. 30 (1996) 253–263. Https://Doi.Org/10.1016/S0144-8617(96)00107-5.

[59] M. Corredig, Molecular Characterization Of Commercial Pectins By Separation With Linear Mix Gel Permeation Columns In-Line With Multi-Angle Light Scattering Detection, Food Hydrocoll. 14 (2000) 41–47. Https://Doi.Org/10.1016/S0268-005x(99)00044-2.

[60] O. Yuliarti, L. Matia-Merino, K.K.T. Goh, J. Mawson, M.A.K. Williams, C. Brennan, Characterization Of Gold Kiwifruit Pectin From Fruit Of Different Maturities And Extraction Methods, Food Chem. 166 (2015) 479–485. Https://Doi.Org/10.1016/J.Foodchem.2014.06.055.

[61] C. Wang, W.-Y. Qiu, T.-T. Chen, J.-K. Yan, Effects Of Structural And Conformational Characteristics Of Citrus Pectin On Its Functional Properties, Food Chem. 339 (2021) 128064. Https://Doi.Org/10.1016/J.Foodchem.2020.128064.

[62] R. Kohn, P. Kovac, Dissociation Constants Of D-Galacturonic And D-Glucuronic Acid And Their O-Methyl Derivatives, Chem. Zvesti. 32 (1978) 478–485.

[63] M. Gottschalk, H. Nilsson, H. Roos, B. Halle, Protein Self-Association In Solution: The Bovine B -Lactoglobulin Dimer And Octamer, Protein Science. 12 (2009) 2404–2411. Https://Doi.Org/10.1110/Ps.0305903.

[64] D. Mercadante, L.D. Melton, G.E. Norris, T.S. Loo, M.A.K. Williams, R.C.J. Dobson, G.B. Jameson, Bovine B-Lactoglobulin Is Dimeric Under Imitative Physiological Conditions: Dissociation Equilibrium And Rate Constants Over The Ph Range Of 2.5-7.5, Biophys J. 103 (2012) 303–312. Https://Doi.Org/10.1016/J.Bpj.2012.05.041.

[65] E.A. Permyakov, A-Lactalbumin, Amazing Calcium-Binding Protein, Biomolecules. 10 (2020) 1–50. Https://Doi.Org/10.3390/Biom10091210.

[66] J. Ren, D.I. Stuart, K.R. Acharya, A-Lactalbumin Possesses A Distinct Zinc Binding Site, Journal Of Biological Chemistry. 268 (1993) 19292–19298. Https://Doi.Org/10.1016/S0021-9258(19)36512-3.

[67] C. Barbana, M.D. Perez, C. Pocovi, L. Sanchez, Z. Wehbi, Interaction Of Human A-Lactalbumin With Fatty Acids: Determination Of Binding Parameters, Biochemistry (Moscow). 73 (2008) 711–716. Https://Doi.Org/10.1134/S0006297908060126.

[68] T. Kamijima, A. Ohmura, T. Sato, K. Akimoto, M. Itabashi, M. Mizuguchi, M. Kamiya, T. Kikukawa, T. Aizawa, M. Takahashi, K. Kawano, M. Demura, Heat-Treatment Method For Producing Fatty Acid-Bound Alpha-Lactalbumin That Induces Tumor Cell Death, Biochem Biophys Res Commun. 376 (2008) 211–214. Https://Doi.Org/10.1016/J.Bbrc.2008.08.127.

[69] S. Aits, L. Gustafsson, O. Hallgren, P. Brest, M. Gustafsson, M. Trulsson, A.-K. Mossberg, H.-U. Simon, B. Mograbi, C. Svanborg, Hamlet (Human A-Lactalbumin Made Lethal To Tumor Cells) Triggers Autophagic Tumor Cell Death, Int J Cancer. 124 (2009) 1008–1019. Https://Doi.Org/10.1002/Ijc.24076.

[70] J. Pettersson, A.-K. Mossberg, C. Svanborg, A-Lactalbumin Species Variation, Hamlet Formation, And Tumor Cell Death, Biochem Biophys Res Commun. 345 (2006) 260–270. Https://Doi.Org/10.1016/J.Bbrc.2006.04.081.

[71] S.E. Permyakov, I. V. Pershikova, T.I. Khokhlova, V.N. Uversky, E.A. Permyakov, No Need To Be Hamlet Or Bamlet To Interact With Histones: Binding Of Monomeric A-Lactalbumin To Histones And Basic Poly-Amino Acids, Biochemistry. 43 (2004) 5575–5582. Https://Doi.Org/10.1021/Bi049584y.

[72] Y. Delgado, M. Morales-Cruz, C.M. Figueroa, J. Hernández-Román, G. Hernández, K. Griebenow, The Cytotoxicity Of Bamlet Complexes Is Due To Oleic Acid And

Independent Of The A-Lactalbumin Component, Febs Open Bio. 5 (2015) 397–404. Https://Doi.Org/10.1016/J.Fob.2015.04.010.

[73] O. Pryshchepa, G.N. Sagandykova, P. Pomastowski, V. Railean-Plugaru, A. Król, A. Rogowska, A. Rodzik, M. Sprynskyy, B. Buszewski, A New Approach For Spontaneous Silver Ions Immobilization Onto Casein, Int J Mol Sci. 20 (2019). Https://Doi.Org/10.3390/Ijms20163864.

Streszczenie

Dysertacja pt. *Układy koloidalne oraz ich odziaływania z wybranymi metalami ciężkimi* odnosi się do badań przeprowadzonych nad charakteryzowaniem odziaływań zachodzących pomiędzy pektynami, beta-laktoglobuliną, alfa-laktoalbuminą oraz wybranymi jonami metali: kadmu, miedzi, cynku, srebra. Badania nad pektynami oraz indukowanym poprzez kationy kadmu oraz miedzi procesem żelowania ukazały, że następują zmiany w wielkości oraz konformacji cząstek żelu oraz obecność kadmu prowadzi do zmniejszenia wewnątrzcząsteczkowego elektrostatycznego odpychania. Beta-laktoglobulina jest białkiem, który może być wyizolowane z łatwo dostępnego i taniego produktu ubocznego przemysłu mleczarskiego - izolatu białek serwatkowych w skali (pół)preparatywnej w wysokiej czystości. Tożsamość białka została potwierdzona oraz dokonano złożonej charakterystyki. Wykazano między innymi, że skład elektrolityczny roztworu ma wpływ na stabilność koloidalną białka. Białko wykazuje tendencje do spontanicznego występowania w formach oligomerycznych, których równowaga zależy od pH środowiska oraz przy pH blisko punktu izoelektrycznego również od stężenia białka w roztworze. Alfa-laktoalbumina w badaniach została scharakteryzowana fizykochemicznie. Wyznaczono punkt izoelektryczny oraz masy molowe izoform białka. Białko stanowiło bazę do syntetyzowanych kompleksów z jonami cynku oraz srebra. Wykazano, że charakter wiązania obu jonów metali jest odmienny. Syntetyzowane produkty wykazywały kilka potencjalnie atrakcyjnych właściwości biologicznych pod kątem potencjalnych zastosowań w układach *in vivo.*

Abstract

PhD thesis entitled *Colloidal systems and their interactions with selected heavy metals* refer to research conducted on the characterization of interactions taking place between pectin, beta-lactoglobulin, alpha-lactalbumin and selected metal ions (cadmium, copper, zinc, silver). Studies on pectin and the gelation process induced by cadmium and copper cations have shown that there are changes in the size and conformation of gel particles and the presence of cadmium leads to a decrease in intramolecular electrostatic repulsion. Beta-lactoglobulin is a protein that can be isolated from an easily available and cheap by-product of the dairy industry - whey protein isolate on a (semi)preparative scale in high purity. The identity of the protein was confirmed and complex characterization was performed. Among other things, it was shown that the electrolytic composition of the solution affects the colloidal stability of the protein. The protein tends to spontaneously occur in oligomeric forms, the equilibrium of which depends on the pH of the environment and, at pH close to the isoelectric point, also on the protein concentration in the solution. Alpha-lactalbumin in the research was characterized physiochemically. The isoelectric point and molar mass of protein isoforms were determined. The protein was the basis for the synthesized complexes with zinc and silver ions. It was shown that the nature of the bonding of both metal ions is different. The synthesized products showed several potentially attractive biological properties for potential applications in *in vivo* systems.

Słowa kluczowe:

Koloidy; oddziaływania; techniki analityczne; metale; stabilność koloidalna; spektrometria mas; techniki separacyjne

Keywords:

Colloids; interactions, analytical techniques, metals, colloidal stability, mass spectrometry; separation techniques

Dorobek naukowy

Aktywność naukowa

Stacjonarne studia doktoranckie na kierunku chemia rozpocząłem w październiku 2018 roku. Jednostką prowadzącą program studiów był Wydział Chemii Uniwersytetu Mikołaja Kopernika w Toruniu. Badania były wykonane w Katedrze Chemii Środowiska i Bioanalityki jak również w Interdyscyplinarnym Centrum Nowoczesnych Technologii UMK w Toruniu pod nadzorem promotora pracy *prof. zw. dr hab*. Bogusława Buszewskiego, *czł. rzecz. PAN i EASA*.

Do tego momentu, jestem współautorem w 18 publikacjach oraz prezentowałem wyniki badań na 8 konferencjach naukowych (komunikaty ustne oraz postery). W ciągu odbywania studiów doktoranckich byłem wykonawcą w dwóch grantach NCN (OPUS 14 oraz Sonata 11) oraz w nadal trwającym projekcie naukowym OPUS 18 „*Nowe strategie otrzymywania związków bioaktywnych na bazie krzemu*". Uzyskałem wsparcie finansowe na przeprowadzenie badań naukowych z puli środków Wydziału Chemii UMK Granty Młodych Naukowców w trzech edycjach.

Odbyłem krótkoterminowe staże/ wizyty naukowe na Wydziale Chemii UAM w Poznaniu oraz profesor Joanny Szpunar w jednostce IPREM (Institute of Analytical Sciences and Physico-Chemistry for Environment and Materials) będącej częścią Uniwersytetu UPPA (Université de Pau et des Pays de l'Adour) w Pau we Francji. Podczas tych dwóch wizyt zdobywałem wiedzę oraz umiejętności w specjalności spektrometrii mas z indukcyjnie sprzężoną plazmą pod kątem oznaczania pierwiastków oraz specjacji. Dodatkowo byłem uczestnikiem dwóch szkoleń z zakresu stosowania techniki asymetrycznego frakcjonowania w polu sił przepływu oraz wielokątowego rozproszenia światła w celu separowania oraz charakteryzowania makrocząsteczek.

Uzyskałem wsparcie finansowe na wyjazd na zagraniczną konferencje naukową w konkursie PROM NAWA. Byłem również nagrodzony zespołową nagroda Rektora Uniwersytetu Mikołaja Kopernika w Toruniu - III stopnia, za osiągnięcia uzyskane w dziedzinie naukowej w 2021 roku.

Zdecydowana większość prac badawczych dotyczyła tematyki charakteryzacji koloidów oraz oznaczania pierwiastków. Kolejną tematyką było przeprowadzanie syntez, charakterystyki oraz wykonywania badań nad potencjalnymi aplikacjami nowych kompleksów na bazie jonów metali oraz białka. Koloidami, które wybrałem do badań, były polisacharydy: pektyny oraz chitozan oraz białka: beta-latoglobulina, alfa-laktoalbumina, laktoferyna oraz frakcji (αS_1, β, κ) kazein. Pierwiastkami, które oznaczałem najczęściej, były kadm, miedz, cynk, srebro oraz krzem w różnych postaciach oraz formach. Technikami, które szczególnie często wykorzystywałem w swoich badaniach, były spektrometria mas z indukcyjnie sprzężoną plazmą oraz laserowa jonizacja/desorpcja wspomagana matrycą oraz technika asymetrycznego frakcjonowania w polu sił przepływu z detekcją wielokątowego rozproszenia światła.

Publikacje:

1. **Golebiowski, Adrian** & Kowalkowski, Tomasz & Buszewski, Bogusław. (2020). Molecular parameters of low methoxylated pectin affected by gelation with copper and cadmium cations. *Bioactive Carbohydrates and Dietary Fibre*. 21. 100211. 10.1016/j.bcdf.2020.100211. CiteScore=5.3 PM=70

2. **Golebiowski, Adrian** & Pomastowski, Paweł & Rodzik, Agnieszka & Król-Górniak, Anna & Kowalkowski, Tomasz & Górecki, Marcin & Buszewski, Bogusław. (2020). Isolation and Self-Association Studies of Beta-Lactoglobulin. *International Journal of Molecular Sciences*. 21. 10.3390/ijms21249711. IF: 6.628 PM=140

3. Rogowska, Agnieszka & Railean, Viorica & Pomastowski, Paweł & Walczak-Skierska, Justyna & Król-Górniak, Anna & **Golebiowski, Adrian** & Buszewski, Bogusław. (2021). The Study on Molecular Profile Changes of Pathogens via Zinc Nanocomposites Immobilization Approach. *International Journal of Molecular Medical Science*. 22. 5395. 10.3390/ijms22105395. IF: 6.628 PM=140

4. Słota, Emilia & Vasylechko, Volodymyr & Patsay, Ihor & **Golebiowski, Adrian** & Sprynskyy, Myroslav & Buszewski, Bogusław & Poddubnaya, Olga & Puziy, Alexander. (2022). The use of H-form clinoptilolite to preconcentrate trace amounts of Nd(III) from aqueous solution under dynamic conditions. *Microporous and Mesoporous Materials*. 333. 111739. 10.1016/j.micromeso.2022.111739. IF 5.876 PM=100

5. Buszewska-Forajta, Magdalena & Monedeiro, Fernanda & **Golebiowski, Adrian** & Adamczyk, Przemysław & Buszewski, Bogusław. (2022). Citric Acid as a Potential Prostate Cancer Biomarker Determined in Various Biological Samples. *Metabolites*. 12. 10.3390/metabo12030268. IF 5.531 PM=100

6. Lupa, Dawid & Plazinski, Wojciech & Michna, Aneta & Wasilewska, Monika & Pomastowski, Paweł & **Golebiowski, Adrian** & Buszewski, Bogusław & Adamczyk, Zbigniew. (2022). Chitosan characteristics in electrolyte solutions: Combined molecular dynamics modeling and slender body hydrodynamics. *Carbohydrate Polymers*. 292. 119676. 10.1016/j.carbpol.2022.119676. IF 10.723 PM=140

7. Pryshchepa, Oleksandra & Pomastowski, Paweł & Rafińska, Katarzyna & **Golebiowski, Adrian** & Rogowska, Agnieszka & Monedeiro-Milanowski, Maciej & Sagandykova, Gulyaim & Michalke, Bernhard & Schmitt-Kopplin, Ph & Gloc, Michał & Dobrucka, Renata & Kurzydłowski, Krzysztof & Buszewski, Bogusław. (2022). Synthesis, Physicochemical Characterization, and Antibacterial Performance of Silver–Lactoferrin Complexes. *International Journal of Molecular Sciences*. 23. 7112. 10.3390/ijms23137112. IF: 6.628 PM=140

8. Orzoł, Aleksandra & **Golebiowski, Adrian** & Szultka-Mlynska, Malgorzata & Glowacka, Katarzyna & Pomastowski, Paweł & Buszewski, Bogusław. (2022). ICP-MS Analysis of Cadmium Bioaccumulation and Its Effect on Pea Plants (Pisum sativum L.). *Polish Journal of Environmental Studies*. 31. 10.15244/pjoes/149259. CiteScore=2.8 PM=40

9. Pryshchepa, Oleksandra & Rafińska, Katarzyna & **Golebiowski, Adrian** & Sugajski, Mateusz & Sagandykova, Gulyaim & Madajski, Piotr & Buszewski, Bogusław & Pomastowski, Paweł. (2022). Synthesis and physicochemical characterization of bovine lactoferrin supersaturated complex with iron (III) ions. *Scientific Reports*. 12. 12695. 10.1038/s41598-022-15814-2. IF: 5.516 PM=140

10. **Golebiowski, Adrian** & Pomastowski, Paweł & Rafińska, Katarzyna & Žuvela, Petar & Wong, M.W. & Madajski, P. & Buszewski, Bogusław. (2022). Binding of silver ions to alpha-lactalbumin. *Journal of Molecular Structure*. 1270. 133940. 10.1016/j.molstruc.2022.133940. IF: 3.841 PM=70

11. Rodzik, Agnieszka & Król-Górniak, Anna & Railean, Viorica & Sugajski, Mateusz & **Golebiowski, Adrian** & Horne, David & Michalke, Bernhard & Sprynskyy, Myroslav & Pomastowski, Paweł & Buszewski, Bogusław. (2022). Study on zinc ions binding to the individual casein fractions: αS1-, β- and κ-casein. *Journal of Molecular Structure*. 1272. 134251. 10.1016/j.molstruc.2022.134251. IF: 3.841 PM=70

12. **Golebiowski, Adrian** & Pomastowski, Paweł & Rafińska, Katarzyna & Žuvela, Petar & Wong, Ming & Pryshchepa, Oleksandra & Madajski, Piotr & Buszewski, Bogusław. (2022). Functionalization of Alpha-Lactalbumin by Zinc Ions. *ACS Omega*. 7, 43, 10.1021/acsomega.2c03674. IF: 4.132 PM=70

13. Railean, Viorica & Buszewska- Forajta, Magdalena & Rodzik, Agnieszka & **Golebiowski, Adrian** & Pomastowski, Paweł & Buszewski, Bogusław. (2022). In Vivo Efficacy of Wound Healing under External (Bio)AgNCs Treatment: Localization Case Study in Liver and Blood Tissue. International Journal of Molecular Sciences. 24. 434. 10.3390/ijms24010434. IF: 6.628 PM=140

14. Rogowska, Agnieszka & Pryshchepa, Oleksandra & Som, Narayan & Spiewak, Piotr & **Golebiowski, Adrian** & Rafińska, Katarzyna & Dobrucka, Renata & Kurzydłowski,

Krzysztof & Buszewski, Bogusław & Pomastowski, Paweł. (2023). Study On The Zinc Ions Binding To Human Lactoferrin. *Journal of Molecular Structure*. 1282. 135149. 10.1016/j.molstruc.2023.135149. IF: 6.628 PM=140

15. Dyrda-Terniuk, Tetiana & Pryshchepa, Oleksandra & Rafińska, Katarzyna & Kolankowski, Mateusz & **Golebiowski, Adrian** & Gloc, Michał & Dobrucka, Renata & Kurzydłowski, Krzysztof & Pomastowski, Paweł. (2023). Immobilization Of Silver Ions Onto Casein. *Colloids and Surfaces A: Physicochemical and Engineering Aspects*. 667, 131390, 10.1016/j.colsurfa.2023.131390. IF: 5.518 PM=70

16. Rogowska, Agnieszka & Szultka-Mlynska, Malgorzata & Kanawati, Basem & Pomastowski, Paweł & Arendowski, Adrian & **Golebiowski, Adrian** & Schmitt-Kopplin, Phillipe & Fordymacka, Marta & Sukiennik, Jarosław & Krzywik, Julia & Buszewski, Bogusław. (2023). Advanced Mass Spectrometric Techniques for the Comprehensive Study of Synthesized Silicon-Based Silyl Organic Compounds: Identifying Fragmentation Pathways and Characterization. *Materials*. 16. 3563. 10.3390/ma16093563. IF: 4.042 PM=140

17. **Golebiowski, Adrian** & Buszewski, Bogusław. (2023). Characterization of colloidal particles of a biological and metallic nature, *Microchemical Journal*, 108864, https://doi.org/10.1016/j.microc.2023.108864. IF: 5.304 PM=70

18. Orzoł, Aleksandra & Cruzado-Tafur, Edith & **Golebiowski, Adrian** & Rogowska, Agnieszka & Pomastowski, Paweł & Górecki, Ryszard & Buszewski, Bogusław & Szultka-Mlynska, Malgorzata & Glowacka, Katarzyna. (2023). Comprehensive Study of Si-Based Compounds in Selected Plants (Pisum sativum L., Medicago sativa L., Triticum aestivum L.). *Molecules*. 28. 4311. 10.3390/molecules28114311. IF: 5.110 PM=140

Konferencje

1.**Adrian Gołębiowski**, Tomasz Kowalkowski, Bogusław Buszewski, Analiza pektyn techniką asymetrycznego frakcjonowania w polu sił przepływu z detekcją wielokątowego rozproszenia światła (A4F-MALS), XII Międzynarodowa Konferencja Naukowa „Chromatografia Jonowa i Techniki Pokrewne 2018", Zabrze 17-18 kwiecień 2018 [komunikat]

2. **Adrian Gołębiowski**, Tomasz Kowalkowski, Changing the radius of gyration of low methoxylated pectin during gelation process with copper and cadmium cations, 6 Naukowa Konferencja Naukowa Monitoring i Analiza Wody, 10 12 Marca 2019 Przysiek [poster]

3. **Golebiowski, Adrian**, Pomastowski, Paweł, Rodzik, Agnieszka, Król-Górniak, Anna, Kowalkowski, Tomasz, Górecki, Marcin, Buszewski, Bogusław, Isolation and multi aspects characteristic of beta - lactoglobulin from whey protein isolate, QUO VADIS Life Sciences 23-27 Czerwiec 2021 Opole [komunikat]

4. **Adrian Gołębiowski**, Tomasz Kowalkowski, Agnieszka Rodzik, Pawel Pomastowski, Boguslaw Buszewski, Characterization of β-lactoglobulin from whey protein isolate, 35th

Conference of the European Colloid and Interface Society (ECIS), Ateny wrzesień, 05-10 2021 [poster]

5. **Adrian Gołębiowski**, Aleksandra Orzoł, Małgorzata Szultka-Młyńska, Katarzyna Głowacka, Sylwia Milarska, Paweł Pomastowski, Agnieszka Rogowska, Bogusław Buszewski, Opracowanie procedury analitycznej oznaczania krzemu i kadmu w materiale roślinnym, „Fizykochemia granic faz – metody instrumentalne", Lublin, 22 – 26 sierpnia 2021 [poster]

6. Aleksandra Orzoł, Małgorzata Szultka-Młyńska, Katarzyna Głowacka,Sylwia Milarska, Paweł Pomastowski, Agnieszka Rogowska, **Adrian Gołębiowski**, Bogusław Buszewski, Effect of cadmium toxicity and silicon supplementation on hydroponically pea plants, Quo Vadis Life Sciences Conference, Opole, czerwiec 23-27 2021[poster]

7. **Adrian Gołębiowski**, Aleksandra Orzoł, Małgorzata Szultka-Młyńska, Katarzyna Głowacka, Mateusz Cichorek, Paweł Pomastowski, Edith CruzadoTafur, Bogusław Buszewski, Detection cadmium speciation in pea plants after Cd-stress and Si-treatment, ISSS Ljubljana 28 czerwiec 2022 [komunikat]

8. **Adrian Gołębiowski**, Aleksandra Orzoł, Małgorzata Szultka-Młyńska, Katarzyna Głowacka, Mateusz Cichorek, Paweł Pomastowski, Edith CruzadoTafur, Bogusław Buszewski, Dobór parametrów analizy specjacyjnej kadmu w próbkach grochu zwyczajnego (Pisum sativum L.), POKOCHA 2022 Łódź 19-23 czerwca 2022 [komunikat]

Granty

1. Doktorant stypendysta; Grant Opus 18 finansowany przez Narodowe Centrum Nauki, nr 2019/35/B/ST4/02791, pt. Nowe strategie otrzymywania związków bioaktywnych na bazie krzemu, kierownik: dr hab. Małgorzata Szultka-Młyńska, prof. UMK (01.2021 – obecnie)

2. Wykonawca; Grant Opus 14 finansowany przez Narodowe Centrum Nauki, nr 2017/27/B/ST4/02628, pt. Synteza kompleksowych związków srebra i cynku na bazie kazein i białek serwatki oraz nanocząstek srebra i tlenku cynku przez probiotyczne bakterie kwasu mlekowego, kierownik: dr hab. Paweł Pomastowski, prof. UMK (01.2020 – 12.2020)

3. Wykonawca; Grant Sonata 11 finansowany przez Narodowe Centrum Nauki, nr 2016/21/D/ST4/03730, pt. Wpływ hormonów, wkaźników biochemicznych i epidemiologicznych oraz zmian w profilach lipidomicznych na proces powstawania nowotworu prostaty, kierownik: dr Magdalena Buszewska- Forajta (11.2020 – 12.2020)

4. Kierownik; Grant Młodych Naukowców, nr 492/2020, pt. „Wpływ pH, siły jonowej i stosunku masowego biopolimerów na syntezę kompleksów beta-laktoglobuliny z pektynami"

5. Kierownik; Grant Młodych Naukowców, nr 2092/2019, pt. „Izolacja beta-laktoglobuliny z izolatu białek serwatkowych w skali preparatywnej"

6. Kierownik; Grant Młodych Naukowców, nr 2092/2019, pt. „Fizykochemiczna i termo-grawimetryczna charakterystyka pektyn wysokometylowych”

Staże

1. Staż w IPREM (Institute of Analytical Sciences and Physico-Chemistry for Environment and Materials) będącej częścią Uniwersytetu UPPA (Université de Pau et des Pays de l'Adour) w Pau we Francji 15 dniowy od 4 lipca 2022

2. Tygodniowy staż na Wydziale Chemii UAM w Poznaniu, styczeń 2020

Nagrody i osiągnięcia

1. Zespołowa nagroda Rektora Uniwersytetu Mikołaja Kopernika w Toruniu - III stopnia, za osiągnięcia uzyskane w dziedzinie naukowej w 2021 roku

2. Uzyskanie dofinansowania na zagraniczną konferencje naukową w ramach projektu PROM NAWA - Międzynarodowa wymiana stypendialna doktorantów i kadry akademickiej na UMK

Szkolenia

1. Seminarium Protein Formulation and Characterization oraz Characterization of Molecular Structure of Synthetic and Natural Polymers by Separation Techniques with Advanced Detectors, 23 maja 2018 w Warszawie

2. Dwudniowe seminarium “Next generation strategies and insights on large molecule characterization”, 28,29 maja 2019 w Zabrzu

UNIWERSYTET MIKOŁAJA KOPERNIKA W TORUNIU
Wydział Chemii

Pełne wersje publikacji

[P1]

Golebiowski, Adrian & Buszewski, Bogusław

Characterization of colloidal particles of a biological and metallic nature

Microchemical Journal,
https://doi.org/10.1016/j.microc.2023.108864.

Microchemical Journal 191 (2023) 108864

Contents lists available at ScienceDirect

Microchemical Journal

journal homepage: www.elsevier.com/locate/microc

Review Article

Characterization of colloidal particles of a biological and metallic nature

Adrian Gołębiowski [a,b], Bogusław Buszewski [a,c,*]

[a] Department of Environmental Chemistry and Bioanalytics, Faculty of Chemistry, Nicolaus Copernicus University, Gagarin 7, 87-100 Torun, Poland
[b] Centre for Modern Interdisciplinary Technologies, Nicolaus Copernicus University, Wileńska 4, 87-100 Torun, Poland
[c] Prof. Jan Czochralski Kuyavian-Pomeranian Science and Technology Center in Przysiek near Torun, Parkowa 1, 87-134 Przysiek, Poland

ARTICLE INFO

Keywords:
Colloid
Analytical technique
Size
Zeta–potential
Metal nanoparticles

ABSTRACT

The work concerns the application of selected analytical techniques to characterize colloidal species of biological and metallic nature. Techniques used to determine particle size distributions, molar mass and zeta-potential, chemical speciation, and interacting elements with colloids were discussed. Some analytical techniques used are the basic research tools, the research results are then used to develop and postulate new mechanisms of interactions between colloidal particles and elements. The complementarity and scope of the techniques used and their limitations, were conferred. Also, possible solutions to the encountered limitations in using techniques have been presented. These physicochemical properties of colloids are crucial in describing and understanding colloid stabilization phenomena and their interactions with other compounds. Thematic scope applies to colloids with biological and metallic origin, which are widespread and utilized in numerous industries. The application of analytical techniques is the elementary source of information about the physicochemical properties of the colloidal system and it is the beginning of the process of developing new materials as well as controlling the quality of already existing colloid-based material and properties of the existing ones and monitoring the interaction of colloids with the environment in living organisms.

1. Introduction

The colloidal system consists of dispersed and dispersant phases. According to the IUPAC definition, the dispersed phase creates particles of size between 1 nm and 1000 nm (as a value of one of the three dimensions). Compounds forming the dispersed phase can form compounds of inorganic or organic origin, whereby the term biocolloid can be distinguished, defined by a colloidal entity derived from organic matter [1]. The dispersant phase is composed of substances in gas, liquid or solid state of mater.

Colloidal particles are created by the association and aggregation of small chemical molecules precursors into larger in size complexes or degradation bulk materials into particles. Examples of species which create dispersed phase are: silica, iron (oxy)hydroxide, and various aluminum silicate minerals and also oxides of aluminum and manganese, elemental sulfur, and metal sulfides. Another interesting group of species that creates colloidal dispersion are macromolecular biopolymers (starch, proteins, polysaccharides, fat micelles), humic acids [2], systems blood cells dispersed in serum (for example, red or white blood cells) or dust particles as well as bacteria or virus-like particles dispersed in liquid or gas (for example in air).

The colloidal system has specific properties which can be used to distinguish from compounds forming real solutions. Colloids, due to their bigger particles, demonstrate specific movement of particles in liquid medium (Brownian motion) as well as diffusion and significant sedimentation rate in the medium. Colloids possess optical properties such as Tyndall effect and light scattering onto particles which could be used in the classification of colloids from real solution as well as electrical properties (electrokinetic potential, electroosmosis) due to their charge transfer reaction properties.

High diversity within this species group causes polydisperse formation in particle sizes, molar masses, electrokinetic potential, etc. In fact, such complex system requires complimentary analytical techniques for characterization and for analysis of the components that make up real solutions. For a colloidal system, the phenomena on the particle surface and interface become especially important; dispersant and dispersed. Diversity in chemical structure and surface is a result of synthesis or chemical composition. For example, proteins consists of many different

* Corresponding author at: Department of Environmental Chemistry and Bioanalytics, Faculty of Chemistry, Nicolaus Copernicus University, Gagarin 7, 87-100 Torun, Poland.
E-mail address: bbusz@umk.pl (B. Buszewski).

https://doi.org/10.1016/j.microc.2023.108864
Received 28 March 2023; Received in revised form 9 May 2023; Accepted 10 May 2023
Available online 15 May 2023

amino acids.

One of the crucial aspects in colloid chemistry is the recognition and characterization of the phenomenon of colloid agglomeration, i.e. the clustering of individual and separated particles of the dispersed phase into large adducts. Attraction between particles could be correlated with predominance of attractive van der Vaals force in terms of repulsive force. This phenomenon is characteristic of colloids not sufficiently stabilized in the dispersing phase; e.g. can be induced or the process balance controlled by changes in pH, ionic strength or the addition of other (usually ionic) components to the system, due to screnning effect to active functional groups. Simply and directly, the phenomenon of agglomeration could be tracked and monitored by particle size measurements, as the result is an agglomerate with significantly larger sizes than individual particles – frequently apearded in analysed solution. One of the main tools for tracking and characterizing the phenomenon of agglomeration is the measurement of the zeta-potential of the colloidal system that directly it is correlated to the partical size. This aspect is associated with the surface chemistry of the colloid particle in the dispersed system and electric charge locanlized onto particle surface due to different mechanism of creation (Section 4).

The surface heterogeneity resulting from the structure of the colloid is significant for predicting and describing the phenomena of rheology and surface micro-structure [3] and modification of colloidal surface by chemical action, self-assembly or phase separation phenomenon. Surface heterogeneity was observed in a study wherein researchers have shown that spherical polystyrene latex particles adhere to the end of the surface of *Escherichia coli* bacteria and only one bacterial particle at the same time in a majority number of cases (90%), which may indicate a strong orientation effect, which is caused by the heterogeneity of the bacterial particle surface [4]. Another aspect is the effect, the type of dissipative phase. When it is a liquid phase, for example, water, it exerts a special influence on the formation of the solvation shell around the colloid particle, thus determining the occurrence of subsequent processes such as acid-base reactions and interactions, adhesion processes and others [5]. Different characteristics, for example, the ability to sorb on the surface of a colloid of a substance (sorption of metals on particles of bacteria in the air), will be exhibited by a colloid dispersed in the gas phase than in the water phase.

The work aims to introduce analytical technique utilized for characterization colloids distributions of: size, molar mas, zeta-potential as well as chemical speciation and interacting elements with colloids; including proposed mechanisms of interaction of colloids with elements. The range of techniques used, their complementarity, and limitations were discussed. Subsequently, in individual sections, the issues resulting from these analyses were discussed, i.e., the phenomena responsible for stabilizing colloids, their interaction with other compounds, and their presence in living organisms.

Fig. 1 schematically shows the key topics discussed in the paper.

In recent years, the awareness of the society regarding the pollution of the environment and the burdening of this environment by the use of harmful chemicals in laboratories has been constantly growing. Also, the awareness of reducing the consumption of energy used for, for example, the operation of research equipment, leads to the optimization of analytical methodologies or changes in the approaches to performing instrumental analyses. Continuously raising awareness and transferring knowledge about green analytical chemistry is therefore especially important for analytical chemists [6] who usually use chemicals and research equipment. Tools have been developed to assess the "grenn" nature of the entire analytical procedure, such as software ComplexGAPI [7]. However, in this paper, it is worth to raise a debate about the green nature of part of the analytical procedure, which is the conducting analysis by analytical technique. Therefore, in the present study the size characterization and molar mass of colloidal particles (section 2) in context of complimentary techniques such as static light scattering (SLS), dynamic light scattering (DLS), nanoparticle tracking analysis (NTA), ICP/MS, scanning electron microscopy (SEM),transmission electron microscopy (TEM), mass spectrometry (for example MALDI)) electrophoretic mobility based the zeta-potential measurement (section 3),size exclusion chromatography (SEC), flow field flow fractionation (FFFF) in section 2 as well as section 6 were debated. For these techniques, the measurement time per sample is rather short and could be reduced by optimizing the general metodology, especially in the case of separation techniques. Techniques which work in a vacuum tend to consume amounts of electricity, however, it can be reduced by

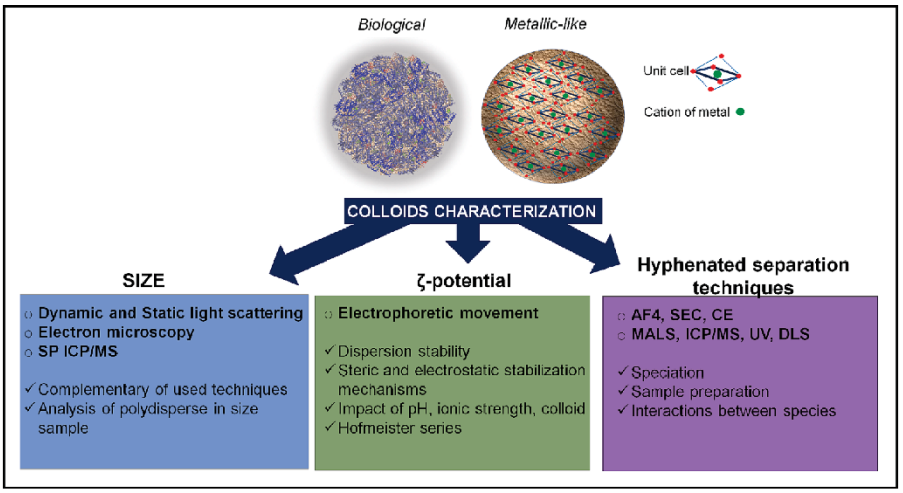

Fig. 1. List of issues discussed in the paper. The characterization of biological and metallic colloids is discussed through particle size parameters, zeta-potential and coupled separation techniques.

decreasing of the total number of samples submitted for analysis through careful planning and modeling of experiments. Analysis with these techniques is possible in environmentally friendly solvent with totally reduction of the most toxic reagents. The amount of sample and consumption of reagents could be reduced by using appropriate tools such as low-volume cuvettes with in terms of light scattering techniques or shorter chromatographic column or smaller volume analytic channel.

2. The size and molar mass of colloidal particles

The size and mass of colloidal particles are two of the key parameters describing the physicochemical properties of colloidal particles. In contrast to compounds create real solution, the colloidal particles have larger size and characteristic distributions giving them unique properties and applications. As particle size increases, the surface area, diffusion coefficient and effective charge decrees, and simultaneously, the ability to scatter light and sedimentation rate increases.

The final result of the measurement of particle size distribution or molecular weight is usually a graph (sometimes in the form of a histogram), which shows the distribution of recorded particle sizes as a function of the intensity of the measured signal. The value of the measured signal can be determined by intensity, volume, or number. The shape of an individual fraction could be described as bell-like curve. Individual fractions could be described mathematically through gaussian curve and with parameters such as median and polydispersity index as a parameter describe spread of the distribution [8]. If the sample is homogeneous in size (within the fraction), the polydispersity index is about 1 or the farther from unity the fraction is heterogeneous.

The choice of analytical technique used will also depend on the state of matter of the sample. For the characterization of solid and liquid particles, the most popular are techniques based on light, neutron or X-ray scattering [9], laser diffraction onto particles, nanoparticle track analysis (NTA), microscopy techniques such as scanning electron microscopy (SEM) and transmission electron microscopy (TEM) as well as the single particle inductively coupled plasma (SP-ICP/MS) technique, which is relatively young technique in the laboratory and dedicated to elemental-like particles which shape of particles could be described as sphere [10].

Fig. 2 shows examples of colloids on a size scale as well as a typical working range of selected analytical techniques used in the laboratory to determine size distributions of colloidal particles. To the comparison in size scale, a water molecule and a hair are also marked to visualize the compounds which are classified as small molecule and macro-object.

Techniques based on static light scattering (SLS) and dynamic light scattering (DLS) as well as SP ICP/MS do not have a designated parameter like the detection limit, understood as the smallest particle giving a measurable analytical signal in the context of background (noise) signal. In general, the intensity of the signal from a scattering of light from a particle is directly proportional to the particle size (mass), their concentration and the square of the increment refractive index value (Eq. (1)). Therefore, the lowest measurable signal (in terms of signal noise) depends on the sample characteristics as well as measurement condition (relation between colloid and dispersant phase).

$$I_{signal} \propto M_w C \left(\frac{dn}{dc}\right)^2 \quad (1)$$

Importantly for SLS measurement is type of scattering, isotropic or anisotropic in particle size context. The lower limit for particle size determination values of around 10 nm is related to the beginning of the process of anisotropic scattering of light onto particles at these particle size values.

As a result of isotropic scattering, the intensity of scattered light is the same in all directions and independent on the detection angles from the center of the particle; this type of scattering is observed for small particles (below 10 nm, approximately). In anisotropic scattering, the intensity of registered signal from scattering depends on the observation angle. The relationship of the intensity of scattered light and observation (detection) angle is expressed in the Rayleigh equation (Eq. (2))

$$\frac{K_{opt} C}{R_{\varnothing}} = \frac{1}{M_W P_{\varnothing}} + 2A_2 \times C \quad (2)$$

where K_opt is the optical constant, R_∅ is the excess Rayleigh scattering ratio, M_W is weighted-average molar mass at concentration C, P_∅ is particle scattering function, A_2 is second viral coefficient. Graphical representation of transformed form of Rayleigh equation could be Zimm plot, where extrapolation of experimental values (scattered light at

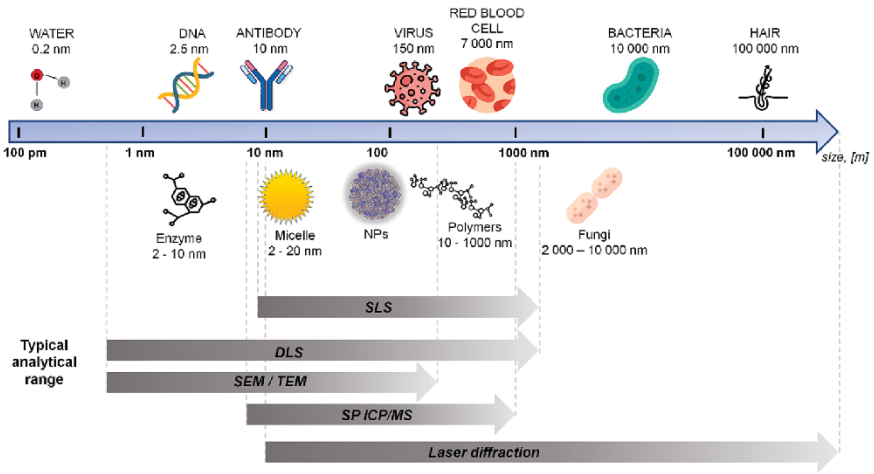

Fig. 2. Examples of colloids of biological nature representing typical values of the size of single objects with typical occurred analytical range of techniques implemented to size characterization.

different angles for anisotropically scattered particle) to angle at ∅=0 and C = 0 gives M_W and radius of gyration vales.

However, DLS measurements in batch (in comparison to flow-through analysis) mode may allow measurements of particle sizes below 10 nm since the measured value depends directly on the diffusion coefficient and not on typical light scattering. Moreover, detection of smallest particles and measurement precision is highly related with sample optical purity [11] as well as instrumental set-up (especially detection arrangement) [12].

Fluctuation of scattered light (in time) onto particles in continuous motion in medium (Brownian motion) is a starting point in DLS measurement. The hydrodynamic radius R_H is calculated from diffusion coefficient parameter based on Stokes-Einstein equation (Eq. (3)) while bigger particle diffuses slowly and scatter more light than smaller.

$$D - \frac{kT}{f} - \frac{kT}{6\Pi\eta R_H} \tag{3}$$

where k is Boltzmann constant, T is absolute temperature, η is dynamic viscosity and D is translational diffusion coefficient.

The lower limit of the analytical range of the technique SP ICP/MS (Fig. 2) could be correlated to element ionization potential and particle concentration in sample as well as background level at specific mass to charge ratio and transport efficiency during sample introduction to plasma [13]. Moreover, this technique provides the ability to measure particles in the entire definition range of colloids for some elements and particle form. Subsequent technique for size determination could be microscopy based techniques (SEM, TEM), while the particle concentration must be high enough to reach turbid initial sample solution, in general, to ensure the detection of particles.

In turn, the upper limits result from the fact that a particle suspended in a medium (for techniques examining particles in a liquid medium) must exhibit measurable Brownian motion and thus be in a colloidal state. Particles that are too large and tend to sediment significantly should not be analyzed using diffusion or light scattering-related techniques. The borderline between colloidal and non-colloidal is difficult to generalize for the whole group of colloids due to significantly different structures and, therefore the upper limit of the analytical range also. The polar structure of a particle which under specific conditions (pH, ionic strength, temperature, etc.) is electrically charged (have significant values of zeta-potential) and therefore are electrostatically stabilized. Another stabilization mechanism is steric exclusion, which in both mechanisms gives possibilities to characterize particles at larger sizes (including agglomerates) and therefore such systems can be characterized in a broader size range. For the SP ICP/MS technique, it is essential to transport the particles efficiently to the analytical parts of the spectrometer (plasma torch through the system of cones and ion lenses) to the mass analyzer through the most used nebulizer and spray chamber, through which too large particles are sterically excluded.

The size of the colloid particles R can be related to the molar mass M of these particles by a relationship (Eq. (4)):

$$M - KR^{d_f} \tag{4}$$

where constant K depends on the particle shape and density, and d_f is fractal dimension, a parameter describes particle shape. For linear particles, d_f is 1 and for compact spherical particle, exponent is 3 [14].

To determine molar mass distribution, techniques based on light scattering, viscosity, sedimentation rate and mass spectrometry techniques (ionization techniques such as electrospray ESI, fast atom bombardment FAB or matrix assisted laser/desorption ionization MALDI) could be used [15]. The techniques listed above can be distinguished by the system in which the measurement is made. Mass spectrometry techniques are based on the transfer of compounds from the solid or liquid sample to the gaseous state in a (high) vacuum, while measurements with the other listed technique can be made in the dispersed phase. In complementary studies, light scattering (SLS) and mass spectrometry (MALDI-TOF/MS) techniques were used to characterize the process of pH-dependent self-association of beta-lactoglobulin in dispersant and both techniques lead to identical conclusions; protein is monomeric at pH equal 3.0, dimeric at pH 7.0 and at pH 5.0 create forms from dimer to octamer [16].

Alternative techniques to determine the size of molecules are size exclusion chromatography (SEC) or technique from a family of field flow fractionation (FFF). Calculation of particle size based on the results from the determination of retention time after SEC or FFF analysis are, however limited to substances with calibration standards are present, because even colloids of the same size show different retention times or elution volumes depending on the chemical structure of the compounds due to versatility in conformations, shape and creation ordered structures [17].

2.1. Complementary techniques in size determination

These techniques, apart from the dependence on the shape of the particles, lead to different types of particle size distribution. The result of DLS measurement leads to obtaining size distribution by intensity. This type of distribution is notably sensitive to detect larger particle in the sample since, the larger particle is the more intensity of scattered light signal produce (**Eq. (1)**). If the intensity type of size distribution is monomodal and monodisperse in size (by Pdi) it is possible to convert the native type of distribution from DLS (by intensity) to number or volume types of size distribution based on the Mie theory [18], the transformation between intensity and numerical size distributions types is done by the Mie scattering formula. These calculations could result in more sensitive analysis of smaller in size particles in the sample. Number type distribution shows the quantity relationship of particle in a sample while volume-based distribution reveals particles volume relations in the sample (approximated to a sphere). The correct result of the transformation of distribution also requires full knowledge of the components of the samples (optical constants), the homogeneity of the composition in terms of density and shape.

Using analytical techniques based on different theoretical and experimental foundations and assumptions leads to obtain complementary information about the components of the sample. For example, using techniques based on DLS or SLS leads to obtaininghe values of hydrodynamic and gyration radii, respectively [19]. The hydrodynamic radius of a particle is related to the size of hard and spherical particle which has the same diffusion coefficient while radius of gyration is the value of distance from the mass focal point of a particle.

For microscopy-based size determination, the particle's shape, sample preparation protocol, and measurement environment have a significant impact. The authors indicated the impact of shrinking of the particles during the drying process before SEM analysis as a source of change in particle size of polyalkylcyanoacrylate nanoparticles as the authors were received significantly different median and distribution of size after comparative study using of scanning electron microscopy, DLS and analytical ultracentrifugation [20]. The TEM analysis leads to obtaining well-defined characterization size, shape and morphology of particles with high resolution and precision. However, the analysis result is a two-dimensional image of (frequently) nonhomogeneoushape and polydisperse in size particles value and leads to number-based size distribution [21].

In comparative studies of size determination of pigments, number-type size distribution during DLS measurement correlates with size distribution obtained from transmittance electron microscopy (TEM) measurement while intensity-type distribution overestimate median value [22]. The intensity-based type of distribution highlights the larger particles in the sample, because bigger particles give more intense scattering intensities.

Nanoparticle Tracking Analysis (NTA) is an analytical technique which measure hydrodynamic radius, similar to DLS, from diffusion coefficient measurement; however, in contrast to DLS, the detection is

based on the microscopic assessment of position change of particle after illumination their by laser. The result gives better particle fraction resolution for polydisperse in size sample compared to DLS and produces number-based type of distribution. that recalculation number-based distribution (from NTA) to intensity-type does not explain differences in registered distribution parameters obtained from DLS analysis, due to the necessity of using ahape-dependent model [23]. Determination of the particle size distribution by the SLS technique leads to obtaining weighted-average size distribution which is orthogonal to DLS and TEM analyses [24] and the average value is often lower for weighted-average size distribution.

2.2. Shape of particles

Techniques based on the measurement diffusion of particles in a medium (DLS, NTA) to calculate particle hydrodynamic size (based on Eq. (3) for example) are shape and shape-model dependent techniques. From the definition of the concept of hydrodynamic radius, it follows strictly that the value of the size of the measured particle refers to a hard and spherical particle that shows the same diffusion (diffusion coefficient) in the medium. In general, only spherical particles have homogeneous properties in size determination. Any change in particle shape (from spherical to non-spherical) and surface properties could potentially affect significant change in diffusion speed of particles in medium. One example could be a conformational change in polymer structure which leads to re-equilibria in surface active group availability.

The size measurement results will depend on the particle's orientation in relation to the detector (the phenomenon is particularly visible in microscopy). Only spherical particles are homogeneous when measuring particle size [25].

The shape factor 'ρ' which contributes to particle shape of a particle can be determined in dispersed state (studies where impact of liquid environment could be important) as the ratio of the gyration to hydrodynamic radii extracellular nanoparticles were characterized as spherical [26], synthetized peptide–liposome complexes were characterized as coated sphere [27].

2.3. Analysis of polydisperse in size samples- problem meaning

The dependence of the intensity of the scattered light on particles is described by the particle radius power relationship with the exponent of 6 [28]. For this reason, DLS and SLS techniques are characterized by their high sensitivity. However, this means that the direct analysis of a complex mixture of particles with a significant polydisperse will reduce the sensitivity and precision of measurement for smaller particles especially, often even leading to a complete loss of the signal for the smallest particles. For example, in research, smaller fraction of dextran particles in the presence of a fraction of large ones were not detectable [29]. Polydisperse sample analysis using DLS may lead to incorrect measurement results due to theow resolution between the measured fractions [30]. Analyzing a polydisperse sample using the DLS technique, it may be helpful to use the CONTIN algorithm, which made it possible to correctly determine the particle size distribution of the microgel suspension [31]. The CONTIN algorithm is one of the possible types of deconvolution of raw experimental data resulting from the measurement of the interaction of apparatus laser light on particles moving as a result of Brownian motion [32].

2.4. Analysis of polydisperse in size samples- using separation technique

Another possible solution is to use a separation technique that maintain homogenous in the determination of particle size and molar mass. Additionally, sizing the monodisperse particles at gives opportunity to minimize multiple scattering onto particles phenomena in highly concentrated suspension [33]. Separation of complex sample into fractions is significant when analyzing substances that tend to agglomerate, thus practically the predominant group of colloids. Multi-angle light scattering detector (SLS based) is typically used in coupled separation techniques such as asymmetric flow field flow fractionation (AF4) or size exclusion chromatography (SEC).

To obtain the separation techniques based on the mechanisms of differences in particle size and particle diffusion coefficient (SEC, AF4) as well as charge (capillary electrophoresis CE) were used. Fig. 3 shows the mechanisms behind AF4 and SEC techniques schematically.

In the case of the AF4 technique (upper panel) Fig. 3, the separation of the sample takes place in the open channel, in which one of the walls is covered with a semi-permeable membrane with strictly selected pore size values. The membrane pore size value determines the smallest particle size retained by the membrane and separated in the channel, while particles smaller than the membrane pore size are removed from the separation solution. The mechanism is used during the semi-preparative purification of the sample and the removal of unwanted sample components during the separation process. The sample is distributed through the canal during the injection stage. Then, experimentally selected flow values lead to the concentration of sample components in a narrow band close to the lower surface of the channel. In addition to the directional forces that attract the sample particles to the membrane, diffusion also affects the particles. Too low experimentally obtained recovery of substances after separation may result from the excessive predominance of focusing forces in relation to the diffusion value. However, the recovery values are also affected by the interaction of the analyte with the membrane structure. During the separation (separation method) there is a change in the value of the created flows, which results in the fact that particles of successively larger sizes (smaller diffusion) can float towards the central part of the channel cross-section in which the linear value of the flow is the highest due to the presence of laminar flow characteristics. Finally, during the normal type of elution, the order of particle size eluting from the channel and entering the detector is from smallest to largest particles.

In the case of utilizing the SEC technique (lower panel) Fig. 3, the components of the sample are introduced into the column filled with a porous stationary phase (the key values are pore diameter and pore size homogeneity) and transported along the channel through a mobile phase (usually a buffer solution). The separation mechanism (according to the main theories and assumptions) is based on the steric exclusion of particles of larger and larger sizes since larger particles (in hydrodynamic volume) penetrate the pores of the stationary phase to a smaller and smaller extent, while particles whose size exceeds the value that would allow inside the pores are eluted in or near the dead volume of the column. Smaller and smaller particles penetrate more deeply into the pores and therefore stay longer in the volume of the stationary phase. After separation, the sample components are classified from the largest (largest hydrodynamic volume) to the smallest.

The separation technique for separating a mixture of biocolloid forms has been used in research to characterize the mass and size of bovine albumin serum protein particles. A theoretical monomer mass of this protein is about 66 kDa and it shows a significant tendency to oligomerization or agglomeration in medium. When batch molar mass determination analysis was performed the result indicates incorrect value of 85 kDa, however, the use of a separation technique (SEC) allows for the separation of these forms and accurate characterization individual forms of mixtures [34]. Changing the separation mechanism from SEC to Ion Exchange Chromatography may allow for the analysis of a wider group of proteins and for more precise determination of the substances' size and molar mass parameters due to the greater number ofptimizing parameters and their influence on the analysis results [35]. Another possibility is using AF4 technique to separate oligomeric forms of beta-lactoglobulin and by using ultraviolet (UV) and multi angle light scattering (MALS) detection system characterize them; protein forms represent pH and concentration dependent relationship, in acidic condition is monomer, at pH 7 is dimer however, at pH protein occurs from dimeric to octameric forms [16].

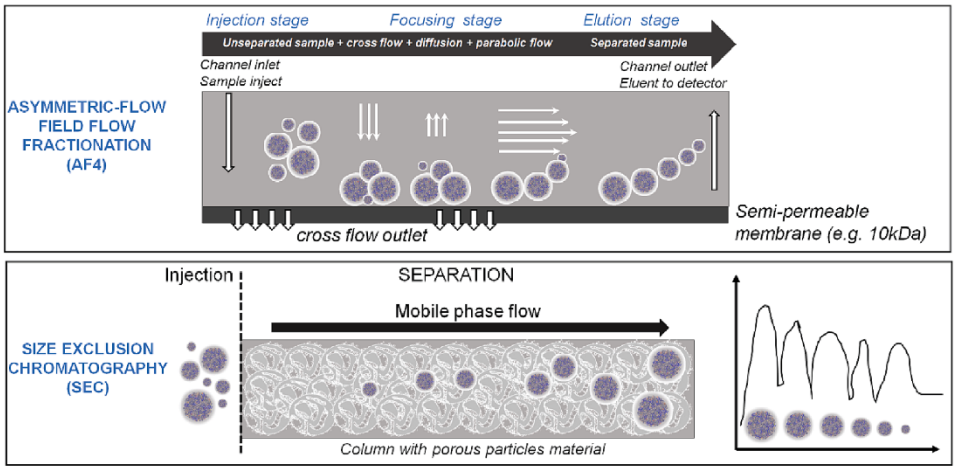

Fig. 3. Schema of separation mechanisms used in the AF4 technique (upper panel) and SEC (lower panel).

The subsequent problem that can be encountered during the measurements is the phenomenon of light absorption by particles which could be found in many examples of proteins containing chromophores, for example, [Fe-S] cluster. The solution to this problem and for fluorescent samples may be changing the laser wavelength, using laser filter caps or using corrections algorithms[36].

However, the use of separation techniques comes with its own disadvantages such as the low recovery of substances after the separation process, possible changes in the conformation of substances or even degradation of certain compounds that are particularly sensitive to the separation process. Many of the inconveniences encountered especially during protein analysis using SEC can be avoided by switching to milder separation technique as AF4, however, the analysis with it requires in-depth optimization [37]. After SEC or AF4 separations for many groups of substances, lower than complete recovery of species is caused by mostly attractive interactions of separated substances with stationary phase in SEC or membrane in AF4. This is especially visible for highly charged (ionic) substances such biopolymers. In case analysis of typhoid Vi polysaccharides where discrepancy in substance recovery after AF4 and SEC analysis were varied between 61.8 % and 7.8 %, respectively [38]. The recovery achieved in AF4 could be higher than after SEC separation due to much lower surface contact of substance with membrane comparedo stationary phase surface in SEC, and recovery is around 80–90 % for separations of biopolymers [39,40]. Even if the experimental conditions theoretically prevent the loss of substance due to the interaction of the particles with the AF4 semi-permeable membrane [41,42]. Thus, during the AF4 method optimization, the correct compromise between resolution and recovery in practice is made.

3. The zeta-potential of colloidal particles

The role of the particle surface and the solid/liquid interfaces becomes decisive while interactions between particles and dispersed phase are considered. The zeta-potential parameter determines the electric charge that is present at the interface (slipping plane) between the adsorption layer (Stern) and the secondary layer of ions interacting with the particle-adsorption layer component [43] (Fig. 4). It is believed that colloidal particles can acquire a surface electric charge as a result of Brownian motion in the dispersing phase due to the friction of the surface and movement of the colloidal particles with molecules of the dissipating phase Surface of colloidal particle can have an electric charge resulting from being native character ions in liquid after the dissolution, ionic surfactant (ad)(chemi) sorption, dissociation of chemical groups, ion exchange reaction and isomorphic substitution of some groups [44,45]. The surface electric charge of particle forces the movement of other ions presented in bulk medium. The electric charge located on the surface of the particle attracts oppositely charged ions (Stern layer) in the first. In return, this layer diffuses ions from the opposite (diffuse layer) sign.

The zeta-potential parameter is one of the key parameters used to describe and predict colloidal suspension stability [46]. If the absolute value exceeds 30 mV, it means that the suspension is stabilized electrostatically, by electrostatic repulsion between particles (Fig. 5), which in turn prevents them from combining larger clusters (agglomerates) and create larger particles. Particles reaching the significant size and not stabilized (electrostatically or sterically) have a tendency to precipitate and sedimentation or creaming from the suspension.

The stability of colloids in medium can be described and predicted using the DLVO theory. The acronym for the term comes from the names of the theorists; Derjaguin-Landau-Verwey-Overbeek. The central hypothesis of the theory is the fact that the van der Valls (attractive) and electrostatic Coulomb (repulsive) forces between particles and within individual particles are present and act simultaneously, the sum of which determines the resultant value that acts on two particles: $F_{DLVO} = F_{attractive} + F_{repulsive}$ [47]. A graphical representation of forces acting onto particles in terms of distance between particles takes form of local minima and maxima depending on the distance between the interacting particles, while at close distances (below about 10 nm) the electrostatic repulsion between the complexes of the particle layers (Stern and diffusion) dominates. As the space between the particles increases, attractive forces begin to appear. For spherical particles of radius R at separation d, Hamaker constant A, the van der Waals energy is given as (Eq. (5))

$$V_d = \frac{-AR}{12d} \tag{5}$$

Hamaker constantly describes the chemical composition of particle and due to the fact that A has positive sign the attraction between the two identical particle is always attractive and therefore separation

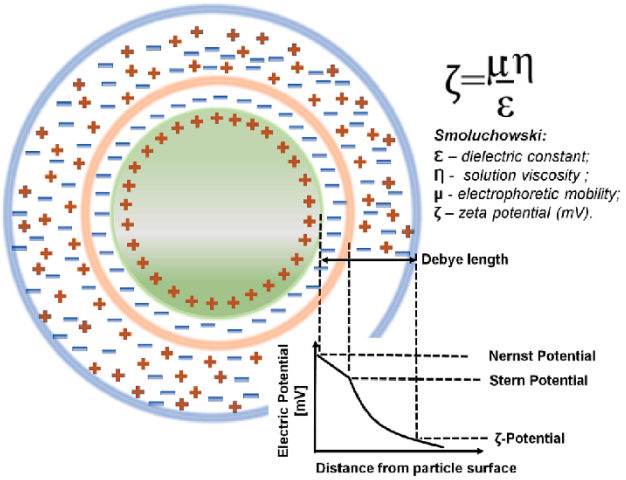

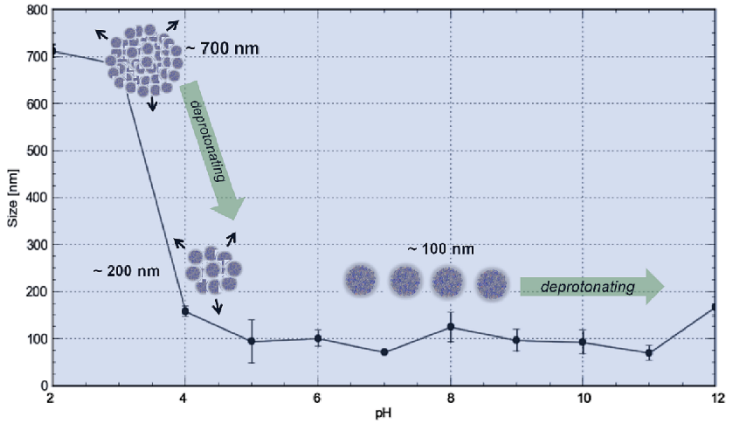

Fig. 4. Schema showing the formation of layers of adsorbed ions on an electrically charged colloidal particle resulted in an electrokinetic potential.

distance is factor that decide about agglomeration process.

Surface potential and diffusion are strongly conditioned by proton transfer reaction or load on electrokinetic stability (Fig. 4). An agglomerating particle in given conditions (a cluster of many particles) may exceed the critical value of density (mass to volume ratio) at which sedimentation of these particles from the suspension will occur. In general, the larger the particle size, the higher the absolute zeta potential should be present to stabilize these particles. Depending on the specific chemical structure of the particle, one of the mechanisms that allow the formation of the structure of the electrically charged surface of the particle and their change in value may be acid-base reactions.

The zeta-potential of a suspension can be determined by means of various instruments: streaming current, streaming potential, electro-acoustic, electro-osmosis and electrophoresis movement [46]. The most popular is the device based on the movement of charged particles in liquid suspension with external voltage applied and particles illuminated by laser radiation and light scattering detection. The electrophoretic velocity of the particle is written in (Eq. (6))

$$v_E = \mu E \tag{6}$$

where μ is named electrophoretic mobility and articulated in terms of a ζ-potential by Smoluchowski formula (Eq. (7)):

$$\mu = \frac{\epsilon\epsilon_0}{\eta}\zeta (\text{for } \kappa\alpha >> 1) \tag{7}$$

where ϵ and ϵ_0 are the relative dielectric constant and the electrical permittivity of a vacuum, respectively, η is the solution viscosity.

One of the key parameters and assumptions is the so-called Debye length parameter κ [48] which is linear proportional with hydrated cation radius [49] and electrolyte concentration [50]. The

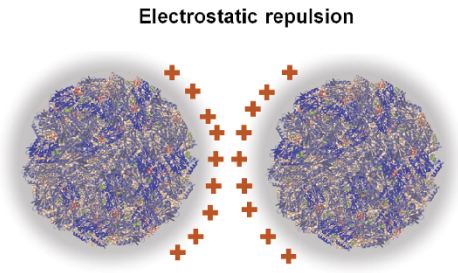

Fig. 5. Electrostatic repulsion (repulsion of single-sign charges) as one of the stabilization mechanisms between colloidal particles.

Smoluchowski form of the electrophoretic mobility equation (Eq. (7)) is particularly useful for the analysis of submicron particles in the medium with significant values of electrolyte concentrations and were ionic radius of particles in relation to Debye lenght parameter is $\kappa\alpha \gg 1$. However, when analyzing a significantly smaller colloidal particle at low electrolyte concentrations or non-aqueous systems ($\kappa\alpha \ll 1$), a Huckel approximation in the electrophoretic mobility relationship with zeta-potential should be considered (Eq. (8))

$$\mu = \frac{2}{3}\frac{\varepsilon\varepsilon_0}{\eta}\zeta (\text{for } \kappa\alpha << 1) \tag{8}$$

However, it was demonstrated that the Henry function $f_H\,\kappa\alpha$ (Eq. (9)) [51] provides the most widely assumed electrophoretic mobility versus zeta-potential relationship in the case of nonfunctionalized metallic nanoparticle [52].

$$\mu = \frac{2}{3}\frac{\varepsilon\varepsilon_0}{\eta}\zeta f_H \kappa\alpha (\text{for } \kappa\alpha << 1) \tag{9}$$

The work of W. Wilson indicated that the Smoluchowski model used for most virus and bacterial particles is correct [53]. However, it has been shown that the Smoluchowski approximation (for large particles in a medium with high ionic strength) is correct for bacteria, while for viruses it is better to use the Henry approximation [54]. In research conducted on the interaction (adsorption) of alkali metal ions to phosphatidylcholine vesicles,Henry parameters were applied to functions depending on particle radius and electrolyte concentration [55]. Increased concentration of electrolyte $NaNO_3$ reduces electrophoretic mobility of Fe_3O_4 nanoparticles due to more effective charge neutralization of particles at given pH [56].

3.1. Impact of pH

The pH of the environment has the greatest impact on the zeta-potential value, the effect of ionic strength and colloid concentration is significant [57]. pH dependance of zeta-potential determination (in function ionic strength for example) is often conducted to colloid isoelectric point determination.

The pH of the environment usually has the most significant influence on the zeta-potential of the suspension. Changes in pH affect the value of the charge located on the surface of the colloidal particle. At an acidic medium conditions, colloid possesses positive zeta potential as a result of protonation of functional groups such as organic residue (proteins, polysaccharides or lipids) onto bio-ZnO nanocomposite [58] carboxyl, amine/hydroxyl, phosphate/hydrogen phosphate groups on the surface of native yeast cells [59] or amino acids in protein [60]. The isoelectric point is the pH point at which the net charge is zero. As the pH decreases further, the groups deprotonate and the zeta-potential decreases to negative values [61,62]. Electrokinetic stabilization at absolute values above 30 mV results from the repulsive action of colloids with the same sign. In turn, the primary change of the charge on the particle's surface entails a change, even reorientation if the surface charge is opposite to the original, of the structure and properties of the near-surface; Stern and diffusion layers.

The relationship of biocolloid pKa and environment pH determines the protonation reaction direction. It has been shown that soluble forms of chitosan (pKa around 6.2) are characterized by positive zeta-potential due to protonation of amino group (functional group of chitosan); at pH 7 the heaviest 300 kDa – 72 kDa) forms of chitosan are insoluble because of (insufficient) deprotonation of functional groups, while pH below 6 ensures solubility of all forms of chitosan [63]. It has been shown that the dispersed forms of caseins become stable after more than 1 h of the process [60].

In turn, the zeta-potential determination and optimalization the physicochemical condition of system could be used to determine the condition where colloid does not have an electrostatic stabilization mechanism. The colloidal particle near the isoelectric point has many interesting properties such as: the highest tendency to agglomeration, minimal solubility, frequently possesses specific conformation and its highly lyophobic. In this specific condition the flocculation process is the most effective as well [64].

3.2. Adsorption of the second colloid onto particle

Determination of the zeta-potential of a mixture of two colloids allows to determine the conditions favorable for the synthesis and to determine the stability of the complex depending on the measurement conditions. However, sometimes high net zeta-potential of suspension does not guarantee stability [56]. Therefore, it was postulated the presence of steric mechanism of stabilization. The presence of a second colloid can improve the system's stability through the steric exclusion effect [65] (Fig. 6). Functional groups of colloidal species are sterically blocked. In an extreme acidic or alkaline environment, where most of the colloids is positively or negatively charged, respectively, the two species' repulsion occurs. However, at pH environment close to pI of colloids, some functional residues could possess oppositely charged moieties followed by electrostatic attraction between them. For example, it has been shown that beta-lactoglobulin can form complexes with pectins, and with a higher percentage of pectin functional groups bound (the degree of esterification of carboxyl groups), the effective pH range in which the formation of complexes occurs decreases [66]. The acid-base properties of the carboxyl group (the carrier can be pectins) and their concentration can be used to improve the stability of many other colloids (for example saybean oil bodies suspension) that are particularly sensitive to degradation in the acidic pH range, which is important in order to optimize new formulations for the food industry,

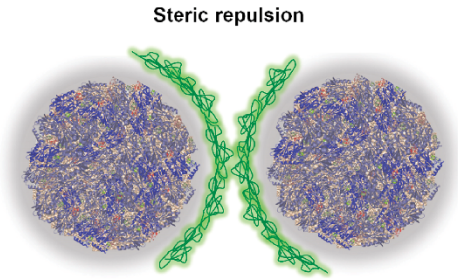

Fig. 6. The tendency to attraction and consequently aggregation of two particles could be reduced significantly by steric mechanism, structural high in size particle is blocks functional groups of particles sterically.

(yoghurt) and other naturally acidic food products [67]. For use value to use in products, for example in food industry, new materials based on colloids, zeta-potential measurements can be used to develop and optimize materials and environmental conditions in which complexes are in a coacervate state [68,69].

When measuring zeta-potential, stability can also be evaluated by the deviation parameter and zeta-potential value distribution. The widening of the distribution or the increase in the deviation of the average zeta-potential value is particularly common for biocolloids with a specific structure, for example proteins; in an extremely acidic (pH below 2–3) or alkaline (above pH 9) environment, the protein may lose its quaternary structure and consequently its biological activity [16,70].

3.3. Impact of adsorption of specific ions onto particle

The zeta potential of the suspension depends on the qualitative and quantitative composition of the suspension. However, it has been proven that specific ions (cations and anions) can exert a different effect on the zeta-potential because they can interact in a way other than just the interaction of charges. The Hofmeister series could describe this relationship.

The Hofmeister series was introduced as a postulate to explain the impact of ions on the phenomenon of protein denaturation. There is an order of anions:

$$CO_3^{2-} > SO_4^{2-} > S_2O_3^{2-} > H_2PO_4^- > F^- > Cl^- > Br^- > NO_3^- > I^- > ClO_4^- > SCN^-.$$

and cations:

$$N(CH_3)_4^+ > NH_4^+ > Cs^+ > Rb^+ > Na^+ > Li^+ > Ca^{2+} > Mg^{2+} > Zn^{2+} > Ba^{2+}.$$

Anions at the left from chloride and cations at the right of sodium are considered as have a high hydration potential and tend to unfold the protein and increase the protein solubility [71]. Initially, the mechanism of action of these series on the release of proteins was seen in changes in bulk water structure by added ions. However, it is known that the specific interaction between ions and macromolecules as well as interactions with water molecules in the first hydration shell of the macromolecule are important [72]. It was shown that the micelle size decreased with Hofmeister series of anions and cations due to increased polarizability potential of cations [73]. The effect of adsorption of series of cations and anions on the lysozyme solubility were studied. The results showed reverse sequence for anions at low concentration, which was discussed through thebility of the more polarizable anions to enhanced interactions by ion-surface interfaces [74]. More hydrated ions can thickness reduction of electric double layer [75].The zeta potential of manganese ferrite particles was lowest at pH 4 suspended in water, and then in citrate and acetate buffers [76].

The zeta-potential measurement technique is a handy tool used to determine the isoelectric point of colloids. Rodzik et al. determined isoelectric point of beta-lactoglobulin at pH = 4.6 [77]. However, this protein's isoelectric point condition varies with environment specificitytype of counterion) and change from 5.3 to 7.6 [16]. Impact of specific ions on isoelectric point was observed in wider group of biomolecules [78]. Ionic surfactants impact of isoelectric point of ZnO particles [79]. According to the Hofmeister series, the zeta-potential of the suspension of galactomannan changes [80]. Using the Hofmeister series, it is possible to interpret the phenomena of specific adsorption of ions to the surface of colloids, not only through the valence of the ions. Adsorption of ions with different levels of hydration to the strongly hydrophobic surface of cellulose particles may occur through the participation of entropic phenomena consisting in the release of hydration water from the structures of the coordination network of ions [81].

4. Mechanism of metallic substance interactions with colloids

Concerning the interaction of metals with colloids or structures of metallic nanoparticles, the mechanisms of synthesis of this type of materials can be elucidated in the first place. Structures of metallic nanoparticles can be obtained using bottom-up or top-down technologies. This means carrying out processes consisting of the agglomeration of smaller individual particles in the solution or the use of processes to reduce and fragmentarge particles, respectively [82]. In turn, for biopolymer particles, the metallic deposit may be present as a result of specific or non-specific adsorption or chemisorption processes [83]. The bacterial cell wall is made of, among others, acids whose functional groups (carboxyl, phosphate) are capable to acid-base reactions and, depending on the environmental conditions (pH) and specific value of pKa of acids, an electrically charged colloidal particle core is formed to which metal ions can attach [84]. The pH condition, the absolute critical parameter, determines the level and character of ionization of active functional groups onto particle [85]. The adsorption of cadmium to bacterial structures showedhat the process does not depend on the type of bacteria (gram positive and negative) but is conditioned by the concentration of functional groups in the bacterial structure, their pKa constants and metal binding constants [86]. Alireza Fathollahi et al. conducted a *meta*-analysis on the biosorption of various metals on many types of bacteria and, as a result of the analysis, estimated the optimal (highest sorption efficiency) conditions for the biosorption process as pH values between 6 and 7.5 for lived bacteria strains as well as sorption effectiveness, contact time (between bacteria strains and metals), optimal temperature depending on type of metal ions [87]. Table 1 summarizes several papers focusing on characterizing the interactions of metal ions with bacteria using instrumental techniques. The works focused mainly on optimizing the biosorption process by determining the optimal conditions and characterizing and postulating the mechanisms of the biosorption process.

The FT IR (Fourier-transform infrared spectroscopy) technique plays a special role in characterizing the interactions between bacteria and metals by determining functional groups that may participate in metal binding by bacteria and thus lead to the presentation of postulated binding mechanisms. Bacteria secrete specific substances called "Extracellular polymeric substances" (EPS) which could be many of proteins and polysaccharides, uronic acids, humic substances, lipids etc. [88]. Due to presence of functional groups such carboxyl, thiol/phosphate, and amino/hydroxyl could bind ions from media through electrostatic interactions. The acidic constants (pKa) of the EPS fell into three ranges of 3.5–4.0, 5.9–6.7, and 8.9–9.8 [89]. Conducting the SEM-EDX technique, it was shown that part of Pb bound by *Phanerochaete chrysosporium* occurs in the form of precipitated associated with EPS located on the surface of bacteria [90]. In Fig. 7 it was showed a comparison of a possible mechanism of metal ion sorption/interaction with bacteria cell.

Similarly, the mechanism of metal binding to the structure of biocolloids (proteins, for example) takes place through the electrostatic attraction between inversely charged centers of metal ions and functional groups of the protein [70] However, it has been shown that the interaction of a group of metals (Zn(II), Cr(III), Cd(II), Cu(II), Pb(II), and Ni(II)) with a protein is not homogeneous and is a process specific to a biopolymer - metal characteristic and reaction environment conditions [91]. In Fig. 8 it was demonstrated schema of possible and postulated in literature mechanism of metal ion binding/interaction with proteins through functional groups of amino acids residue.

5. Characterization of metal-like (bio)colloids and metals interaction with colloidal particles with using ICP-MS: Direct sampling and sample solubilization

The element concentrations in bio composite samples (metal-like colloids and metal-colloid particles) could be determined by analytical

Table 1
Comparison of the tested metal ions with a group of different bacteria by means of instrumental techniques.

Chemical Element	Biocolloid	Analytical techniques	Main outcome	Reference
Cd, Cu, Pb	*Pseudomonas azotoformans*	MIC determination, ICP OES, 16S rDNA, FT IR	• Binding to ionizable groups –OH, –NH and COOH present on the cell surface Optimal removal effectiveness at pH 6.0, 2 g/L of biomass and initial concentration of each metal 25 mg/L Removal efficiency was as follow: Cd 33.1 %, Cu 53.9 % and Pb 81.9 %	[92]
Cd, Cu, Cr(III), Ni	Bacteria: *Pseudomonas, Bacillus, Micrococcus, Escherichia, Streptococcus, Enterobacter, Staphylococcus Fungi: Aspergillus niger, Penicillium notatum and Aspergillus flavus*	UV–VIS	• the highest removal effectiveness in bacteria series was determined for Cr 89.67% and for Cu 90.89% by Pseudomonas aeruginosa at 20 ppm on day 21 and 15 ppm on day 14, respectively P. notatum showed highest biosorption rate for cadmium at 10 ppm with 77.67%. Aspergillus niger showed highest biosorption rate for nickel with 81.07% after 28 days of incubation	[93]
Zn, Pb	*Oceanobacillus profundus*	UV–VIS, ICP OES, CLSM	• maximum removal percentage for Pb was 97% at an initial concentration of 50 mg/L whereas maximum removal percentage for Zn was at 54% at an initial concentration of 2 mg/L obtained at pH 6 and 30 °C. proposed sorption mechanism by interaction metal ions with carboxyl, sulfate, and phosphate presented in EPS	[94]
Cr (VI)	*Pseudomonas alcaliphila strain NEWG-2*	SEM-EDX, FT IR, 16S rRNA, flame-AAS	• sorption effectiveness 96.60% of 200 mg/L of Cr (VI) using yeast extract (5.6 g/L), glucose (4.9 g/L), pH of 7 phenolic, carbonyl ester, acetyl, carboxylate, alkanes and carbonyl were participated in ion binding	[95]
ZnO and TiO_2 nanoparticles	*Serratia* sp., *Bacillus* sp., *Morganella* sp., *Citrobacter freundii and Lysinibacillus* sp.	ICP OES	• bacteria were able to gradually uptake nZnO and nTiO_2 in concentrations varying from 1 to 50 mg/L	[96]
Zn	XZN4 strain	UV–VIS, SEM, FT IR, flame AAS	• removal of zinc(II) by bacteria was single-molecule layer adsorption model take place Optimal removal rates were obtained at a pH between 5 and 6 and at pH 5 was 81.5% pH higher than 6 leads to stop the process due to starts metal oxide forming shriveled shape and crystal precipitation on the surface of particles peptidoglycan, polysaccharide, phospholipid, and other functional groups participate in sorption	[97]
Pb	*Gelidium amansii*	ICP OES, FT IR, SEM EDX,	• sorption optimum conditions: initial Pb^{2+} concentration of 200 mg/L, temperature 45 °C, pH 4.5, biomass of 1 g/L and contact time of 60 min carbonyl, methylene, phosphate, carbonate and phenolic groups participate in binding	[98]

Abbreviations: ICP OES inductively coupled plasma optical emission spectroscopy, EDX Energy-dispersive X-ray spectroscopy, flame AAS Atomic absorption spectroscopy with flame ionization source, 16S rRNA 16S ribosomal RNA, CLSM Confocal laser scanning microscopy.

techniques based on elemental spectroscopy or mass spectrometry (absorption and emission spectroscopy), mass spectrometry or X-ray fluorescence. The important feature to achieve sensitive elemental analysis at ultra-trace concentration level is choice of excitation sources; utilization of ICP (inductively coupled plasma) gives the most effective transfer process ofingle ions production from atoms [99] and using this ionization source gives possibility to characterize most of the elements. Flame or graphite furnace ionization techniques (especially used with AAS) could also be used; however, using these types of ionization sources is dedicated to quite higher element concentration in sample [100]. Samples in solid or liquid states of matter could be analyzed by sample introducing system selection; from the solid-state laser ablation introduction system connected to ionization source [101] or dissolved (as well as dispersed liquid state) sample by peristaltic pump.

5.1. Sample solubilization

The main task of carrying out the sample preparation stage by means of mineralization is to dissolve the sample and simplify the matrix by oxidation to simple compounds. Using highly efficient ICP excitation sources, it is theoretically possible to determine the quantification of the element in a sample's biological matrix without the prior process of effective mineralization (decomposition) of the sample. However, the analysis of the total content of the element together with carried out mineralization brings benefits because of reducing the carbon content in the sample, which reduces the subsequent matrix and drift effects [102]. The analysis of colloidal samples of a metallic nature also does not theoretically require mineralization if the particles are stably suspended in the medium and do not show too large sizes that could lead to clogging of the nebulizer. Moreover, sample mineralization with using concentrated inorganic acids brings many benefits. Acids with high metal dissolving and oxidizing power such as nitric acid (V) is a typical choice for the mineralization of Cu-Al layered double hydroxide materials [103] and other types of samples [104,105]. Nitric acid is commonly used as mixture with concentrated hydrochloric acid [77]. Fusion of sample with fluxes (for example $Li_2B_4O_7$ and $LiBO_2$) for determination of Fe, Al, Si, Ca, and Mg could be successfully used [106].

5.2. Sample preparation to SP ICP/MS

Another aspect is the preparation of the sample to the SP ICP/MS analysis. This specific technique can answer the total concentration of the element in the colloidal particles as well as the size of the colloid particles. Particle size determination using this technique can be beneficial for spherical particles. Sample preparation for SP ICP/MS requires suspension of the colloidal sample in a liquid that does not cause degradation of the colloid structure and the release of the element from the particles. Carful and adequate sample dilution is particularly

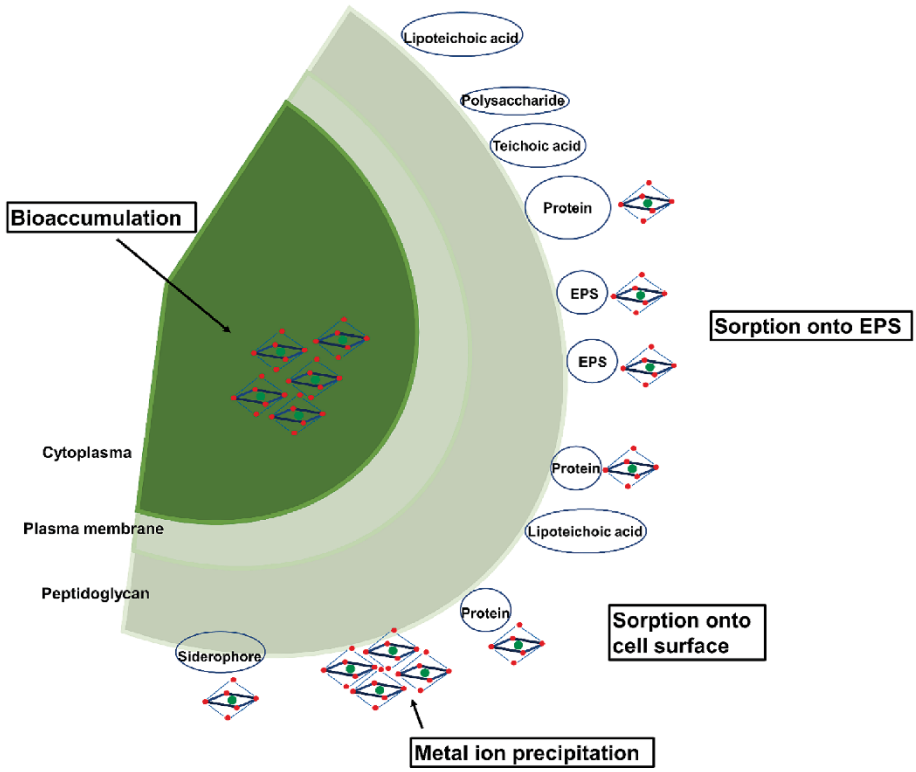

Fig. 7. Possible and collection of postulated in literature mechanisms of metal ion sorption onto bacteria.

important to characterize single particle during the analysis time [107]. Sample dispersed in ultra-pure water (spectral pure) is the most common medium if it provides stability and does not interfere with the analysis, such as ZnO NPs [108] and silica nanoparticle [109].

6. Separation and speciation of metal (bio)colloids by hyphenated techniques

Speciation is the section of analytical chemistry consisting of the determination of the forms of the element present in the sample and can be combined with quantitative analysis of these forms as well as identification and characterization of the new compounds in samples. The elements usually do not occur in an accessible form in a living organism but in a bound, complex form, and they could interact with colloidal compounds. The specific combination of the metal with the compound determines properties such as: solubility and thus bioavailability, diffusion or toxicological and other features [110]. An especially important issue is the study of speciation of metallic nanoparticles, especially of elements considered beneficial to the environment, harmful or toxic, to learn about these substances' toxicological and environmental consequees [111].

6.1. Speciation analysis

The stages of speciation analysis are as follows: defining the scope of research and the purpose, sampling, and preparation of the sample for analysis, followed by, in the classical approach of conducting speciation analysis, the separation of forms of an element is performed using separation techniques followed by detection of forms combined with their identification (especially important for forms of elements for which no standards are available or the sample matrix is different) [112]. Most chemical elements occur in the orgasms of the living in the form associated with ligands, but not all elements interact with biopolymers. The most common biopolymers are proteins and polysaccharides, whose monomers composed of functional groups containing S, N, and O atoms are often the metal ions' binding site[113]. The affinities of metal ions for particular atoms of a compound's coordination center can be interpreted, generalized, and predicted by the theory of hard and soft acids and bases (HSAB) [114]. Ions with electric charge dispersed onto highly ionic radius particles such Cu, Zn, Cd, Hg, Ag atoms have a special affinity for binding through S atoms (similarly high ionic radius and relatively low charge) of functional groups to proteins, while Mo, Mn, Fe, Co, Ni, Cu, Zn through O and N, while Ca, Sr, Ba, La, Pb with polysaccharides through oxygen atoms [113].

It should be emphasized that the speciation analysis performed by the mass spectrometry technique consisting in monitoring the signal at

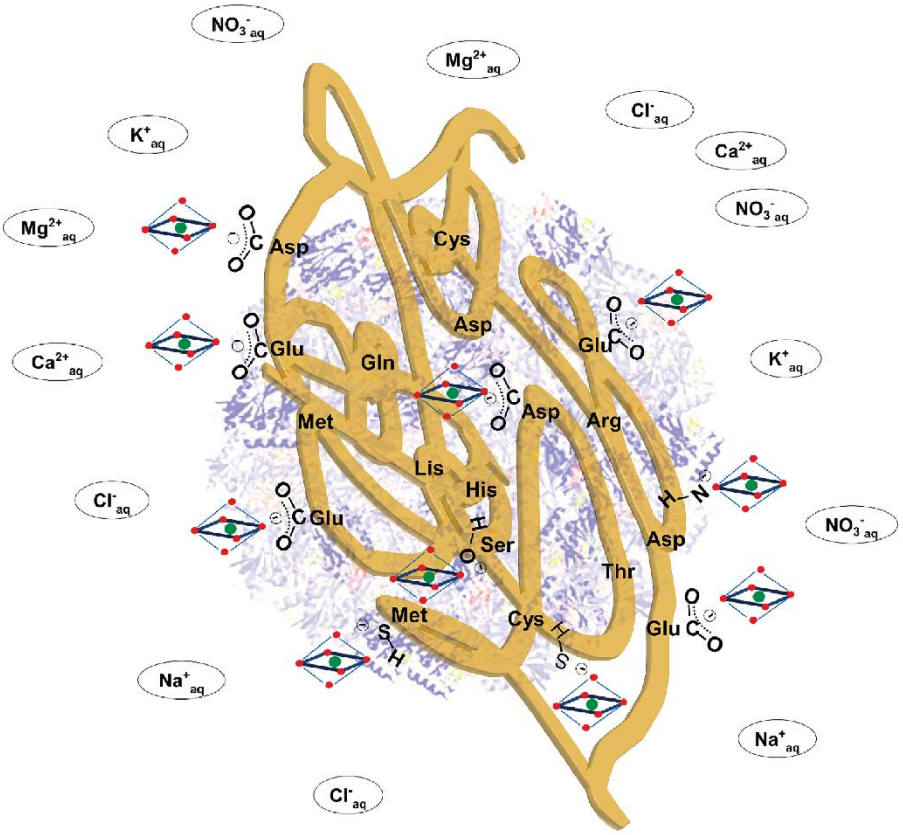

Fig. 8. Metal ions can interact with proteins through the presence of functional groups located in individual amino acid residues.

m/z 32, which corresponds to the measurement with singly ionized sulfur atoms with the highest abundance, is commonly used as a determinant to monitor biologically active substances containing sulfur. However, the analysis using the ICP/MS technique in a system with a single quadruple mass analyzer does not achieve the expected high sensitivity of the analysis due to the presence of an intense background signal coming from the polyatomic ion: $[^{16}O^{16}O]^{+}$. It has been shown that using a sector-type mass analyzer allows for significantly higher sensitivity analys of sulfur characterization [115].

With accordance with the HSAB theory, copper (I) cation has been determined to form complexes with human metallothionein (high sulfur content in peptide) [116]. Zn, Fe, S and P have been shown to accumulate most in bran and embryo organs and most of the Fe content is bound to P from phytic acid (myo-inositol-1,2,3,4,5,6-hexakisphosphate) (IP6) with $Fe_4(IP6)_{18}$ stoichiometry, in turn, most of the Zn is bound to S as 3 kDa compounds [117]. It was shown that, in direct competition, albumin-bound free fatty acids significantly decrease the binding capacity of albumin for Zn^{2+} [118]. Manganese, cadmium, copper, zinc and cobalt interact with 17–44 kDa in mass compounds in the young barley plant [119]. Lead was identified in the high-molecular fraction of pectin compounds through interactions with two main components homogalacturonan and rhamnogalacturonan I in plant samples (mostly by carboxylic residue) [120]. Also, in higher plants, the most frequently reported compound interacting with cadmium are phytochelatins (few calasses of oligopeptides of glutathione and cysteine amino acids- high nitrogen and sulfur content) [121]. Iron oxide (Fe_3O_4) nanoparticles size, elemental concentration and interaction with blood compounds were studied by coupled AF4 with ICP/MS techniques and it has been showed that particle radius of gyration increased from 15 to 28 nm to 40–120 nm as well as polydisperse index after mixing [122]. Gold nanoparticles in human plasma were studied using the CE-ICP/MS technique, where it was determined that albumin and transferrin are responsible to binding with nanoparticles [123]. The bioavailability of AgNPs to rat organs and its transformation were investigated and it has been shown that silver from AgNPs is present in the kidneys in a complex form with metallothionein, in turn, in the liver with proteins with masses from 25 kDa to 70 kDa [124].

Elemental detection using ICP/MS allows determiningltra-trace concentration of Ag from engineered nanoparticle in real samples (from 0.08 to 0.4 μg/L, depending on the Ag form and nanoparticle size) [125]. Application of SP ICP/MS for characterization of Ag and Au nanoparticles can answer the speciation in relation to the size of the

particles in the sample [126]. However, for the same samples, the use of AF4-MALS-ICP/MS gives the opportunity to characterize smaller and biggeranoparticles (wider analytical range of nanoparticles) [126]. Utilizing the AF4 technique to separate pectin-cadmium and pectin-copper complexes after gelation process showed creation of highly cross-linked gel structures and coupling AF4 with ICP/MS could be utilized as airect method to monitor cadmium and copper sorption kinetics [127]. AF4-MALS-ICP/MS allows to characterize particle size, conformation, molar mass, and element content in each fraction. Due to presence of semi-permeable membrane in AF4 channel the purification of sample from low molecular weight impurities (smaller than membrane pore) and/or biologically active form of species vs inactive form were obtained [40,128-130].

7. Concluding remarks and future perspective

The paper debates about selected analytical techniques used to determine parameters of particular importance for the characterization of colloidal particles of a biological and metallic nature.

Characterizing the particle size distribution of colloids is a complex process. The sample to be analyzed is preferably homogeneous, the dispersion in particle size present in the sample makes it difficult to obtain accurate results. The solutions used to obtain accurate results are discussed. The use of various techniques brings the possibility of obtaining complementary data regarding the size distribution as well as characterizing the shape of particles.

The phenomena at the interface (the surface of the particle of the dispersed phase and the dispersing phase) are of decisive importance when it comes to the phenomenon of stabilization of the colloid in the medium as well as the interaction of the colloidal particle with other elements and elements in the medium. The structure of the colloid according to the Gay-Chapman model of the diffusion layer and the resulting zeta-potential were discussed. The importance, determination of the distribution of values and the consequences (stability) of the existence of a charge between the Stern and diffusion layers were debated.

Discussions were undertaken on the possibility of sample preparation to characterize the content of elements in a colloidal particle as well as the particle size using a specific SP ICP/MS technique. An attempt was made to explain the mechanism of the interaction of colloidal particles with elements and to determine the forms of elements in the form associated with collides in a wide range of sample types.

Based on the analysis of the works, the influence of the polydispersion of the sample is visible. Therefore, it is recommended to take steps to analyze the most homogeneous systems to obtain accurate measurement results. The use of separation techniques is one of the most commonly used solutions to obtain a homogeneous sample for characterization. However, the nature of the sample, the electrokinetic potential of the system as well as the dependence on environmental/experimental variables (especially pH) and parameters associated with the analytical technique have an impact on the loss of time (often significant) of the sample during analysis and thus loss of information about the complete composition and properties of the sample. Therefore, it also seems reasonable to recommend optimizing, creating new analytical methods that allow for the highest possible selectivity, resolution as well as high recoveries.

One of the separation techniques directly dedicated to the analysis of colloidal compounds is the AF4 technique. Combining this separation technique with many different detection techniques simultaneously also gives a vast spectrum of possibilities for exploring and characterizing a colloidal system. The use of the features of this apparatus, such as the presence of a semi-permeable membrane, gives the possibility of sample purification as a filter, similarly to the use of special membranes during the dedicated stage of sample purification or solvent exchange. Therefore, it seems attractive to use this property to carry out an on-line process of sample purification with separation and characterization of particles, also of a metallic nature.

Declaration of Competing Interest

The authors declare that they have no known competing financial interests or personal relationships that could have appeared to influence the work reported in this paper.

Data availability

No data was used for the research described in the article.

Acknowledgement

The authors would like to extend your sincere thank to Dr. Viorica Railean-Plugaru from Centre for Modern Interdisciplinary Technologies, Faculty of Biological and Veterinary Sciences, Nicolaus Copernicus University in Torun, Poland for valuable contribution and help in the preparation, editing of the manuscript as well as designing and processing of the figures.

References

[1] T.S. Steenhuis, V.L. Morales, M.E. Cakmak, A.E. Salvucci, W. Zhang, Biocolloids: Transport and Retention in Soils, in: J. Gliński, J. Horabik, J. Lipiec (Eds.), Encyclopedia of Agrophysics, Springer, Netherlands, Dordrecht, 2011, pp. 66–70, https://doi.org/10.1007/978-90-481-3585-1_244.
[2] S. Jeong, G. Naidu, T. Leiknes, S. Vigneswaran, 4.3 Membrane Biofouling: Biofouling Assessment and Reduction Strategies in Seawater Reverse Osmosis Desalination, in: E. Drioli, L. Giorno, E. Fontananova (Eds.), Comprehensive Membrane Science and Engineering (Second Edition), Elsevier, Oxford, 2017, pp. 48–71, https://doi.org/https://doi.org/10.1016/B978-0-12-409547-2.12261-9.
[3] G. Wang, J.W. Swan, Surface heterogeneity affects percolation and gelation of colloids: dynamic simulations with random patchy spheres, Soft Matter 15 (2019) 5094–5108, https://doi.org/10.1039/c9sm00607a.
[4] J.F. Jones, J.D. Feick, D. Imoudu, N. Chukwumah, M. Vigeant, D. Velegol, Oriented adhesion of escherichia coli to polystyrene particles, Appl. Environ. Microbiol. 69 (2003) 6515–6519, https://doi.org/10.1128/AEM.69.11.6515-6519.2003.
[5] B. Buszewski, S. Bocian, A. Felinger, Artifacts in liquid-phase separations-system, solvent, and impurity peaks, Chem. Rev. 112 (2012) 2629–2641, https://doi.org/10.1021/cr200182j.
[6] A. Kurowska-Susdorf, M. Zwierżdżyński, A.M. Bevanda, S. Talić, A. Ivanković, J. Płotka-Wasylka, Green analytical chemistry: social dimension and teaching, TrAC Trends Anal. Chem. 111 (2019) 185–196, https://doi.org/10.1016/j.trac.2018.10.022.
[7] J. Płotka-Wasylka, W. Wojnowski, Complementary green analytical procedure index (ComplexGAPI) and software, Green Chem. 23 (2021) 8657–8665, https://doi.org/10.1039/D1GC02318G.
[8] J.J. Lietor-Santos, C. Kim, M.L. Lynch, A. Fernandez-Nieves, D.A. Weitz, The role of polymer polydispersity in phase separation and gelation in colloid-polymer mixtures, Langmuir 26 (2010) 3174–3178, https://doi.org/10.1021/la903127a.
[9] B. Chu, T. Liu, Characterization of nanoparticles by scattering techniques, 2000.
[10] F. Laborda, E. Bolea, J. Jiménez-Lamana, Single particle inductively coupled plasma mass spectrometry: a powerful tool for nanoanalysis, Anal. Chem. 86 (2014) 2270–2278, https://doi.org/10.1021/ac402980q.
[11] M. de Kanter, J. Meyer-Kirschner, J. Viell, A. Mitsos, M. Kather, A. Pich, C. Janzen, Enabling the measurement of particle sizes in stirred colloidal suspensions by embedding dynamic light scattering into an automated probe head, Measurement (Lond). 80 (2016) 92–98, https://doi.org/10.1016/j.measurement.2015.11.024.
[12] M. Kaszuba, D. McKnight, M.T. Connah, F.K. McNeil-Watson, U. Nobbmann, Measuring sub nanometre sizes using dynamic light scattering, J. Nanopart. Res. 10 (2008) 823–829, https://doi.org/10.1007/s11051-007-9317-4.
[13] A. Laycock, N.J. Clark, R. Clough, R. Smith, R.D. Handy, Determination of metallic nanoparticles in biological samples by single particle ICP-MS: a systematic review from sample collection to analysis, Environ. Sci. Nano 9 (2022) 420–453, https://doi.org/10.1039/d1en00680k.
[14] S. Lazzari, L. Nicoud, B. Jaquet, M. Lattuada, M. Morbidelli, Fractal-like structures in colloid science, Adv. Colloid Interface Sci. 235 (2016) 1–13, https://doi.org/10.1016/j.cis.2016.05.002.
[15] C. Comby-Zerbino, X. Dagany, F. Chirot, P. Dugourd, R. Antoine, R. Antoine, The emergence of mass spectrometry for characterizing nanomaterials at atomically precise nanoclusters and beyond, Mater Adv. 2 (2021) 4896–4913, https://doi.org/10.1039/d1ma00261a.
[16] A. Gołębiowski, P. Pomastowski, A. Rodzik, A. Król-Górniak, T. Kowalkowski, M. Górecki, B. Buszewski, Isolation and self-association studies of beta-lactoglobulin, Int. J. Mol. Sci. 21 (2020) 1–21, https://doi.org/10.3390/ijms21249711.
[17] D.M. Meunier, J.W. Lyons, J.J. Kiefer, Q.J. Niu, L.M. DeLong, Y. Li, P.S. Russo, R. Cueto, N.J. Edwin, K.J. Bouck, H.C. Silvis, C.J. Tucker, T.H. Kalantar,

Determination of particle size distributions, molecular weight distributions, swelling, conformation, and morphology of dilute suspensions of cross-linked polymeric nanoparticles via size-exclusion chromatography/differential viscometry, Macromolecules 47 (2014) 6715–6729, https://doi.org/10.1021/ma501420z.
[18] U. Nobbmann, A. Morfesis, Light scattering and nanoparticles, Mater. Today 12 (2009) 52–54, https://doi.org/10.1016/S1369-7021(09)70164-6.
[19] K. Haydukivska, V. Blavatska, J. Paturej, Universal size ratios of Gaussian polymers with complex architecture: radius of gyration vs hydrodynamic radius, Sci. Rep. 10 (2020), https://doi.org/10.1038/s41598-020-70649-z.
[20] A. Bootz, V. Vogel, D. Schubert, J. Kreuter, Comparison of scanning electron microscopy, dynamic light scattering and analytical ultracentrifugation for the sizing of poly(butyl cyanoacrylate) nanoparticles, Eur. J. Pharm. Biopharm. 57 (2004) 369–375, https://doi.org/10.1016/S0939-6411(03)00193-0.
[21] S.B. Rice, C. Chan, S.C. Brown, P. Eschbach, L. Han, D.S. Ensor, A.B. Stefaniak, J. Bonevich, A.E. Vladár, A.R.H. Walker, J. Zheng, C. Starnes, A. Stromberg, J. Ye, E.A. Grulke, Particle size distributions by transmission electron microscopy: an interlaboratory comparison case study, Metrologia 50 (2013) 663–678, https://doi.org/10.1088/0026-1394/50/6/663.
[22] T.G.F. Souza, V.S.T. Ciminelli, N.D.S. Mohallem, A comparison of TEM and DLS methods to characterize size distribution of ceramic nanoparticles, J. Phys. Conf. Ser. 733 (2016) 012039.
[23] A. Kim, W.B. Ng, W. Bernt, N.J. Cho, Validation of size estimation of nanoparticle tracking analysis on polydisperse macromolecule assembly, Sci. Rep. 9 (2019), https://doi.org/10.1038/s41598-019-38915-x.
[24] F. Caputo, A. Arnould, M. Bacia, W.L. Ling, E. Rustique, I. Texier, A.P. Mello, A. C. Couffin, Measuring particle size distribution by asymmetric flow field flow fractionation: a powerful method for the preclinical characterization of lipid-based nanoparticles, Mol. Pharm. 16 (2019) 756–767, https://doi.org/10.1021/acs.molpharmaceut.8b01033.
[25] P. Arenas-Guerrero, Á.V. Delgado, K.J. Donovan, K. Scott, T. Bellini, F. Mantegazza, M.L. Jiménez, Determination of the size distribution of non-spherical nanoparticles by electric birefringence-based methods, Sci. Rep. 8 (1) (2018), https://doi.org/10.1038/s41598-018-27840-0.
[26] K. Kogej, D. Božič, B. Kobal, M. Herzog, K. Černe, Application of dynamic and static light scattering for size and shape characterization of small extracellular nanoparticles in plasma and ascites of ovarian cancer patients, Int. J. Mol. Sci. 22 (23) (2021) 12946.
[27] P. Iavicoli, P. Urbán, A. Bella, M.G. Ryadnov, F. Rossi, L. Calvolai, Application of asymmetric flow field-flow fractionation hyphenations for liposome-antimicrobial peptide interaction, J. Chromatogr. A 1422 (2015) 260–269, https://doi.org/10.1016/j.chroma.2015.10.029.
[28] A.v. Malm, J.C.W. Corbett, Improved dynamic light scattering using an adaptive and statistically driven time resolved treatment of correlation data, Sci. Rep. 9 (2019) 13519, https://doi.org/10.1038/s41598-019-50077-4.
[29] L.M.T. Ramirez, C. Rihouey, F. Chaubet, D. Le Cerf, L. Picton, Characterization of dextran particle size: how frit-inlet asymmetrical flow field-flow fractionation (FI-AF4) coupled online with dynamic light scattering (DLS) leads to enhanced size distribution, J. Chromatogr. A 1653 (2021) 462404.
[30] C.M. Hoo, N. Starostin, P. West, M.L. Mecartney, A comparison of atomic force microscopy (AFM) and dynamic light scattering (DLS) methods to characterize nanoparticle size distributions, J. Nanopart. Res. 10 (2008) 89–96, https://doi.org/10.1007/s11051-008-9435-7.
[31] A. Scotti, W. Liu, J.S. Hyatt, E.S. Herman, H.S. Choi, J.W. Kim, L.A. Lyon, U. Gasser, A. Fernandez-Nieves, The CONTIN algorithm and its application to determine the size distribution of microgel suspensions, J. Chem. Phys. 142 (23) (2015) 234905.
[32] K. Franks, V. Kestens, A. Braun, G. Roebben, T.P.J. Linsinger, Non-equivalence of different evaluation algorithms to derive mean particle size from dynamic light scattering data, J. Nanopart. Res. 21 (2019), https://doi.org/10.1007/s11051-019-4630-2.
[33] R. Ragheb, U. Nobbmann, Multiple scattering effects on intercept, size, polydispersity index, and intensity for parallel (VV) and perpendicular (VH) polarization detection in photon correlation spectroscopy, Sci. Rep. 10 (2020), https://doi.org/10.1038/s41598-020-78872-4.
[34] D.J. Slotboom, R.H. Duurkens, K. Olieman, G.B. Erkens, Static light scattering to characterize membrane proteins in detergent solution, Methods 46 (2008) 73–82, https://doi.org/10.1016/j.ymeth.2008.06.012.
[35] H. Amartely, O. Avraham, A. Friedler, O. Livnah, M. Lebendiker, Coupling multi angle light scattering to ion exchange chromatography (iex-mals) for protein characterization, Sci. Rep. 8 (2018), https://doi.org/10.1038/s41598-018-25246-6.
[36] C. Velours, J. Zhou, P. Zecchin, N. He, M. Salameh, M.-P. Golinelli-Cohen, B. Golinelli-Pimpaneau, Determination of the absolute molar mass of [fe-s]-containing proteins using size exclusion chromatography-multi-angle light scattering (SEC-MALS), Biomolecules 12 (2) (2022) 270.
[37] M. Marioli, W.T. Kok, Recovery, overloading, and protein interactions in asymmetrical flow field-flow fractionation, Anal. Bioanal. Chem. 411 (2019) 2327–2338, https://doi.org/10.1007/s00216-019-01673-w.
[38] C. Bayart, E. Jean, M. Paillagot, A. Renoud, A. Raillard, J. Paladino, M. le Borgne, Comparison of SEC and AF4 analytical tools for size estimation of typhoid Vi polysaccharides, Anal. Methods 11 (2019) 4851–4858, https://doi.org/10.1039/c9ay00145j.
[39] I.K. Ventouri, A. Astefanei, E.R. Kaal, R. Haselberg, G.W. Somsen, P. J. Schoenmakers, Asymmetrical flow field-flow fractionation to probe the dynamic association equilibria of β-D-galactosidase, J. Chromatogr. A 1635 (2021) 461719.
[40] M. Marioli, W.T. Kok, Continuous asymmetrical flow field-flow fractionation for the purification of proteins and nanoparticles, Sep. Purif. Technol. 242 (2020) 116744.
[41] B. Meisterjahn, S. Wagner, F. von der Kammer, D. Hennecke, T. Hofmann, Silver and gold nanoparticle separation using asymmetrical flow-field flow fractionation: Influence of run conditions and of particle and membrane charges, J. Chromatogr. A 1440 (2016) 150–159, https://doi.org/10.1016/j.chroma.2016.02.059.
[42] B. Moreira-Alvarez, A.L. Larraga-Urdaz, A. Fuentes-Cervantes, M.L. Fernandez-Sánchez, J.M. Costa-Fernández, J.R. Encinar, AF4-UV/VIS-MALS-ICPMS/MS for the characterization of the different nanoparticulated species present in oligonucleotide-gold nanoparticle conjugates, Talanta 256 (2023) 124309.
[43] P. Sennett, J.P. Olivier, Colloidal dispersions, electrokinetic effects, and the concept of zeta potential, Ind. Eng. Chem. 57 (8) (1965) 32–50.
[44] C. Schreuer, S. Vandewiele, T. Brans, F. Strubbe, K. Neyts, F. Beunis, Single charging events on colloidal particles in a nonpolar liquid with surfactant, J. Appl. Phys. 123 (1) (2018) 015105.
[45] M.H. Derkani, A.J. Fletcher, M. Fedorov, W. Abdallah, B. Sauerer, J. Anderson, Z. J. Zhang, Mechanisms of surface charge modification of carbonates in aqueous electrolyte solutions, Colloids and Interfaces. 3 (4) (2019) 62.
[46] C. Cano-Sarmiento, D.I. Téllez-Medina, R. Viveros-Contreras, M. Cornejo-Mazón, C.Y. Figueroa-Hernández, E. García-Armenta, L. Alamilla-Beltrán, H.S. García, G. F. Gutiérrez-López, Zeta potential of food matrices, Food Eng. Rev. 10 (2018) 113–138, https://doi.org/10.1007/s12393-018-9176-z.
[47] B. Buszewski, P. Pomastowski, Wpływ heterogeniczności powierzchni biokoloidów na ich rozdzielanie elektroforetyczne, Wiad Chem. 69 (2015) 823–846. https://www.scopus.com/inward/record.uri?eid=2-s2.0-85033405372&partnerID=40&md5=094e4195cae80f7621d531ba875db705.
[48] G.V. Lowry, R.J. Hill, S. Harper, A.F. Rawle, C.O. Hendren, F. Klaessig, U. Nobbmann, P. Sayre, J. Rumble, Guidance to improve the scientific value of zeta-potential measurements in nanoEHS, Environ. Sci. Nano 3 (5) (2016) 953–965.
[49] M.A. Brown, Z. Abbas, A. Kleibert, R.G. Green, A. Goel, S. May, T.M. Squires, Determination of surface potential and electrical double-layer structure at the aqueous electrolyte-nanoparticle interface, Phys. Rev. X 6 (2016), https://doi.org/10.1103/PhysRevX.6.011007.
[50] M.A. Brown, A. Goel, Z. Abbas, Effect of electrolyte concentration on the stern layer thickness at a charged interface, Angew. Chem. 128 (2016) 3854–3858, https://doi.org/10.1002/ange.201512025.
[51] J.W. Swan, E.M. Furst, A simpler expression for Henry's function describing the electrophoretic mobility of spherical colloids, J. Colloid Interface Sci. 388 (2012) 92–94, https://doi.org/10.1016/j.jcis.2012.08.026.
[52] T.L. Doane, C.H. Chuang, R.J. Hill, C. Burda, Nanoparticle ζ -potentials, Acc. Chem. Res. 45 (2012) 317–326, https://doi.org/10.1021/ar200113c.
[53] W.W. Wilson, M.M. Wade, S.C. Holman, F.R. Champlin, Status of methods for assessing bacterial cell surface charge properties based on zeta potential measurements, J. Microbiol. Methods 43 (2001) 153–164, https://doi.org/10.1016/s0167-7012(00)00224-4.
[54] A.L. Polaczyk, J.E. Amburgey, A. Alansari, J.C. Poler, M. Propato, V.R. Hill, Calculation and uncertainty of zeta potentials of microorganisms in a 1:1 electrolyte with a conductivity similar to surface water, Colloids Surf A Physicochem Eng Asp 586 (2020) 124097.
[55] B. Klasczyk, V. Knecht, R. Lipowsky, R. Dimova, Interactions of alkali metal chlorides with phosphatidylcholine vesicles, Langmuir 26 (2010) 18951–18958, https://doi.org/10.1021/la103631y.
[56] D.J. Pochapski, C. Carvalho Dos Santos, G.W. Leite, S.H. Pulcinelli, C.V. Santilli, Zeta potential and colloidal stability predictions for inorganic nanoparticle dispersions: effects of experimental conditions and electrokinetic models on the interpretation of results, Langmuir 37 (2021) 13379–13389, https://doi.org/10.1021/acs.langmuir.1c02056.
[57] M.G. Carneiro-Da-Cunha, M.A. Cerqueira, B.W.S. Souza, J.A. Teixeira, A. A. Vicente, Influence of concentration, ionic strength and pH on zeta potential and mean hydrodynamic diameter of edible polysaccharide solutions envisaged for multinanolayered films production, Carbohydr. Polym. 85 (2011) 522–528, https://doi.org/10.1016/j.carbpol.2011.03.001.
[58] A. Król-Górniak, V. Railean, P. Pomastowski, T. Płociński, M. Gloc, R. Dobrucka, K.J. Kurzydłowski, B. Buszewski, Comprehensive study upon physicochemical properties of bio-ZnO NCs, Sci. Rep. 13 (2023), https://doi.org/10.1038/s41598-023-27564-w.
[59] A. Rogowska, P. Pomastowski, M. Złoch, V. Railean-Plugaru, A. Król, K. Rafińska, M. Szultka-Młyńska, B. Buszewski, The influence of different pH on the electrophoretic behaviour of saccharomyces cerevisiae modified by calcium ions, Sci. Rep. 8 (2018), https://doi.org/10.1038/s41598-018-25024-4.
[60] A. Rodzik, P. Pomastowski, V. Railean-Plugaru, M. Sprynskyy, B. Buszewski, The study of zinc ions binding to αS1-, β-and κ-casein, Int. J. Mol. Sci. 21 (2020) 1–18, https://doi.org/10.3390/ijms21218096.
[61] S. Świątek, P. Komorek, G. Turner, B. Jachimska, β-Lactoglobulin as a potential carrier for bioactive molecules, Bioelectrochemistry 126 (2019) 137–145, https://doi.org/10.1016/j.bioelechem.2018.12.006.
[62] L.C.d. Oliveira, J.R. Barbosa, S.d.C.A. Ribeiro, M.A.M.d. Vasconcelos, B.A. d. Aguiar, G.V.d.S. Pereira, G.A. Albuquerque, F.N.L.d. Silva, R.L. Crizel, P. H. Campelo, L.d.F.H. Lourenço, Improvement of the characteristics of fish gelatin – gum arabic through the formation of the polyelectrolyte complex, Carbohydr. Polym. 223 (2019) 115068.

[63] S.H. Chang, H.T.V. Lin, G.J. Wu, G.J. Tsai, pH Effects on solubility, zeta potential, and correlation between antibacterial activity and molecular weight of chitosan, Carbohydr. Polym. 134 (2015) 74–81, https://doi.org/10.1016/j.carbpol.2015.07.072.
[64] E. Ofir, Y. Oren, A. Adin, Electroflocculation: the effect of zeta-potential on particle size, Desalination 204 (2007) 33–38, https://doi.org/10.1016/j.desal.2006.03.533.
[65] M.K.A. Ali, H. Xianjun, Colloidal stability mechanism of copper nanomaterials modified by ionic liquid dispersed in polyalphaolefin oil as green nanolubricants, J. Colloid Interface Sci. 578 (2020) 24–36, https://doi.org/10.1016/j.jcis.2020.05.092.
[66] O.G. Jones, U. Lesmes, P. Dubin, D.J. McClements, Effect of polysaccharide charge on formation and properties of biopolymer nanoparticles created by heat treatment of β-lactoglobulin-pectin complexes, Food Hydrocoll. 24 (2010) 374–383, https://doi.org/10.1016/j.foodhyd.2009.11.003.
[67] L. Wu, Q. Yue, M. Kang, M. Zhong, B. Qi, Y. Li, Stabilization of soybean and peanut oil bodies using apple pectin under acidic conditions, Colloids Surf A Physicochem Eng Asp 655 (2022) 130263.
[68] F. Pir Cakmak, A.T. Grigas, C.D. Keating, Lipid Vesicle-Coated Complex Coacervates, Langmuir 35 (2019) 7830–7840, https://doi.org/10.1021/acs.langmuir.9b00213.
[69] H. Espinosa-Andrews, K.E. Enríquez-Ramírez, E. García-Márquez, C. Ramírez-Santiago, C. Lobato-Calleros, J. Vernon-Carter, Interrelationship between the zeta potential and viscoelastic properties in coacervates complexes, Carbohydr. Polym. 95 (2013) 161–166, https://doi.org/10.1016/j.carbpol.2013.02.053.
[70] P. Pomastowski, M. Sprynskyy, P. Zuvela, K. Rafińska, M. Milanowski, J.J. Liu, M. Yi, B. Buszewski, Silver-Lactoferrin Nanocomplexes as a Potent Antimicrobial Agent, J. Am. Chem. Soc. 138 (2016) 7899–7909, https://doi.org/10.1021/jacs.6b02699.
[71] B. Kang, H. Tang, Z. Zhao, S. Song, Hofmeister series: insights of ion specificity from amphiphilic assembly and interface property, ACS Omega 5 (2020) 6229–6239, https://doi.org/10.1021/acsomega.0c00237.
[72] Y. Zhang, P.S. Cremer, Interactions between macromolecules and ions: the Hofmeister series, Curr. Opin. Chem. Biol. 10 (2006) 658–663, https://doi.org/10.1016/j.cbpa.2006.09.020.
[73] C.A. Ericsson, O. Söderman, V.M. Garamus, M. Bergström, S. Ulvenlund, Effects of temperature, salt, and deuterium oxide on the self-aggregation of alkylglycosides in dilute solution. 1. n-Nonyl-β-D-glucoside, Langmuir. 20 (2004) 1401–1408, https://doi.org/10.1021/la035613e.
[74] M. Boström, D.F. Parsons, A. Salis, B.W. Ninham, M. Monduzzi, Possible origin of the inverse and direct hofmeister series for lysozyme at low and high salt concentrations, Langmuir 27 (2011) 9504–9511, https://doi.org/10.1021/la202023r.
[75] M.V. Manilo, N.I. Lebovka, S. Barany, Effects of sort and concentration of salts on the electrosurface properties of aqueous suspensions containing hydrophobic and hydrophilic particles: validity of the Hofmeister series, J. Mol. Liq. 276 (2019) 875–884.
[76] C. Moreno-Castilla, Á. Naranjo, M. Victoria López-Ramón, E. Siles, J.J. López-Peñalver, J.M.R. de Almodóvar, Influence of the hydrodynamic size and ξ potential of manganese ferrite nanozymes as peroxidase-mimicking catalysts at pH 4 in different buffers, J. Catal. 414 (2022) 179–185, https://doi.org/10.1016/j.jcat.2022.09.010.
[77] B. Buszewski, A. Rodzik, V. Railean-Plugaru, M. Sprynskyy, P. Pomastowski, A study of zinc ions immobilization by β-lactoglobulin, Colloids Surf. A Physicochem Eng. Asp. 591 (2020), 124443, https://doi.org/10.1016/j.colsurfa.2020.124443.
[78] S. Salgin, U. Salgin, S. Bahadir, Zeta potentials and isoelectric points of biomolecules: the effects of ion types and ionic strengths, accessed April 28, 2023, Int. J. Electrochem. Sci. 7 (2012) 12404–12414, http://www.electrochemsci.org/papers/vol7/71212404.pdf.
[79] R. Marsalek, Particle size and zeta potential of ZnO, APCBEE Proc. 9 (2014) 13–17, https://doi.org/10.1016/j.apcbee.2014.01.003.
[80] Y. Tao, J. Ma, C. Huang, C. Lai, Z. Ling, Q. Yong, Effects of the Hofmeister anion series salts on the rheological properties of Sesbania cannabina galactomannan, Int. J. Biol. Macromol. 188 (2021) 350–358, https://doi.org/10.1016/j.ijbiomac.2021.08.030.
[81] R. Prathapan, R. Thapa, G. Garnier, R.F. Tabor, Modulating the zeta potential of cellulose nanocrystals using salts and surfactants, Colloids Surf A Physicochem Eng Asp 509 (2016) 11–18, https://doi.org/10.1016/j.colsurfa.2016.08.075.
[82] N. Abid, A.M. Khan, S. Shujait, K. Chaudhary, M. Ikram, M. Imran, J. Haider, M. Khan, Q. Khan, M. Maqbool, Synthesis of nanomaterials using various top-down and bottom-up approaches, influencing factors, advantages, and disadvantages: a review, Adv. Colloid Interface Sci. 300 (2022) 102597.
[83] S. Barber-Zucker, B. Shaanan, R. Zarivach, Transition metal binding selectivity in proteins and its correlation with the phylogenomic classification of the cation diffusion facilitator protein family, Sci. Rep. 7 (2017), https://doi.org/10.1038/s41598-017-16777-5.
[84] J.B. Fein, C.J. Daughney, N. Yee, T.A. Davis, A chemical equilibrium model for metal adsorption onto bacterial surfaces, Geochim. Cosmochim. Acta 61 (1997) 3319–3328, https://doi.org/10.1016/S0016-7037(97)00166-X.
[85] Y.L. Li, M. Xin, D. Xie, S. Fan, J. Ma, K. Liu, F. Yu, Variation in extracellular polymeric substances from enterobacter sp. and their pb 2+ adsorption behaviors, ACS Omega 6 (14) (2021) 9617–9628.
[86] N. Yee, J. Fein, Cd adsorption onto bacterial surfaces: a universal adsorption edge? Geochim. Cosmochim. Acta 65 (2001) 2037–2042, https://doi.org/10.1016/S0016-7037(01)00587-7.
[87] A. Fathollahi, N. Khasteganan, S.J. Coupe, A.P. Newman, A meta-analysis of metal biosorption by suspended bacteria from three phyla, Chemosphere 268 (2021) 129290.
[88] P. Gupta, B. Diwan, Bacterial Exopolysaccharide mediated heavy metal removal: a Review on biosynthesis, mechanism and remediation strategies, Biotechnol. Rep. 13 (2017) 58–71, https://doi.org/10.1016/j.btre.2016.12.006.
[89] Z.-B. Yue, Q. Li, C.-C. Li, T.-h. Chen, J. Wang, Component analysis and heavy metal adsorption ability of extracellular polymeric substances (EPS) from sulfate reducing bacteria, Bioresour. Technol. 194 (2015) 399–402.
[90] N. Li, J. Liu, R. Yang, L. Wu, Distribution, characteristics of extracellular polymeric substances of Phanerochaete chrysosporium under lead ion stress and the influence on Pb removal, Sci. Rep. 10 (2020), https://doi.org/10.1038/s41598-020-74983-0.
[91] D. Liu, Z. Li, W. Li, Z. Zhong, J. Xu, J. Ren, Z. Ma, Adsorption behavior of heavy metal ions from aqueous solution by soy protein hollow microspheres, Ind. Eng. Chem. Res. 52 (2013) 11036–11044, https://doi.org/10.1021/ie401092f.
[92] A. Choińska-Pulit, J. Sobolczyk-Bednarek, W. Łaba, Optimization of copper, lead and cadmium biosorption onto newly isolated bacterium using a Box-Behnken design, Ecotoxicol. Environ. Saf. 149 (2018) 275–283, https://doi.org/10.1016/j.ecoenv.2017.12.008.
[93] O.A. Oyewole, S.S.L.T. Zobeashia, E.O. Oladoja, R.O. Raji, E.E. Odiniya, A. M. Musa, Biosorption of heavy metal polluted soil using bacteria and fungi isolated from soil, SN Appl Sci. 1 (2019), https://doi.org/10.1007/s42452-019-0879-4.
[94] W. Mwandira, K. Nakashima, S. Kawasaki, A. Arabelo, K. Banda, I. Nyambe, M. Chirwa, M. Ito, T. Sato, T. Igarashi, H. Nakata, S. Nakayama, M. Ishizuka, Biosorption of Pb (II) and Zn (II) from aqueous solution by Oceanobacillus profundus isolated from an abandoned mine, Sci. Rep. 10 (2020), https://doi.org/10.1038/s41598-020-78187-4.
[95] N.E.A. El-Naggar, A.Y. El-khateeb, A.A. Ghoniem, M.S. El-Hersh, W.E.I.A. Saber, Innovative low-cost biosorption process of Cr6— by Pseudomonas alcaliphila NEWG-2, Sci. Rep. 10 (2020), https://doi.org/10.1038/s41598-020-70473-5.
[96] V. Weber, I. Kamika, M.N.B. Momba, Comparing the effect of zinc oxide and titanium dioxide nanoparticles on the ability of moderately halophilic bacteria to treat wastewater, Sci. Rep. 11 (2021), https://doi.org/10.1038/s41598-021-96413-5.
[97] J. Huang, J. Wang, L. Jia, Removal of zinc(II) from livestock and poultry sewage by a zinc(II) resistant bacteria, Sci. Rep. 10 (2020), https://doi.org/10.1038/s41598-020-78138-x.
[98] N.E.A. El-Naggar, R.A. Hamouda, I.E. Mousa, M.S. Abdel-Hamid, N.H. Rabei, Biosorption optimization, characterization, immobilization and application of Gelidium amansii biomass for complete Pb2— removal from aqueous solutions, Sci. Rep. 8 (2018), https://doi.org/10.1038/s41598-018-31660-7.
[99] A.A. Ammann, Inductively coupled plasma mass spectrometry (ICP MS): A versatile tool, J. Mass Spectrom. 42 (2007) 419–427, https://doi.org/10.1002/jms.1206.
[100] V. Yeung, D.D. Miller, M.A. Rutzke, Atomic Absorption Spectroscopy, Atomic Emission Spectroscopy, and Inductively Coupled Plasma-Mass Spectrometry, in: S.S. Nielsen (Ed.), Food Analysis, Springer International Publishing, Cham, 2017, pp. 129–150, https://doi.org/10.1007/978-3-319-45776-5_9.
[101] N.L. Lahaye, S.S. Harilal, P.K. Diwakar, A. Hassanein, Characterization of laser ablation sample introduction plasma plumes in fs-LA-ICP-MS, J. Anal. At. Spectrom 29 (2014) 2267–2274, https://doi.org/10.1039/c4ja00200h.
[102] S. Liu, Z. Han, X. Kong, J. Zhang, Z. Lv, G. Yuan, Organic matrix effects in inductively coupled plasma mass spectrometry: a tutorial review, Appl. Spectrosc. Rev. 57 (2022) 461–489, https://doi.org/10.1080/05704928.2021.1897991.
[103] G. Layrac, S. Harrisson, M. Destarac, C. Gérardin, D. Tichit, Comprehensive study of the formation of stable colloids of Cu[sbnd]Al layered double hydroxide assisted by double hydrophilic block copolymers, Appl. Clay Sci. 193 (2020), https://doi.org/10.1016/j.clay.2020.105673.
[104] W. Bartz, M. Górka, J. Rybak, R. Rutkowski, A. Stojanowska, The assessment of effectiveness of SEM- EDX and ICP-MS methods in the process of determining the mineralogical and geochemical composition of particulate matter deposited on spider webs, Chemosphere 278 (2021) 130454.
[105] F. Laborda, J. Jiménez-Lamana, E. Bolea, J.R. Castillo, Selective identification, characterization and determination of dissolved silver(i) and silver nanoparticles based on single particle detection by inductively coupled plasma mass spectrometry, J. Anal. At. Spectrom 26 (2011) 1362–1371, https://doi.org/10.1039/c0ja00098a.
[106] N. Tang, N. Siebers, P. Leinweber, K.U. Eckhardt, S. Dultz, V. Nischwitz, E. Klumpp, Implications of free and occluded fine colloids for organic matter preservation in arable soils, Environ. Sci. Tech. 56 (2022) 14133–14145, https://doi.org/10.1021/acs.est.2c01973.
[107] N.D. Donahue, E.R. Francek, E. Kiyotake, E.E. Thomas, W. Yang, L. Wang, M. S. Detamore, S. Wilhelm, Assessing nanoparticle colloidal stability with single-particle inductively coupled plasma mass spectrometry (SP-ICP-MS), Anal. Bioanal. Chem. 412 (2020) 5205–5216, https://doi.org/10.1007/s00216-020-02783-6.
[108] L. Fréchette-Viens, M. Hadioui, K.J. Wilkinson, Quantification of ZnO nanoparticles and other Zn containing colloids in natural waters using a high sensitivity single particle ICP-MS, Talanta 200 (2019) 156–162, https://doi.org/10.1016/j.talanta.2019.03.041.
[109] M.D. Montaño, B.J. Majestic, Å.K. Jämting, P. Westerhoff, J.F. Ranville, Methods for the detection and characterization of silica colloids by microsecond spICP-MS, Anal. Chem. 88 (2016) 4733–4741, https://doi.org/10.1021/acs.analchem.5b04924.

[110] D.M. Templeton, The importance of trace element speciation in biomedical science, Anal. Bioanal. Chem. 375 (8) (2003) 1062–1066.
[111] M. Auffan, J. Rose, M.R. Wiesner, J.Y. Bottero, Chemical stability of metallic nanoparticles: a parameter controlling their potential cellular toxicity in vitro, Environ. Pollut. 157 (2009) 1127–1133, https://doi.org/10.1016/j.envpol.2008.10.002.
[112] B. Michalke, Element speciation definitions, analytical methodology, and some examples, Ecotoxicol. Environ. Saf. 56 (2003) 122–139, https://doi.org/10.1016/S0147-6513(03)00056-3.
[113] J. Szpunar, R. Lobinski, A. Prange, Hyphenated techniques for elemental speciation in biological systems, Appl. Spectrosc. 57 (2003) 102A–112A, https://doi.org/10.1366/000370203321558128.
[114] H. Xu, D.C. Xu, Y. Wang, Natural indices for the chemical hardness/softness of metal cations and ligands, ACS Omega 2 (2017) 7185–7193, https://doi.org/10.1021/acsomega.7b01039.
[115] S. Studzińska, S. Mounicou, J. Szpunar, R. Łobiński, B. Buszewski, New approach to the determination phosphorothioate oligonucleotides by ultra high performance liquid chromatography coupled with inductively coupled plasma mass spectrometry, Anal. Chim. Acta 855 (2015) 13–20, https://doi.org/10.1016/j.aca.2014.12.010.
[116] A. Melenbacher, N.C. Korkola, M.J. Stillman, The pathways and domain specificity of Cu(i) binding to human metallothionein 1A, Metallomics 12 (2020) 1951–1964, https://doi.org/10.1039/D0MT00215A.
[117] D.P. Persson, T.H. Hansen, K.H. Laursen, J.K. Schjoerring, S. Husted, Simultaneous iron, zinc, sulfur and phosphorus speciation analysis of barley grain tissues using SEC-ICP-MS and IP-ICP-MS, Metallomics 1 (2009) 418–426, https://doi.org/10.1039/B905688B.
[118] J.P.C. Coverdale, J.P. Barnett, A.H. Adamu, E.J. Griffiths, A.J. Stewart, C. A. Blindauer, A metalloproteomic analysis of interactions between plasma proteins and zinc: elevated fatty acid levels affect zinc distribution, Metallomics 11 (2019) 1805–1819, https://doi.org/10.1039/C9MT00177H.
[119] L. Ruzik, A. Dyoniziak, Natural deep eutectic solvents as a key metal extractant for fractionation in speciation analysis, Molecules 27 (3) (2022) 1063.
[120] K. Poleć-Pawlak, R. Ruzik, E. Lipiec, M. Ciurzyńska, H. Gawrońska, Investigation of Pb(ii) binding to pectin in arabidopsis thaliana, J. Anal. At. Spectrom 22 (2007) 968–972, https://doi.org/10.1039/b704157h.
[121] Y. Zhao, M. Gouda, G. Yu, C. Zhang, L. Lin, P. Nie, W. Huang, H. Ye, Y. Ye, C. Zhou, Y. He, Analyzing cadmium-phytochelatin2 complexes in plant using terahertz and circular dichroism information, Ecotoxicol. Environ. Saf. 225 (2021) 112800.
[122] K.C. Nwoko, A. Raab, L. Cheyne, D. Dawson, E. Krupp, J. Feldmann, Matrix-dependent size modifications of iron oxide nanoparticles (Ferumoxytol) spiked into rat blood cells and plasma: characterisation with TEM, AF4-UV-MALS-ICP-MS/MS and spICP-MS, J. Chromatogr. B Anal. Technol. Biomed. Life Sci. 1124 (2019) 356–365, https://doi.org/10.1016/j.jchromb.2019.06.029.
[123] M. Matczuk, K. Anecka, F. Scaletti, L. Messori, B.K. Keppler, A.R. Timerbaev, M. Jarosz, Speciation of metal-based nanomaterials in human serum characterized by capillary electrophoresis coupled to ICP-MS: a case study of gold nanoparticles, Metallomics 7 (2015) 1364–1370, https://doi.org/10.1039/c5mt00109a.
[124] J. Jiménez-Lamana, F. Laborda, E. Bolea, I. Abad-Álvaro, J.R. Castillo, J. Bianga, M. Ho, K. Bierla, S. Mounicou, L. Ouerdane, S. Gaillet, J.-M. Rouanet, J. Szpunar, An insight into silver nanoparticles bioavailability in rats, Metallomics 6 (2014) 2242–2249, https://doi.org/10.1039/c4mt00200h.
[125] J. Soto-Alvaredo, M. Montes-Bayón, J. Bettmer, Speciation of silver nanoparticles and silver(I) by reversed-phase liquid chromatography coupled to ICPMS, Anal. Chem. 85 (2013) 1316–1321, https://doi.org/10.1021/ac302851d.
[126] B. Bocca, B. Battistini, F. Petrucci, Silver and gold nanoparticles characterization by SP-ICP-MS and AF4-FFF-MALS-UV-ICP-MS in human samples used for biomonitoring, Talanta 220 (2020) 121404.
[127] A. Gołębiowski, T. Kowalkowski, B. Buszewski, Molecular parameters of low methoxylated pectin affected by gelation with copper and cadmium cations, Bioact. Carbohydr. Diet. Fibre 21 (2020) 1–2, https://doi.org/10.1016/j.bcdf.2020.100211.
[128] K. Eskelin, M. Lampi, F. Meier, E. Moldenhauer, D.H. Bamford, H.M. Oksanen, Asymmetric flow field flow fractionation methods for virus purification, J. Chromatogr. A 1469 (2016) 108–119, https://doi.org/10.1016/j.chroma.2016.09.055.
[129] A.A. Levanova, M. Lampi, K. Kalke, V. Hukkanen, M.M. Poranen, K. Eskelin, Native rna purification method for small rna molecules based on asymmetrical flow field-flow fractionation, Pharmaceuticals. 15 (2) (2022) 261.
[130] J. Kotoucek, R. Hezova, A. Vrablikova, F. Hubatka, P. Kulich, S. Macaulay, D. Roessner, M. Raska, I. Psikal, J. Turanek, Characterization and purification of pentameric chimeric protein particles using asymmetric flow field-flow fractionation coupled with multiple detectors, Anal. Bioanal. Chem. 413 (2021) 3749–3761, https://doi.org/10.1007/s00216-021-03323-6.

UNIWERSYTET
MIKOŁAJA KOPERNIKA
W TORUNIU
Wydział Chemii

[P2]

Golebiowski, Adrian & Kowalkowski, Tomasz & Buszewski, Bogusław

Molecular parameters of low methoxylated pectin affected by gelation with copper and cadmium cations

Bioactive Carbohydrates and Dietary Fibre
10.1016/j.bcdf.2020.100211.

Bioactive Carbohydrates and Dietary Fibre 21 (2020) 100211

Contents lists available at ScienceDirect

Bioactive Carbohydrates and Dietary Fibre

journal homepage: http://www.elsevier.com/locate/bcdf

Molecular parameters of low methoxylated pectin affected by gelation with copper and cadmium cations

Adrian Gołębiowski [a,b], Tomasz Kowalkowski [a,b,*], Bogusław Buszewski [a,b]

[a] Department of Environmental Chemistry & Bioanalytics, Faculty of Chemistry, Nicolaus Copernicus University in Torun, 7 Gagarina St., 87- 100, Torun, Poland
[b] Centre for Modern Interdisciplinary Technologies, Nicolaus Copernicus University in Torun, 4 Wileńska St., 87- 100, Torun, Poland

ARTICLE INFO

Keywords:
Pectin
Radius of gyration
Copper
Cadmium
Egg-box model
Asymmetrical flow field flow fractionation (AF4)
Inductively coupled plasma mass spectrometry (ICP-MS)

ABSTRACT

The basic feature of aqueous low-methoxylated pectin solution is the ability to form gels in the presence of cations. In this study, the changes in the pectin fractions after gelling with copper and cadmium cation in the water solution were analyzed by asymmetrical flow field flow fractionation coupled with multi-angle light scattering detector. Content of cadmium in pectin fractions were measured by hyphenated inductively coupled plasma mass spectrometer. Two fractions of native pectin were obtained, which were eluted through the normal mode. The average radius of gyration for these fractions was 593 and 671 nm, respectively. After ionotropic induced gelation of pectin, the fractionation takes place on steric mode. Size of pectin complexes reduces in the second fraction and the new fraction is created. Complexes with both cation metals have both concentration and time dependent the molecular characteristic. The increase of metal concentration leads to small sizes of complexes in the second fraction. The size is growing with the time due to partial aggregation. The content of the bounded cadmium is highest in the first fraction and rise with the time.

1. Introduction

Pectins are a hetero polysaccharide polymers containing α-(1–4)-D-galacturonic acid units (Mohnen, 2008; Voragen, Coenen, Verhoef, & Schols, 2009) and important elements of primary cell wall and middle lamella in plants and fruits. They are used in many industries (Dranca & Oroian, 2018) e.g. in food (Naqash, Masoodi, Rather, Wani, & Gani, 2017), pharmacy (G. A. Morris, Kök, Harding, & Adams, 2010), as anti-corrosion agents (Fiori-Bimbi, Alvarez, Vaca, & Gervasi, 2015) and biosorbents (Jakóbik-Kolon, Bok-Badura, Karoń, Mitko, & Milewski, 2017). Pectins are classified according to the degree of esterification (DE). They could be high methoxylated (HM) with a DE above 50% or low methoxylated (LM) with lower DE. The applied extraction method and the source of pectin have influence on their chemical properties.

The basic feature of aqueous pectin solution is the ability to form gels. The mechanism of gel formation depends on the degree of esterification. HM-pectin gels in the presence of another saccharide and at a narrower, acidic pH range. Hydrogen bonds and hydrophobic interactions are used in the formation of complexes between carboxylic groups of each chain of pectin and interactions between methyl groups (Yuliarti, Hoon, & Chong, 2017). In the case of LM-pectin, it gels in presence of metal cation in wider pH range, with lack of saccharides, according to the egg-box model. The cation binds two chains of pectin in the junction zones. Gelling of pectin with calcium ion was firstly studied by Morris in 1982 (E. R. Morris, Powell, Gidley, & Rees, 1982). Moreover, pectin forms gels in the presence of mono-, tri- and other divalent cations (Gamonpilas, Krongsin, Methacanon, & Goh, 2015). The presence of monovalent ions, e.g. sodium, decreases repulsive forces between negatively charged anionic carboxylic groups present in chain of the pectin (pH < pK_a carboxylic groups in galacturonic acid). Selectivity of binding ions (Celus et al., 2018; Thibault & Rinaudo, 1986) decreases in the following order: copper, lead ≫ zinc, cadmium, nickel > calcium (Dronnet, Renard, Axelos, & Thibault, 1996) according to Irving-Williams theory (Irving & Williams, 1953) and it is connected with the ionic radius. Gelation of pectin can occur in a higher temperature. The mechanism of this process is based on hydrophobic interaction between methyl pectin groups.

Pectin can be characterized by many techniques available in the modern laboratory. In majority of works, rheology studies of pectin solution are conducted. Size exclusion chromatography (SEC) connected with variable detectors e.g. multi angle light scattering (MALS), ultra violet (UV), refractive index (RI), intrinsic viscosity (IV) is the most

* Corresponding author. Department of Environmental Chemistry & Bioanalytics, Faculty of Chemistry, Nicolaus Copernicus University in Torun, 7 Gagarina St., 87- 100, Torun, Poland.
E-mail address: tomasz.kowalkowski@umk.pl (T. Kowalkowski).

https://doi.org/10.1016/j.bcdf.2020.100211
Received 12 June 2019; Received in revised form 14 January 2020; Accepted 21 January 2020
Available online 24 January 2020

popular technique for pectin fractionation (Muñoz-Almagro, Rico-Rodriguez, Villamiel, & Montilla, 2018).

An alternative technique is asymmetrical field flow fractionation (AF4) (Kowalkowski, Buszewski, Cantado, & Dondi, 2006). This technique is the most popular from field flow fractionation (FFF) separation techniques family, there was discovered and described by Gidings in the mid-1960s. Others are Split Flow Thin Cell Fractionation (SPLITT) (Szparaga, Kowalkowski, & Buszewski, 2018) and thermal (TFFF) and electric field (EIFFF).

Combining AF4 with MALS (Thielking & Kulicke, 1998) allows investigating a native solution of pectin and pectin-heavy metal complexes, exploring the changes in the fraction profile, size and molar mass distribution, as well as the conformation changes during the gelling process.

A number of researches about the pectins and their interactions with metal's cations have been performed since 80's of last century. Pectin complexation with ions leads to the gel matrix formation. The characterization of these particles may be performed by many analytical techniques. One of those techniques is light scattering methods (E. R. Morris et al., 1982). By using it information about radius of gyration (R_g), molar mass and also conformation of particles can be obtained. However, the sample must be homogenous in structure with monodispersed distribution of particle size shape and the chemical composition. Therefore the light scattering detector is usually coupled with separation techniques like size exclusion chromatography (SEC) or flow field-flow fractionation (F4) which is able to separate a complex sample to individual components.

Comparing with SEC, AF4 is a more suitable technique for highly branched, large molecules with bigger polydispersity index (PDi) (Nilsson, 2013; Podzimek, 2011). Pectin, and its gels, is a complex sample characterized by high polydispersity in size, therefore, we have chosen asymmetric flow field-flow fractionation with multiangle light scattering detector (AF4-MALS) to obtain the whole information about the molecular parameters of pectins.

A separation process, in the case of the normal mode, is based on the difference in diffusion coefficients of the analytes. In the open tubular narrow ribbon-like channel a laminar flow is maintained. The downstream wall is called accumulation wall and contains a semi-permeable membrane. The second flow, called a crossflow, is generated through this membrane and acts as a perpendicular force. Generally, in the AF4, three the elution models are possible: normal, steric and hyper-layer model. A wide range of particle sizes are present in these three models of elution, from the smallest particles in the order of a few nanometers through colloidal particles, up to large particles (e.g. cells) or agglomerates in the size of a micrometer. In the normal mode, the external, separation force – the cross flow attracts particles to the accumulation wall. A solvent permeates the membrane pores. In turn, the particles are too big to leave the channel through the membrane pores. Therefore, these create a narrow band just next to the membrane. However, the force acting in the opposite direction pulls away particles from the wall towards the central part of the channel, in a process called the Brown diffusion. Smaller particle have a higher diffusion coefficient then bigger particles, therefore, they wander to the central part of the channel. In the channel, there are laminar flow conditions, so the flow velocity is highest in the middle of channel and it is the smallest near an accumulation wall. So, in the normal mode, the smallest particles elute before the bigger ones (Baalousha, Stolpe, & Lead, 2011).

The aim of this study was to characterize changes in the pectin fraction, and consequently molecular parameters (radius of gyration - R_g, molar mass - M_w, fractal dimensions, and polydispersity index - Pdi) and cadmium content as well as distribution in pectin gel network after ionotropic induced gelation with copper and cadmium cations. The goal was achieved using AF4 system on-line coupled with MALS and inductively coupled plasma mass spectrometer (ICP-MS) as detectors.

2. Materials and methods

2.1. Materials and sample preparation

LM Pectin from citrus peel (Lot: SLBN9007V) was purchased from Sigma-Aldrich. As supplier stated content of galacturonic acid and methoxyl is 80.2% and 7.6%, respectively. We have use this material without additional a purification.

Pectin (3 mg/mL) was dissolved in pure water Milli-Q in a flask, applying magnetic stirrer for 120 min for complete dissolution. Appropriate volumes of cadmium and copper standards were added to this solution, respectively. Concentration of copper and cadmium was in the range of 3–100 mg/L. This solution was mixed for respective times (e.g. 1 h, 2 h etc.).

2.2. Methods

2.2.1. AF4-MALS

AF2000 Multi Flow system (Postnova, Germany), equipped with analytical channel of 335 mm in length and 60 mm in width, and 350 μm spacer was used. 10 kDa of regenerated cellulose was used as a channel membrane. Multi-angle light scattering (MALS) detector PN3621 (Postnova, Germany) was used for data acquisition and set at 35 °C with 80% laser (λ = 532 nm) power. All fractograms presented in results section showing the signal registered at 44° angle. Evaluation of the MALS signal was performed using AF2000 Control software. The specific refractive index increment value (dn/dc) was set to 0.145 mL/g. A UV detector was set to 210 nm. Radius of gyration (R_g) was obtained directly from MALS by using random coil model. Water was used as a carrier liquid in the study and was prepared in the Milli-Q system (Millipore, USA). Before the analysis, the carrier liquid was filtered using 0.1 μm nylon membrane (Merck Millipore, Poland). All AF4-MALS analyses were performed in room temperature. The detector flow rate, injection time, cross flow rate, and elution time were also optimized. Detector flow rate was 0.5 mL/min. The injection volume was 10 μL. The first step of the analysis, focusing step, consisted of a combination of three flows through the channel responsible for proper separation. The injection flow was 0.20 mL/min, the focus pump 1.8 mL/min and the cross flow was 1.50 mL/min. This step continued for 10 min. After the focusing step, 3 min of transition was added prior to the elution step. During this time, the focus flow was reduced to 0 mL/min. The cross flow was maintained for 5 min. After that, a linear decrease to the value of 0 mL/min was set within the next 3 min.

The value of radius of gyration is an approximation of the molecule size, as it explains the mass average (root mean square) distance of each point in a molecule from the molecule's center of gravity. The expression allowing to obtain the radius of gyration is the Zimm plot (Eq. (1)) (Wu & Lattuada, 2013):

$$\frac{K \times c}{R(\theta, c)} = \frac{1}{M_w P(\theta)} + 2A_2 c \tag{1}$$

where $R(\theta, c)$ excess Rayleigh ratio as a function of scattering angle θ and concentration c, K is the optical constant $K = \frac{4\pi^2 \left(\frac{dn}{dc}\right)^2 n_0^2}{N_A \lambda_0^4}$, where expression $\left(\frac{dn}{dc}\right)$ is the increment refractive index, n_0 is refractive index of solvent, λ_0 is wavelength of laser source and N_A is Avogadro number. M_w is the weighted-average molar mass of compound, A_2 is the second virial expansion of the osmotic pressure. In $P(\theta)$ is named form factor and express the angular dependence of scattered light and contains the radius of gyration (Eq. (2)):

$$P(\theta) \sim 1 - \frac{16\pi^2 n_0^2}{3\lambda_0^2} < R_g^2 > sin^2\frac{\theta}{2} \tag{2}$$

Thus, by carrying out the light scattering measurement we obtain relationship between intensity of the scattered light probes and intensity of the laser which is excess in the $R(\theta,c)$. From Zimm's plot (Eq. (1)), the dependence of $\frac{K}{R(\theta,c)}$ of $sin^2\frac{\theta}{2}$ at double interpolation concentration and angle $c,\ \theta \underset{lim\to 0}{\to} 0$, radius of gyration is obtained from slopes.

2.2.2. AF4-ICP-MS

Inductively coupled plasma mass spectrometer detector (Shimadzu ICP-MS 2030) was directly coupled with AF4-UV-MALS sector system through capillary tube (inner diameter 0.5 mm). Time resolved measurements (TRM) mode was applied to perform analyses. Processing of peaks consist of manual baseline integration between 13 and 23 min of analyses in case pectin-cadmium complexes analysis.

2.2.2.1. Performing calibration curve for cadmium content. ICP-MS condition is described in Table 1. Tip flow was 0.5 mL/min and others pumps were not generate flow (0 mL/min). Injecting of increased amounts of 100 μL solution of cadmium (from 0 μg to 2 μg cadmium) (full loop injection mode) to AF4 channel and eluted to ICP-MS system.

2.2.2.2. Analysis of cadmium content and distribution in pectin-cadmium complexes. AF4 experimental methods were as in A4F-MALS section and ICP_MS method is present in Table 1. Pectin (3 mg/mL) was dissolved in water Milli-Q for complete dissolution. After that time cadmium standard solution was added to obtain concentration of 20 mg Cd/L.

To our best knowledge hyphenation of AF4 with ICP system is innovative in the case of monitoring bounded heavy metal to pectin. In one run we obtained information about molecular parameters and concentration of adsorbed metal.

2.2.3. ζ-potential characteristic of pectin in pure water condition

Pectin was dissolved in pure water Milli-Q to reach concentration of 0.05% (w/v). After complete dissolution and hydration of pectin, disposable folded capillary cell (DTS1070) was filled paying attention to avoid air bubbles in the capillary. Malvern Zetasizer NanoZS (Malvern Panalytical Ltd, UK) instrument was used to measure electrophoretic mobility of pectin by applying the Smoluchowski approximation in Hanry equation (f (κα) = 1.5). Temperature was set to 25 °C and equilibrium time was 2 min. Auto-mode was chosen to generation data (3 runs with 10–30 repetitions each). Experimental condition was selected automatically by the system.

3. Results and discussion

3.1. Molecular characteristic pectin and pectin complexes with copper and cadmium

The chemical structure of pectin, physicochemical condition of solution and cations metal have impact on ionotropic formation of pectin gels. During dissolving of pectin in water different physicochemical processes take place and lead to formation of viscous solution (Einhorn-Stoll, 2018). We perform the fractionation of low methoxylated pectin from citrus peel in aquatic conditions without the addition of any buffer salts. Comparison of fractograms from analyses carrying out over the period of three days is presented in Fig. 1. Two fractions of particles were separated with different radius of gyration, molar mass, and consequently diffusion coefficient. In accordance to the retention time, the particles from the first fraction are eluted between 13 and 16 min of analysis, during the transition step. The second fraction is eluted between 20 and 28 min.

Table 1
ICP-MS experimental conditions.

Monitored mass	Cd 111
Radio frequency power	1.20 kW
Sampling Depth	5 mm
Plasma Gas	8.0 L/min (Ar)
Auxiliary Gas	1.10 L/min
Carrier Gas	0.70 L/min
Cell Gas	6 mL/min (He)
Cell Voltage	−21 V
Energy Filter	7.0 V
Chamber Temperature	5 °C

From this fractograms and Table 2, which presents molecular parameters from whole section of analyses, one can see that the mean radius of gyration of these particles in specified fractions. The fractionation of pectin in this condition proceeds under the normal mode fractionation. The repeatability of analyses is satisfactory in terms of both, retention times and radius of gyration values. This phenomenon may be explained by the fact that, pectin dissolved in pure water has high colloidal stability. No additional fraction of particles after prolonging (3 days) pectin in solution was observed, which can stand for the agglomeration process. Additionally, we not recorded significant increase in radius of gyration in obtained fractions. The ζ potential describes the colloidal stability of colloids in solution. Obtained by us ζ-potential of pectin in pure water was 0.25 ± 0.49 V. This value close to zero apparently testifies about electroneutrality pectin in pure water. The cause of this is low conductivity of medium. Low content of ions did not provides electrophoretic mobility and electro osmosis pectin between a electrodes and makes it impossible the creation the double diffuse layers. Zeta-potential is electrokinetic potential at bounded and free phases on colloid particle. In pure water condition a source of ions comes from pectin dissociation and ionic soluble contamination. At such conditions the adsorption layer is very small. However, as reported by other authors, pectin is a highly negative charged (highly negative ζ-potential) particle when they are dissolved in pure water (no buffer conditions, pH neutral) (Jonassen, Treves, Kjøniksen, Smistad, & Hiorth, 2013a). Despite application the purification they noted a highly negative ζ-potential. This discrepancy might be caused an additional source of free ions in solution, because it is not possible a measure of ζ-potential in highly pure water condition.

Due to its chemical structure, pectin constitute from many acidic groups of galacturonic acid, which are fully soluble. In our work low methylated pectin (DE 7%) was used ensuring that rest of galacturonic acid is dissociated. Negative charges localized on acidic groups prevent to any attractive interactions among pectins chain.

In pure water with pH of 6–7, low methoxylated pectin has a big number of negative centers, because pKa of pectin is about 3.5. In these conditions, galacturonic acid is fully dissociated. Additionally, there are many hydroxyl residues and possible presence of acetyl residues attached to C2 and or C3 of the sugar ring. Such big accumulation of negative charges results in high level of van der Vaal's repulsion forces. This electrostatic repulsion is responsible for extended conformation of chains of pectin, which is reflected in high radius of gyration of native pectin molecules. Agglomeration process in these conditions is less likely. This repulsion force could be considered as intra- and intermolecular interactions. Intra-molecular repulsion occurs because the negative charge located on carboxylic residues increases during the deprotonation process of galacturonic acid and interacts with the negatively charged hydroxyl and acetyl residues of the molecule. Inter molecular repulsion takes place between other chains of the molecule and occurs via repulsion between negatively charged carboxylic groups and hydroxyl groups as well as acetyl residues. These effects explain the recorded radius of gyration of pectin (Fig. 1). However, many authors state that the radius of gyration of pectin is lower (Liu, Guo, Liang, Liu, & Chen, 2017; Nakauma et al., 2017, 2016; Yuliarti & Mardyiah Binte Othman, 2018). Those authors investigated the size in the presence of a buffer solution, which is explaining higher R_g value reported in present study. Buffer solutions provide the screening effect to the negative charged centers. The decreasing of net negative charge causes reduction

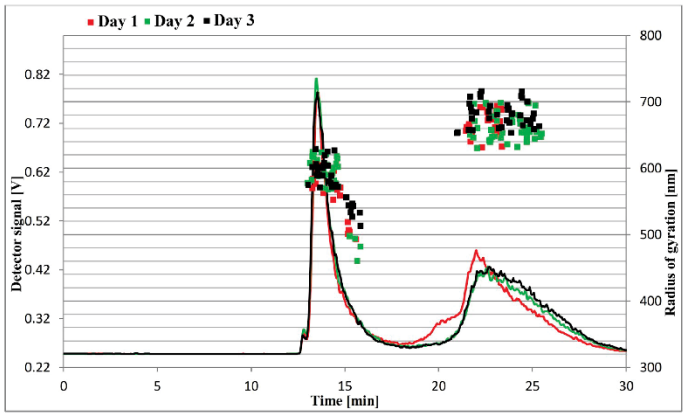

Fig. 1. Stability of native pectin in three days period.

Table 2
Fractal dimensions and polydispersity index (Pdi) for obtained fractions of pectin complexes with copper and cadmium samples.

Sample name	Fraction number								
	1			2			3		
	Fractal dimension	Mw [g/mol]	Pdi	Fractal dimension	Mw [g/mol]	Pdi	Fractal dimension	Mw [g/mol]	Pdi
Native sample Day 1	3.7	2.6*10^8	2.3	2.2	7.8*10^7	1.3	3.0	3.0*10^8	3.1
Native sample Day 2	4.3	3.1*10^8	1.9	4.1	3.3*10^8	1.3	2.1	7.7*10^7	1.3
Native sample Day 3	2.5	3.1*10^8	1.8	3.0	4.5*10^8	1.7	2.7	9.1*10^7	1.7
Pectin with 40 mg Cu/L after 2H	18.3	1.2*10^8	12.1	1.6	5.4*10^7	1.1	2.1	9.5*10^6	1.4
Pectin with 100 mg Cu/L after 1H	14.0	1.6*10^8	11.0	2.2	1.5*10^7	1.2	1.7	8.6*10^6	1.4
Pectin with 100 mg Cu/L after 2H	21.0	1.5*10^8	12.5	2.3	2.6*10^7	1.3	1.7	9.4*10^6	1.4
Pectin with 3 mg Cd/L 0H	34.2	8.7*10^7	21.0	2.1	2.0*10^7	1.1	2.1	2.7*10^7	1.5
Pectin with 3 mg Cd/L 0.5H	59.6	1.4*10^8	22.0	1.7	3.7*10^7	1.8	1.7	3.3*10^7	1.3
Pectin with 3 mg Cd/L 5H	51.9	1.4*10^8	44.0	2.1	4.7*10^7	1.4	8.6	9.1*10^8	7.1
Pectin with 3 mg Cd/L 24H	16.4	1.4*10^8	24.3	1.8	2.2*10^7	1.1	2.1	1.2*10^7	1.5
Pectin with 20 mg Cd/L after 2H	6.8	9.3*10^7	4.3	2.1	4.3*10^7	1.2	2.3	1.0*10^7	1.3
Pectin with 100 mg Cd/L after 0H	1.6	6.7*10^7	1.6	2.0	2.7*10^7	1.1	2.1	3.7*10^6	1.3
Pectin with 100 mg Cd/L after 1H	7.0	7.1*10^7	2.9	2.2	1.9*10^7	1.1	2.0	3.3*10^6	1.5

of the radius of gyration.

Table 2 shows also the data about conformation of pectin using fractal dimensions. Double logarithmic plot radius of gyration and molar mass indicates particles topology. For example, the fractal dimensions equal to 3 lead to spheres, because the increase of sphere mass growth in third power of radius ($M = 4/3\pi R^3$). Pectin particles form 3-dimensional structures.

The addition of cation metal to the pectin solution leads to the gel network formation. Gelling of pectin is based on egg-box model. Firstly, a cation metal attach to carboxylic residue of galacturonic acid. After that, pectin-metal complex combine with another chain of pectin through cations via bridges between two chains of pectin. We carry out ionotropic gelation of pectin with copper and cadmium cations.

Historically, calcium was described cation to the ionotropic gelation firstly. The researchers have carried out experiments with another metal including mono- and tri-valent metals. The physicochemical properties of gel are various according to the metal which was applicable. Calcium, for example, can interact with pectin through only carboxylic residue of galacturonic acid, whereas another metal can attract with hydroxylic residue. The additionally binding site increase strength of binding between pectin and metal and therefore the properties of gels are change. In case of preparation gels with monovalent ions, the mechanism is based on the screening a negatively charged acidic groups and consequently reducing in repulsive forces between galacturonic acid in the ionic form. The moving closer chains of pectin can attract with each other through the hydrophobic and hydrogen binding.

We studied the molecular parameters before and after ionotropic gelation of pectin with copper and cadmium. For this reason, we use pure water as a dispersant. Constituents of buffer solution compete with the analyte about the binding sites of pectin. Jonassen showed a decrease in hydrodynamic radii and ζ-potential of pectin after mixing a pectin solution with NaCl (Jonassen et al., 2013a). Also (Lascol et al., 2016) noted the same trend.

The degree of esterification has a crucial importance for an electrostatic interaction between pectin and ions. The lower DE causes in higher available number of acidic groups which can dissociate. Consequently, higher content of anionic charged groups binds higher amount of cations. From 6 to 10 consecutive non-methylesterified galacturonic acid units are required for formation of stable junction zones with calcium. Thus, the lower esterified pectin creates a higher number of junction zones and the formed gel is stable.

Influence of internal factors of pectin, degree of esterification and molar masses and also external factor which is solvent effect has crucial role for obtained radius of gyration of pectin (Fishman, Chau, Kolpak, & Brady, 2001) Radius of gyration of pectin is a dependent on conformation of particles. After the gel formation, we suppose that firstly radius of

gyration decrease for monomer fractions and secondly the radius of gyration increase for the derivate agglomerate fraction, both due to reduction in electrostatic repulsion. Thirdly, the compactness of structure has grown up because dimeric and other structure has created.

Fig. 2 is presenting the comparisons of fractograms during pectin gelation with copper in various concentrations. Changes are displayed evidently. Firstly, the elution mode is changed from normal to steric model. Bigger particles were eluted before smaller ones. After gelation process pectin changes their structure. Thus the separation force is hydrodynamic lift now. Denser and bigger particles of pectin have too low diffusion coefficient. Another change is the appearance of new fraction. This comprises a tail of first fraction. The retention time of first fraction not alternate but this rise in intensity of the detector signals with concentrations of copper. Radius of gyration particles in the second fraction sharply decrease after gelation process in comparison to the native pectin.

Intensity of signals decreases in the second fraction. The intensity of the signal from MALS detector (Eq. (3)) is directly proportional to weighted-average molar mass M_w, concentration C and square increment of refractive index $\frac{dn}{dc}$:

$$Instensity_{\ MALS\ signals} \cong M_w \times C \times \left(\frac{dn}{dc}\right)^2 \tag{3}$$

It means that an increase of the signal intensity is possible through an increase of these parameters, separately or simultaneously. Particles have higher and lower weighted-average molar mass M_w after gelation process in the first and second fraction, respectively (Table 2). Thus change in molar mass is responsible for those changes in intensity of signals.

We obtain three populations of particles after the gel formation. We suppose that the elution row is like follows: the secondary agglomerate and/or not bound agglomerate; then the complexes of pectin gels; then the smaller complexes of pectin. The first one represents the ectypal agglomerates of pectin-copper gels and the fraction agglomerates. The second one contains the newest creates complexes of pectin-copper which they not overcome further polymerization. The particles have intermediate the radius of gyrations. The third one constitutes the smaller primary pectin-copper complexes.

Increase of the copper concentration from 40 mg Cu/L to 100 mg Cu/L leads to the higher radius of gyration of particles in the second fraction. Increasing the copper concentration in the reaction system provide successive binding of copper cations to the binding site of pectin. The complexes have a smallest intra and intermolecular repulsive potential and both effects are responsible for the formation of higher in size particles.

At the 100 mg Cu/L concentration the radius of gyration also slightly increases with increasing in the time of contact (from 1 to 2 h). The explanation for this can be a partial agglomerates formation.

The creation ultra-high mass particles indicate a sharp rise the fractal dimension (Table 2), especially for the first fraction. Those values indicate highly expanded 3-dimensional structures.

Addition of copper to pectin leads to the creation of coordination complex according to the egg-box model (Einhorn-Stoll, 2018). Copper cations serve as connecting bridges between two pectin chains. Oxygen from carboxylic residues of galacturonic acid is responsible for the linkage with metallic parts. This connection decreases the molecular size, because some part of repulsion is inactivated and the conformation is more concise (Jonassen, Treves, Kjøniksen, Smistad, & Hiorth, 2013b). (Liu et al., 2017) clearly show that pectin has various conformations depending on sources of origin and the applied extraction method, as well as the medium in which pectin is dissolved.

The effect of time of contact on the pectin-cadmium complexes is shown on Fig. 3. After addition of cation metal pectin reduces its R_g due to smaller repulsion forces which are able between a negative charged carboxyl groups of pectin (~neutral pH in the AF4 channel). In comparison to unchanged pectin, the effect of cadmium addition is similar to that for copper. The increase of signal intensity was noticed for the first fraction, while the decrease of radius of gyration was found for the second fraction and the new fraction appeared which elutes between 15 and 16 min. This experiment shows that the creation of the complex is very fast. Over time, the radius of gyration increases slightly, returning to the initial values. Possible explanation is the partial agglomeration process which turns the radius of gyration to a higher value. Extended increase in both content and size of agglomerates causes high value of the fractal dimensions. They crates highly dense and expanded structures in comparison to both the cadmium induces gels and the native pectin (Table 2). After 5 h, in the second fraction fractal dimensions depart from other values. The cause may be noisy signal in this case. Big Pdi values in the first fraction are caused by extremely high molar mass species, which significantly inflated the mean values of mass, especially z-average molar mass which is sensible for high values.

The molecular parameters of pectin are ionically, concentration and

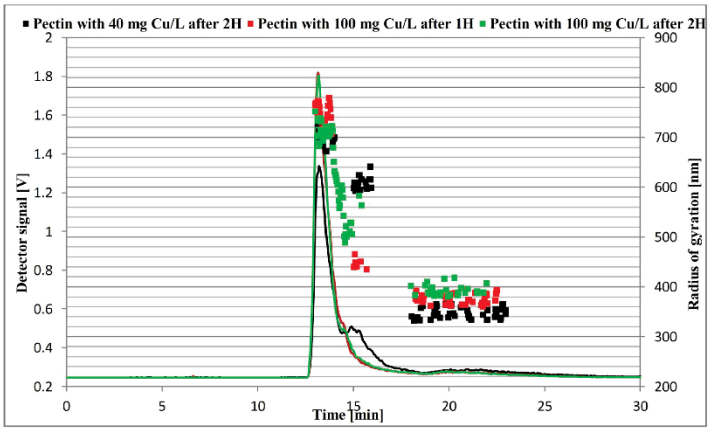

Fig. 2. The impact of copper concentration and Cu^{2+} contact time on gelation process of pectin.

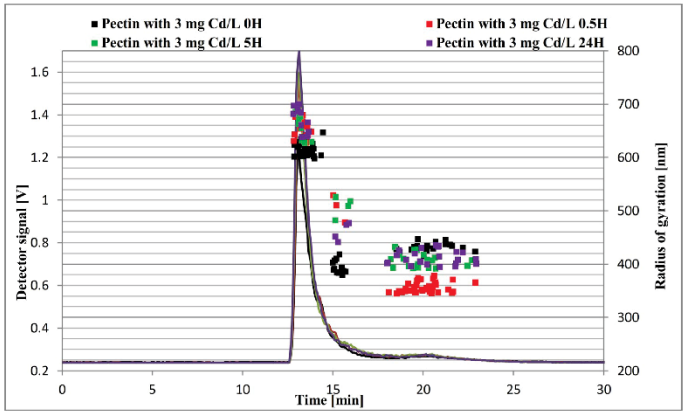

Fig. 3. The impact of contact time on gelation process of pectin with cadmium.

time dependents (Zhang et al., 2018). demonstrates that complexation is strongly dependent on concentration binding ions (in this study - calcium cations) and stoichiometry between the pectin, the cation and the oligoguluronate during the gelation process. In our study this effect is shown too. Higher cadmium concentration leads to the formation smaller in R_g particles (Fig. 4) (in comparison to Fig. 3). The same effect of R_g changes in the second fraction is present. Firstly, particles are dramatic lower then native ones. Secondly, higher concentration leads to smaller particles and thirdly after prolonging time, those increases size due to both possible effects which are described above.

3.2. Content and distribution of cadmium in pectin-cadmium complexes

The response of detector was linear and repeatable in case of coupling AF4-ICP-MS system (Fig. 5). Peaks are wide in time because the difusion phenomena take place both in dynamic flow in AF4 channel and tubing conection between AF4 and ICP-MS. It is worth to notice that cross and focus flows are stoped and only the tip flow transfer anlytes through separation channel to ICP-MS detector.

AF4-ICPMS fractograms of pectin affected by cadmium is present at Fig. 6. The major advantage of AF4-ICP-MS system is the fact that non-bounded cadmium is sack through semipermeable membrane during AF4 relaxation step and consequently only Cd pectin complexes are detected. Some amount of cadmium in native pectin sample was also detected. Possible source of those is technological processing residues or contamination of pectin samples. Cadmium profiles are correlated with pectin profiles from MALS detector. The most amount of metal is bound with pectin from first fraction. During the time, pectin bounds cadmium constantly, after 2 h practically whole Cd amount is bounded. In the new fraction, which due to dispersion is visible as tail of first fraction, cadmium concentration increased mostly during firstly 30 min of gelation process while in the next time points the Cd concentration is raising much slower. In the second fraction cadmium content fluctuates. After 30 min of gelation the Cd concentration is the highest and with the time decreases. Although, taken together both fractions, the concentration of cadmium after 2 h of process is the highest and after 30 min of process is the smallest concentration.

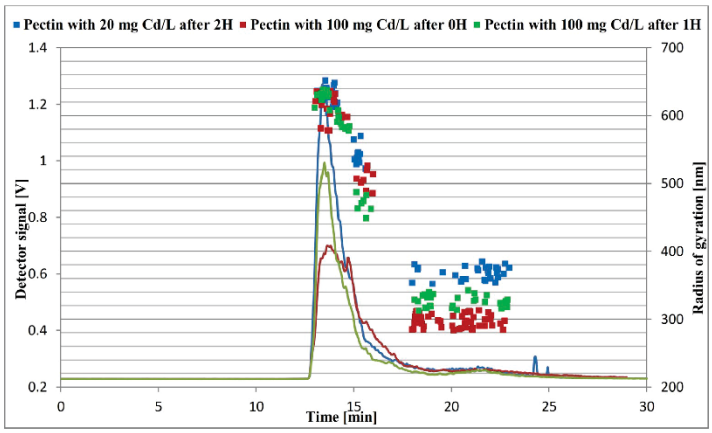

Fig. 4. Fractionation of pectin-cadmium complexes with different both concentrations of cadmium and contact times.

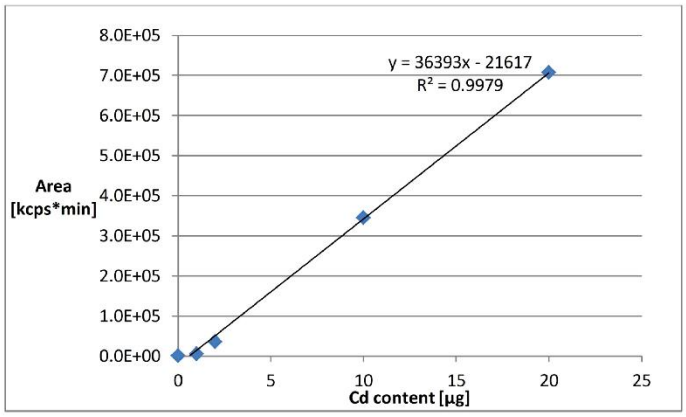

Fig. 5. Calibration curve of cadmium.

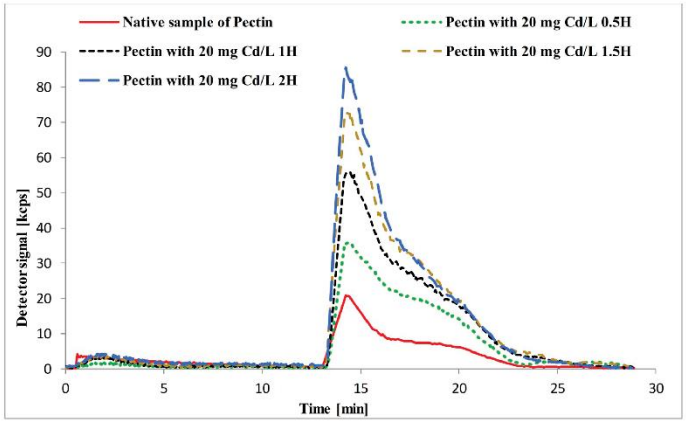

Fig. 6. AF4-ICPMS fractograms obtained for native pectin and with the time of gelation caused by cadmium: 0.5 h; 1 h; 1.5 h and 2 h.

4. Conclusions

This work confirms that molecular parameters of pectins are changing during cadmium and copper induced gelation. We characterize radius of gyration in particular fractions and other parameters. Native pectin in water solution has two fractions of particles and after addition of heavy metal's ions to pectin solution begins the creation of pectin gels. It is manifested in changes in molecular characteristics of pectin particles. The new fraction was created. It constitutes a tail of the first fraction which indicates highly branched 3-dimmensional network. The conformational and molar mass analyses prove the creation ultra-high species. Another change is R_g increase in the first fraction along with increase metal's concentration and time of contact and R_g decrease in the second fraction. Both metal's ions quantitatively contributes the same trend in AF4-MALS profile. The AF4-ICP-MS system was applied first time in the study of pectin-heavy metal's particles. This is powerful tool in characterization metals which are bounded or adsorbed on nanoparticles or are their natural constituents. In this work we monitored cadmium distribution in time and in particular fractions. During the time cadmium content rise most extensively in the first fraction. In the second fraction the content decreases with the time of gelation process.

Declaration of competing interest

Herewith, as an corresponding author, I declare no conflict of interest of all co-authors.

CRediT authorship contribution statement

Adrian Gołębiowski: Investigation, Writing - original draft. **Tomasz Kowalkowski:** Conceptualization, Writing - original draft, Visualization, Writing - review & editing. **Bogusław Buszewski:** Supervision.

Acknowledgements

Declarations of interest: none.

Funding: This research did not receive any specific grant from funding agencies in the public, commercial, or not-for-profit sectors.

References

Baalousha, M., Stolpe, B., & Lead, J. R. (2011). Flow field-flow fractionation for the analysis and characterization of natural colloids and manufactured nanoparticles in environmental systems: A critical review. *Journal of Chromatography A, 1218*(27), 4078–4103. https://doi.org/10.1016/j.chroma.2011.04.063.

Celus, M., Kyomugasho, C., Salvia-Trujillo, L., Van Audenhove, J., Van Loey, A. M., Grauwet, T., et al. (2018). Interactions between citrus pectin and Zn2+ or Ca2+ and associated in vitro Zn2+bioaccessibility as affected by degree of methylesterification and blockiness. *Food Hydrocolloids, 79*, 319–330. https://doi.org/10.1016/j.foodhyd.2018.01.003.

Dranca, F., & Oroian, M. (2018). Extraction, purification and characterization of pectin from alternative sources with potential technological applications. *Food Research International, 113*(February), 327–350. https://doi.org/10.1016/j.foodres.2018.06.065.

Dronnet, V. M., Renard, C. M. G. C., Axelos, M. A. V., & Thibault, J. F. (1996). Characterisation and selectivity of divalent metal ions binding by citrus and sugar-beet pectins. *Carbohydrate Polymers, 30*(4), 253–263. https://doi.org/10.1016/S0144-8617(96)00107-5.

Einhorn-Stoll, U. (2018). Pectin-water interactions in foods – from powder to gel. *Food Hydrocolloids, 78*, 109–119. https://doi.org/10.1016/j.foodhyd.2017.05.029.

Fiori-Bimbi, M. V., Alvarez, P. E., Vaca, H., & Gervasi, C. A. (2015). Corrosion inhibition of mild steel in HCl solution by pectin. *Corrosion Science, 92*, 192–199. https://doi.org/10.1016/j.corsci.2014.12.002.

Fishman, M. L., Chau, H. K., Kolpak, F., & Brady, J. (2001). Solvent effects on the molecular properties of pectins. *Journal of Agricultural and Food Chemistry, 49*(9), 4494–4501. https://doi.org/10.1021/jf0013171.

Gamonpilas, C., Krongsin, J., Methacanon, P., & Goh, S. M. (2015). Gelation of pomelo (Citrus maxima) pectin as induced by divalent ions or acidification. *Journal of Food Engineering, 152*, 17–23. https://doi.org/10.1016/j.jfoodeng.2014.11.024.

Irving, H., & Williams, R. J. P. (1953). 637. The stability of transition-metal complexes. *Journal of the Chemical Society*, 3192–3210. https://doi.org/10.1039/JR9530003192, 0.

Jakóbik-Kolon, A., Bok-Badura, J., Karoń, K., Milko, K., & Milewski, A. (2017). Hybrid pectin-based biosorbents for zinc ions removal. *Carbohydrate Polymers, 169*, 213–219. https://doi.org/10.1016/j.carbpol.2017.03.095.

Jonassen, H., Treves, A., Kjøniksen, A. L., Smistad, G., & Hiorth, M. (2013a). Preparation of ionically cross-linked pectin nanoparticles in the presence of chlorides of divalent and monovalent cations. *Biomacromolecules, 14*(10), 3523–3531. https://doi.org/10.1021/bm4008474.

Jonassen, H., Treves, A., Kjøniksen, A. L., Smistad, G., & Hiorth, M. (2013b). Preparation of ionically cross-linked pectin nanoparticles in the presence of chlorides of divalent and monovalent cations. *Biomacromolecules, 14*(10), 3523–3531. https://doi.org/10.1021/bm4008474.

Kowalkowski, T., Buszewski, B., Cantado, C., & Dondi, F. (2006). Field-flow fractionation: Theory, techniques, applications and the challenges. *Critical Reviews in Analytical Chemistry, 36*(2), 129–135. https://doi.org/10.1080/10408340600713702.

Lascol, M., Bourgeois, S., Guillière, F., Hangouët, M., Raffin, G., Marote, P., et al. (2016). Pectin gelation with chlorhexidine: Physico-chemical studies in dilute solutions. *Carbohydrate Polymers, 150*, 159–165. https://doi.org/10.1016/j.carbpol.2016.05.014.

Liu, C. mei, Guo, X. juan, Liang, R. hong, Liu, W., & Chen, J. (2017). Alkylated pectin: Molecular characterization, conformational change and gel property. *Food Hydrocolloids, 69*, 341–349. https://doi.org/10.1016/j.foodhyd.2017.03.008.

Mohnen, D. (2008). Pectin structure and biosynthesis. *Current Opinion in Plant Biology, 11*(3), 266–277. https://doi.org/10.1016/j.pbi.2008.03.006.

Morris, G. A., Kök, S. M., Harding, S. E., & Adams, G. G. (2010). Polysaccharide drug delivery systems based on pectin and chitosan. *Biotechnology & Genetic Engineering Reviews, 27*(1), 257–284. https://doi.org/10.1080/02648725.2010.10648153.

Morris, E. R., Powell, D. A., Gidley, M. J., & Rees, D. A. (1982). Conformations and interactions of pectins. I. Polymorphism between gel and solid states of calcium polygalacturonate. *Journal of Molecular Biology, 155*(4), 507–516. https://doi.org/10.1016/0022-2836(82)90484-3.

Muñoz-Almagro, N., Rico-Rodriguez, F., Villamiel, M., & Montilla, A. (2018). Pectin characterisation using size exclusion chromatography: A comparison of ELS and RI detection. *Food Chemistry, 252*(January), 271–276. https://doi.org/10.1016/j.foodchem.2018.01.087.

Nakauma, M., Funami, T., Fang, Y., Nishinari, K., Draget, K. I., & Phillips, G. O. (2016). Calcium binding and calcium-induced gelation of sodium alginate modified by low molecular-weight polyuronate. *Food Hydrocolloids, 55*, 65–76. https://doi.org/10.1016/j.foodhyd.2015.10.021.

Nakauma, M., Funami, T., Fang, Y., Nishinari, K., Draget, K. I., & Phillips, G. O. (2017). Calcium binding and calcium-induced gelation of normal low-methoxyl pectin modified by low molecular-weight polyuronate fraction. *Food Hydrocolloids, 69*, 318–328. https://doi.org/10.1016/j.foodhyd.2016.12.035.

Naqash, F., Masoodi, F. A., Rather, S. A., Wani, S. M., & Gani, A. (2017). Emerging concepts in the nutraceutical and functional properties of pectin—a review. *Carbohydrate Polymers, 168*, 227–239. https://doi.org/10.1016/j.carbpol.2017.03.058.

Nilsson, L. (2013). Separation and characterization of food macromolecules using field-flow fractionation: A review. *Food Hydrocolloids, 30*(1), 1–11. https://doi.org/10.1016/j.foodhyd.2012.04.007.

Podzimek, S. (2011). Asymmetric flow field flow fractionation. In *Light scattering, size exclusion chromatography and asymmetric flow field flow fractionation* (pp. 259–305). https://doi.org/10.1002/9780470877975.ch5.

Szparaga, A., Kowalkowski, T., & Buszewski, B. (2018). Mathematical modeling of full feed depletion split-flow lateral-transport thin self-adjustable channels (FFD-SPLITT-SA). *Journal of Chromatography A, 1552*, 67–72. https://doi.org/10.1016/j.chroma.2018.03.045.

Thibault, J. F., & Rinaudo, M. (1986). Chain association of pectic molecules during calcium-induced gelation. *Biopolymers, 25*(3), 455–468. https://doi.org/10.1002/bip.360250306.

Thielking, H., & Kulicke, W. M. (1998). Determination of the structural parameters of aqueous polymer solutions in the molecular, partially aggregated, and particulate states by means of FFFF/MALLS. *Journal of Microcolumn Separations, 10*(1), 51–56. https://doi.org/10.1002/(SICI)1520-667X(1998)10:1<51::AID-MCS7>3.0.CO;2-Y.

Voragen, A. G. J., Coenen, G. J., Verhoef, R. P., & Schols, H. A. (2009). Pectin, a versatile polysaccharide present in plant cell walls. *Structural Chemistry, 20*(2), 263–275. https://doi.org/10.1007/s11224-009-9442-z.

Wu, H., & Lattuada, M. (2013). Light scattering – the application of static light scattering: Zimm plot. In *Molecular Sciences and Chemical Engineering. Molecular Sciences and Chemical Engineering* (pp. 1–9). https://doi.org/10.1016/B978-0-12-409547-2.05431-7.

Yuliarti, O., Hoon, A. L. S., & Chong, S. Y. (2017). Influence of pH, pectin and Ca concentration on gelation properties of low-methoxyl pectin extracted from Cyclea barbata Miers. *Food Structure, 11*, 16–23. https://doi.org/10.1016/j.foostr.2016.10.005.

Yuliarti, O., & Mardyiah Binte Othman, R. (2018). Temperature dependence of acid and calcium-induced low-methoxyl pectin gel extracted from Cyclea barbata Miers. *Food Hydrocolloids, 81*, 300–311. https://doi.org/10.1016/j.foodhyd.2018.03.004.

Zhang, B., Hu, B., Nakauma, M., Funami, T., Nishinari, K., Draget, K. I., et al. (2018). Modulation of calcium-induced gelation of pectin by oligogluronate as compared to alginate. *Food Research International, 1*. https://doi.org/10.1016/j.foodres.2018.08.020. March.

UNIWERSYTET
MIKOŁAJA KOPERNIKA
W TORUNIU
Wydział Chemii

[P3]

Golebiowski, Adrian & Pomastowski, Paweł & Rodzik, Agnieszka & Król-Górniak, Anna & Kowalkowski, Tomasz & Górecki, Marcin & Buszewski, Bogusław

Isolation and Self-Association Studies of Beta-Lactoglobulin

International Journal of Molecular Sciences

10.3390/ijms21249711

International Journal of
Molecular Sciences

MDPI

Article

Isolation and Self-Association Studies of Beta-Lactoglobulin

Adrian Gołębiowski [1,2], Paweł Pomastowski [1], Agnieszka Rodzik [1,2], Anna Król-Górniak [1,2], Tomasz Kowalkowski [1,2], Marcin Górecki [3] and Bogusław Buszewski [1,2,*]

1 Centre for Modern Interdisciplinary Technologies, Nicolaus Copernicus University in Torun, 4 Wilcńska St., 87-100 Torun, Poland; adrian.golebiowski@doktorant.umk.pl (A.G.); p.pomastowski@umk.pl (P.P.); agnieszka.rodzik1@gmail.com (A.R.); annkrol18@gmail.com (A.K.-G.); tomasz.kowalkowski@chem.umk.pl (T.K.)
2 Department of Environmental Chemistry and Bioanalytics, Faculty of Chemistry, Nicolaus Copernicus University in Torun, 7 Gagarina St., 87-100 Torun, Poland
3 Institute of Organic Chemistry, Polish Academy of Sciences, 44/52 Kasprzaka St., 01-224 Warsaw, Poland; gorecki_marcin@interia.pl
* Correspondence: bbusz@umk.pl; Tel.: +48-(56)-665-60-38

Received: 9 November 2020; Accepted: 17 December 2020; Published: 19 December 2020

Abstract: The aim of this study was to investigate isolated β-lactoglobulin (β-LG) from the whey protein isolate (WPI) solution using the column chromatography with SP Sephadex. The physicochemical characterization (self-association, the pH stability in various salt solutions, the identification of oligomeric forms) of the protein obtained have been carried out. The electrophoretically pure β-LG fraction was obtained at pH 4.8. The fraction was characterized by the matrix-assisted laser desorption ionization-time of flight mass spectrometry (MALDI-TOF/TOF MS) technique. The use of the HCCA matrix indicated the presence of oligomeric β-LG forms, while the SA and DHB matrices enabled the differentiation of A and B isoforms in the sample. The impact of sodium chloride, potassium chloride, ammonium sulfate, and sodium citrate in dispersion medium on β-LG electrophoretic stability in solution was also studied. Type of the dispersion medium led to the changes in the isoelectric point of protein. Sodium citrate stabilizes protein in comparison to ammonium sulfate. Additionally, the potential of capillary electrophoresis (CE) with UV detection using bare fused capillary to monitor β-LG oligomerization was discussed. Obtained CE data were further compared by the asymmetric flow field flow fractionation coupled with the multi-angle light scattering detector (AF4-MALS). It was shown that the β-LG is a monomer at pH 3.0, dimer at pH 7.0. At pH 5.0 (near the isoelectric point), oligomers with structures from dimeric to octameric are formed. However, the appearance of the oligomers equilibrium is dependent on the concentration of protein. The higher quantity of protein leads to the formation of the octamer. The far UV circular dichroism (CD) spectra carried out at pH 3.0, 5.0, and 7.0 confirmed that β-sheet conformation is dominant at pH 3.0, 5.0, while at pH 7.0, this conformation is approximately in the same quantity as α-helix and random structures.

Keywords: β-lactoglobulin (β-LG); asymmetric flow field flow fractionation (AF4); oligomeric forms; protein stability

1. Introduction

β-lactoglobulin (β-LG) is a small globular protein from the lipocalin family. It is constituted from 162 amino acid residues. The mass of the monomer is about 18.3 kDa [1]. It is the most abundant bovine whey protein, accounting for more than 50% of the total whey protein [2].

β-LG is an important source of the essential and branched-chain amino acids (leucine, isoleucine, and valine). This protein possesses antioxidant properties, because it contains two disulfide bonds

(Cys-66 to Cys-160, Cys-106 to Cys-119) and one free thiol group (Cys-121) [3]. β-LG is a ligand transport agent. In particular, the affinity to hydrophobic compounds is significant due to the β-barrel structure [4–6].

As a result of whey processing, whey protein hydrolysate (WPH), whey protein concentrate (WPC), and the whey protein isolate (WPI) can be obtained. The WPH can be obtained by heating with acid [7] or enzymatic treatment [8]. β-LG is particularly sensitive to trypsin digestion [9]. The degradation and agglomeration temperature can be achieved at the range of 65–68 °C, depending on the pH and ionic strength [10]. The enzymatic hydrolysis of whey proteins liberates fragments that may contribute to the improvement of functions of the immune, cardiovascular, nervous, and gastrointestinal systems [11]. In contrast, WPC can be obtained as a result of modern membrane-based separation technologies such as ultra-filtration for protein concentration, diafiltration (DF) to remove lactose, minerals and low molecular weight compounds. Depending on their concentration, there are WPCs containing 35%, 50%, 65%, and 80% (*w*/*w*) of proteins. WPI with 90% (*w*/*w*) of protein is considered as a high quality and pure protein concentrate [12].

WPI is a good source of high quality native β-LG. It is important in food and biotechnology [13]. β-LG isolation can be performed by many routes [14,15], e.g., the precipitation by denaturing agents (salts, acids, acetone, temperature). However, these approaches can also lead to undesirable precipitation of other proteins. Column chromatography is a technique that allows for isolation of high purity protein, but the selection of experimental conditions is crucial. β-LG occurs in several isoforms, where the A and B isoforms are dominant [16].

In solution β-LG exists in different oligomeric states, which depend on the pH, the ionic strength, temperature, and protein concentration [17]. The main factor contributing to the oligomerization of β-LG, taking into account the effect of variable pH and ionic strength on dimerization, is the hydrophobic effect. According to theoretical calculations, the hydrophobic effect is the result of a decrease in the area accessible to water when dimers are formed [18]. At room temperature, β-LG occurs mainly as a dimer in unprocessed milk, but below pH = 3.5, β-LG becomes a monomer. Isoform β-LG A forms octamers close to pH = 4.6 at temperature below 20 °C, while β-LG B is less resistant [19].

The circular dichroism spectra recorded in far UV region (far UV-CD) can solve the secondary structure of proteins. Based on the CD spectra, α-helical proteins possess negative bands at 222 nm and 208 nm and a positive one at 193 nm. Proteins with β-sheet conformation have negative bands at 218 nm and positive bands at 195 nm. In turn, the random conformed proteins have very low ellipticity above 210 nm and one band near 195 nm [20]. The main conformation of β-LG is β-sheet at pH close to physiological [4,21–26]. Oligomeric state is dependent in particular on pH; at pH 2.0 it is a stable monomer, while at neutral pH it shows a dimeric state. In strong acidic conditions β-LG chains are highly positively charged, and they repel each other. In neutral pH conditions, the dimeric state is stabilized by hydrogen bonds between the surface AB loop and the anti-parallel β-sheet [27].

Different values of 5.1 [28], 4.8 [29,30], and 5.2 [31] were reported for the isoelectric point of β-LG. The differences can be caused by solvent components, the ionic strength, employed analytical method and fitting of experimental data. The influence of various trivalent cations on the protein surface charge was discussed in literature [32]. The authors showed that multivalent cations could change the protein surface charge more effectively than monovalent cations.

The zeta potential analysis is the most popular technique for determination of the surface charges of biocolloids and investigation their stability in the fluids. It is also used to determine the isoelectric point of colloid particles. The advantages of this technique are connected to the possibility to perform the zeta potential and isoelectric point measurements in a wide range of pH, ionic strength and study of the impact of buffer composition on these parameters. In the case of protein research, the impact of buffer components on protein physicochemical stability and isoelectric point values seems to be the most important. Other techniques like isoelectric focusing (IEF) and capillary isoelectric focusing (CIEF) do not allow for determination of the stability at different pH values, ionic strength, and composition of solvent. However, these techniques are advantageous for high resolution and short time of analysis [33].

The association of β-LG protein has been studied using analytical ultracentrifugation or small angle X-ray scattering [18,34]. However, there are still many questions regarding this process and the factors affecting protein oligomerization. Thus, a new interdisciplinary approach for deeper characterization of β-LG forms is needed. Capillary electrophoresis (CE) is one of such techniques and provides a rapid and efficient protein analysis with a low sample and buffer consumption [35,36]. The technique is typically applied for protein separation [37–39], but recently the use of CE as a screening method for the protein oligomers determinations is attracting attention [40,41]. Therefore, the potential use of CE for rapidly monitoring of β-LG forms at different pH conditions was studied in this paper.

Light scattering techniques can estimate the molar mass of the particles and thus distinguish protein forms in solution. Moreover, the multi-angle light scattering (MALS) detector coupled to the separation technique gives information about the molar mass distribution, the radius of the gyration of polydispersed protein forms. The asymmetric flow field-flow fractionation (AF4) gives opportunity for a "soft" separation with minimal changes of the sample composition during analysis [42]. This approach was developed in the mid-1960s by Giddings [43,44]. Today, the application of the technology is more appropriate for separation of large, highly branched colloids in comparison with other techniques [45]. The oligomeric states and molar mass of α-lactalbumin complexes were successfully investigated by the AF4-MALS technique by S. Dhayal et al. [46]. The formalism used to calculate the particle size and the average weight of molar mass has a crucial impact on the results [47] Proteins, therein the β-LG, were analyzed by the AF4 technique [48]. The authors also discussed a selection of the channel membrane and analyzed an overloading effect.

In turn, a powerful tool for protein identification is the matrix-assisted laser desorption ionization-time of flight mass spectrometry (MALDI-TOF/TOF MS) technique, characterized by high sensitivity, low detection limit (LOD), and simplicity of use. The MALDI-TOF/TOF MS method allows for a simple determination of protein masses, as well as analysis of the peptide fragmentation and localization of the posttranslational modifications of proteins [49].

The aim of this study was to investigate the isolated β-LG from the WPI solution, applying column chromatography. Characterization of the β-LG was carried out by multi-instrumental approaches. The data on the factors affecting the protein characterization has not been thoroughly discussed in the literature. Thus, obtained data presented in the current study shed light on β-LG self-association, which seems to be crucial not only for analytical chemistry, but also for the dairy industry. It shows potential to affect the processing and manufacturing of milk products. In this context, the different physicochemical parameters such as the impact of MALDI-TOF/TOF-MS matrix, solvent composition and pH were tested. The dispersion stability and oligomeric forms of the isolated β-lactoglobulin were characterized by the use of zeta potential measurements, capillary electrophoresis, and asymmetric flow field-flow fractionation (AF4) with the multi-angle light scattering (MALS) detector technique. This innovative complementary approach allowed for detection of oligomeric state of the β-LG at pH 3.0, 5.0 and 7.0. Furthermore, we investigated conformation of protein in these conditions by applying circular dichroism (CD) spectroscopy.

2. Results

2.1. Isolation of β-LG from WPI Solution by Chromatographic Column

β-lactoglobulin was isolated in a 0.2 M citrate buffer at the linear pH gradient (from pH 3.0 to 6.5) by column chromatography. The isolation method was optimized by changing the pH of eluent. The first set up scheme was created using a pH gradient from 3.0 to 6.5 with the increment of 0.5 pH units. The pH 5.0 fraction was enriched mostly with β-LG. However, α-lactalbumin was also collected from the same solution (data not shown). Thus, the pH values of buffer at which fractions were collected were set to 4.2, 4.8, 5.5, and 6.0; consequently, one single band of proteins was observed in the range of 14 and 17 KDa (Figure 1) and fraction at pH 4.8 was mostly enriched by β-LG. The 14 kDa

protein was found in this solution, which can be treated as impurity. However, the intensity of the impurity was low, and it could be seen with utilization of proteins solution of particular fraction with high concentration. The 301.3 mg of dry β-LG was from 0.1 L of WPI concentration of 10 g/L.

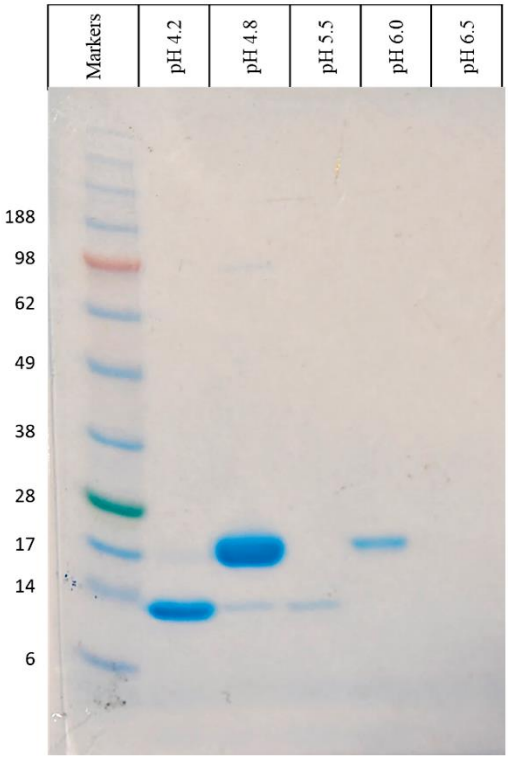

Figure 1. SDS-PAGE electropherogram at reduced condition of fractions from WPI separation.

2.2. Characterization of β-LG by MALDI-TOF/TOF-MS Analysis

In order to characterize β-LG by MALDI-TOF/TOF MS spectrometric method, isolated fractions of WPI at pH values: 4.5, 5.0, 5.5, 6.0, and 6.5 were subjected to electrophoresis in the polyacrylamide gel. Gel electrophoresis was used to determine the purity of protein in the sample. The obtained bands were obtained due to the separation of protein on the basis of the charge-to-weight ratio and indicated the presence of β-LG at about 18 kDa.

MALDI-TOF/TOF MS analysis of intact proteins carried out with two matrices: HCCA and SA. Their application allowed for observation of the presence of β-LG only in the fraction at pH 4.5 for both matrices (Figure S1) In case of both matrices used, the presence of α-lactalbumin (α-LA), which is the second major protein in whey after β-LG, was also observed for the fraction at pH 4.5. For the HCCA matrix, α-LA was also present in the fraction at pH 5.0 and with SA matrix additionally in the pH 5.5 fraction. No proteins were found in the remaining pH 6.0 and pH 6.5 fractions.

Comparing the utilization of both matrices, it was found that it is possible to observe isoforms of the protein with sinapic acid. Masses obtained for the protein with application of HCCA and SA as matrices using the MALDI/TOF MS by the intact approach are shown in Table 1.

Table 1. Masses obtained for HCCA and SA matrices using MALDI TOF/TOF MS in the intact approach.

		pH 4.5		pH 5.0		pH 5.5		pH 6.0	pH 6.5
		Mass [kDa]							
HCCA	β-LG	18.348 ± 0.137		–		–		–	–
	α-LA	14.173 ± 0.137		14.184 ± 0.137		–		–	–
SA	β-LG	18.301 18.382	±0.000	–		–		–	–
	α-LA	14.197 14.415	±0.000	14.190 14.399	±0.000	14.199 14.417	±0.000	–	–

More detailed investigations of the β-LG fraction components were carried out after their tryptic digestion, after which the fingerprints obtained in the positive reflection mode were analyzed. The mass spectra of tryptic peptides obtained for the fraction collected for β-LG are presented in Figure S2 and Table 2.

Table 2. MS and MS/MS identification of β-lactoglobulin peptides isolated from WPI.

Mass [Da]		Intensity	Sequence Range	Sequence from MS/MS
Measured	Theoretical			
837.527	837.476	650.565	158–164	ALPMHIR
1121.531	1121.468	335.855	77–85	WENGECAQK
1193.758	1193.678	188.018	108–117	VLVLDTDYKK
1245.658	1245.584	262.086	141–151	TPEVDDEALEK
1635.868	1633.775	1016.811	141–154	TPEVDDEALEKFDK
1715.902	1715.806	5737.401	165–178	LSFNPTQLEEQCHI
2313.428	2313.259	2143.636	57–76	VYVEELKPTPEGDLEILLQK
2355.446	2355.365	220.694	87–107	HAFKTKIPAVFKIDALNENK
2707.374	2707.376	2194.688	31–56	VAGTWYSLAMAASDISLLDAQSAPLR
2846.512	2846.480	431.587	155–178	ALKALPMHIRLSFNPTQLEEQCHI

2.3. *Characterization of β-LG Zeta Potential*

The zeta potential was investigated in the pH stability range of solvent component and protein. Figure 2 depicts pH the dependence of the β-LG zeta potential dispersed in several media with concentration 0.09% (*w*/*v*): sodium citrate, sodium chloride, potassium chloride, and ammonium sulfate. The zeta potential dependences on four solvent compositions were typical for proteins.

At a pH value lower than the isoelectric point (pI), the zeta potential was positive. In contrast, at a pH value higher than pI, the zeta potential was negative. The highest positive values of the zeta potential were observed in pH 3.0, and the sodium citrate buffer accounted for 26.4 ± 4.1 mV. In that solution, the standard deviations of the zeta potential were also found to be the lowest. The lowest value of the zeta potential at pH 3.0 was observed in the sodium chloride solution, but it was associated with the highest deviation. The isoelectric point of protein varied depending on the individual medium composition. In case of the sodium citrate buffer, it was estimated as 5.3. In turn, the higher value was observed for the other mediums. For example, in the ammonium sulfate solvent the pI reached 7.6. In the sodium citrate buffer, the protein had the lowest zeta potential value in alkaline condition −34.8 ± 4.8 mV. In the other medium conditions, the zeta potential was higher, reaching the zero value with a much higher deviation. The highest values of zeta potential deviation were recorded for the ammonium sulfate solvent in the whole pH range.

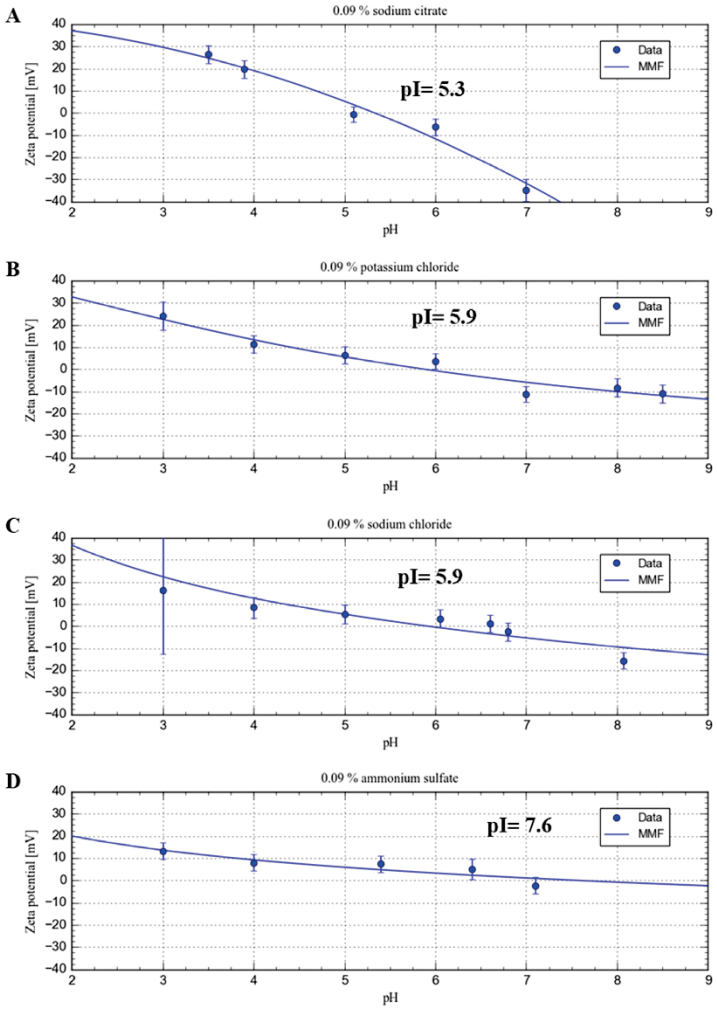

Figure 2. The pH dependence of the zeta potential at 0.09% (*w*/*v*) sodium citrate (**A**), potassium chloride (**B**), sodium chloride (**C**), and ammonium sulfate (**D**). The blue line represents fitted line to the experimental data (sigmoidal fitting, MMF function).

2.4. Characterization of β-LG Oligomerization by CE

The goal of the electrophoretic study was to monitor the β-LG oligomerization process. The Figure 3A–C shows the electropherograms of β-LG at pH 3.0, 5.0, and 7.0, respectively. The sample at pH 3.0 can be characterized by one CE signal zone (1) at the 15.16 min electromigration time

(Figure 3A). In case of protein suspension in the buffer at pH 5.0 (1–8), the number of CE signals occurred at 8 (Table 3, Figure 3B). In contrast application of buffer at pH 7.0 resulted in the observation of three signals (1–3) (Table 3, Figure 3C).

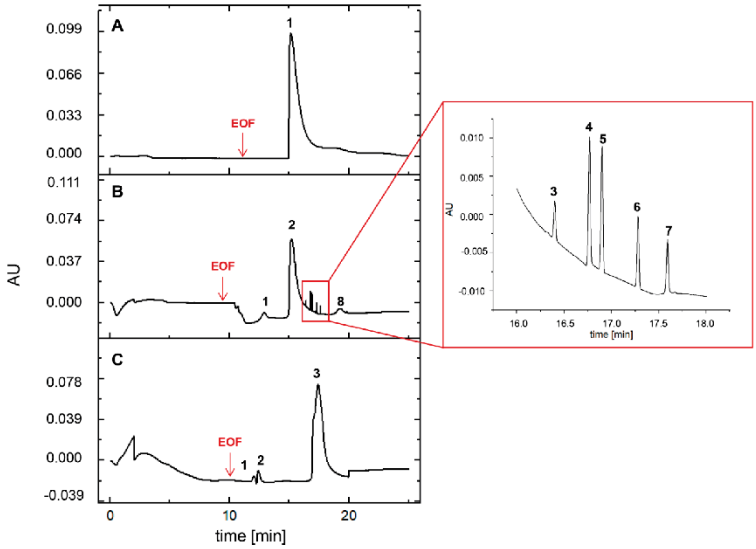

Figure 3. Electropherogram of β-LG at pH 3.0 (**A**), 5.0 (**B**), and 7.0 (**C**). The EOF acronym means the electro-osmotic flow. The compounds (oligomeric forms of protein and impurities) leaving the capillary were signed with subsequent numbers in each electropherogram.

Table 3. Migration times (tm, min), electrophoretic mobility (μe, cm^2/Vs) of β-lactoglobulin obtained at different pH values.

Migration Time (t_m, Min)			Electrophoretic Mobility (μ_e, cm^2/V_s)		
pH = 3	pH = 5	pH = 7	pH = 3	pH = 5	pH = 7
15.16	12.89	1.95	0.003	0.100	−0.001
	15.20	11.99		0.059	0.004
	16.42	12.39		0.049	0.003
	16.75	17.42		0.047	0.001
	16.90			0.046	
	17.29			0.043	
	17.60			0.042	
	19.25			0.035	
	19.83			0.033	

The electrophoretic mobility (μe, cm^2/Vs) value of β- lactoglobulin at pH 5.0 and 7.0 decreased within the CE analysis time (Table 3). Different buffer conditions affect the changes in electrophoretic mobility of β-LG, and consequently, its stability. According to the Smoluchowski equation [50], the zeta potential (ZP) depends proportionally on electrophoretic mobility of particular colloidal particles and inversely proportional to the dielectric constant of the medium. Since the ZP value is a crucial parameter for determination of long term stability of biocolloids. It has been assumed that ZP values between +30 mV and −30 mV typically demonstrate low degree of stability. In addition, deviation from

these values provide higher stability of biocolloids [51,52]. Based on the obtained results, it can be concluded that β-lactoglobulin at pH 5.0 has a high tendency to oligomerization as well as creation of aggregates. In comparison with pH 3.0 and 7.0, electrophoretic separation of β-LG around its isoelectric point (pI) provides the highest number of signals, and consequently, lower electrophoretic mobility rate and dispersion stability were observed (Figure 3B, Table 3).

2.5. Characterization of β-LG Self-Association Using AF4-UV-MALS

The β-LG was characterized by multi-angle light scattering technique in view to investigate the molar masses (molecular form) in 0.09% sodium citrate buffer at three pHs: 3.0, 5.0, and 7.0. To achieve this goal, the AF4 was coupled to the MALS detector. Figure 4 presents the acquired fractograms. The normal mechanism of separation was obtained for all tested conditions. The mass of the first fraction was dominant for all the samples in the whole pH range.

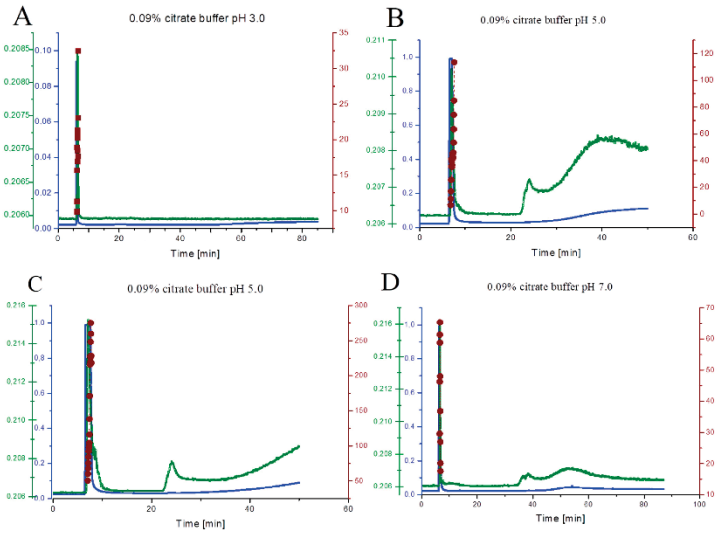

Figure 4. AF4-UV–MALS fractograms of β-LG in 0.09% (*w*/*v*) sodium citrate pH 3.0 (**A**), 5.0 (**B**,**C**), and 7.0 (**D**). The blue scale comes from UV detector (signal in V), green scale from MALS detector (92 angle, signal in V), and brown scale indicates for weighted-average molar mass (kDa).

At pH 3.0, two fractions were recorded. The first fraction, obtained between 5 and 6 min of the analysis, had a mean weight average molar mass of 22.1 ± 0.5 kDa (Figure 4A, Table 4). The second fraction was registered as a weak signal, appearing from about 55 min of the analysis.

Table 4. Mean of weight average molar mass, radius of gyrations, and protein content in the first fraction at pH 3.0, 5.0, and 7.0 from AF4–UV-MALS analyses.

Analysis at pH Buffer	Radius of Gyration [nm]	Mw Average [kDa]	Mass of Fraction from UV [μg]
3	45.1 ± 4.1	22.1 ± 0.5	230 ± 41
5	83.0 ± 35.8	149.0 ± 13.7	176 ± 63
5	115.1 ± 18.4	50.2 ± 12.5	325.2 ± 28.1
7	37.2 ± 7.9	38.7 ± 8.2	161 ± 23

Similarly, at pH 5.0, two fractograms were shown (Figure 4B,C). Both of them present three fractions of protein particles. The Figure 4B shows the particles with a mean weight average molar mass of 50.2 ± 12.5 kDa, while the Figure 4C indicate the presence of particles with a three times higher mass, reaching the mean at 149.0 ± 13.7 kDa. The first fraction was eluted just after the focusing step (from 6.5 min to 8 min of the analysis); the second fraction was eluted after 25 min of the analysis.

At pH 7.0, three fractions were recorded. The first fraction was eluted in the relaxation step (from 6 to 8 min of the analysis). Particles had a mean weight average molar mass of 38.7 ± 8.2 kDa. Another fraction is acquired at the elution step (from 45 to 65 min of the analysis) (Figure 4D).

At pH 5.0, high polydispersity in the first fraction was observed. The second and third fractions represent agglomerates of protein. The molar mass of these species was in the range of 10^5–10^7 kDa.

Figure S6 presents the example SDS-PAGE result from the analysis at pH 3.0. One single band between 14 and 17 kDa was observed. The band from the first fraction was the most intensive. The sample filtrated by the Amicon with the membrane cut off value of 10 kDa also showed bands at the aforementioned range. The results from gel electrophoresis at pH values of 5.0 and 7.0 are presented in Figure S7. At pH value of 5.0, one single band from the first fraction is observed with the range from 14 to 17 kDa, while no bands for the second and third fraction were observed. At pH 7.0, one single band is present at the aforementioned range for the first and third fractions. In case of the second fraction no bands were observed.

2.6. Characterization of β-LG Fraction from AF4-UV-MALS Using MALDI-TOF/TOF MS

The fractions from the AF4-MALS analyses were collected into Eppendorf tubes, concentrated and subjected to the gel electrophoresis as well as the MALDI-TOF/MS analysis in the intact protein mode with utilization of HCCA and DHB matrices (Figures S3 and S4).

Using the HCCA matrix for the obtained three fractions for pH 3.0, the appearance of dimers, trimers, tetramers, and pentamers (in the case of the first fraction) was observed. When the pH increased to 5.0, the same was observed for the first fraction, while no signals were recorded for the second and third fractions. A slightly different situation was observed at pH 7.0; namely, the presence of dimers, trimers, tetramers, and pentamers was observed for fraction one.

For the second fraction, similarly to the applied pH 5.0, no signal from the β-LG was observed, whereas for the third fraction the presence of dimer was detected. On the other hand, the use of the DHB matrix allowed for observation of similarity in the appearance of oligomers for individual fractions at pH 5.0 and 7.0. For pH 3.0 only, the presence of peak corresponding to the β-LG monomer was observed. Additionally, the DHB matrix compared to the HCCA matrix indicated the presence of two genetic forms (isoforms) for each pH. The β-LG masses obtained for the three fractions from the AF4-UV-MALS using the MALDI-TOF/TOF MS are shown in Table S1.

In addition, for three fractions of pH 3.0 obtained by the AF4-UV-MALS, MALDI-/TOF MS were analyzed on diluted (1:10) β-LG samples. Significant differences were observed in comparison with more concentrated samples. For both HCCA and DHB matrices, the β-LG was detected only for the first fraction. When the HCCA matrix was used, the presence of β-LG isomers was found, whereas when the DHB matrix was used, two separate β-LG signals distinguishing A and B β-LG formulas were found (Figure S5).

2.7. Characterization of β-LG Secondary Structure by Far UV-CD

The circular dichroism (CD) spectra obtained in far UV range are presented in Figure 5. Due to the absorbance of citrate buffer, the CD signal was obtained up to 190 nm; thus, the range from 190 to 250 nm were taken into consideration for analysis of the secondary structure. The differences are present according to pH values at which β-LG is dissolved. In the secondary structure range at pH value of 3.0, β-LG has a positive bands at 193 nm and two negative bands at 208 and 222 nm. In value of pH of 5.0, the protein structure exhibits a positive band at 197 nm and negative band at 217 nm.

In contrast, at alkaline condition (pH of 7.0) a positive band is observed at 196 nm and two negative bands are obtained at 212 and 221 nm.

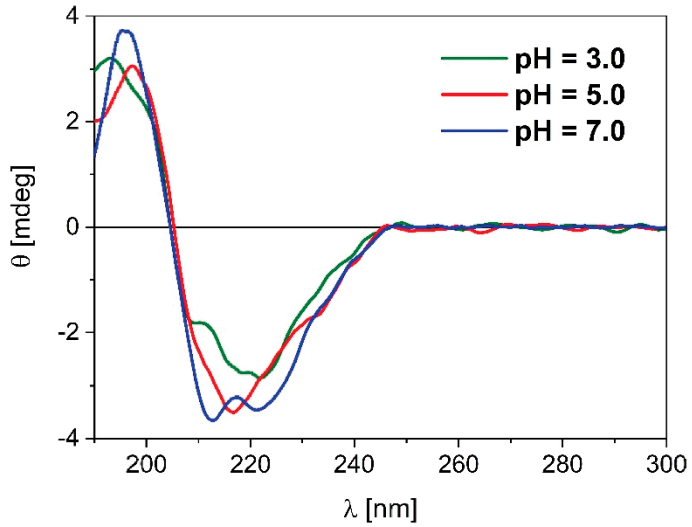

Figure 5. ECD spectra of β-LG carried out at pH 3.0, 5.0, and 7.0 in 0.09% citrate buffer.

3. Discussion

Whey proteins comprise the fraction of ruminant's milk and particularly bovine milk that is soluble at pH 4.6 [53]. They constitute about 20% of the total mass. The β-LG is the most abundant protein in bovine whey. The average concentration of the β-LG in whey is 3–4 g/L [14], but the isolated amount depends on both the procedure and the initial quantity in the milk. The yield of the isolation β-LG was 56%, taking into account the proteins amount in the WPI equal to 90% (according to the manufacturer specification) and the quantity of β-LG in the mass of protein equal to 60%.

Gel electrophoresis analysis was performed for the initial identification of isolated proteins and assessment of purity of the obtained fractions. Single fractions are the electrophoretically pure grade protein solutions (>95%). The comparison of the sample and protein marker bands can be used as a screening method for protein identification. In this way, one can state that the fraction at pH 4.2 is α-lactalbumin. This protein has a monomer form with the molecular mass of about 14 kDa, and it is the second most abundant protein in whey. The fraction at pH 4.8 is a solution of β-LG. The co-elution of α-lactalbumin with this protein was observed, but the concentration effect exists. The isoelectric point of these two proteins is closely localized at the pH scale (pI of α-lactalbumin is about 4.2–4.6) [54]. The optimal selectivity of separation was achieved by a slight pH increase (from 4.0 to 4.2) to elute α-lactoalbumin and a slight pH decrease (from 5.0 to 4.8) to obtain the elution of β-LG. Fractions that are collected at higher pH contain a smaller amount of proteins. To confirm this screening, identification by the MALDI-TOF/TOF MS analysis was performed.

The MALDI-TOF/TOF MS analysis is currently a widely used technique in proteomic research [55].

A key aspect of MALDI-TOF/MS analysis is the matrix. The use of different matrices allows for different protein coverage as well as slight differences in the obtained protein molecular weights [56]. Two matrices were used in this study: HCCA and SA to characterize β-LG obtained by

column chromatography as a control in relation to the MALDI-TOF/MS analysis for β-LG after the AF4-UV-MALS analysis. The chemical structure of the applied matrices consists of a benzene ring that absorbs UV light, hydroxyl groups for simplified mixing with hydrophilic biomolecules, and a carboxyl group that acts as a proton donor [57]. The structural details of the matrix molecule, e.g., the hydrophobicity and hydrophilicity of the compound, exert a great effect on the degree and extent of protein ionization in the matrix-assisted laser desorption [58].

The obtained MALDI-TOF MS spectrum for intact β-LG with the SA matrix showed two peaks with *m*/*z* 18 301.1 ± 0.0 and 18 382.8 ± 0.0 (Figure S1), which can correspond to β-LG B and β-LG A genetic variants [59]. The difference in masses of β-LG A and β-LG B can arise from the substitution of the amino acids such as Asp in position 64 instead of Gly and Val in position 118 instead of Ala [59]. Furthermore, β-LG A showed a higher intensity than β-LG B, indicating a higher content of β-LG A in the sample. Similar was observed using the SA matrix by Hemung et al. reporting higher intensity to β-LG A [60].

In addition, the detected octamers are assigned to be the β-LG A form [61]. Isomers A and B were also observed for α-LA at pH 4.5, 5.0, 5.5. Variant A compared to variant B differs in the presence of Gln at position 10 instead of Arg.

In the case of the β-LG characterization using the HCCA matrix, only one monomeric form was observed.

For the characterization of β-LG AF4-UV-MALS fractions using the MALDI-TOF/TOF MS, the HCCA and DHB matrixes were used. The use of the HCCA matrix allowed obtained of the mass spectrum indicating the presence of the monomer as the main peak and small peaks corresponding to oligomeric β-LG forms. However, the use of DHB matrix, apart from indicating oligomeric forms, indicated the presence of β-LG isoforms.

It is claimed that the absolute zeta potential of the investigated system greater than ±25 mV suggests that the colloidal particles would remain in a stabile dispersion state [62]. The electrostatic repulsion constitutes the next force for the steric mechanism, considering the stability of the dispersed particles in the medium. Unfortunately, at extremely low or high values of pH, the protein can degrade its quaternary structure, losing its biological activity [62]. For this reason, the zeta potential measurements were carried out in a stable range of protein and solvent components. The concentration expressed in mass units (mass/mass or mass/volume) in this study was used. This form of concentration units is frequently used in proteomic studies for proteins as well as dispersants. Therefore, we compare data with other works carried out for various proteins in our lab [55,62,63]. However, this expression of concentrations implies various molar concentrations for different salts component and consequently various ionic strength for dispersants. Therefore, direct comparison of ZP obtained data between them is not adequate.

The positive value of the zeta potential is the result of the protonation of carboxyl and amino groups from amino acid residues. The protonation is the strongest at the lowest pH investigated. However, only in citrate buffer, the zeta potential of β-LG is higher than the value for stabile dispersion. In another medium, the electrostatic stability was lower.

Deviation of zeta potential is also a significant mark of protein stability, because it is a derivate of polydysperity, impurity content, and inherently instability of sol [64] Very high deviation in sodium chloride at pH 3.0 was observed most preferably due to the degradation of protein at acidic conditions. At higher pH, the deprotonation took place and consequently lower zeta potential values were observed. According to the Hofmeister series and our results, it is clearly shown that the protein has different stability in the suspension. The strongest stabilizing agent is citrate buffer, followed by potassium chloride, ammonium sulfate, and sodium chloride. At higher pH values, the lower repulsion forces and the higher attracting forces between particles are present. The stability of protein dispersion depends on neutralization of protein charges due to specific adsorption properties to protein surface. Citrate anions have high affinity to protein cationic junction zones [65]. Another physicochemical parameter, which must be analyzed, is hydration potential of ions. Strong hydrated cations (in this case

sodium in comparison to potassium and ammonium) create a highly stabile complex with carboxylic moieties of glutamic and aspartic residue. In contrast, weakly hydrated anions bind hydrated cations tightly then strongly to amide groups [66].

The pH at which the particle has equal amount of positive and negative charged residues is called the isoelectric point (pI) [67,68]. Consequently, the particles reach pI, when the Stern layer has the same electric potential as the diffusive layer of particle. The solvent components discriminate pI of β-LG. The DLVO theory assumes that the type of counterion and the valences have impact on the diffuse layer. Positive zeta potential values appear when the anions of salts are adsorbed onto the protein particle, and they constitute the Stern layer. Counterions have a variable screening effect on the protein.

The repulsive forces are lower when the higher valance ions are present in the solution. Chloride is a single negative charged species, but citrate anion is higher in size and depending on pH can have charge from minus one to three. The citrate anion is known as a complexing protein agent. Thus, the citrate ions can stabilize the protein by electrostatic and steric mechanisms. In this way, citrate anion stabilizes more evidently the β-LG especially close to its electric equivalence. According to the electro kinetic theory, the higher valance ions bind more strongly to the protein surface than the monovalent ones and neutralize the protein charge more effectively [69]. The thicker Stern layer has impact on the diffuse layer. Thus, the pI is achieved for higher valance ions at more alkaline pH [70]. Świątek et al. [71] discussed relationships between the zeta potential and pH in various ionic strength and buffer compositions.

On the other hand, after exceeding the isoelectric point, the protein net charge is negative. In this case, the cations are counterions. In this work, sodium, potassium, and ammonium cations were assessed. For alkaline solution citrate anion is triple negative charged, and consequently sodium cation has a marginal effect, because the diffusive layer is thin, in comparison with the system when chloride is present as an anion. Sulfate anions are double negative charged species in the entire measured pH range [72]. The single charged ammonium ion also has the lower impact on the zeta potential of protein. Nonetheless, based on the obtained results, one can conclude that the cations in the solution have very low impact on the zeta potential of protein, because their influence is screened by multi charged anions. The zeta potential in the alkaline range is similar, with the exception of triple negative citrate buffer.

The self-association of the bovine β-LG was extensively studied by several physical techniques in the past [73,74].

In our study, capillary electrophoresis with the UV detection was able to separate a few different species of β-LG at pH 5.0. According to electrokinetic theory and based on the electrophoretic mobility, the order of migration is consistent with the β-LG mass. Then, it can be concluded that at pH 5.0 examined protein creates both diverse oligomeric forms (from dimers to octamers) (1–2 and 8 at Figure 3B) as well as the aggregates (3–7 at Figure 3B). On the other hand, the separation at pH 3.0 and pH 7.0 resulted in one and three signals, respectively (Figure 3A,C). Considering the phenomenon called the Tanford transition [18], the β-LG protein at pH close to physiological undergoes reversible conformational change and is mostly dimeric. Mercadante et al. [18] have demonstrated that an increase of the ionic strength strongly promotes the formation of the β-lactoglobulin dimer. Consequently, bovine β-LG is likely to be dimeric at the pH typically associated with milk [75]. However, CE data from our study also showed the formation of one homogenous β-LG fraction at the pH 3.0 (peak 1 at Figure 3A)—and it seems that the protein exhibits similar oligomerization behavior as at pH 7.0. However, the UV-CE detection is not sufficient to distinguish oligomeric forms under these conditions; hence, it was necessary to implement another approach with the AF4-UV-MALS technique.

Our results at acidic conditions show the monomeric state of β-LG, in contrast to the alkaline environment, where β-LG exists as a dimer [18]. Genetic variants β-LG A and β-LG B show structurally high resolution in a monomeric and dimeric state. For the β-LG A variant at low temperatures <10 °C, moderate ionic strength about 0.1 M, and near the isoelectric point about pH, 5.3 there is a low

resolution of structural evidence for octameric form about 144 kDa. In contrast, for genetic variant β-LG B, no oligomerization of higher order is observed [18].

At pH 3.0 in the 0.09% sodium citrate dispersion, the monomer form was dominant. The mean weight average molar mass is quite consistent with the theoretical value. At pH 5.0, the results are unclear, because they indicate various forms of the protein in this condition. Additionally, the separation technique did not isolate these forms onto individual fractions. However, one can state that at pH 5.0, the protein creates from dimer to octamer forms. Two sorted series of the result are shown. The first series indicate the presence of a dimer, trimer, and tetramer form. The second series shows the octamer form. It means the β-LG has dynamic equilibrium between these species and the presence of these individual is not dependent on the pH, ionic strength, and temperature, but the difference in the protein concentration can be decisive. The higher content causes the octamer formation to depend on the concentration in the channel [42]. Thus, under this step, the particle concentration near the membrane rises to maximal values with much bigger content than in the stock solution. This local compacting can enhance the self-association of the β-LG. In turn, lower content entails to the formation of lower associate species. Beside the pH dependency, the ionic strength has a strong impact on the stabilization of the forms [76]. A higher content of salts stabilizes dimer [73], but when exceeding a certain value, it leads to the monomer formation. According to literature, our results confirm the occurrence of the dimeric form of the β-LG at pH 7.0 [73].

In all the analyses, the agglomerate fractions are detected. In reference to the zeta potential results, the repulsion–attraction forces are always present. Citrate ion stabilizes protein effectively in the acidic condition, so the only small amount of aggregate was detected. On the other hand, citrate also has significant reducing capability [77]. At pH close to isoelectric point, the attraction forces are dominant, and consequently, the aggregate is created rapidly [78]. The two fractions of agglomerate are presented. The formation of the agglomerate takes place on the diffuse barrier. At pH 7.0, two fractions of the agglomerate are also detected.

The electrokinetic theory does not explain that phenomena, because a strong negative value of the zeta potential was measured. The creation of the stabile complexes of protein with the citrate ion is the possible reason. Marioli and Kok analyzed the β-LG in 0.15 M PBS buffer at pH 7.2 using AF4 [48]. Fractogram also contained two fractions: dimers were reported in the first fraction. However, authors did not discuss the source of the less intensive second fraction.

The electropherograms (as a control) show that only the β-LG was detected after the separation process. The protein did not degrade under the analysis conditions.

We carried out the CD analysis to obtain information about the main conformation(s) of our system at pH values of 3.0, 5.0, and 7.0. This analysis was supported by the Secondary Structure Estimation (SSE) software from JASCO based on the Principle Component Regression (PCR) method. In acidic condition, the obtained signals indicated mainly β-sheet conformations (38%) with similar amount of random coil structures and some amounts of α-helical conformation (13%). In turn, in pH value of 5.0, β-sheet conformation is still dominant (35%), while the amount of α-helical structure increased about twice (25%). Finally according CD spectra, at pH of 7.0 α-helical, β-sheet and random conformations are approximately at the same amount (*ca.* 30%) in equilibrium of 0.09% citrate buffer. These results are in accordance with works cited in introduction section. The main conformation of β-LG is antiparallel β-pleated sheets with some content of α-helical conformation [26]. Although cited works were focused on neutral and alkaline pH environment (pH 6–9) where β-LG possesses dimeric structure, Wada et al. report β-sheet conformation and no noted differences between pH dependence (5 mM sodium phosphate buffer, pH 7.5 and 5 mM acetate buffer, pH 3.0) [22]

4. Materials and Methods

4.1. Protein Isolation from WPI Solution

WPI was purchased from the Dairy Cooperative Spomlek (Radzyń Podlaski, Poland). The isolation method for the fractionation of protein from the WPI's solution was followed by the Etzel procedure [79] with minor modifications and optimization. Elution solutions have been optimized by small change of pH in comparison with the original patent. In our study, this small change leads to increasing the purity fractions.

Firstly, a 10 g/L solution of the WPI in 0.2 M citrate buffer pH 3.7 was prepared. The solution was adjusted to pH 3.0 against pH meter. Afterwards the soluble protein fraction was clarified from curds, lipids, and other insoluble parts using a centrifuge (14,400 rpm, 1 h, T = 4 °C). After that, the solution was mixed with SP Sephadex C-25 (GE Healthcare Bio-Sciences AB, Sweden), the resin of which was swelled and conditioned prior to separation. The mass ratio of WPI to dry mass of the ion exchanger was 0.33. The chromatographic column was packed with about 40 mL of slurry at room temperature. After washing with water, the elution procedure was performed with increasing pH (from 3.0 to 6.5) conditions. Additionally, the buffer solution at pH 3.0 consisted of 0.02 M EDTA, while buffer solutions pH 6.0 and 6.5 contained calcium chloride 0.05 M. The column was eluted by 1 column volume (CV) of eluents. The fractions at pH 4.2 and 4.8 were collected. The resin was regenerated by eluting with the 2 M sodium chloride solution.

The protein solution was stored at 4 °C. It was concentrated by flushing nitrogen through the solution. Amicon centrifugal filter units (Merck, Darmstadt, Germany) with nominal cut-off value of 10 kDa were used to change the solvent from the citrate buffer to water. The β-LG solution (pH 4.8 fraction) was lyophilized to dry mass. The powder was stored at −80 °C.

4.2. SDS-PAGE Analysis of Protein

Protein solution was analyzed by the SDS-PAGE method using Coomassie Blue R-350 staining and Invitrogen Bolt™ 4–12% Bis-Tris Plus polyacrylamide gel (Thermo Scientific, Waltham, MA, USA) with SeeBlue® Plus2 Pre-Stained Standard (Thermo Scientific, Waltham, MA, USA) in non-reduced and reduced modes with, applying MES Running Buffer.

In case of water samples, protein solution with concentration of about 1 mg/mL was prepared. The protein solution was separated by the AF4 fractionation and was concentrated by flushing nitrogen through the solution. Amicon centrifugal filter units (Merck, Darmstadt, Germany) with nominal cut-off value of 10 kDa were used to change the solvent in the same way as described above. According to the manufacturer procedure (Thermo Scientific, Waltham, MA, USA)), proteins solutions were dissolved in a 2.5 µL Load Sample buffer (LDS), reduced and alkylated using the Sample Reducing Agent (10×) dithiothreitol (DTT) and iodoacetamide (IAA), respectively. Samples for analysis in a non-reduced mode were prepared by dissolving proteins fractions in the LDS buffer. The samples were then heated for 10 min at 70 °C and were introduced to the gel.

The electrophoretic process was performed at 200 V. After the separation process, the gel was stained for 20 min and destaining of the gel was carried out for 24 h in deionized water. The SDS-PAGE was performed also after the AF4-UV-MALS separation in order to confirm the purity of the fraction collected. The fractions were concentrated and analyzed as described above.

4.3. Characterisation of β-LG by MALDI-TOF/TOF MS Analysis

For this part of the study mass spectrometer MALDI-TOF/TOF (Bruker Daltonics, Bremen, Germany) equipped with a modified Nd:YAG laser operating at the wavelength of 355 nm and frequency of 2 kHz was used. The reagents used in the MALDI-TOF/TOF MS analysis were purchased from Sigma-Aldrich (Steinheim, Germany) with the highest commercially available degree of purity. The α-cyano-4-hydroxycinnamic acid (HCCA), 3,5-dimethoxy-4-hydroxycinnamic acid (sinapic acid—SA) and 2,5-dihydroxybenzoic acid (DHB) were used as a matrix and Protein Calibration

Standard II for intact analysis and Peptide Calibration Standard II applied for the PMF study (all from Bruker Daltonics, Bremen, Germany) were used for calibration.

The spectrometric analysis for both intact and digested protein samples was performed in three stages. Stage I—gel electrophoresis according to the procedure described in Part 2.2 to check the purity of the obtained protein fraction. Stage II—the digestion of proteins in-gel with trypsin according to Bruker Proteomic protocols for mass spectrometry [80]. β-LG was dissolved in the buffer 10 mM ammonium bicarbonate (NH4HCO3, ABC) and incubated at 37 °C with trypsin overnight. Subsequently, the extraction of peptides was carried out by addition of 10 µL of 50% ACN with 1% TFA. Stage III—both intact and digested samples were applied to ground steel targets purchased from Bruker Daltonics (Bremen, Germany) using dry droplet method and spectrometric analysis.

The MS spectra of β-LG intact were recorded in a linear positive mode in the range of *m/z* 5000–100,000, while the peptide fingerprint mass spectra (PMF) of protein digested with trypsin was recorded in a reflectron positive mode in the range of *m/z* 500–3500. In both cases, the measurements were carried out at an accelerating voltage of 25 kV. To determine the fragment spectra, the laser-induced fragmentation technique (LIFT) in the same *m/z* range was used. The peptides obtained after the tryptic digestion of β-LG were identified using the BioTools software (Bruker Daltonics, Bremen, Germany). All data was collected manually, and the mass tolerance was set to 0.3 Da for the spectra and calibrated internally on immonium ions at laser power 80% and attenuation 27% for the MS/MS analysis.

4.4. Zeta Potential (ζ) Determination for β-LG

Different solutions at 0.09% (*w/v*) concentration were prepared: sodium and potassium chloride at pH range from 3.0 to 8.5 and sodium citrate, ammonium sulfate at pH range from 3.5 to 7.0 was also prepared. The sodium hydroxide, hydrochloric, sulfuric, or citric acids (1 M and 0.1 M acid and base solutions) (all reagents from Sigma-Aldrich, Steinheim, Germany) were added to the solution to obtain required pH values against pH meter. In this way, mixing of different ions was avoided. β-LG solutions at 0.4 mg/mL in all of these dispersants were prepared. The sample was loaded to DTS1070 cuvette (Malvern, Worcestershire, UK), and zeta potential was determined by Malvern Zetasizer NanoZS apparatus (Malvern, Worcestershire, UK).

Smoluchowski's approximation ($f(\kappa\alpha) = 1.5$) in Henry's equation (Equation (1)) was used [81]:

$$\mu_e = \frac{2\varepsilon_r \epsilon_O \zeta f(\kappa\alpha)}{3\nu} \quad (1)$$

where ε_r is the relative permittivity, ϵ_O is the permittivity of a vacuum, ζ is the zeta potential (mV), $f(\kappa\alpha)$ is Henry's function, and ν is the viscosity (cP) of the liquid medium at the experimental temperature (25 °C). Measurements were performed in the automatic mode selection of the voltages and number of runs. Each measurement was performed in triplicate.

4.5. Characterization of β-LG by CE

The sample of β-LG was suspended in 0.09% citrate buffer at pH = 3.0, 5.0 and 7.0, respectively. CE analysis was performed using PA 800 plus (Beckman Coulter system, Brea, CA, USA) equipped with a DAD with the use of fused silica capillary (I.D. = 50 µm; Ltot = 67 cm; Leff = 50 cm; Beckman Coulter Inc., USA). Before use, a new capillary was rinsed with 0.1 M NaOH, deionized water, and the running background electrolyte (BGE) for 10 min. The protein samples were injected into the capillary with a pressure mode (3 psi, 5 s) and the analysis was performed at a constant voltage (10 kV) and the temperature of 23 °C. The sample at pH = 7 was analyzed in reverse polarity. The signal was monitored at λ = 214 nm. Between the runs, the capillaries were washed with 0.1 M NaOH, deionized water, and BGE for 2 min each. As the EOF marker, thiourea at 1 mg/mL concentration was used.

The electrophoretic mobility of β-LG during the CE assay was calculated from the Equation (2):

$$\mu_e = \frac{L_{tot}L_{eff}}{V}\left(\frac{1}{t_m - t_{EOF}}\right) \quad (2)$$

where μ_e is an electrophoretic mobility [cm2/V*s], L_{tot} is the total length of the capillary [cm], L_{eff} is the length to the detector [cm], t_m is the migration time [s], t_{EOF} is the EOF migration time [s], and V is the applied potential [V].

4.6. Characterization of β-LG by AF4-UV-MALS

Solutions of β-LG at the final concertation of 3 mg/mL were prepared in 0.09% (*w*/*v*) citrate buffer at pH 3.0, 5.0, and 7.0 values. The AF2000 Multi Flow system (Postnova Analytics GmbH, Landsberg am Lech, Germany) was used in this research. The used apparatus configuration has been the same as [45]. The specific refractive index increment value (dη/dc) of β-LG was set at 0.185 mL/g, and the extinction coefficient was of 0.960 mL/g cm. The UV detector acquires data at 280 nm. Berry model was used to calculate molar masses and the radius of gyration (Rg). Citrate buffer 0.09% at certain pH was used as a carrier liquid and prepared from the Milli-Q system (Merck Millipore, MA, USA)) and were filtered using 0.1 µm nylon membrane (Merck Millipore, Warsaw, Poland). All fractionation analyses were performed at room temperature. Conditions of AF4 fractionations were showed in Table 5, and the cross-flow program during elution is presented in Figure S8.

Table 5. The focusing parameters of method at three experimental conditions.

pH	Focus			
	Injection Flow [mL/min]	Injection Time [min]	Initial Cross Flow [mL/min]	Transition Time [min]
3.0	0.1	5.0	3.0	1.0
5.0	0.2		1.0	3.0
7.0	0.1		1.0	2.0

4.7. Characterization of β-LG by Far UV Circular Dichroism (UV–CD)

The sample of β-LG (0.3 mg/mL) was suspended in 0.09% citrate buffer at pH = 3.0, 5.0, and 7.0, respectively. Far UV circular dichroism (UV–CD) was performed using J-815 spectrometer (JASCO, Cremella (LC), Italy). The experimental conditions were as follows: sensitivity: high, response: 1 sec, band width: 1 nm, scanning speed: 50 nm/min, accumulation: 10, data pitch: 0.2 nm. All data were background-corrected against citrate buffer in certain pH. All data were acquired in the range from 300 to 190 nm at room temperature using the quartz cell with a path length of 0.02 cm. For estimation of the secondary structural composition, the ECD spectra were submitted to the JASCO Secondary Structure Estimation (SSE) software based on the Principal Component Regression method (PCR). The multivariate analysis allowed us to obtain quantitative data of α-helix, β-sheet, turns, and random coil contents from experimental CD spectra.

5. Conclusions

The β-LG was isolated from the WPI solution. The fast flow column chromatographic technique was used. The electrophoretic purity of the isolated protein was achieved. The MALDI-TOF/TOF MS analyses assisted for the identification of protein. Additionally, the matrices used in the studies allowed us to distinguish the protein isoform A and B. The pH correlation with the zeta potential in four solvent compositions was studied. The medium components have significant impact on the protein stability and the isoelectric point. The capillary electrophoresis with the UV detection was applied for the protein oligomerization screening. Obtained data were further confirmed by AF4-UV-MALS. Multi-angle light scattering was used to characterize the self-association of β-LG in citrate buffer at pH: 3.0, 5.0, and 7.0. The monomer was present at acidic condition. At pH 5.0, the forms from dimer to octamer were observed, wherein the AF4 system did not separate these forms into individual fractions. The equilibria also depend on the protein concentration. At pH 7.0, the β-LG forms a dimer.

The SDS-PAGE and MALDI-TOF/TOF MS analyses after the AF4 separation process were used to identify the purity of the fraction. It showed that the separation process did not have a negative impact on the protein structure. The far circular dichroism (CD) spectra carried out at pH 3.0, 5.0, and 7.0 confirmed that the β-sheet conformation is dominant at pH 3.0, 5.0, while at pH 7.0 this conformation is approximately in the same quantity as a-helix and random structures.

Supplementary Materials: The following are available online at http://www.mdpi.com/1422-0067/21/24/9711/s1.

Author Contributions: Conceptualization, A.G., P.P., T.K. and B.B.; Data curation, M.G.; Formal analysis, A.G., P.P. and T.K.; Funding acquisition, P.P.; Investigation, A.G., A.R. and A.K.-G.; Methodology, A.G., P.P., A.R. and A.K.-G.; Project administration, P.P. and B.B.; Software, T.K.; Supervision, B.B.; Validation, A.G.; Visualization, A.G., A.R., A.K.-G. and T.K.; Writing—original draft, A.G., P.P., A.R., A.K.-G. and T.K. All authors have read and agreed to the published version of the manuscript.

Funding: This work was financially supported by the National Science Centre within the framework 35 of Opus 14 project No. 2017/27/B/ST4/02628 (2018–2021) and Young Scientist Grant on Faculty of Chemistry NCU (No. 2092/2019).

Acknowledgments: Paweł Pomastowski and Bogusław Buszewski are members of Toruń Center of Excellence "Towards Personalized Medicine" operating under Excellence Initiative-Research University.

Conflicts of Interest: The authors declare no conflict of interest. The funders had no role in the design of the study; in the collection, analyses, or interpretation of data; in the writing of the manuscript, or in the decision to publish the results.

References

1. Elzoghby, A.O.; Elgohary, M.M.; Kamel, N.M. *Implications of Protein- and Peptide-Based Nanoparticles as Potential Vehicles for Anticancer Drugs*, 1st ed.; Elsevier Inc.: Amsterdam, The Netherlands, 2015; Volume 98.
2. Tai, C.S.; Chen, Y.Y.; Chen, W.L. β -Lactoglobulin influences human immunity and promotes cell proliferation. *Biomed. Res. Int.* **2016**, *2016*. [CrossRef] [PubMed]
3. Sakai, K.; Sakurai, K.; Sakai, M.; Hoshino, M.; Goto, Y. Conformation and stability of thiol-modified bovine beta-lactoglobulin. *Protein Sci.* **2000**, *9*, 1719–1729. [PubMed]
4. Swain, B.C.; Subadini, S.; Rout, J.; Sakshi; Mishra, P.P.; Sahoo, H.; Tripathy, U. Biophysical study on complex formation between β-Lactoglobulin and vitamin B12. *Food Chem.* **2020**, *312*, 126064. [CrossRef] [PubMed]
5. Mensi, A.; Choiset, Y.; Rabesona, H.; Haertlé, T.; Borel, P.; Chobert, J.M. Interactions of β-lactoglobulin variants A and B with vitamin A. Competitive binding of retinoids and carotenoids. *J. Agric. Food Chem.* **2013**, *61*, 4114–4119. [CrossRef]
6. Yang, M.C.; Guan, H.H.; Liu, M.Y.; Lin, Y.H.; Yang, J.M.; Chen, W.L.; Chen, C.J.; Mao, S.J.T. Crystal structure of a secondary vitamin D3 binding site of milk β-lactoglobulin. *Proteins Struct. Funct. Genet.* **2008**, *71*, 1197–1210. [CrossRef] [PubMed]
7. Carrillo, W.; Guzmán, X.G.; Vilcacundo, E. Native and heated hydrolysates of milk proteins and their capacity to inhibit lipid peroxidation in the Zebrafish larvae model. *Foods* **2017**, *6*, 81. [CrossRef] [PubMed]
8. Witono, Y.; Taruna, I.; Windrati, W.S.; Azkiyah, L.; Sari, T.N. 'Wader' (*Rasbora jacobsoni*) protein hydrolysates: Production, biochemical, and functional properties. *Agric. Agric. Sci. Procedia* **2016**, *9*, 482–492. [CrossRef]
9. Lisak, K.; Toro-Sierra, J.; Kulozik, U.; Bozanic, R.; Cheison, S.C. Chymotrypsin selectively digests β-lactoglobulin in whey protein isolate away from enzyme optimal conditions: Potential for native α-lactalbumin purification. *J. Dairy Res.* **2013**, *80*, 14–20. [CrossRef]
10. Rabbani, G.; Ahmad, E.; Zaidi, N.; Fatima, S.; Khan, R.H. PH-induced molten globule state of Rhizopus Niveus lipase is more resistant against thermal and chemical denaturation than its native state. *Cell Biochem. Biophys.* **2012**, *62*, 487–499. [CrossRef]
11. Dullius, A.; Goettert, M.I.; de Souza, C.F.V. Whey protein hydrolysates as a source of bioactive peptides for functional foods—Biotechnological facilitation of industrial scale-up. *J. Funct. Foods* **2018**, *42*, 58–74. [CrossRef]
12. Madureira, A.R.; Pereira, C.I.; Gomes, A.M.P.; Pintado, M.E.; Xavier Malcata, F. Bovine whey proteins—Overview on their main biological properties. *Food Res. Int.* **2007**, *40*, 1197–1211. [CrossRef]
13. Maté, J.; Krochta, J. β-Lactoglobulin separation from whey protein isolate on a large scale. *J. Food Sci.* **2006**, *59*, 1111–1114. [CrossRef]

14. Hahn, R.; Schulz, P.M.; Schaupp, C.; Jungbauer, A. Bovine whey fractionation based on cation-exchange chromatography. *J. Chromatogr. A* **1998**, *795*, 277–287. [CrossRef]
15. Imafidon, G.I.; Farkye, N.Y.; Spanier, A.M. Isolation, purification, and alteration of some functional groups of major milk proteins: A review. *Crit. Rev. Food Sci. Nutr.* **1997**, *37*, 663–689. [CrossRef] [PubMed]
16. Berino, R.P.; Báez, G.D.; Ballerini, G.A.; Llopart, E.E.; Busti, P.A.; Moro, A.; Delorenzi, N.J. Interaction of vitamin D3 with beta-lactoglobulin at high vitamin/protein ratios: Characterization of size and surface charge of nanoparticles. *Food Hydrocoll.* **2019**, *90*, 182–188. [CrossRef]
17. Adams, J.J.; Anderson, B.F.; Norris, G.E.; Creamer, L.K.; Jameson, G.B. Structure of bovine β-lactoglobulin (variant A) at very low ionic strength. *J. Struct. Biol.* **2006**, *154*, 246–254. [CrossRef] [PubMed]
18. Mercadante, D.; Melton, L.D.; Norris, G.E.; Loo, T.S.; Williams, M.A.K.; Dobson, R.C.J.; Jameson, G.B. Bovine β-lactoglobulin is dimeric under imitative physiological conditions: Dissociation equilibrium and rate constants over the pH range of 2.5–7.5. *Biophys. J.* **2012**, *103*, 303–312. [CrossRef]
19. Verheul, M.; Pedersen, J.S.; Roefs, S.P.F.M.; De Kruif, K.G. Association behavior of native β-lactoglobulin. *Biopolymers* **1999**, *49*, 11–20. [CrossRef]
20. Greenfield, N.J. Using circular dichroism spectra to estimate protein secondary structure. *Nat. Protoc.* **2007**, *1*, 2876–2890. [CrossRef]
21. Loch, J.I.; Bonarek, P.; Lewiński, K. Conformational flexibility and ligand binding properties of ovine β-lactoglobulin. *Acta Biochim. Pol.* **2019**, 66. [CrossRef]
22. Wada, R.; Fujita, Y.; Kitabatake, N. Effects of heating at neutral and acid pH on the structure of β-lactoglobulin A revealed by differential scanning calorimetry and circular dichroism spectroscopy. *Biochim. Biophys. Acta Gen. Subj.* **2006**, *1760*, 841–847. [CrossRef] [PubMed]
23. Rodrigues, R.M.; Avelar, Z.; Vicente, A.A.; Petersen, S.B.; Pereira, R.N. Influence of moderate electric fields in β-lactoglobulin thermal unfolding and interactions. *Food Chem.* **2020**, 304. [CrossRef] [PubMed]
24. Comaa, A.I.; Nsonzi, F.; Sedman, J.; Ismail, A.A. Enhanced unfolding of Bovine β-Lactoglobulin structure using microwave treatment: A multi-spectroscopic study. *Food Biophys.* **2016**, *11*, 370–379. [CrossRef]
25. Güler, G.; Džafić, E.; Vorob'Ev, M.M.; Vogel, V.; Mäntele, W. Real time observation of proteolysis with Fourier transform infrared (FT-IR) and UV-circular dichroism spectroscopy: Watching a protease eat a protein. *Spectrochim. Acta Part. A Mol. Biomol. Spectrosc.* **2011**, *79*, 104–111. [CrossRef]
26. Simões, L.S.; Abrunhosa, L.; Vicente, A.A.; Ramos, O.L. Suitability of β-lactoglobulin micro- and nanostructures for loading and release of bioactive compounds. *Food Hydrocoll.* **2020**, *101*. [CrossRef]
27. Khorsand Ahmadi, S.; Mahmoodian Moghadam, M.; Mokaberi, P.; Reza Saberi, M.; Chamani, J. A comparison study of the interaction between β-lactoglobulin and retinol at two different conditions: Spectroscopic and molecular modeling approaches. *J. Biomol. Struct. Dyn.* **2015**, *33*, 1880–1898. [CrossRef]
28. Engelhardt, K.; Lexis, M.; Gochev, G.; Konnerth, C.; Miller, R.; Willenbacher, N.; Peukert, W.; Braunschweig, B. PH effects on the molecular structure of β-lactoglobulin modified air-water interfaces and its impact on foam rheology. *Langmuir* **2013**, *29*, 11646–11655. [CrossRef]
29. Harnsilawat, T.; Pongsawatmanit, R.; McClements, D.J. Characterization of β-lactoglobulin-sodium alginate interactions in aqueous solutions: A calorimetry, light scattering, electrophoretic mobility and solubility study. *Food Hydrocoll.* **2006**, *20*, 577–585. [CrossRef]
30. Jachimska, B.; Świątek, S.; Loch, J.I.; Lewiński, K.; Luxbacher, T. Adsorption effectiveness of β-lactoglobulin onto gold surface determined by quartz crystal microbalance. *Bioelectrochemistry* **2018**, *121*, 95–104. [CrossRef]
31. Zhang, X.; Hemar, Y.; Lv, L.; Zhao, T.; Yang, Y.; Han, Z.; Li, M.; He, J. Molecular characterization of the β-lactoglobulin conjugated with fluorescein isothiocyanate: Binding sites and structure changes as function of pH. *Int. J. Biol. Macromol.* **2019**, *140*, 377–383. [CrossRef]
32. Roosen-Runge, F.; Heck, B.S.; Zhang, F.; Kohlbacher, O.; Schreiber, F. Interplay of pH and binding of multivalent metal ions: Charge inversion and reentrant condensation in protein solutions. *J. Phys. Chem. B* **2013**, *117*, 5777–5787. [CrossRef]
33. Righetti, P.G. Determination of the isoelectric point of proteins by capillary isoelectric focusing. *J. Chromatogr. A* **2004**, *1037*, 491–499. [CrossRef] [PubMed]
34. Crowther, J.M.; Lassé, M.; Suzuki, H.; Kessans, S.A.; Loo, T.S.; Norris, G.E.; Hodgkinson, A.J.; Jameson, G.B.; Dobson, R.C.J. Ultra-high resolution crystal structure of recombinant caprine β-lactoglobulin. *FEBS Lett.* **2014**, *588*, 3816–3822. [CrossRef] [PubMed]

35. Chen, F.-T.A.; Evangelista, R.A. Protein analysis by capillary electrophoresis. In *Handbook of Capillary Electrophoresis Applications*; Springer: Dordrecht, The Netherlands, 1997; pp. 173–197.
36. Dawod, M.; Arvin, N.E.; Kennedy, R.T. Recent advances in protein analysis by capillary and microchip electrophoresis. *Analyst* **2017**, *142*, 1847–1866. [CrossRef] [PubMed]
37. Recio, I.; Molina, E.; Ramos, M.; de Frutos, M. Quantitative analysis of major whey proteins by capillary electrophoresis using uncoated capillaries. *Electrophoresis* **1995**, *16*, 654–658. [CrossRef] [PubMed]
38. Pomastowski, P.; Sprynskyy, M.; Buszewski, B. The study of zinc ions binding to casein. *Colloids Surf. B Biointerfaces* **2014**, *120*, 21–27. [CrossRef] [PubMed]
39. Recio, I.; Olieman, C. Determination of denatured serum proteins in the casein fraction of heat-treated milk by capillary zone electrophoresis. *Electrophoresis* **1996**, *17*, 1228–1233. [CrossRef]
40. Paracha, S.; Hestekin, C. Field amplified sample stacking of amyloid beta (1-42) oligomers using capillary electrophoresis. *Biomicrofluidics* **2016**, *10*, 033105. [CrossRef]
41. Gates, A.T.; Lowry, M.; Fletcher, K.A.; Murugeshu, A.; Rusin, O.; Robinson, J.W.; Strongin, R.M.; Warner, I.M. Capillary electrophoretic screening for the inhibition of homocysteine thiolactone-induced protein oligomerization. *Anal. Chem.* **2007**, *79*, 8249–8256. [CrossRef]
42. Kowalkowski, T.; Buszewski, B.; Cantado, C.; Dondi, F. Field-flow fractionation: Theory, techniques, applications and the challenges. *Crit. Rev. Anal. Chem.* **2006**, *36*, 129–135. [CrossRef]
43. Giddings, J.C. A new separation concept based on a coupling of concentration and flow nonuniformities. *Sep. Sci.* **1966**, *1*, 123–125. [CrossRef]
44. Giddings, J.C. The conceptual basis of field-flow fractionation. *J. Chem. Educ.* **1973**, *50*, 667–669. [CrossRef]
45. Gołębiowski, A.; Kowalkowski, T.; Buszewski, B. Molecular parameters of low methoxylated pectin affected by gelation with copper and cadmium cations. *Bioact. Carbohydr. Diet. Fibre* **2020**, 100211. [CrossRef]
46. Dhayal, S.K.; Gruppen, H.; de Vries, R.; Wierenga, P.A. Controlled formation of protein nanoparticles by enzymatic cross-linking of α-lactalbumin with horseradish peroxidase. *Food Hydrocoll.* **2014**, *36*, 53–59. [CrossRef]
47. Andersson, M.; Wittgren, B.; Wahlund, K.G. Accuracy in multiangle light scattering measurements for molar mass and radius estimations. Model calculations and experiments. *Anal. Chem.* **2003**, *75*, 4279–4291. [CrossRef] [PubMed]
48. Marioli, M.; Kok, W.T. Recovery, overloading, and protein interactions in asymmetrical flow field-flow fractionation. *Anal. Bioanal. Chem.* **2019**, *411*, 2327–2338. [CrossRef]
49. Redeker, V.; Vinh, J.; Le Caer, J.P.; Rossier, J. Characterization of posttranslational modifications of proteins by MALDI-TOF MS: Application to the study of tubulin. *Analusis* **1998**, *26*, 22–26. [CrossRef]
50. Sze, A.; Erickson, D.; Ren, L.; Li, D. Zeta-potential measurement using the Smoluchowski equation and the slope of the current-time relationship in electroosmotic flow. *J. Colloid Interface Sci.* **2003**, *261*, 402–410. [CrossRef]
51. Wilson, W.W.; Wade, M.M.; Holman, S.C.; Champlin, F.R. Status of methods for assessing bacterial cell surface charge properties based on zeta potential measurements. *J. Microbiol. Methods* **2001**, *43*, 153–164. [CrossRef]
52. Kłodzińska, E.; Szumski, M.; Dziubakiewicz, E.; Hrynkiewicz, K.; Skwarek, E.; Janusz, W.; Buszewski, B. Effect of zeta potential value on bacterial behavior during electrophoretic separation. *Electrophoresis* **2010**, *31*, 1590–1596. [CrossRef]
53. Indyk, H.E.; Hart, S.; Meerkerk, T.; Gill, B.D.; Woollard, D.C. The β-lactoglobulin content of bovine milk: Development and application of a biosensor immunoassay. *Int. Dairy J.* **2017**, *73*, 68–73. [CrossRef]
54. Morr, C.V.; Ha, E.Y.W. Whey protein concentrates and isolates: Processing and functional properties whey protein concentrates and isolates: Processing and functional properties. *Crit. Rev. Food Sci. Nutr.* **1993**, *33*, 431–476. [CrossRef] [PubMed]
55. Buszewski, B.; Rodzik, A.; Railean-Plugaru, V.; Sprynskyy, M.; Pomastowski, P. A study of zinc ions immobilization by β-lactoglobulin. *Colloids Surf. A Phys. Eng. Asp.* **2020**, *591*, 124443. [CrossRef]
56. Lewis, J.K.; Wei, J.; Siuzdak, G. Matrix-assisted laser desorption/ionization mass spectrometry in peptide and protein analysis. *Encycl. Anal. Chem.* **2006**, 5880–5894. [CrossRef]
57. Fukuyama, Y. MALDI Matrix Research for Biopolymers. *Mass Spectrom.* **2015**, *4*, A0037. [CrossRef] [PubMed]
58. Beavis, R.C.; Chaudhary, T.; Chait, B.T. a-Cyano-4-hydroxycinnamic acid as a matrix for matrixassisted laser desorption mass-spectrometry. *Org. Mass Spectrom.* **1992**, *27*, 156–158. [CrossRef]

59. Qin, B.Y.; Jameson, G.B.; Bewley, M.C.; Baker, E.N.; Creamer, L.K. Functional implications of structural differences between variants A and B of bovine β-lactoglobulin. *Protein Sci.* **2008**, *8*, 75–83. [CrossRef]
60. Hemung, B.O.; Li-Chan, E.C.Y.; Yongsawatdigul, J. Identification of glutaminyl sites on β-lactoglobulin for threadfin bream liver and microbial transglutaminase activity by MALDI-TOF mass spectrometry. *Food Chem.* **2009**, *115*, 149–154. [CrossRef]
61. Godovac-Zimmermann, J.; Krause, I.; Buchberger, J.; Weiss, G.; Klostermeyer, H. Genetic variants of bovine β-lactoglobulin. A novel wild-type β-lactoglobulin W and its primary sequence. *Biol. Chem. Hoppe. Seyler.* **1990**, *371*, 255–260. [CrossRef]
62. Pomastowski, P.; Sprynskyy, M.; Žuvela, P.; Rafińska, K.; Milanowski, M.; Liu, J.J.; Yi, M.; Buszewski, B. Silver-lactoferrin nanocomplexes as a potent antimicrobial agent. *J. Am. Chem. Soc.* **2016**, *138*, 7899–7909. [CrossRef]
63. Pryshchepa, O.; Sagandykova, G.N.; Pomastowski, P.; Railean-Plugaru, V.; Król, A.; Rogowska, A.; Rodzik, A.; Sprynskyy, M.; Buszewski, B. A new approach for spontaneous silver ions immobilization onto casein. *Int. J. Mol. Sci.* **2019**, *20*, 3864. [CrossRef] [PubMed]
64. Uskoković, V.; Odsinada, R.; Djordjevic, S.; Habelitz, S. Dynamic light scattering and zeta potential of colloidal mixtures of amelogenin and hydroxyapatite in calcium and phosphate rich ionic milieus. *Arch. Oral Biol.* **2011**, *56*, 521–532. [CrossRef] [PubMed]
65. Salis, A.; Monduzzi, M. Not only pH. Specific buffer effects in biological systems. *Curr. Opin. Colloid Interface Sci.* **2016**, *23*, 1–9. [CrossRef]
66. Okur, H.I.; Hladílková, J.; Rembert, K.B.; Cho, Y.; Heyda, J.; Dzubiella, J.; Cremer, P.S.; Jungwirth, P. Beyond the Hofmeister series: Ion-specific effects on proteins and their biological functions. *J. Phys. Chem. B* **2017**, *121*, 1997–2014. [CrossRef]
67. Rabbani, G.; Ahmad, E.; Khan, M.V.; Ashraf, M.T.; Bhat, R.; Khan, R.H. Impact of structural stability of cold adapted Candida antarctica lipase B (CaLB): In relation to pH, chemical and thermal denaturation. *RSC Adv.* **2015**, *5*, 20115–20131. [CrossRef]
68. Cleaves, H.J. Isoelectric Point. In *Encyclopedia of Astrobiology*; Gargaud, M., Amils, R., Quintanilla, J.C., Cleaves, H.J., Irvine, W.M., Pinti, D.L., Viso, M., Eds.; Springer: Berlin/Heidelberg, Germany, 2011; p. 858. ISBN 978-3-642-11274-4.
69. Kalayan, J.; Henchman, R.H.; Warwicker, J. Model for counterion binding and charge reversal on protein surfaces. *Mol. Pharm.* **2020**. [CrossRef]
70. Kumar, S.; Yadav, I.; Ray, D.; Abbas, S.; Saha, D.; Aswal, V.K.; Kohlbrecher, J. Evolution of interactions in the protein solution as induced by mono and multivalent ions. *Biomacromolecules* **2019**, *20*, 2123–2134. [CrossRef]
71. Świątek, S.; Komorek, P.; Jachimska, B. Adsorption of β-lactoglobulin A on gold surface determined in situ by QCM-D measurements. *Food Hydrocoll.* **2019**, *91*, 48–56. [CrossRef]
72. Rabbani, G.; Kaur, J.; Ahmad, E.; Khan, R.H.; Jain, S.K. Structural characteristics of thermostable immunogenic outer membrane protein from Salmonella enterica serovar Typhi. *Appl. Microbiol. Biotechnol.* **2014**, *98*, 2533–2543. [CrossRef]
73. Sakurai, K.; Oobatake, M.; Goto, Y. Salt-dependent monomer-dimer equilibrium of bovine β-lactoglobulin at pH 3. *Protein Sci.* **2008**, *10*, 2325–2335. [CrossRef]
74. Gottschalk, M.; Venu, K.; Halle, B. Protein self-association in solution: The bovine pancreatic trypsin inhibitor decamer. *Biophys. J.* **2003**, *84*, 3941–3958. [CrossRef]
75. Kontopidis, G.; Holt, C.; Sawyer, L. Invited review: β-lactoglobulin: Binding properties, structure, and function. *J. Dairy Sci.* **2004**, *87*, 785–796. [CrossRef]
76. Hoque, M.; Gupta, J.; Rabbani, G.; Khan, R.H.; Saleemuddin, M. Behaviour of oleic acid-depleted bovine alpha-lactalbumin made LEthal to tumor cells (BAMLET). *Mol. Biosyst.* **2016**, *12*, 1871–1880. [CrossRef] [PubMed]
77. Garcia-Hernandez, C.; Freese, A.K.; Rodriguez-Mendez, M.L.; Wanekaya, A.K. In situ synthesis, stabilization and activity of protein-modified gold nanoparticles for biological applications. *Biomater. Sci.* **2019**, *7*, 2511–2519. [CrossRef] [PubMed]
78. Rabbani, G.; Ahmad, E.; Zaidi, N.; Khan, R.H. pH-Dependent conformational transitions in Conalbumin (Ovotransferrin), a Metalloproteinase from hen egg white. *Cell Biochem. Biophys.* **2011**, *61*, 551–560. [CrossRef] [PubMed]

79. Etzel, M.R. Isolating β-Lactoglobulin and α-Lactalbumin by Eluting from a Cation Exchanger without Sodium Chloride. U.S. Patent 5986063, 16 November 1999.
80. Shevchenko, A.; Wilm, M.; Vorm, O.; Mann, M. Mass spectrometric sequencing of proteins from silver-stained polyacrylamide gels. *Anal. Chem.* **1996**, *68*, 850–858. [CrossRef]
81. Bukackova, M.; Rusnok, P.; Marsalek, R. Mathematical methods in the calculation of the zeta potential of BSA. *J. Solut. Chem.* **2018**, *47*, 1942–1952. [CrossRef]

Materiały uzupełniające do publikacji

Isolation and Self-Association Studies of Beta-Lactoglobulin

Są również dostępne pod adresem:

https://www.mdpi.com/1422-0067/21/24/9711/s1

UNIWERSYTET MIKOŁAJA KOPERNIKA W TORUNIU
Wydział Chemii

Isolation and Self-Association Studies of Beta-Lactoglobulin

A. Gołębiowski[1, 2], P. Pomastowski[1], A. Rodzik[1, 2], A. Król-Górniak[1, 2], T. Kowalkowski[1, 2] M. Górecki[3], and B. Buszewski[1, 2*]

[1] Centre for Modern Interdisciplinary Technologies, Nicolaus Copernicus University in Torun, 4 Wileńska St., 87- 100 Torun Poland

[2] Department of Environmental Chemistry & Bioanalytics, Faculty of Chemistry, Nicolaus Copernicus University in Torun, 7 Gagarina St., 87- 100 Torun Poland

[3] Institute of Organic Chemistry, Polish Academy of Sciences, 44/52 Kasprzaka St., 01-224 Warsaw, Poland

* Corresponding author: bbusz@umk.pl; Tel: +48 (56) 665-60-38

Supplemented tables and figures to the manuscript

Table S1. β-LG masses for three fractions with AF4-UV-MALS using MALDI-TOF/TOF MS.

			Fraction 1		Fraction 2		Fraction 3	
			Mass of β-LG [kDa]					
HCCA	pH 3	Monomers	18.356	± 0.066	18.362	± 0.066	18.362	± 0.066
		Dimers	36.639		36.661		36.661	
		Trimers	55.029		55.024		55.018	
		Tetramers	73.387		73.389		73.374	
		Pentamers	91.732		–		–	
	pH 5	Monomers	18.371	± 0.308	–		–	
		Dimers	36.737		–		–	
		Trimers	55.109		–		–	
		Tetramers	73.493		–		–	
		Pentamers	91.834		–		–	
	pH 7	Monomers	18.339	± 0.000	–		18 341	± 0.000
		Dimers	36.675		–		36 718	
		Trimers	55.051		–		–	
		Tetramers	73.421					
		Pentamers	91.636					
DHB	pH 3	Monomers	18.280 18.369	± 0.088	18.364 18.280	± 0.088	18.369 18.281	± 0.088
		Dimers	–		–		–	
		Trimers	–		–		–	
		Tetramers	–		–		–	
		Pentamers	–		–		–	
	pH 5	Monomers	18.291 18.380	± 0.000	–		–	
		Dimers	36.741					
		Trimers	55.025		–		–	
		Tetramers	73.460		–		–	
		Pentamers	91.838		–		–	
	pH 7	Monomers	18.289 18.377	± 0.000			18.294 18.379	± 0.000
		Dimers	36.742		–		36.736	
		Trimers	55.025		–		55.090	
		Tetramers	73.384		–		73.416	
		Pentamers	91.793					

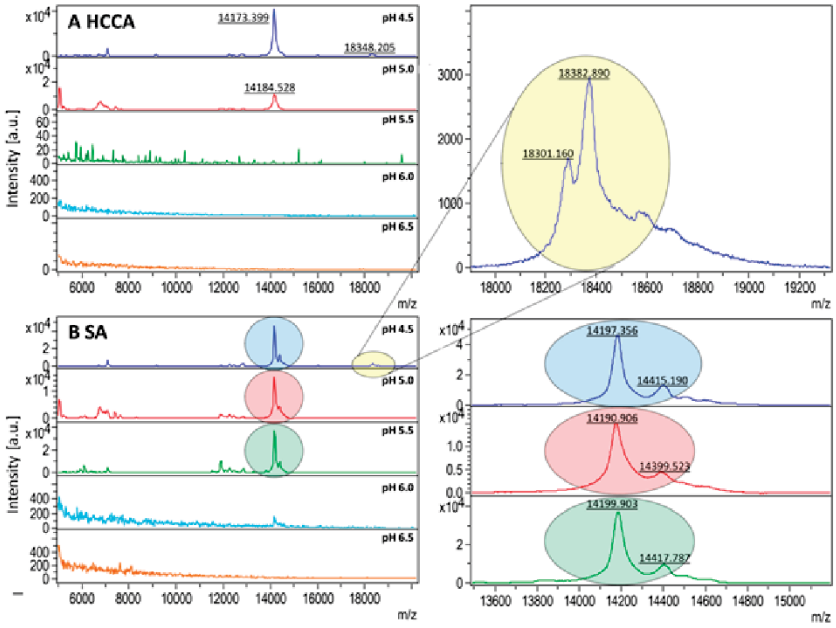

Fig. S1 MALDI-TOF/TOF MS spectrums of intact proteins. Two matrices: α-cyano-4-hydroxycinamic acid (HCCA) – A and 3,5-dimethoxy-4-hydroxycinnamic acid (sinapic acid, SA) – B were used.

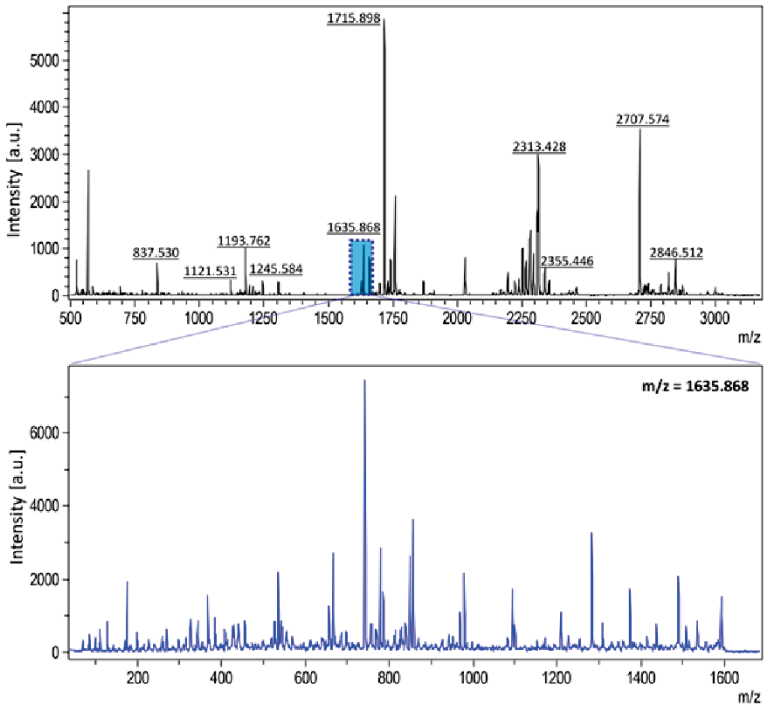

Fig. S2 MALDI-TOF/TOF MS spectrum of tryptic digests of protein sample. Sample peak at m/z 1635.868 was investigated.

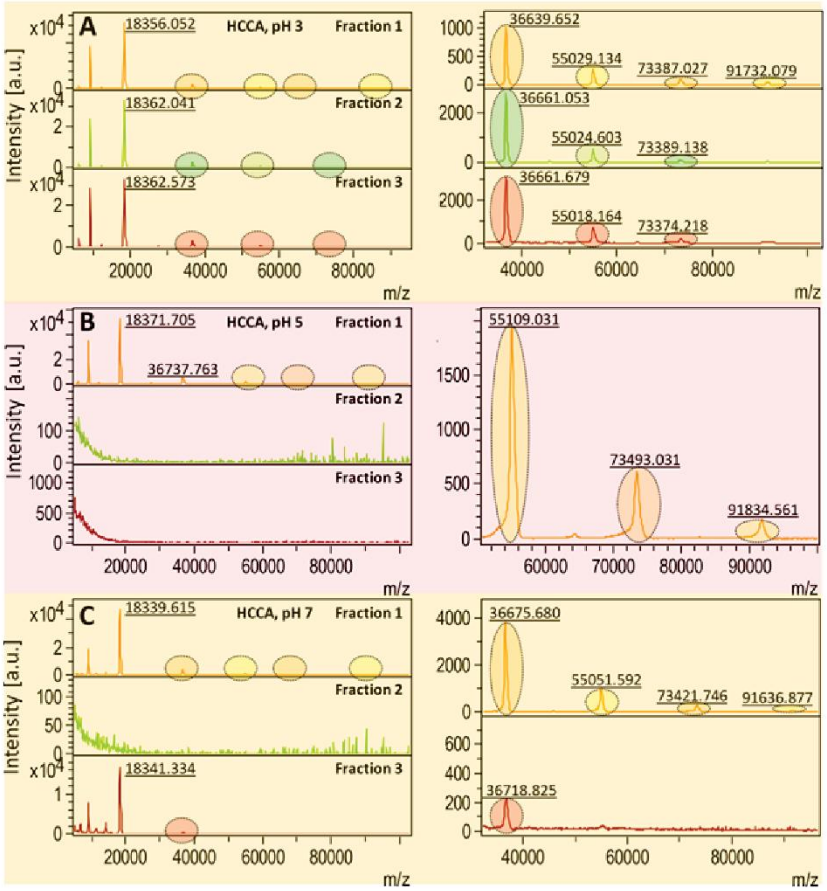

Fig. S3 MALDI-TOF/TOF MS spectrums of intact proteins. Two matrices: α-cyano-4-hydroxycinamic acid (HCCA) – A and 3,5-dimethoxy-4-hydroxycinnamic acid (sinapic acid, SA) – B were used.

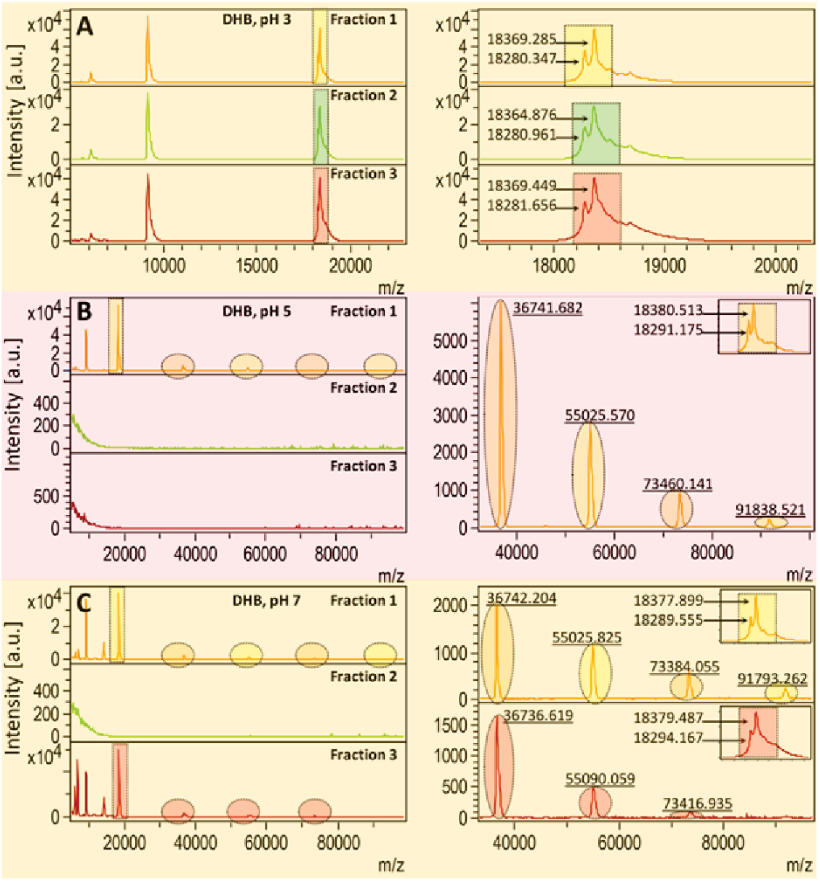

Fig. S4 MALDI-TOF/TOF MS intact protein analyses of three fractions after AF4-UV-MALS characterization. The DHB matrix was shown.

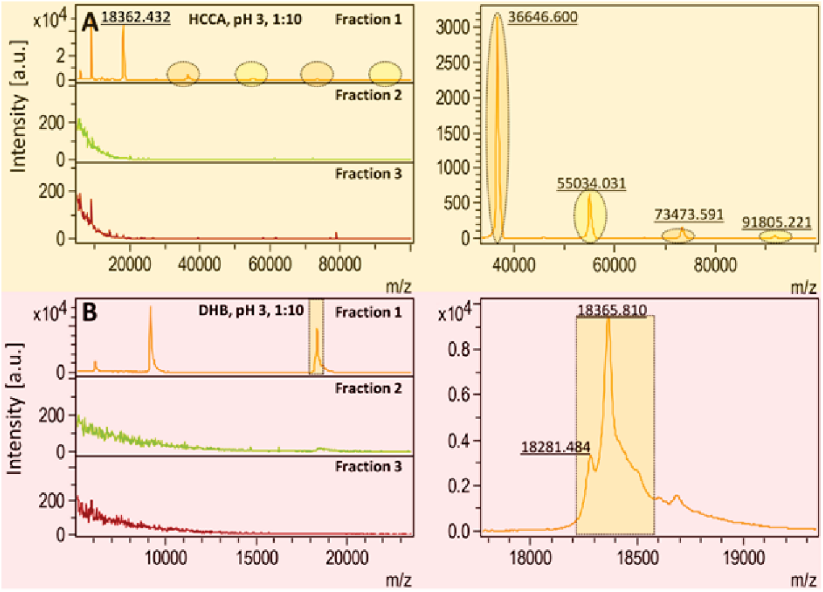

Fig. S5 MALDI-TOF/TOF MS intact protein analyses of three fractions after AF4-UV-MALS characterization. Comparison of the matrixes.

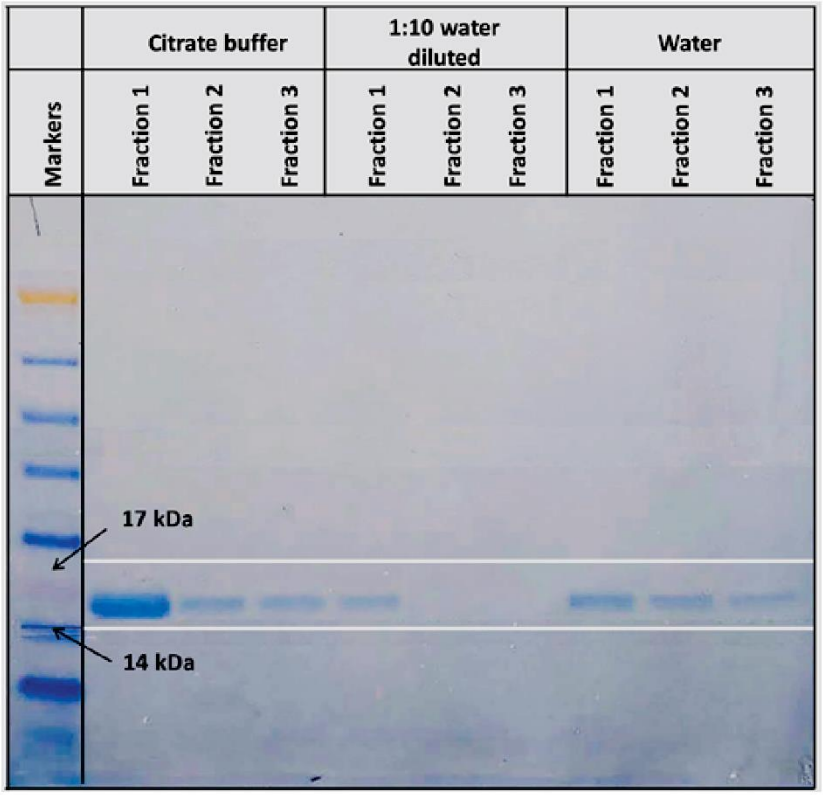

Fig. S6 The SDS-PAGE electropherogram of β-LG fractions after the AF4-UV-MALS characterization in 0.09% citrate buffer at pII 3.0. From the left to the right, fractions in citrate buffer, diluted with water 1:10, and water samples (after desalting step on Amicon membrane).

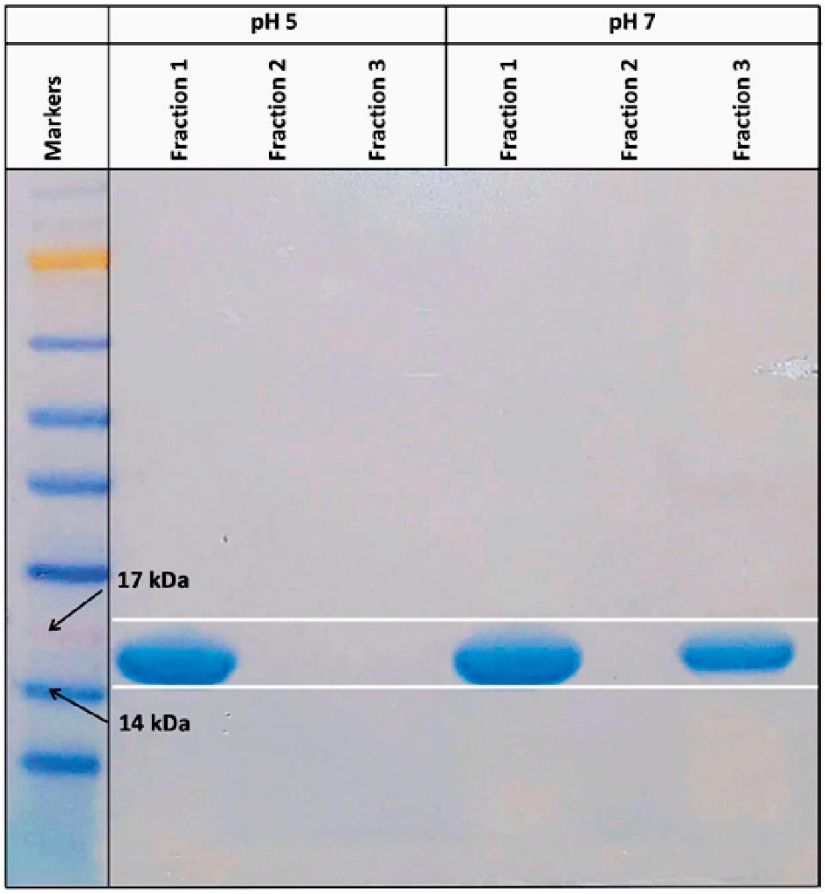

Fig. S7 SDS-PAGE of three fractions of the protein samples at pH 5.0 and 7.0 from AF4-UV-MALS characterization.

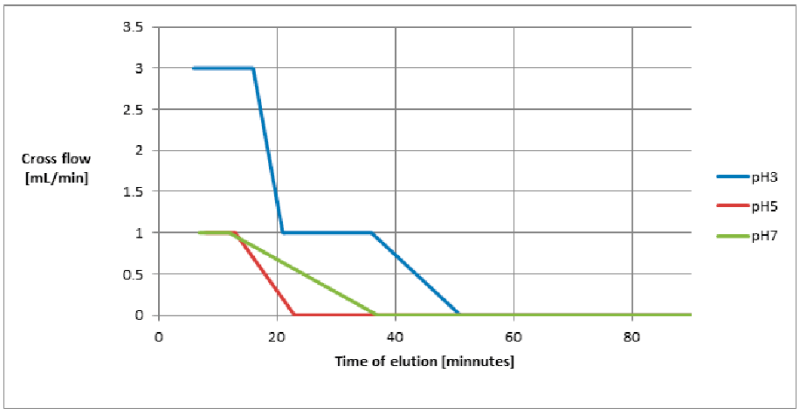

Fig. S8. The cross flow gradients during the elution at different pH.

UNIWERSYTET
MIKOŁAJA KOPERNIKA
W TORUNIU
Wydział Chemii

[P4]

Golebiowski, Adrian & Pomastowski, Paweł & Rafińska, Katarzyna & Žuvela, Petar & Wong, Ming & Pryshchepa, Oleksandra & Madajski, Piotr &

Buszewski, Bogusław

Functionalization of Alpha-Lactalbumin by Zinc Ions

ACS Omega

10.1021/acsomega.2c03674

ACS OMEGA

http://pubs.acs.org/journal/acsodf

Article

Functionalization of Alpha-Lactalbumin by Zinc Ions

Adrian Gołębiowski, Paweł Pomastowski,* Katarzyna Rafińska, Petar Zuvela, Ming Wah Wong, Oleksandra Pryshchepa, Piotr Madajski, and Bogusław Buszewski

Cite This: *ACS Omega* 2022, 7, 38459−38474

Read Online

ACCESS | Metrics & More | Article Recommendations | Supporting Information

ABSTRACT: Alpha-lactalbumin (α-LA) and binding of zinc cations to protein were studied. Molecular characteristics of protein was determined by MALDI-TOF/MS and electrophoresis SDS-PAGE, and also, for complexes, it was determined by spectroscopic techniques (ATR-FT-IR and Raman) and microscopic techniques (SEM along with an EDX detector and also TEM). The pH dependence of zeta potential of α-LA was determined in saline solution. The zinc binding to the protein mechanism was investigated; zinc binding to protein kinetics, the molecular modeling by the DFT method, and electron microscopy (SEM and TEM) for microstructure observation were performed. The experiments performed indicate a quick binding process (equilibrium takes place after 2 min of incubation) which occurs onto the surface of α-LA. Zinc cations change the conformation of the protein and create spherical particles from the morphological point of view. DFT studies indicate the participation of acidic functional groups of the protein (aspartic acid and glutamic acid residues), and these have a decisive influence on the interaction with zinc cations. Application studies of general toxicity and cytotoxicity and bioavailability were conducted.

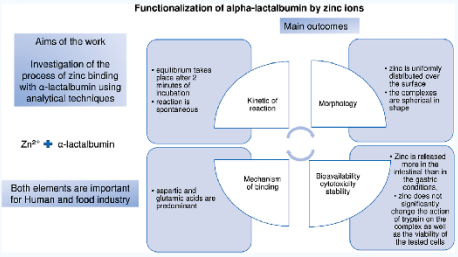

1. INTRODUCTION

Alpha-lactalbumin (α-LA) is a protein, which constitutes 123 amino acids and has a molar mass of the monomer of about 14 kDa.[1] It is the most relevant milk protein in humans (about one-quarter of mass). It is present in all mammalian species, but the content differs in individual organisms.[2,3] Protein is a part of lactase synthetase, and its source of relevant amino acids, consequently, plays a key role in nutrition of organisms, especially infants.[4,5] The structural similarity to lysosomes is noted, but proteins have different properties and play different roles in living organisms.[6] The α-helix has the highest content in the overall conformation of a protein in its native state and undergoes a self-cross-linking reaction.[7] α-LA occurs as holo and apo forms, and calcium ions are tightly bound (which appear as the holo form) to the calcium binding site.[8] Protein has also secondary binding sites.[9] The properties of protein are strictly depending on the protein form. The holo form of α-LA (calcium-bound state) increases the stability of protein,[6,10,11] although the apo form of protein gives higher opportunity to bind other metal ions.[12,13] However, other ions such as sodium, divalent, and trivalent ions compete with each other to binding sites of α-LA.[14,15] This protein is one of the most acidic proteins (the isoelectric point is from 4.2 to 4.6).[16] In differentiation to beta-lactoglobulin, the main protein in bovine milk, α-LA, does not have free thiol residues, and consequently, at elevated temperature and under denaturated conditions, it does not create a gel structure.[17] The characteristic property of α-LA is creating the molten globule state of protein under acidic conditions or using specific denaturated conditions.[18] Protein in this state is known to be a specific transport agent and can possess lethal activity to tumor cells. The HAMLET (human α-LA makes lethal to tumor cells) and BAMLET (bovine α-LA makes lethal to tumor cells) approaches are extensively studied as anti-tumor agents.[19,20] α-LA protein has the ability to bind trace amounts of metals (Zn, Fe, Mn, *etc.*) and release them during digestion in the gastrointestinal tract. This is especially important for the supply of micronutrients during the nutrition of infants, in particular.[21] Therefore, research on the synthesis and characterization of this type of connection, such as protein micronutrients (zinc), is important from a scientific and industrial point of view. In addition, the synthesis mechanism (especially the participation of individual amino acids) and the action and factors affecting the characteristics of this type of complexes have not yet been fully understood.

Zinc is noted as a *trans*-metal element. Zinc has five isotopes (64, 66, 67, 68, and 70 amu) which make up an average

Received: June 13, 2022
Accepted: October 14, 2022
Published: October 21, 2022

https://doi.org/10.1021/acsomega.2c03674
ACS Omega 2022, 7, 38459−38474

molecular weight of 65.38 units. In consideration of the chemical activity, it is a reducing agent, and in biological fluids, it exhibits a double valence state. In solution, the zinc ion is hydrated, and the coordination compounds are created. Zinc ions are coordinated commonly by six water molecules.[22] Zinc ions are one of the necessary micronutrients. It is found in all plants and animals, which may prove its popularity. It is essential in maintaining homeostasis and the proper functioning of the immune system and growth; however, excessive supplementation has negative effects similar to the deficiency of an element in the body;[23] however, zinc in the body is participating in signal transduction as a second messenger.[24] It is a cofactor of many enzymes, and it constitutes catalytic activity in many biological reactions.[25] Thus, taking protein−zinc complexes can promote healthy growth of all humans.[26] A zinc ion possesses affinity to oxygen and sulfur atoms especially. Thus, zinc creates complexes with α-LA due to interaction with amino acid moieties: glutamic and aspartic acids and also histidine.[6] There are two sets of binding places on the surface of the protein. The first was a bond of the order 10^4 to 10^5, and the second was a bond of approximately 10^3.[27,28] Binding of metal to protein occurs gradually in relation to the molar ratio of protein to zinc. The zinc−protein complex shows lower thermal stability than the holo protein form, leading, in consequence, to aggregation and higher susceptibility to digestion with proteolytic enzymes.[27] The bovine α-LA structure and its complexes with zinc were studied using the techniques of circular dichroism and nuclear magnetic resonance. The binding of zinc to the holo form did not lead to large structural changes but to small local changes only.[11] Single and slight structural changes of the protein in the form of apo and holo after binding with zinc were noticed using the Fourier transform infrared spectroscopy (FT-IR) technique.[10]

The zinc complexes of α-LA are not yet fully understood. There is a lack of extensive research into the in-depth characterization of both the protein and the zinc complex. Therefore, the aim of this work was to investigate α-LA and protein−zinc complexes. Multidisciplinary research was carried out using advanced instrumental and computational simulations techniques (MALDI-TOF-MS/MS, PAGE, ATR-FT-IR and Raman spectroscopy, physicochemical stability in solution by zeta potential determination, kinetic study of zinc binding using ICP−MS to trace zinc concentration determination, complex stability in synthetic physiological fluids, morphology studies by SEM, TEM, and molecular dynamics simulation by DFT calculations). Extended knowledge of this type of connection can be valuable in understanding and describing the mechanism of the formation of the α-LA−Zn complexes and using this knowledge for supplementation both as a source of endogenic protein and using it as a carrier of the necessary minerals.

2. MATERIALS AND METHODS

The commercial standard of α-LA was used in all experiments. The protein was bought from Sigma-Aldrich (Sigma-Aldrich, Steinheim, Germany). The supplier states that the purity of the material is higher than 85% (SDS-PAGE method).

2.1. Characterization of α-LA by SDS-PAGE. The purity of the product and molar mass of protein were assessed by applying the SDS-PAGE technique using a method adopted from ref 29 with modifications. Electrophoresis was performed using the Thermo Scientific apparatus (Thermo Scientific, Waltham, MA, USA). The used gel was Invitrogen Bolt 4−12% Bis-Tris Plus (Thermo Scientific, Waltham, MA, USA). The markers of protein mass were SeeBlue Plus2 Pre-Stained Standard (Thermo Scientific, Waltham, MA, USA). The gel was stained using the Coomassie Blue method. The protein solution of about 2 mg/mL was prepared in double-deionized water. Two additional 10-fold serial dilutions of stock samples were prepared. The reduced and nonreduced modes were utilized. Samples were prepared according to a manufacturer (Invitrogen) procedure. Briefly, protein solution was dispersed in a 2.5 μL load sample buffer (LDS). Reduction and alkylation were prepared using the sample reducing agent (10×)—dithiothreitol (DTT) and iodoacetamide (IAA), respectively. The samples were then heated for 10 min at 70 °C and introduced to the gel. Nonreduced samples were prepared without the last step (reduction and alkylation). Running buffer was MES. The electrophoresis process was executed at a voltage of 200 V. After the separation process, the gel was stained for 20 min. The discoloration was carried out at least for 24 h in double-deionized water at room temperature.

2.2. Characterization of α-LA by the MALDI-TOF/TOF MS Technique. The MALDI-TOF/TOF MS technique in the linear positive mode (*intact*) for molar mass determination and in the reflectron positive mode for investigation of peptide fingerprint mass spectra (PMF) after the protein digestion procedure with trypsin were used. The method[29,30] was adopted with modifications. A MALDI-TOF/TOF mass spectrometer (Bruker Daltonics, Bremen, Germany) equipped with a modified Nd:YAG laser operating at a wavelength of 355 nm and frequency of 2 kHz was used. The reagents were purchased from Sigma-Aldrich (Steinheim, Germany) with the highest commercially available degree of purity. The α-cyano-4-hydroxycinnamic acid (HCCA) was used as a matrix in the reflectron mode, while 3,5-dimethoxy-4-hydroxycinnamic acid (sinapic acid—SA) was used in the linear mode (all from Bruker Daltonics, Bremen, Germany). The calibration was carried out applying Peptide Calibration Standard II and Protein Calibration Standard II all from Bruker Daltonics (Bremen, Germany) for PMF and intact analyses, respectively. The dried droplet method was applied in intact analysis, while for PMF analysis, the Bruker Proteomic protocols for mass spectrometry were applied.[31] The MS spectra of α-LA intact were recorded in the range of m/z 5000−50,000, while the peptide fingerprint mass spectra (PMF) of protein digested with trypsin were recorded in the range of m/z 700−3500. In both cases, the measurements were carried out at an accelerating voltage of 25 kV. To determine the fragmentation spectra, the laser-induced fragmentation technique (LIFT) in the same m/z range was used. The peptides obtained after the tryptic digestion of α-LA were identified using BioTools software (Bruker Daltonics, Bremen, Germany). All data were collected manually, and the mass tolerance was set to 0.3 Da for the spectra and calibrated internally on immonium ions at a laser power of 60% and an attenuation of 27% for the MS/MS analysis.

2.3. Characterization of α-LA Saline Using Laser Doppler Velocimetry and Phase Analysis Light Scattering (PALS) (M3-PALS). Zeta potential values were determined in the pH range from 2 to 8. α-LA solution (0.4 mg/mL) was prepared in 0.09% (w/v) NaCl. The method was adopted from refs 29 and 30 with modifications. After protein was dissolved, the pH was adjusted to a certain value against the pH meter (1 M HCl and 1 M NaOH solutions were used

https://doi.org/10.1021/acsomega.2c03674
ACS Omega 2022, 7, 38459−38474

to correction) (first, solution at a pH of 2 was prepared). A portion of solution was loaded to the DTS 1070 cuvette (Malvern, Worcestershire, UK), and zeta potential was determined using the Malvern Zetasizer NanoZS apparatus (Malvern, Worcestershire, UK). After completion of measurement, the sample was turn back to stock protein solution. The solution was used again; the solution was mixed with the remaining solution, and another sample was prepared (pH correction and application to the cuvette). Protein solution was adjusted to a higher pH by dropwise addition of acid or alkali solution to reach the pH about 0.5 units higher than that of the previous sample. Smoluchowski's approximation in Henry's equation was used. Measurements were performed at room temperature, with automatic selection of voltages and the number of runs for software. For the result, three replications of run were averaged. To process data, the sigmoidal model was used.

2.4. Synthesis of α-LA Complexes with Zinc; Kinetic Study of Zinc Binding to Protein by the ICP−MS Technique. *2.4.1. General Synthesis Method.* The sample preparation protocol was adopted from refs 30 and 32 modifications. The protein stock solution with a concentration of 5 mg/mL was prepared in pH 4.5 in 0.09% (w/V) NaCl solution. The pH was adjusted to pH of the protein isoelectric point (pH 4.5). Zinc solution with a concentration of 60 mg/L was prepared under the same conditions as a protein from the nitrate salt (Sigma-Aldrich, Steinheim, Germany). The solutions were mixed in the volume ratio 1:1.

2.4.2. Kinetic Study of Zinc Binding. The samples were incubated at room temperature by constantly stirring at 900 rpm on a Thermomixer. Times of incubation were 2, 5, 10, 20, and 30 min and 1, 2, 4, and 6 h. After reaching incubation time, the unbound metal fraction solution was separated on Amicon Ultracell 3 kDa (Merck, Darmstadt, Germany). The solution was centrifuged for 15 min at 4 °C, 14,000 rpm. The filtrate solution was diluted (dilution factor 200) in 1% HNO_3 solution (Suprapure grade) (Merck, Darmstadt, Germany). The initial zinc concentration was determined as well. The calibration curve method was used to obtain the concentration result in samples. Zinc standard solution (Sigma-Aldrich, Steinheim, Germany) was diluted to the appropriate region of concentrations. Scandium was used as an internal standard. In this research, Shimadzu ICPMS 2030 (Shimadzu, Kyoto, Japan) was used. The collision reaction cell with the helium mode was used. The signals at m/z of 66 and 67 were monitored. The binding kinetics was determined as the difference between the initial zinc concentration and not bound fraction of zinc by the protein. The experimental data were analyzed using zero-order, pseudo-zero kinetics, and Weber−Morris intraparticle models. The fitting was performed by the least-squares method. Also, the thermodynamic parameters such as the amount of zinc bound to protein Q_t, distribution coefficient K_d, and Gibbs free energy of adsorption were displayed.[32,33]

2.5. Preparation of Complexes for Further Studies. According to the kinetic study, the complex sample was incubated for about 10 min. The unbound metal fraction was separated as in 2.4. Section. The supernatant was excluded, the remaining solution was centrifuged (14,000 rpm, 20 °C) using the Amicon 3 kDa membrane (Merck, Darmstadt, Germany), and the pellet was washed twice with deionized water. The solution was recovered from the membrane. The complexes were lyophilized (FreeZone Labconco, Kansas City, US). Dried complexes were stored at −20 °C.

2.6. Characterization of α-LA Complexes with Zinc by Spectroscopic Techniques (ATR-FTIR and Raman). The sample was probed to characterization by attenuated total reflection Fourier transform infrared spectroscopy (ATR-FTIR) using an Alpha FTIR spectrometer apparatus (Bruker, Billerica, Massachusetts, USA).[30,32] Spectra were obtained in the range 400−4000 cm^{-1}. The dried sample was attached to the measurement window.

Raman spectra were recorded using a Raman spectrometer (Senterra, Bruker Optik).[30,32] The protein was dissolved in small volume of water. A tiny droplet of suspension was injected to glass. The spectra were recorded in the region 4000−400 cm^{-1} at the wavelength 532 nm as excitation light, with a power of approximately 20 mW, and the spectrum was counted two times at 30 s. The spectroscopic data were processed with OPUS software.

2.7. Characterization of α-LA Complexes with Zinc by Microscopic Techniques: SEM, SEM−EDX, and TEM. To obtain information about morphology, topography, and quantitative analysis of elements in protein and complexes, analysis using scanning electron microscopy (SEM) along with EDX was carried out.[30,32] The apparatus used were as follows: SEM (Quanta 3D) and SEM−EDX instrument [1430 VP (LEO Electron Microscopy Ltd, UK)]. The dried powder was applied on the carbon tape.

TEM microscopy gives higher resolution and deeper view into the morphological structure. The dried material of complexes was dispersed in anhydrous ethanol and applied on a carbon lacey copper grid. Measurements were performed using the TEM apparatus (model G2 F20X-Twin 200 kV, FEI).

2.8. Characterization of α-LA Complexes with Zinc by Molecular Dynamics. Molecular dynamics (MD) study was performed according to the protocol of Pomastowski *et al.*[34] and Žuvela *et al.*[35] The α-LA was analyzed in the apo form, and their complexes with zinc were characterized. Solvation in a TIP3P water box with a variable side length, depending on the size of the system, was performed. Due to the limited volume of solvation boxes, the amounts (in moles) of α-LA−Zn solutions were downscaled with constant scaling factors (to fully preserve the concentration ratios for Zn−α-LA); from initial zinc concentration of 30 mg/L in mixture, the n(ions) per protein. molecule is 2.57 and scaled of 39.

Structures of the proteins used for the computational characterization are as in ref 36. α-LA was characterized with its holo form (Ca^{2+} cation bound within its structure). The native ions were preserved in all the APO structures and their complexes since they define the protein functions. To account for nonbonded interactions of Zn^{2+} with α-LA, parameters compatible with the TIP3P water model were obtained from Li *et al.*;[37,38] briefly, $R_{min}/2$ is 1.271, epsilon is 0.00330286, and sigma is 0.226466.

Electrostatic neutralization with Na^+ or Cl^- ions, EM to remove bad contacts and structural clashes, heating to 298.15 K at a constant volume, and equilibration of density by subjecting systems to constant were carried out. A pressure of 1 bar and a temperature of 298.15 K—*NPT* ensemble—were used; production MD simulations in the *NVT* ensemble were used. MD simulations were carried out using GROMACS 5.1.2 software using the AMBER ff99-SB-ILDN force field.[39] Visual

https://doi.org/10.1021/acsomega.2c03674
ACS Omega 2022, 7, 38459−38474

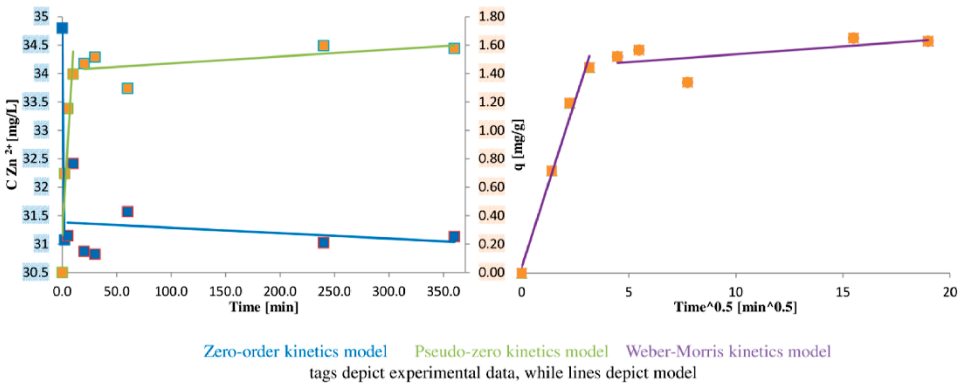

Figure 1. Zinc kinetics of binding to α-LA.

Molecular Dynamics (VMD) 1.9.3 software and Python 3.9 were used for visualization and data analysis.

2.9. Binding Interaction of Zn^{2+} with Aspartate and Glutamate Residues by DFT Calculation. To shed light on the interaction of the zinc ion (Zn^{2+}) and α-LA protein, density functional theory (DFT) calculations, using Gaussian 16 Programs,[40] were carried out to examine various possible 1:1 Zn^{2+}−Asp^{-} and Zn^{2+}−Glu^{-} complexes. The M06-2X functional[41] was employed for the DFT calculations. Geometry optimizations were performed at the M06-2X/6-31+G** level. Higher-level M06-2X/6-311++G(3df,2p) single-point energies were used to compute the binding free energies of various complexes at 298 K (ΔG_{298}). The solvation effect of aqueous medium (ε = 78.4) was modeled with an implicit solvation model SMD.[42]

2.10. Application of Zinc−α-LA Complexes; Stability in Synthetic Physiological Fluids. Dissolution of zinc from the complexes was studied in four model synthetic fluids: gastric and intestinal with and without specific enzymes (pepsin and pancreatin for gastric and intestinal, respectively). The fluid was prepared as in ref 30. The sample was weighted on an analytical balance and dissolved in dissolution fluid. The solution was transferred to Amicon centrifugal device 3 kDa (Merck, Darmstadt, Germany). After 24 h of incubation time, the released zinc solution was separated by applying centrifugation (15 min, 14,000 rpm, 10 °C). The filtered solution was diluted (dilution factor 100) in 1% HNO_3 (Merck Suprapure, Darmstadt, Germany). The quantitative analysis of zinc by the ICP−MS technique was performed as described in 2.4. Section.

2.11. Peptic Digestion Kinetics. For the study, the modified protocol from Pryshchepa *et al.*[43] was utilized. The digestion was performed in simulated gastric fluid prepared as follows: 2.0 g of NaCl was mixed with 80 mL of 1 M HCl and diluted to 1000 mL. The working pepsin (Sigma-Aldrich, Steinheim, Germany) solution with a concentration of 50 U/mL was prepared in simulated gastric fluid from stock solution (2000 U/mL in deionized water). The native α-LA and its complex with zinc were suspended in deionized water to a concentration of 10 mg/mL. The reaction mixture was prepared with an enzyme-to-substrate ratio of 0.5 U:100 μg by adding 80 μL of simulated gastric fluid, 10 μL of working pepsin solution, and 10 μL of protein or its complex solution to the Eppendorf tube. Final concentration of the protein in the solution was 1 mg/mL. Next, the mixture was incubated at 37 °C for 5, 15, 30, and 45 min. Termination of the reaction was performed by the addition of 0.7 M Na_2CO_3 at 35% of the reaction volume, that is, 35 μL was added to the reaction mixture. The control samples were prepared, where instead of protein/complex solution, 10 μL of reaction buffer was added to the reaction mixture. The control samples were incubated during 45 min. The SDS-PAGE analysis was performed in the reduced mode according to the procedure described in 2.1. Section with Perfect Color Protein Ladder (EURx Sp. z o. o, Gdansk, Poland) as a protein MW marker.

2.12. Biological Activity of Zinc−α-LA Composites. References 4445−46 were utilized in developing this part of research (with some modifications). L929 and Caco-2 cell lines were purchased from ECACC (European Collection of Authenticated Cell Cultures operated by Public Health England) (Sigma). Both cell lines were cultured in DMEM supplemented with 10% (v/v) fetal bovine serum, 2 mM glutamine, 100 U/mL penicillin, and 100 μg/mL streptomycin (Sigma). The cells were passaged by trypsinization with 0.25% trypsin/EDTA every 3−4 days. For assays, cells were cultured on 96-well plates at a density of 2×10^5 cells/mL and incubated for 24 h. When cells were attached to the bottom of the plate, the medium was replaced with a new one containing tested Ag complexes and incubated for 24 h. In control, the medium was replaced with a fresh one without tested substances. A silver nitrate control was performed to differentiate the cell response to various forms of silver compounds. After 24 h, 10% (v/v) of thiazolyl blue tetrazolium bromide (MTT) solution (5 mg/mL in PBS) was added to each well and incubated for 4 h at 37 °C. After that, medium from wells was removed, and the formazan crystals were dissolved in DMSO for 10 min by mixing. Absorbance was measured using a microplate reader (Multiskan, ThermoFisher) at 570 and 650 nm as background absorbance.

The LDH release assay was performed using a Lactate Dehydrogenase Activity Assay Kit (MAK066, Sigma). Cell cultures were prepared as for MTT assay, and cultured cells were incubated with the zinc complex and zinc nitrate to induce cytotoxicity and subsequently release enzyme lactate

https://doi.org/10.1021/acsomega.2c03674
ACS Omega 2022, 7, 38459−38474

dehydrogenase (LDH). The medium with released LDH was transferred to a new plate and mixed with 50 μL of the reaction mixture. Absorbance was measured at λ = 450 nm using a multimode microplate reader (Varioskan TM LUX Thermo Fisher Scientific, Waltham, MA, USA). Results are presented as a percent of activity in comparison to the control.

The level of reactive oxygen species was measured with a Fluorometric Intracellular ROS kit (MAK144, Sigma-Aldrich). Cell cultures were prepared as for MTT assay, and cultured cells were incubated with the zinc complex and zinc nitrate to induce ROS for 24 h. After the incubation time, 100 μL of master reaction mix was added to each well and incubated for 30 min. The fluorescence intensity was measured at λ_{ex} = 540/λ_{em} = 570 nm using a multimode microplate reader (Varioskan TM LUX, Thermo Fisher Scientific, Waltham, MA, USA). Results are presented as a percent of activity in comparison to the control.

To check the amount of silver ions obtained from α-LA composites, L929 cells were incubated for 24 h with the Zn complex and $Zn(NO_3)_2$ at a concentration of 0.05 mM for 24 h. After that time, cells were washed two times with Dulbecco's PBS, trypsinized with 0.25% trypsin, and again washed with Dulbecco's PBS. The obtained cell pellet was mineralized with nitric acid.

3. RESULTS AND DISCUSSION

3.1. Characterization of α-LA by SDS-PAGE. Figure S1 shows a gel electropherogram from α-LA analysis under reducing and nonreducing conditions. One single band occurs under these conditions. The band is around 14 kDa with respect to the standard markers. The initial use of concentrated protein solution (2 mg/mL) results in a wider band (lanes on the left side of the mode for reducing and nonreducing). The α-LA protein has a molar mass of about 14 kDa (from the amino acid sequence). The presence of one band in this region proves the purity and electrophoretic stability of the protein product. In particular, no band above 17 kDa for the marker was recorded. At this region of mass, it would come from the β-lactoglobulin, a protein which, next to α-LA, is a constituent of bovine whey proteins.[47,48]

Table 1. Thermodynamic Parameters Obtained from the Kinetic Study of Zinc Binding to α-LA

parameters	value [units]
C_e	3.7 [mg/L]
Q_e	1.58 [mg/g]
K_D	47.3
ΔG	−9.45 [kJ/mol]

3.2. Characterization of α-LA by the MALDI-TOF/TOF MS Technique. For further characterization of α-LA, mass spectrometry analyzes were performed using the MALDI technique. In order to obtain the molecular weight of the protein, the intact analysis was performed using the linear positive mode. Sinapic acid was used as a matrix while preparing the sample. Figure S2 shows the mass spectra. The most intense signal was recorded at an m/z of 14,166. This value indicates the α-LA adducts probably with hydrogen or sodium ions.[49] A matrix and trifluoric acid are the source of these ions.[50,51] The molecular weight value corresponds to the theoretical value for α-LA. Other peaks above the monomeric form can be distinguished. Peaks at m/z: 14,386, 14,496, and 14,599 correspond to other protein forms. Molar mass values of proteins will be differentiated by many factors (protein origin, post-translational modifications, and calcium content).[1,52,53] The protein can be glycosylated at the asparagine moiety.[54,55] Consequently, many isoforms can be characterized.[56,57] The spectrum also shows a peak from the dimeric form occurring at m/z 28,326 and trimeric form (at m/z 42,495) and a low intensity peak from the doubly ionized form of the pseudo-molecular ion at an m/z of 7081. The choice of the matrix is crucial for observation and the stability of protein oligomers and isoforms under measurement conditions. The sinapic acid matrix can also distinguish oligomeric and isoform forms of β-lactoglobulin, while the HCCA matrix (another typical matrix used in proteomic studies) does not allow this. Jin and Manabe determined the molar mass of the monomer of α-LA for 14.18 KDa and discussed the effect of the residual content of foreign ions as impurities, especially sodium, and residual, nonwashed stain after unfolding the electropherogram, which have a measurable effect on the obtained results.[58] Ham *et al.* determined the mass of the protein at around 14.2 kDa with an uncertainty of 4−105 Da for various samples prepared from Cow, Saanen, Toggenberg, and Alpine and found that the differences in the masses obtained were not significant.[59] Svensson determined the molar mass at 14,088 kDa, and the difference between the determined and theoretical mass calculated from the amino acid sequence (14,078 KDa) attributed to post-translational modification (glycosylation and phosphorylation).[60] In summary, our results are consistent with above-presented studies, and the differences in the determined masses result from (1) the origin of the protein, (2) post-translational modifications, and (3) residual impurities.

Protein identification was carried out by obtaining a unique peptide sequence after digesting the protein with trypsin. The corresponding peptide sequences are shown in Table S1. The resulting collection of peptides allows the identity of the protein to be established as α-LA.

3.3. Characterization of α-LA Saline Solution by Zeta Potential Determination. In order to investigate the stability of the α-LA solution in 0.09% NaCl (w/V), the zeta potential relationship was determined as a function of pH. The graph of this relationship is shown in Figure S3. The course of the dependence of zeta potential on pH is typical for a protein. We move from a solution in a strongly acidic environment where the measured zeta potential is strongly positive (above +20 mV) to an environment with higher pH values where the zeta potential approaches neutral values. A solution that exhibits a zeta potential absolute value greater than 25 mV is considered to be colloidally stable by the action of electrostatic repulsion between the colloid particles.[34] In this case, it can be considered that the α-LA solution can be considered electrostatically stable only at the highest acidity of the solution. The protein shows a positive charge (it is positively electrostatically charged) due to protonation of amino acid functional groups. At pH 2, all amino acid residues are protonated initially. The amino acids with the most acidic properties in protein are the glutamic and aspartic acids. On the basis of the pKa values of these groups (3.22 and 2.77), at these pH values, exactly half of the content of these acids is deprotonated (neglecting the effect of the remaining amino acid groups on the pK_a value in α-LA). α-LA has 12 aspartic acid residues and 7 glutamic residues in its chain. This is a large proportion of acid functional groups in the protein

https://doi.org/10.1021/acsomega.2c03674
ACS Omega 2022, 7, 38459−38474

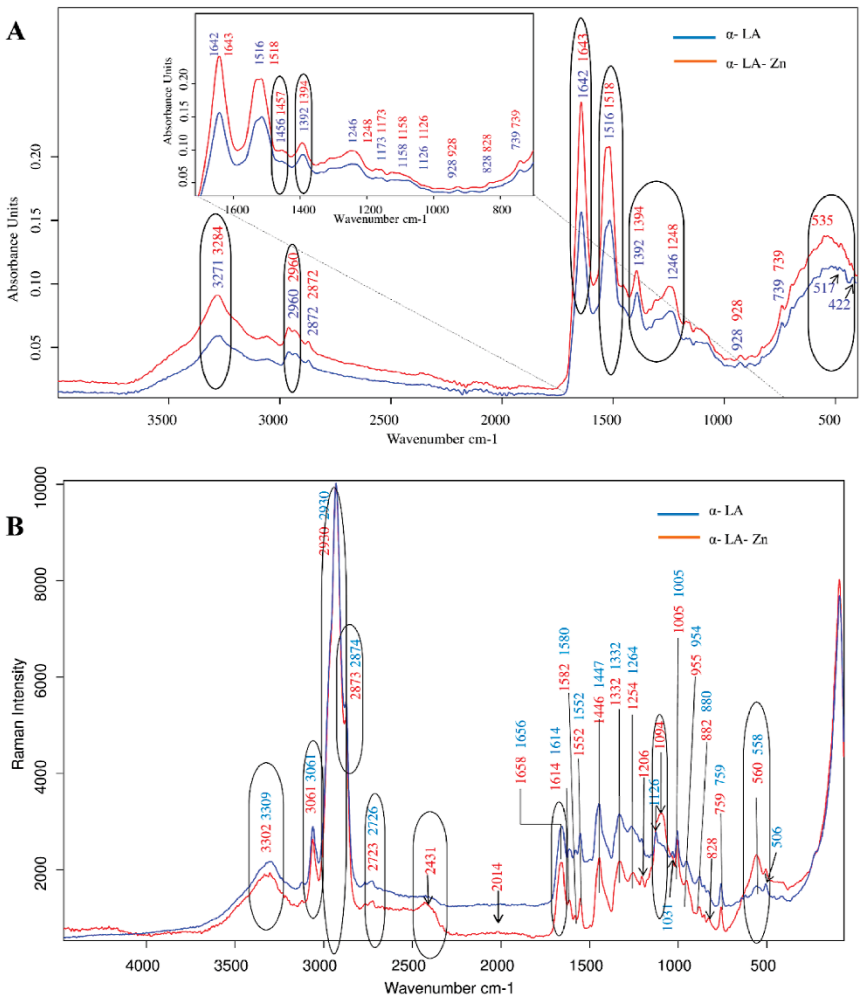

Figure 2. (A) ATR-IR spectrum of α-LA (blue line) and α-LA complexes with zinc (red line); (B) Raman spectrum of α-LA (blue line) and α-LA complexes with zinc (red line).

structure, considering that α-LA has a total of 123 amino acid residues. At higher pH values, deprotonation begins to take place on amino acids with more and more basic properties (successively with polar and neutral side chain properties, acid amides, aliphatic moieties, and residues with basic side chain properties). The pH point at which the resultant of the positive and negative charges on the protein is zero is called the isoelectric point. This value for α-LA is 4.5 using the sigmoidal model.[61,62] The charge of the protein, both dissociated and protonated groups, is equal to zero, and at this pH, we recorded the isoelectric point of the protein in a solution of 0.09% NaCl. The isoelectric point value is within the range of the literature values for α-LA. The value of the isoelectric point is a function of the composition of the solution.[48] The solution under these conditions shows a number of properties: the protein is the least soluble, and the electrostatic repulsion between the individual groups of the protein is the lowest. This causes the protein under these conditions to have the greatest tendency to aggregate.[63] The formed large particle clusters often sediment, and phase separation can occur. Moving toward the alkaline environment, the solution shows negative values of the zeta potential. They stabilize at around −25 mV at a pH of around 6.5. Under these conditions, the protein regains its electrostatic stability through ionization of

https://doi.org/10.1021/acsomega.2c03674
ACS Omega 2022, 7, 38459−38474

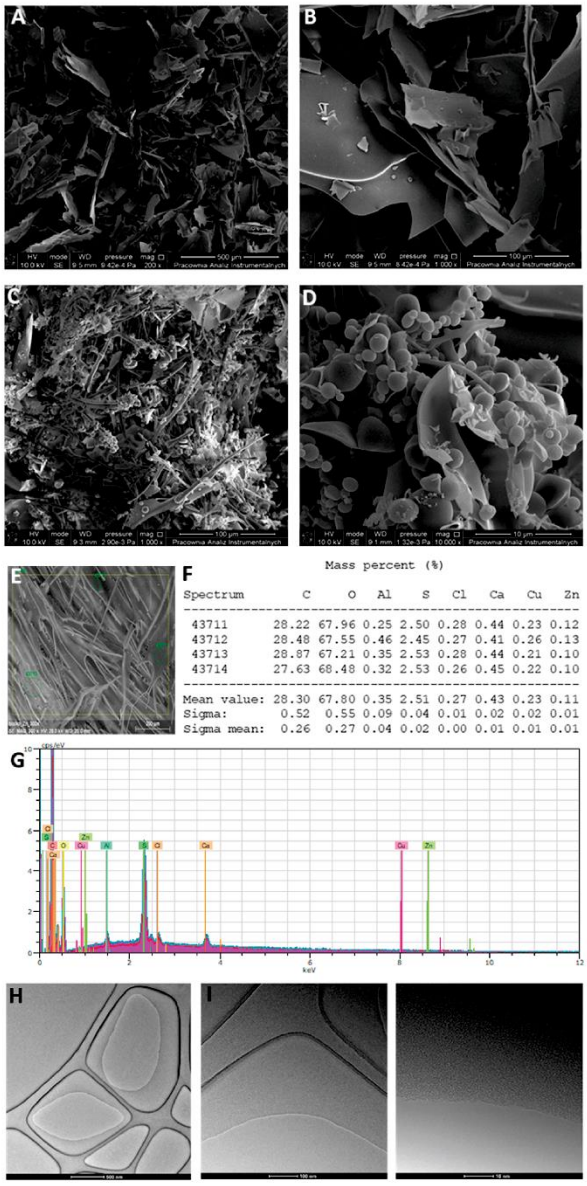

Figure 3. (A,B) SEM pictures of the α-LA protein with different magnifications of the sample place; (C–E) SEM pictures of the Zn–α-LA complex with different sample place magnifications; (F) SEM–EDX imaging, photograph of the sample; (G) spectrum from the selected image; (G) list of characterized elements with the content of individual elements in the material; and (H–J) TEM pictures of the Zn–α-LA complex with different bars.

https://doi.org/10.1021/acsomega.2c03674
ACS Omega 2022, 7, 38459–38474

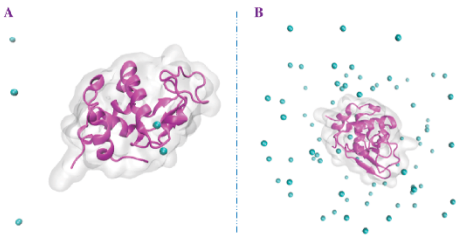

Figure 4. Modeled structures: α-LA with its apo form (A) and modeled complex with zinc cations (with a concentration of 30 mg Zn/L in the reagent mixture) (B).

Table 2. Participation of Amino Acids of α-LA in Interaction with Zinc Cations at Studied Concentration of Metal

AA	1A4V−Zn^{2-} (39) n(bind. sites)	1A4V−Zn^{2+} (39) %(bind. sites)
GLU	**830**	**43.252**
ASP	**994**	**51.798**
CYS	4	0.208
HIS	0	0.000
TYR	4	0.208
TRP	0	0.000
PHE	3	0.156
MET	9	0.469
ARG	0	0.000
LYS	21	**1.094**
	1865	

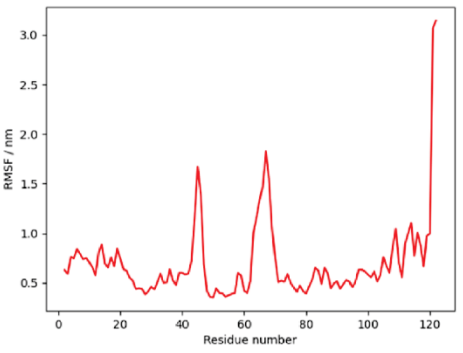

Figure 5. Flexibility analysis of α-LA−Zn complexes.

individual functional groups of the protein. Relatively low values of the zeta potential deviation can be interpreted as an indicator of the lack of protein degradation, especially at extremely acidic and alkaline pH solutions, and consequently chemical stability to a harsh acid environment. However, the deviations arise with the acidity of medium. This trend of protein degradation by acid hydrolysis in very low pH will be visible particularly in dissolution studies of bound zinc cations in acidic artificial physiological fluid (Section 3.9).

3.4. Kinetic Study and Thermodynamic Data of Zinc Binding to Protein by the ICP−MS Technique. Figure 1 shows the dependence of unbound zinc concentration to α-LA as a function of the duration of kinetic experiment. Three different models of the fitting and interpretation of the results are presented: kinetic zero-order, pseudo-zero, and intraparticle diffusion models by Weber−Morris. Based on zero-order and pseudo-zero kinetic relationship, two stages of the ongoing process can be distinguished. The first stage is a rapid decrease in the concentration of zinc in the remaining solution. The second stage is leading to the stabilization of the concentration of zinc in the solution. The first stage is very quick. The reaction rate constant is 1.864 mg min per liter. Already, in the first measuring point (2 min of incubation), the concentration range is reached, which, based on the further course, can be called equilibrium. The second stage can be described as the stabilization and equilibrium stage, where the concentration of zinc in the solution fluctuates with respect to the equilibrium concentration. The reaction rate constant for this step (calculated with respect to the zero-order kinetic model) is equal to 7.3×10^{-5} mg min per liter. It can be concluded that the process of zinc binding by α-LA is very fast (after 2 min of incubation, the equilibrium is established), and the complexes were stable under the experimental conditions during the experiment. The intraparticle diffusion model is a fit of the experimental values in the system of coordinates of the adsorbed amount of zinc by the proteins to the root of the process duration. Experimental data show a gradual increase in the amount of zinc bound to the protein as a function of time. Stability in the recorded q values is visible at later measuring points. The Weber−Morris model is based on the linear dependence of q on the root of time. It is evident that the α-LA binding process for zinc is not linear for complete measuring time dimensions. Equilibrium values are shown; in particular, the Q_c value of 1.58 mg/g says that 1 g of protein binds 1.58 mg of zinc. The presented two models of matching the results allow concluding about the mechanism of the process. Based on the model of the zero-order kinetics, it can be stated that the process is fast, the rate-limiting stage is the diffusion of zinc cations to the surface of the protein structure, and the functional groups are available on the surface. It should be emphasized that the process is located on the surface. There are no additional steps of zinc binding through α-LA (a symptom would be a further, stepwise decrease in the recorded concentration in the remaining solution or an equilibrium increase in the q value). In other words, no further diffusion of zinc cations into the interior of the protein structure is observed. Detection of a further stepwise increase in the amount of zinc by the protein would be visible using the Weber−Morris model.[64]

The amount of bound zinc by protein under equilibrium conditions ranged from 30.05 mg/g for casein mixtures, from 5.16 to 6.85 mg/g for individual forms of casein, and 8.16 mg/g for bound zinc by beta-lactoglobulin based on studies performed in our research unit.[30,32,33] It can be seen that the α-LA protein does not show much value of binding zinc ions from the solution. This may be due to the availability of zinc binding sites for the holo protein. In addition, it is known that the sites are located on the surface, and the experiment was conducted under the pH conditions at the isoelectric point, where accessibility to the surface is the lowest. Buszewski *et al.* also noted the effect of the molar mass of a protein on the value of the bound portion of the metal by the protein. The smaller the protein, the lower the possible availability of appropriate functional groups and, consequently, the number

https://doi.org/10.1021/acsomega.2c03674
ACS Omega 2022, 7, 38459−38474

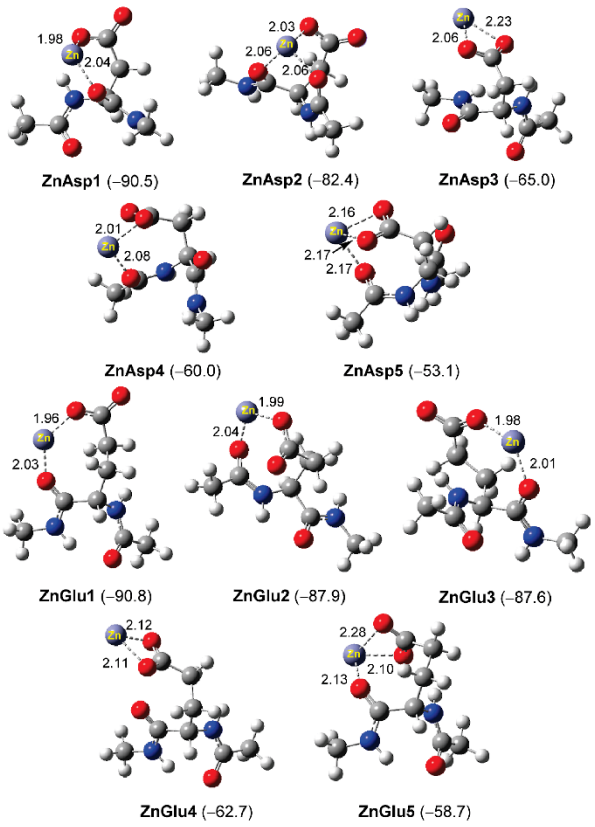

Figure 6. Optimized geometries of various conformations of Zn^{2+}−Asp^{-} (**ZnAsp1**−**ZnAsp5**) and Zn^{2+}−Glu^{-} (**ZnGlu1**−**ZnGlu5**) complexes. Interaction distances are in Å, and binding free energies (ΔG_{298}) are in kJ/mol.

of active centers capable of interacting.[30] Hence, α-LA protein is the smallest protein, in terms of molecular weight, tested in our research group. α-LA has a numerically low content of functional groups that are able to interact with zinc ions compared to heavier proteins, which have far more active functional groups to absorb cations. The influence of the process conditions through the prism of zinc cations and possibly the influence of conformation of the zinc aqua complex and charge localized on the surface (which is positive in the pH of the process) occur. The process at pH 4.5 determines the value of the electrostatic attraction force in relation to the protein structure. The net charge of α-LA is zero, but the active functional groups (aspartic and glutamic acids in particular) are fully deprotonated and negatively charged. In addition, the pH value of the isoelectric point determines the conformation of the protein, where the presence of polar groups available for interaction is the highest due to the hydrophobic effect occurring at around pH of isoelectric point of protein. Thus, the process binding of zinc for α-LA is surface-localized only. Table 1 shows the thermochemical data from the kinetic experimental data. The value of the Gibbs enthalpy is negative. Thus, reaction has a spontaneous tendency to occur. There is a visible correlation between the quoted other protein studies tested in our team and the values of Gibbs enthalpy for the study of zinc binding. Gibbs enthalpy is lower for heavier proteins compared to α-LA. Great importance here is the entropy effect, which assumes more favorable changes from the thermochemical point of view for these systems, where, as a result, a more disordered system is formed. This can manifest itself in conformation changes, ion-exchange reactions,and so forth.

3.5. Characterization of α-LA Complexes with Zinc by Spectroscopic Techniques. Figure 2A shows the infrared spectra of the α-LA protein (as a control) and α-LA complex with zinc ions. Noteworthy is the fact that selective increases in absorbance for specific vibrations took place for α-LA complexes with zinc compared to the control. In the beginning of interpretation from the highest wavelength region, the first bands at 3271 cm^{-1} (control) and 3284 cm^{-1} (α-LA−Zn) correspond to the vibration of the amine group N−H of amide

https://doi.org/10.1021/acsomega.2c03674
ACS Omega 2022, 7, 38459−38474

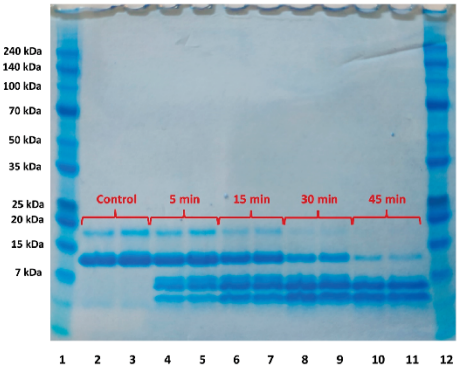

Figure 7. SDS-PAGE presenting peptic digestion kinetics, where bands of native α-LA are presented on 2, 4, 6, 8, and 10 and the bands of the complex of α-LA with zinc are presented on 3, 5, 7, 9, and 11.

I.[65] Changes in the frequency of stretching vibrations (N−H) in this respect between control and complex compounds are the result of changes in the values of the share of hydrogen bonds. The consecutive bands located at lower frequencies are responsible for the stretching vibrations of the aliphatic C−H and also of the amine groups. Another range in which the vibration bands are observed is the vibration range of amide I. In this range, vibrations from the carbonyl group C═O have their very strong band (1642 and 1643 cm^{-1} for control and complexes, respectively).[66] Another band can be attributed to the vibration of amide II. The N−H and C−N groups have their vibrations here. Two consecutive bands present at about 1456 and 1392 cm^{-1} are responsible for the C−H bending vibration of the amino acid groups. The next bands are the vibrations of the amide III group coming from the N−H bending and C−N stretching vibrations. Subsequent bands come from the vibrations of aromatic amino acid groups,[67] unless there were any drastic changes in the IR spectrum of the α-LA and after the formation of complexes with zinc, which is consistent with the literature data. The greatest changes in the distribution of the bands were noted for the region with the lowest vibration frequencies. This region, from aromatic vibrations, and the environment around these groups probably change (*e.g.*, conformational).[68] The region of the participation of individual conformations (ρ-helix, β-sheet, β-turns, and random coil) can be attributed to the vibration of amide III.[69] Especially, in the enlargement of the fingerprint region, there is a visible change in the relative intensity of the vibration between the native structure and the binding to zinc. Thus, the protein conformation change after binding with zinc is very possible. After the binding of the protein with the zinc, a band at 535 cm^{-1} was visible, while before the binding, bands at 517 and 422 cm^{-1} were visible.

Figure 2B shows the Raman spectrum of the α-LA protein before binding and its complex with zinc. Similar to the IR technique, Raman is a complementary technique, which, unlike IR, especially shows vibrations from groups with a low difference in electronegativity in the group, while IR shows vibrations of ionic groups in particular. Also starting the description from the bands at the highest frequencies toward the lower ones, the first band at around 3300 comes from the stretching vibration of the N−H amino group. A clue that it is a vibration of the amino group may be the intensity of the vibration, which we judge as an average. Vibrations of other groups with a similar range (O−H or ═C−H) have a weak intensity in the Raman spectrum. The change in the frequency of this protein oscillation after binding may also be the result of changes in the orientation of the hydrogen bond. The next bands at 3061, 2930 cm^{-1}, and around 2873 cm^{-1} are the vibration bands of ═C−H and C−H, respectively. The bands at around 2723 and 2431 cm^{-1} are responsible for S−H vibrations, while after the binding of zinc to the protein, the second band is not visible.[70] The band at around 1658 cm^{-1} is responsible for amide I vibrations. The carbonyl group of glutamic and aspartame amino acids gives the band from the C═O stretching vibration.[71] Then, the spectra show a rich set of bands derived from vibrations of individual amino acid groups (fingerprint region).[71,72] The two bands were significantly enhanced in intensity compared to the control. The bands at 1094 and 560 can be attributed to C−S aliphatic and aromatic vibrations, respectively.[70,72]

3.6. Characterization of α-LA Complexes with Zinc by Microscopic Techniques. Figure 3A,B shows the results of surface imaging and examination of the surface morphology of α-LA protein by the SEM method. The surface is flat and continuous without visible bulges, flooding,and so forth. The petals rarely show small clusters of particles that can be assessed as impurities. Figure 3C,D shows the characteristics of the Zn complex with α-LA. After the zinc binding process by α-LA, visible changes took place on the surface. When assessing the photograph with the smallest magnification, we can see clusters of particles that are significantly whiter and brighter (Figure 6C). This effect can be attributed to the bound zinc ions on the surface of the metal−protein composite. Additionally, it can be assessed that these places are located rather evenly, without segregation. In addition, the metal deposit is rather in the surface layers, with a visible scaly structure from the protein in the deeper layers of the material. Moving on to photographs with larger enlargements, the surface structure is visible. There are numerous particles in the shape of spheres, tightly adhering to the surface of the protein. The whiter shade of these beads as mentioned earlier is due to the zinc-rich material. The deposit globules adhere tightly to each other, forming large clusters which, when enlarged further, appear as a compact surface. Image 6E shows a low-resolution image taken during EDX imaging. It shows a dense, compact structure. From the marked area, spectra of the selected elements were collected. The image 6F shows the spectra of individual elements. In addition to zinc, which is evenly distributed (low Sigma value) (Figure 3G), there are other elements coming from the protein, the mesh in which the sample was placed (Cu) and typical contamination of the sample from, for example, water (Cl).

Figure 3H,I,J shows the TEM image of the material after the zinc binding process by α-LA. Each image shows an amorphous form of the material in greater zoom. There are no visible clusters or clumps of particles that could indicate the formation of zinc oxide nanoparticles on the surface of the protein or the precipitation of zinc to a metallic form.[73] On this basis, it can be concluded that the process of zinc binding to α-LA proceeds in accordance with the electrostatic attraction of zinc ions to the oppositely charged functional groups of the protein, without the charge transfer process (oxidation or reduction).[74]

https://doi.org/10.1021/acsomega.2c03674
ACS Omega 2022, 7, 38459−38474

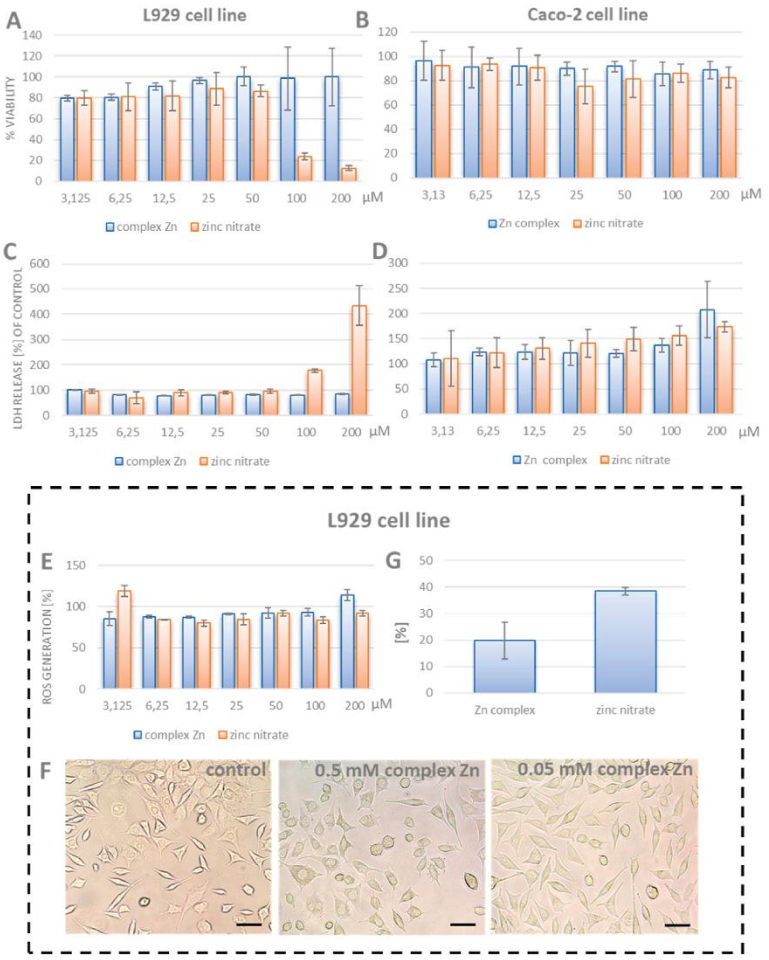

Figure 8. (A,B) L929 and Caco-2 cell viability after treatment with the Zn complex and Zn ions measured by the MTT method; (C,D) LDH leakage level of L929 and Caco-2 cells treated with Zn ions and the Zn complex; (E) concentration-dependent ROS generation by Zn ions and the Zn complex in L929 cells; (F) morphology of L929 cells treated with the Zn complex; and (G) % of silver taken up by L929 cells from the Zn complex and zinc nitrate. For (A−E), * indicates statistically significant differences ($p \leq 0.001$) between the sample and control according to one-way ANOVA and the Tukey post hoc test. For (G), * indicates statistically significant differences ($p \leq 0.001$) between the uptake of zinc from the Zn complex and zinc nitrate according to one-way ANOVA and the Tukey post hoc test.

3.7. Characterization of α-LA Complexes with Zinc by MD Simulations. Figure 4 depicts the modeled structure of protein and the complex with zinc cations with concentration used in all studies (30 mg Zn/L). These structures were obtained after the energy minimization procedure.

Table 2 shows the percentage of participation of amino acid residues in interaction with zinc. Analyzed interactions between Zn cations and GLU, ASP, CYS, HIS, TYR, TRP, PHE, MET, ARG, and LYS with a distance threshold of 0.35 nm were examined. Glu and Asp amino acids are dominating with interaction with zinc cations, while smaller contribution has lysine with interaction.

The flexibility of the four key regions decreases with the increase in zinc concentration. At around residues 15−20, 30−50, 60−80, 100−120, 15−20: 3 turn-helix (310), 30−50: hydrogen-bonded turn, extended strand (beta sheet), 60−80: same as 30−50 + *a* 3-turn helix, 100−120: four-turn helix (alpha), three turn-helix and random coil were detected (Figure 5).

https://doi.org/10.1021/acsomega.2c03674
ACS Omega 2022, 7, 38459−38474

3.8. Binding Interactions of Aspartate and Glutamate Residues toward Zn^{2+} (aq). The MD simulations have demonstrated the dominant occurrence of aspartate and glutamate residues, which indicated that the negatively charged Asp^- and Glu^- residues are the strongest Zn^{2-} binders. DFT calculations were performed to further shed light on the possible binding modes and interaction energies of Zn^{2+} with aspartate and glutamate residues. To this end, various possible conformations of 1:1 Zn^{2+}−Asp^- and Zn^{2+}−Glu^- complexes were investigated. The Asp^- and Glu^- residues were modeled with two units of amide linkage and capped with methyl groups in order to investigate the interaction of Zn^{2+} with the protein polypeptide backbone. The solvation effect in an aqueous environment was modeled using the implicit SMD solvation model. The optimized geometries and binding free energies ($Zn^{2+} + AA^- \rightarrow Zn^{2+}$−$AA^-$, ΔG_{298}) of the five lowest energy conformations of Zn^{2+}−Asp^- and Zn^{2+}−Glu^- complexes (**ZnAsp1**−**ZnAsp5** and **ZnGlu1**−**ZnGlu5**, respectively) are summarized in Figure 6. As expected, mondentate/bidentate interaction between the Zn^{2+} cation and the negatively charged carboxyl group (COO^-) represents the key interaction, which readily attributed to the strong electrostatic attraction between Zn^{2+} and COO^-. Simultaneous coordination of Zn^{2+} with the carboxyl group of the backbone, *via* carbonyl oxygen, is observed in most complexes. The $Zn^{+}\cdots$O (carbonyl) interaction distances, 2.01−2.17 Å, are comparable to those in Zn^{2+}−COO^- interactions, 1.96−2.28 Å. Several tri-coordinated Zn^{2+} complexes, namely, **ZnAsp2**, **ZnAsp5**, and **ZnGlu5**, were observed. However, these conformations are less stable due to the unfavorable entropy effect. For both Zn^{2+}−Asp^- and Zn^{2+}−Glu^- complexes, the lowest energy conformation, namely, **ZnAsp1** and **ZnGlu1**, respectively, corresponds to a coordination geometry with the zinc ion two-coordinated with carboxyl and carbonyl (side chain) groups. The calculated binding free energies (ΔG_{298}) of various conformations of both Zn^{2+}−AA^- complexes fall in the range −53.1−−90.8 kJ/mol (Figure 6). This indicates that the formation of the Zn^{2+}−AA^- complex is energetically favorable. The calculated strong binding affinity supports the experimental observation of the interaction of Zn^{2+} ions with aspartate and glutamate residues of α-LA protein.

3.9. Application of Zinc−α-LA Complexes; Stability in Synthetic Physiological Fluids and Biological Activity. This section of research focuses on contents of zinc released from the complex under four different conditions simulating the stomach and intestine conditions. About 10% of zinc, which was initially bound to the protein, was released in an acidic environment. No effect of the enzyme was noted. The pepsin was unable to cause the effect of dissolving zinc from the complex and degrading the protein into short peptides that could pass into the solution tested under the conditions of this experiment. In the alkaline environment without the participation of the enzyme, the release value of less than 10% was also noted, which confirms the stability of the complex to the alkaline environment. However, the action of this alkaline medium together with the pancreatin enzyme causes the release of a significant amount of zinc (41.4%), and consequently, it can be assessed that the complex is not stable under these conditions. Rodzik *et al.* studied the release of zinc from complexes with β-lactoglobulin.[30] The stability of the complex in both environments (gastric and intestinal fluid) acting on the complex without the enzyme is noted. However, along with the enzymes, zinc was released from the complex. In this case, the complex is insensitive to the enzyme acting in the acidic medium, unlike the studies in ref 30. As in the studies by Rodzik *et al.*, the influence of the pancreatin enzyme in the intestinal fluid was noted here. This may be due to the action of the enzyme trypsin, which degrades protein into peptides, which is part of the release solution.[30]

Furthermore, the peptic digestion kinetics was performed to visually demonstrate the digestive stability of the synthesized complex. Figure 7 presents the resulting SDS-PAGE for performed digestions.

The results of the peptic digestion revealed that complete α-LA hydrolysis was not achieved even after 45 min. Instead, in the previous work of our group, the kinetics of bovine lactoferrin (bLTF) digestion was performed. After 30 min, there were no intact bLTF in the solution,[43] while almost 50% of α-LA at this time point still was unchanged. It is noteworthy to mention that for bLTF digestion, a lower enzyme-to-protein ratio was utilized (0.1 U/100 μg) which indicates much higher susceptibility to peptic hydrolysis. The proteins' digestion susceptibility with enzymes is dependent on the structure of the protein. More tightly folded sequences reveal lower susceptibility to enzymatic degradation.[75] bLTF has a hinge region connecting N- and C-lobes which seems to be the most preferable place for the enzymatic action. Moreover, it was reported that bLTFs' N-lobe treated with pepsin can easily release antibacterial peptide lactoferricin. Additionally, the digestion appears more intense upon the loss of the iron from the structure which occurs under acidic conditions.[76] Instead, α-LA under acidic conditions forms a highly stable molten globule which may be a reason for its increased stability against peptic digestion.[77] The digestion kinetics of the complex of α-LA with zinc did not differ from the kinetics of native protein. Interestingly, the peptic digestion of α-LA cause the formation of three peptides with masses lower than 7 kDa, and two of them remain unchanged even after 45 min of the process. It may be concluded that zinc from the complex should remain bonded to these peptides. Instead, for the complex of bLTF with Ag, a slightly lower degradation rate for the protein was observed, but much faster digestion of peptides occurred. The respective differences may be due to the changes in the tertiary structure caused by Ag incorporation.[43] It is noteworthy to mention that in Permyakov *et al.* work,[27] the tryptic digestion of α-LA was performed in the presence of Zn^{2+} ions. They have utilized both the trypsin and chymotrypsin for the digestion. It was shown that in the case of trypsin, the presence of Zn^{2+} increases the digestion rate in all utilized Zn/protein ratios. Instead, for chymotrypsin, the acceleration began at somewhat higher metal concentration. The differences may be connected to the differences in their specificity: trypsin cleaves at peptide bonds containing basic residues, while chymotrypsin cleaves at peptide bounds adjacent to aromatic residues. Pepsin is a protein that also preferentially hydrolyzes peptide bonds between the aromatic amino acids which may explain the observed results as the batch sorption analysis did not show the high Zn^{2+} sorption by α-LA.[78]

Cytotoxicity of Zn−α-LA composites and Zn ions was determined by MTT and LDH methods on human epithelial colorectal adenocarcinoma Caco-2 cell lines and L929 murine fibroblast cell lines. L929 cells are used in ISO 10993-5 and ISO 10993-12 norms for biological and clinical evaluation of medical devices. Caco-2 cells, due to many morphological and biochemical similarities to enterocytes—intestinal absorptive cells, are used as *in vitro* models to study absorption of orally

https://doi.org/10.1021/acsomega.2c03674
ACS Omega 2022, 7, 38459−38474

administered drugs. Cell viability was tested using two spectrophotometric assays: MTT (3-(4,5-dimethylthiazol-2-yl)-2,5-diphenyl tetrazolium bromide) and LDH (lactate dehydrogenase) release. MTT test is based on the ability of mitochondrial enzyme dehydrogenase to transfer yellow tetrazolium dye into formazan crystals. The level of obtained formazan crystals is directly proportional to cell viability. Therefore, the level of formazan crystals in the control, untreated sample is set to 100% viability. In the LDH assay protocol, the level of lactate dehydrogenase that is released into the culture medium following the loss of membrane integrity is measured. LDH activity is recognized as an indicator of cell membrane integrity.

As shown in Figure 8A,B, the MTT results demonstrated that in L929 cells, Zn in the form of complex did not decrease the viability of cells in the whole range of tested concentrations, that is, up to 200 μM. However, zinc ions were more toxic and lowered the viability of cells to 20% at a concentration of 100 μM. Caco-2 cells were less sensitive to both forms of Zn than L929 cells. One of the reasons for the difference may be that L929 cells belong to the normal cell line, while Caco-2 cells are from malignant tissue, colorectal adenocarcinoma.

To monitor the membrane damage of more susceptible L929 cells, LDH test was performed (Figure 8C,D). The results of this assay show that the lactate dehydrogenase release is mostly very similar for zinc complexes in the whole range tested and comparable with the control. For zinc ions, a significant increase in the dehydrogenase released was observed at the concentration 200 μM, which indicates damage to the integrity of the membrane. For cells, Caco-2 levels of released lactate dehydrogenase were only slightly elevated in the range 6.25−200 μM.

One of the aspects of cytotoxicity is oxidative stress. In order to detect reactive oxygen species after treatment with zinc ions and complexes, a fluorometric intracellular ROS kit that detects, in particular, superoxide and hydroxyl radicals was applied (Figure 8E). Studies showed that the level of ROS for cells treated with zinc ions and zinc complexes was comparable with control cells. Also, a comparison of the morphology of cells treated with various concentrations of zinc complexes did not reveal any significant changes compared to control cells.

To check the amount of zinc ions taken from the protein complexes, L929 cells were incubated for 24 h with zinc complexes and for comparison with zinc nitrate (Figure 8G). Results showed that the level of adsorbed zinc was two times higher for zinc nitrate than for zinc complexes. However, many studies indicate that at higher zinc concentrations, zinc uptake is by passive diffusion (for review, 68). Lower values of zinc taken by cells from zinc complexes indicate another, more safe mechanism of zinc absorption. However, further studies especially on Caco-2 cells are necessary for understanding the transport mechanism of zinc complexes.

CONCLUSIONS

This article presents the physicochemical characteristics of α-LA and the synthesis of the complex of the protein with zinc ions. The binding process was investigated with several analytical techniques. The work shows that the binding process is fast and zinc ions are bound to the surface of protein particles in solution, while aspartic and glutamic acids are particularly active functional groups in metal ion binding. The solubility, bioavailability, and cytotoxicity of these complexes were also tested.

ASSOCIATED CONTENT

Supporting Information

The Supporting Information is available free of charge at https://pubs.acs.org/doi/10.1021/acsomega.2c03674.

SDS-PAGE analysis of the α-LA standard; mass spectra of α-LA recorded in the linear positive mode by MALDI-TOF MS; identified peptide sequence characteristic for α-LA, protein recorded with MALDI-TOF MS in the collision mode after digestion reaction with trypsin; and pH dependence of zeta potential for protein suspension in 0.09% (w/V) NaCl (PDF)

AUTHOR INFORMATION

Corresponding Author

Pawel Pomastowski − *Centre for Modern Interdisciplinary Technologies, Nicolaus Copernicus University in Torun, 87-100 Torun, Poland;* orcid.org/0000-0002-1594-0623; Email: p.pomastowki@umk.pl

Authors

Adrian Gołębiowski − *Centre for Modern Interdisciplinary Technologies, Nicolaus Copernicus University in Torun, 87-100 Torun, Poland; Department of Environmental Chemistry and Bioanalytics, Faculty of Chemistry, Nicolaus Copernicus University in Torun, 87-100 Torun, Poland;* orcid.org/0000-0001-9321-286X

Katarzyna Rafińska − *Department of Environmental Chemistry and Bioanalytics, Faculty of Chemistry, Nicolaus Copernicus University in Torun, 87-100 Torun, Poland*

Petar Zuvela − *Department of Chemistry, National University of Singapore, 117543 Singapore, Singapore;* orcid.org/0000-0001-6481-2241

Ming Wah Wong − *Department of Chemistry, National University of Singapore, 117543 Singapore, Singapore;* orcid.org/0000-0003-2162-1220

Oleksandra Pryshchepa − *Centre for Modern Interdisciplinary Technologies, Nicolaus Copernicus University in Torun, 87-100 Torun, Poland; Department of Environmental Chemistry and Bioanalytics, Faculty of Chemistry, Nicolaus Copernicus University in Torun, 87-100 Torun, Poland*

Piotr Madajski − *Department of Chemistry of Materials Adsorption and Catalysis, Faculty of Chemistry, Nicolaus Copernicus University in Torun, 87-100 Torun, Poland*

Bogusław Buszewski − *Centre for Modern Interdisciplinary Technologies, Nicolaus Copernicus University in Torun, 87-100 Torun, Poland; Department of Environmental Chemistry and Bioanalytics, Faculty of Chemistry, Nicolaus Copernicus University in Torun, 87-100 Torun, Poland*

Complete contact information is available at: https://pubs.acs.org/10.1021/acsomega.2c03674

Notes

The authors declare no competing financial interest.

ACKNOWLEDGMENTS

This work was financially supported by the National Science Centre within the framework of Opus 14 project no. 2017/27/B/ST4/02628 (2018−2021). A.G., P.P., K.R., O.P., and B.B.

are members of Toruń Center of Excellence "Towards Personalized Medicine" operating under Excellence Initiative-Research University. Authors would like to acknowledge Interdisciplinary Centre for Mathematical and Computational Modelling (ICM) at the University of Warsaw within the framework of the Virtual Library of Science program, subsidized by the Ministry of Science and Higher Education for financial support of Open Access publishing.

REFERENCES

(1) Beg, O. U.; Bahr-lindstrom, H.; Zaidi, Z. H.; Jornvall, H. The primary structure of alpha-lactalbumin from camel milk. *Eur. J. Biochem.* **1985**, *147*, 233−239.
(2) Heine, W. E.; Klein, P. D.; Reeds, P. J. The Importance of α-Lactalbumin in Infant Nutrition. *J. Nutr.* **1991**, *121*, 277−283.
(3) Jackson, J. G.; Janszen, D. B.; Lonnerdal, B.; Lien, E. L.; Pramuk, K. P.; Kuhlman, C. F. A multinational study of α-lactalbumin concentrations in human milk. *J. Nutr. Biochem.* **2004**, *15*, 517−521.
(4) Lien, E. L. Infant formulas with increased concentrations of α-lactalbumin. *Am. J. Clin. Nutr.* **2003**, *77*, 1555S.
(5) Davis, A. M.; Harris, B. J.; Lien, E. L.; Pramuk, K.; Trabulsi, J. α-Lactalbumin-rich infant formula fed to healthy term infants in a multicenter study: plasma essential amino acids and gastrointestinal tolerance. *Eur. J. Clin. Nutr.* **2008**, *62*, 1294−1301.
(6) Permyakov, E. A. α-Lactalbumin, Amazing Calcium-Binding Protein. *Biomolecules* **2020**, *10*, 1210.
(7) Saricay, Y.; Wierenga, P. A.; de Vries, R. Changes in Protein Conformation and Surface Hydrophobicity upon Peroxidase-Catalyzed Cross-Linking of Apo-α-lactalbumin. *J. Agric. Food Chem.* **2014**, *62*, 9345−9352.
(8) Chrysina, E. D.; Brew, K.; Acharya, K. R. Crystal Structures of Apo- and Holo-bovine α-Lactalbumin at 2.2-Å Resolution Reveal an Effect of Calcium on Inter-lobe Interactions. *J. Biol. Chem.* **2000**, *275*, 37021−37029.
(9) Permyakov, S. E.; Veprintsev, D. B.; Brooks, C. L.; Permyakov, E. A.; Berliner, L. J. Zinc binding in bovine ?-lactalbumin: Sequence homology may not be a predictor of subtle functional features. *Protein Struct. Funct. Genet.* **2000**, *40*, 106−111.
(10) Prestrelski, S. J.; Byler, D. M.; Thompson, M. P.; Byler, D. M.; Thompson, M. P. Effect of metal ion binding on the secondary structure of bovine.alpha.-lactalbumin as examined by infrared spectroscopy. *Biochemistry* **1991**, *30*, 8797−8804.
(11) Tanaka, N.; Kunugi, S. Influence of zinc (II) binding on the structure of bovine α-lactalbumin. *Int. J. Pept. Protein Res.* **1996**, *47*, 154−160.
(12) Segawa, T.; Sugai, S. Interactions of Divalent Metal Ions with Bovine, Human, and Goat α-Lactalbumins1. *J. Biochem.* **1983**, *93*, 1321−1328.
(13) Permyakov, E. A.; Morozova, L. A.; Kahnichenko, L. P.; Derezhkov, V. Y. Interaction of α-lactalbumin with Cu2+. *Biophys. Chem.* **1988**, *32*, 37−42.
(14) Desmet, J.; Haezebrouck, P.; Van Cauwelaert, F. Thermodynamic data on the binding of six M2+-ions to bovine, goat, and human α-lactalbumin. *J. Inorg. Biochem.* **1991**, *42*, 139−145.
(15) Kronman, S. C.; Bratcher, M. J. Conformational changes induced by zinc and terbium binding to native bovine alpha-lactalbumin and calcium-free alpha-lactalbumin. *J. Biol. Chem.* **1984**, *259*, 10887−10895.
(16) Bramaud, C.; Aimar, P.; Daufin, G. Thermal isoelectric precipitation of ?-lactalbumin from a whey protein concentrate: Influence of protein-calcium complexation. *Biotechnol. Bioeng.* **1995**, *47*, 121−130.
(17) Kurz, F.; Hengst, C.; Kulozik, U. RP-HPLC Method for Simultaneous Quantification of Free and Total Thiol Groups in Native and Heat Aggregated Whey Proteins. *MethodsX* **2020**, *7*, 101112.
(18) Rösner, H. I.; Redfield, C. The Human α-Lactalbumin Molten Globule: Comparison of Structural Preferences at pH 2 and pH 7. *J. Mol. Biol.* **2009**, *394*, 351−362.
(19) Hoque, M.; Gupta, J.; Rabbani, G.; Khan, R. H.; Saleemuddin, M. Behaviour of Oleic Acid-Depleted Bovine Alpha-Lactalbumin Made LEthal to Tumor Cells (BAMLET). *Mol. Biosyst.* **2016**, *12*, 1871−1880.
(20) Yarramala, D. S.; Prakash, P.; Ranade, D. S.; Doshi, S.; Kulkarni, P. P.; Bhaumik, P.; Rao, C. P. Cytotoxicity of apo bovine α-lactalbumin complexed with La3+ on cancer cells supported by its high resolution crystal structure. *Sci. Rep.* **2019**, *9*, 1780.
(21) Layman, D. K.; Lönnerdal, B.; Fernstrom, J. D. Applications for α-lactalbumin in human nutrition. *Nutr. Rev.* **2018**, *76*, 444−460.
(22) Krężel, A.; Maret, W. The Biological Inorganic Chemistry of Zinc Ions. *Arch. Biochem. Biophys.* **2016**, *611*, 3−19.
(23) Ibs, K.-H.; Rink, L. Immunity Enhanced by Trace Elements Zinc-Altered Immune Function 1. *J. Nutr.* **2003**, *133*, 1452S.
(24) Haase, H.; Rink, L. Multiple Impacts of Zinc on Immune Function. *Metallomics* **2014**, *6*, 1175−1180.
(25) Wellenreuther, G.; Cianci, M.; Tucoulou, R.; Meyer-Klaucke, W.; Haase, H. The Ligand Environment of Zinc Stored in Vesicles. *Biochem. Biophys. Res. Commun.* **2009**, *380*, 198−203.
(26) Lönnerdal, B.; Lien, E. L. Nutritional and Physiologic Significance of α-Lactalbumin in Infants. *Nutr. Rev.* **2003**, *61*, 295−305.
(27) Permyakov, E. A.; Shnyrov, V. L.; Kalinichenko, L. P.; Kuchar, A.; Reyzer, I. L.; Berliner, L. J. Binding of Zn(II) ions to α-lactalbumin. *J. Protein Chem.* **1991**, *10*, 577.
(28) Atri, M. S.; Saboury, A. A.; Moosavi-Movahedi, A. A.; Kavousi, K.; Ariaeenejad, S. Effects of Zinc Binding on the Structure and Thermal Stability of Camel Alpha-Lactalbumin. *J. Therm. Anal. Calorim.* **2015**, *120*, 481−488.
(29) Gołębiowski, A.; Pomastowski, P.; Rodzik, A.; Król-Górniak, A.; Kowalkowski, T.; Górecki, M.; Buszewski, B. Isolation and Self-Association Studies of Beta-Lactoglobulin. *Int. J. Mol. Sci.* **2020**, *21*, 9711.
(30) Buszewski, B.; Rodzik, A.; Railean-Plugaru, V.; Sprynskyy, M.; Pomastowski, P. A study of zinc ions immobilization by β-lactoglobulin. *Colloids Surf., A* **2020**, *591*, 124443.
(31) Shevchenko, A.; Wilm, M.; Vorm, O.; Mann, M. Mass Spectrometric Sequencing of Proteins from Silver-Stained Polyacrylamide Gels. *Anal. Chem.* **1996**, *68*, 850−858.
(32) Rodzik, A.; Pomastowski, P.; Railean-Plugaru, V.; Sprynskyy, M.; Buszewski, B. The Study of Zinc Ions Binding to αS1-, β- and κ-Casein. *Int. J. Mol. Sci.* **2020**, *21*, 8096.
(33) Pomastowski, P.; Sprynskyy, M.; Buszewski, B. The Study of Zinc Ions Binding to Casein. *Colloids Surf., B* **2014**, *120*, 21−27.
(34) Pomastowski, P.; Sprynskyy, M.; Żuvela, P.; Rafińska, K.; Milanowski, M.; Liu, J. J.; Yi, M.; Buszewski, B. Silver-Lactoferrin Nanocomplexes as a Potent Antimicrobial Agent. *J. Am. Chem. Soc.* **2016**, *138*, 7899−7909.
(35) Żuvela, P.; Liu, J. J.; Yi, M.; Pomastowski, P. P.; Sagandykova, G.; Belka, M.; David, J.; Bączek, T.; Szafrański, K.; Żołnowska, B.; Sławiński, J.; Supuran, C. T.; Wong, M. W.; Buszewski, B. Target-Based Drug Discovery through Inversion of Quantitative Structure-Drug-Property Relationships and Molecular Simulation: CA IX-Sulphonamide Complexes. *J. Enzyme Inhib. Med. Chem.* **2018**, *33*, 1430−1443.
(36) Chandra, N.; Brew, K.; Acharya, K. R. Structural Evidence for the Presence of a Secondary Calcium Binding Site in Human α-Lactalbumin,. *Biochemistry* **1998**, *37*, 4767−4772.
(37) Li, P.; Song, L. F.; Merz, K. M. Systematic Parameterization of Monovalent Ions Employing the Nonbonded Model. *J. Chem. Theory Comput.* **2015**, *11*, 1645−1657.
(38) Li, P.; Roberts, B. P.; Chakravorty, D. K.; Merz, K. M. Rational Design of Particle Mesh Ewald Compatible Lennard-Jones Parameters for +2 Metal Cations in Explicit Solvent. *J. Chem. Theory Comput.* **2013**, *9*, 2733−2748.

https://doi.org/10.1021/acsomega.2c03674
ACS Omega 2022, 7, 38459−38474

(39) Lindorff-Larsen, K.; Piana, S.; Palmo, K.; Maragakis, P.; Klepeis, J. L.; Dror, R. O.; Shaw, D. E. Improved Side-Chain Torsion Potentials for the Amber Ff99SB Protein Force Field. *Proteins: Struct., Funct., Bioinf.* **2010**, *78*, 1950−1958.
(40) Frisch, M.; Trucks, G.; Schlegel, H.; Scuseria, G.; Robb, M.; Cheeseman, J.; Scalmani, G.; Barone, V.; Petersson, G.; Nakatsuji, H.; et al. *Gaussian 16*, Revision A; Gaussian Inc., 2016.
(41) Zhao, Y.; Truhlar, D. G. The M06 Suite of Density Functionals for Main Group Thermochemistry, Thermochemical Kinetics, Noncovalent Interactions, Excited States, and Transition Elements: Two New Functionals and Systematic Testing of Four M06-Class Functionals and 12 Other Functionals. *Theor. Chem. Acc.* **2008**, *120*, 215−241.
(42) Marenich, A. V.; Cramer, C. J.; Truhlar, D. G. Universal Solvation Model Based on Solute Electron Density and on a Continuum Model of the Solvent Defined by the Bulk Dielectric Constant and Atomic Surface Tensions. *J. Phys. Chem. B* **2009**, *113*, 6378−6396.
(43) Pryshchepa, O.; Pomastowski, P.; Rafińska, K.; Gołębiowski, A.; Rogowska, A.; Monedeiro-Milanowski, M.; Sagandykova, G.; Michalke, B.; Schmitt-Kopplin, P.; Gloc, M.; Dobrucka, R.; Kurzydlowski, K.; Buszewski, B. Synthesis, Physicochemical Characterization, and Antibacterial Performance of Silver-Lactoferrin Complexes. *Int. J. Mol. Sci.* **2022**, *23*, 7112.
(44) Rekha, S.; Anila, E. I. In Vitro Cytotoxicity Studies of Surface Modified CaS Nanoparticles on L929 Cell Lines Using MTT Assay. *Mater. Lett.* **2019**, *236*, 637−639.
(45) Fotakis, G.; Timbrell, J. A. In Vitro Cytotoxicity Assays: Comparison of LDH, Neutral Red, MTT and Protein Assay in Hepatoma Cell Lines Following Exposure to Cadmium Chloride. *Toxicol. Lett.* **2006**, *160*, 171−177.
(46) van Meerloo, J.; Kaspers, G. J. L.; Cloos, J. Cell Sensitivity Assays: The MTT Assay. In *Cancer Cell Culture: Methods and Protocols*; Cree, I. A., Ed.; Humana Press: Totowa, NJ, 2011; pp 237−245.
(47) Maté, J.; Krochta, J. ?-Lactoglobulin Separation from Whey Protein Isolate on a Large Scale. *J. Food Sci.* **1994**, *59*, 1111−1114.
(48) Gołębiowski, A.; Pomastowski, P.; Rodzik, A.; Król-Górniak, A.; Kowalkowski, T.; Górecki, M.; Buszewski, B. Isolation and Self-Association Studies of Beta-Lactoglobulin. *Int. J. Mol. Sci.* **2020**, *21*, 9711.
(49) Fuchs, B.; Süß, R.; Schiller, J. An Update of MALDI-TOF Mass Spectrometry in Lipid Research. *Prog. Lipid Res.* **2010**, *49*, 450−475.
(50) Chinthaka, S. D. M.; Rodgers, M. T. Sodium Cation Affinities of Commonly Used MALDI Matrices Determined by Guided Ion Beam Tandem Mass Spectrometry. *J. Am. Soc. Mass Spectrom.* **2012**, *23*, 676−689.
(51) Zhang, J.; Knochenmuss, R.; Stevenson, E.; Zenobi, R. The Gas-Phase Sodium Basicities of Common Matrix-Assisted Laser Desorption/Ionization Matrices. *Int. J. Mass Spectrom.* **2002**, *213*, 237−250.
(52) Rout, P. K.; Verma, M. Post Translational Modifications of Milk Proteins in Geographically Diverse Goat Breeds. *Sci. Rep.* **2021**, *11*, 5619.
(53) Giuffrida, M. G.; Cavaletto, M.; Giunta, C.; Neuteboom, B.; Cantisani, A.; Napolitano, L.; Calderone, V.; Godovac-Zimmermann, J.; Conti, A. The Unusual Amino Acid Triplet Asn-Ile-Cys Is a Glycosylation Consensus Site in Human α-Lactalbumin. *J. Protein Chem.* **1997**, *16*, 747−753.
(54) Shewale, J. G.; Sinha, S. K.; Brew, K. Evolution of alpha-lactalbumins. The complete amino acid sequence of the alpha-lactalbumin from a marsupial (Macropus rufogriseus) and corrections to regions of sequence in bovine and goat alpha-lactalbu. *J. Biol. Chem.* **1984**, *259*, 4947−4956.
(55) Picariello, G.; Ferranti, P.; Mamone, G.; Roepstorff, P.; Addeo, F. Identification of N-Linked Glycoproteins in Human Milk by Hydrophilic Interaction Liquid Chromatography and Mass Spectrometry. *Proteomics* **2008**, *8*, 3833−3847.
(56) Giufrida, J.; Cantisani, A.; Napoutano, L.; Conti, A.; Godovac-zimmermann, J. The Amino-Acid Sequence of Two Isoforms of α-Lactalbumin from Donkey(Equus asinus)Milk is Identical. *Biol. Chem. Hoppe Seyler* **1992**, *373*, 931−936.
(57) Girardet, J. M.; N'negue, M. A.; Egito, A. S.; Campagna, S.; Lagrange, A.; Gaillard, J. L. Multiple forms of equine α-lactalbumin: evidence for N-glycosylated and deamidated forms. *Int. Dairy J.* **2004**, *14*, 207−217.
(58) Jin, Y.; Manabe, T. High-Efficiency Protein Extraction from Polyacrylamide Gels for Molecular Mass Measurement by Matrix-Assisted Laser Desorption/Ionization-Time of Flight-Mass Spectrometry. *Electrophoresis* **2005**, *26*, 1019−1028.
(59) Ham, J. S.; Han, G. S.; Jeong, S. G.; Seol, K. H.; Jang, A. R.; Oh, M. H.; Kim, D. H.; Park, Y. W. Determination of Molecular Weights of Caprine Milk Proteins by Matrix-Assisted Laser Desorption/Ionization Mass Spectrometry. *J. Dairy Sci.* **2012**, *95*, 15−19.
(60) Svensson, M.; Sabharwal, H.; Håkansson, A.; Mossberg, A. K.; Lipniunas, P.; Leffler, H.; Svanborg, C.; Linse, S. Molecular Characterization of α-Lactalbumin Folding Variants That Induce Apoptosis in Tumor Cells. *J. Biol. Chem.* **1999**, *274*, 6388−6396.
(61) Peleg, Y.; Unger, T. Resolving Bottlenecks for Recombinant Protein Expression in E. coli. *Methods Mol. Biol.* **2012**, *800*, 173−186.
(62) Calgaroto, S.; Wilberg, K. Q.; Rubio, J. On the Nanobubbles Interfacial Properties and Future Applications in Flotation. *Miner. Eng.* **2014**, *60*, 33−40.
(63) Krebs, M. R. H.; Domike, K. R.; Donald, A. M. Protein Aggregation: More than Just Fibrils. *Biochem. Soc. Trans.* **2009**, *37*, 682−686.
(64) Ramírez-Rodríguez, T.; de Landa Castillo-Alvarado, F. Application of the Intra-Particle Diffusion Model for Activated Carbon Fibers in an Aqueous Medium. *Mater. Res. Soc. Symp. Proc.* **2011**, *1373*, 424.
(65) Barth, A. Infrared Spectroscopy of Proteins. *Biochim. Biophys. Acta, Bioenerg.* **2007**, *1767*, 1073−1101.
(66) Prestrelski, S. J.; Byler, M. D.; Thompson, M. P. Infrared spectroscopic discrimination between alpha- and 3(10)-helices in globular proteins. Reexamination of Amide I infrared bands of alpha-lactalbumin and their assignment to secondary structures. *Int. J. Pept. Protein Res.* **1991**, *37*, 508−512.
(67) Barth, A. The Infrared Absorption of Amino Acid Side Chains. *Prog. Biophys. Mol. Biol.* **2000**, *74*, 141−173.
(68) Lafaut, J. P.; Van Dael, H. Calcium binding effects on the structure of α-lactalbumin. *J. Mol. Struct.* **1986**, *143*, 449−452.
(69) Cai, S.; Singh, B. R. Identification of β-turn and random coil amide III infrared bands for secondary structure estimation of proteins. *Biophys. Chem.* **1999**, *80*, 7−20.
(70) Bazylewski, P.; Divigalpitiya, R.; Fanchini, G. In situ Raman spectroscopy distinguishes between reversible and irreversible thiol modifications in l-cysteine. *RSC Adv.* **2017**, *7*, 2964−2970.
(71) Zhu, G.; Zhu, X.; Fan, Q.; Wan, X. Raman Spectra of Amino Acids and Their Aqueous Solutions. *Spectrochim. Acta, Part A* **2011**, *78*, 1187−1195.
(72) Jenkins, A. L.; Larsen, R. A.; Williams, T. B. Characterization of Amino Acids Using Raman Spectroscopy. *Spectrochim. Acta, Part A* **2005**, *61*, 1585−1594.
(73) Pomastowski, P.; Król-Górniak, A.; Railean-Plugaru, V.; Buszewski, B. Zinc Oxide Nanocomposites-Extracellular Synthesis, Physicochemical Characterization and Antibacterial Potential. *Materials* **2020**, *13*, 4347.
(74) Buszewski, B.; Žuvela, P.; Król-Górniak, A.; Railean-Plugaru, V.; Rogowska, A.; Wong, M. W.; Yi, M.; Rodzik, A.; Sprynskyy, M.; Pomastowski, P. Interactions of Zinc Aqua Complexes with Ovalbumin at the Forefront of the Zn2+/ZnO-OVO Hybrid Complex Formation Mechanism. *Appl. Surf. Sci.* **2021**, *542*, 148641.
(75) Fu, Z.; Akula, S.; Thorpe, M.; Hellman, L. Marked Difference in Efficiency of the Digestive Enzymes Pepsin, Trypsin, Chymotrypsin, and Pancreatic Elastase to Cleave Tightly Folded Proteins. *Biol. Chem.* **2021**, *402*, 861−867.

https://doi.org/10.1021/acsomega.2c03674
ACS Omega 2022, 7, 38459−38474

(76) Takayama, Y. Lactoferrin Structure Function and Genetics. *Lactoferrin and its Role in Wound Healing*; Springer Netherlands, 2012; pp 43−66.
(77) Nicoleta, S.; Rapeanu, G. An Overview of Bovine α-Lactalbumin Structure and Functionality. *Ann. Univ. Dunarea Jos Galati, Fasc. VI* **2010**, *34*, 82.
(78) Wang, R.; Edrington, T. C.; Storrs, S. B.; Crowley, K. S.; Ward, J. M.; Lee, T. C.; Liu, Z. L.; Li, B.; Glenn, K. C. Analyzing Pepsin Degradation Assay Conditions Used for Allergenicity Assessments to Ensure That Pepsin Susceptible and Pepsin Resistant Dietary Proteins Are Distinguishable. *PLoS One* **2017**, *12*, No. e0171926.

https://doi.org/10.1021/acsomega.2c03674
ACS Omega 2022, 7, 38459−38474

Materiały uzupełniające do publikacji

Functionalization of Alpha-Lactalbumin by Zinc Ions

Są również dostępne pod adresem:

https://pubs.acs.org/doi/10.1021/acsomega.2c03674

UNIWERSYTET MIKOŁAJA KOPERNIKA W TORUNIU
Wydział Chemii

Supporting Information

Functionalization of alpha-lactalbumin by zinc ions

Adrian Gołębiowski[1,2], Paweł Pomastowski[1*], Katarzyna Rafińska[2], Petar Zuvela[3], Ming Wah Wong[3], Oleksandra Pryshchepa[1,2], Piotr Madajski[4], Bogusław Buszewski[1,2]

[1] Centre for Modern Interdisciplinary Technologies, Nicolaus Copernicus University in Torun, 4 Wileńska St., 87-100 Torun, Poland
[2] Department of Environmental Chemistry and Bioanalytics, Faculty of Chemistry, Nicolaus Copernicus University in Torun, 7 Gagarina St., 87-100 Torun, Poland
[3] Department of Chemistry, National University of Singapore, 3 Science Drive 3, 117543, Singapore
[4] Department of Chemistry of Materials Adsorption and Catalysis, Faculty of Chemistry, Nicolaus Copernicus University in Torun, Gagarina 7, 87-100 Torun, Poland

[*] Correspondence: p.pomastowki@umk.pl

Contents

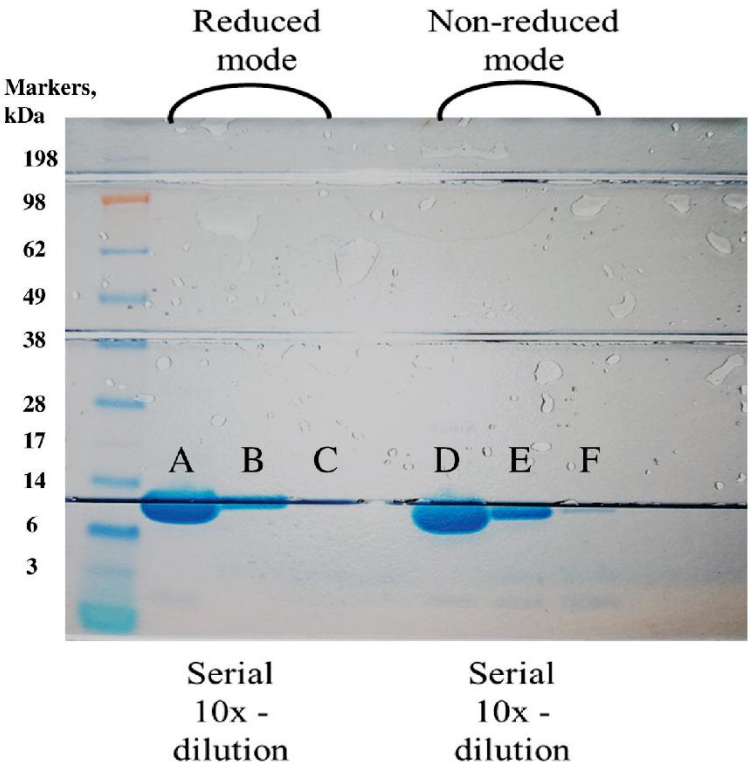

Figure S1. SDS-PAGE of α-LA. The reduced and non-reduced conditions were applied. Three 10X serial dilution was analyzed.

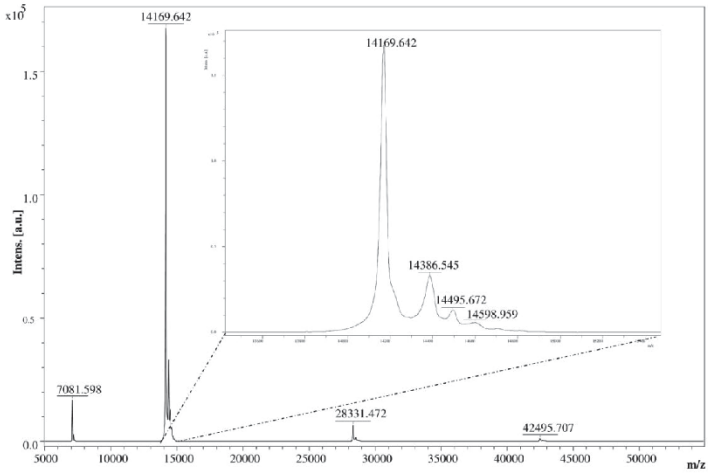

Figure S2. Mass spectrum for α-LA obtained in Intact mode of MALDI-TOF-MS spectrometer.

Table S1. MS and MS/MS identification of α-LA peptides.

Mass [Da]		Intensity	Sequence Range	Sequence from MS/MS
Measured	Theoretical			
710.330	710.329	33013.490	25 - 29	CEVFR
1091.520	1091.519	4357.889	134 - 141	LDQWLCEK
1200.666	1200.652	203435.100	118 - 127	VGINYWLAHK
1699.774	1699.755	4108.163	99 - 112	FLDDDLTDDIMCVK
2003.818	2003.818	1341.993	82 - 98	DDQNPHSSNICNISCDK

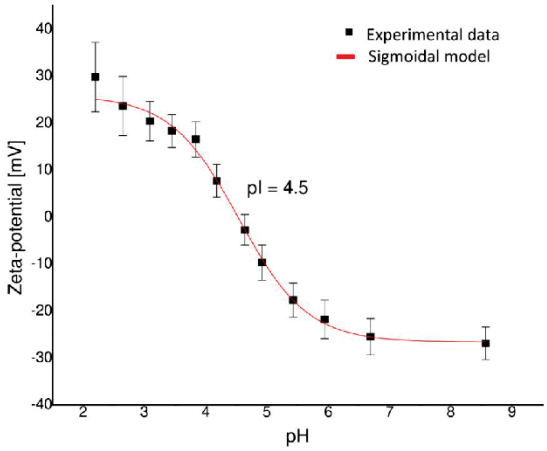

Figure S3. Zeta-potential dependence of α-LA on the pH in a saline solution.

UNIWERSYTET MIKOŁAJA KOPERNIKA W TORUNIU
Wydział Chemii

[P5]

Golebiowski, Adrian & Pomastowski, Paweł & Rafińska, Katarzyna & Žuvela, Petar & Wong, M.W. & Madajski, P. & Buszewski, Bogusław

Binding of silver ions to alpha-lactalbumin

Journal of Molecular Structure

10.1016/j.molstruc.2022.133940

Journal of Molecular Structure 1270 (2022) 133940

Contents lists available at ScienceDirect

Journal of Molecular Structure

journal homepage: www.elsevier.com/locate/molstr

Binding of silver ions to alpha-lactalbumin

A. Gołębiowski[a,b], P. Pomastowski[a,*], K. Rafińska[b], P. Žuvela[c], M.W. Wong[c], P. Madajski[d], B. Buszewski[a,b]

[a] Centre for Modern Interdisciplinary Technologies, Nicolaus Copernicus University in Toruń, 4 Wileńska St., Toruń 87-100, Poland
[b] Department of Environmental Chemistry and Bioanalytics, Faculty of Chemistry, Nicolaus Copernicus University in Toruń, 7 Gagarina St., Toruń 87-100, Poland
[c] Department of Chemistry, National University of Singapore, 3 Science Drive 3, 117543, Singapore
[d] Department of Chemistry of Materials Adsorption and Catalysis, Faculty of Chemistry, Nicolaus Copernicus University in Toruń, Gagarina 7, Toruń 87-100, Poland

ARTICLE INFO

Article history:
Received 1 June 2022
Revised 9 August 2022
Accepted 12 August 2022
Available online 13 August 2022

Keywords:
Metal-protein complexes
ICP-MS
Spectroscopic technique
Alpha-lactalbumin
Silver
Molecular dynamics

ABSTRACT

The process and product of silver ions binding to alpha-lactalbumin (α-LA) were studied and discussed in this paper. The aim of the work was to explain the mechanism of reaction using interdisciplinary research. The kinetic study shows that binding equilibrium of silver to α-LA is achieved after 2 min. Process was fitted to pseudo-zero, zero and Weber-Morris models and can be distinguished by two distinct steps: firstly, graduate decline in silver concentration in solution and second step of silver concentration equilibration. The determined thermodynamic parameters showed that the reaction can occur spontaneously. Complementing the experiments, molecular dynamic simulations and DFT calculations have shown that aspartic and glutamic residues have the most significant contribution in the silver binding process. Spectroscopic (ATR-FT-IR and Raman) methods were used to compare structure of native protein and after binding of silver and they confirmed that the binding occurs with participation of acidic residues of protein. Morphology and information about surface of particles were determined using scanning electron microscopy (SEM) and transmission electron microscopy (TEM) (with energy dispersive X-ray spectroscopy - EDX). Such experiments have shown that silver forms nearly homogeneous metallic structure onto protein. Silver has shown to be released from complexes in synthetic intestine physiological fluids in the highest quantity in stomach with comparison to mimicked intestine system. Cytotoxicity study showed better biocompatibility and bioavailability of composite than control.

1. Introduction

Silver is a chemical element belonging to the group of heavy metals and in its cation (Ag^+) form it can exhibit toxic properties. Its toxic properties against microbes can, in fact, be used in medical treatments such as pressure ulcer therapy [1]. Typically, in this type of therapy silver compounds of reduced toxicity are used. Therefore, synthesis and characterization of new compounds of silver (silver-protein for example) are being actively developed [2–4]. Silver bound to high molecular weight matrix compound reduces the toxicity to the living organism. Some matrices are capable of slow, controlled and targeted dissolution process of silver which can lead to antimicrobial activity [5]. The dissolution mechanism can be described as a "Trojan horse" which assumes the nanoparticles as carrier in the transfer process of high amount of silver ions between cell membranes [6]. The interactions of silver ions with proteins proved to be effective, safe and showed controlled and modulated cytotoxic properties against a certain group of microorganisms. The protein in these combinations acts as a carrier for silver and provides a kind of protective coat that allows for the controlled release of safe doses of silver throughout the entire body [7,8]. The nature of silver uptake by biocolloids very often results in obtaining silver in the form of nanoparticles [9]. Often the biocolloid itself is the source and carrier for the reaction of reducing silver in ionic form to reduced, zero-valance Ag^0 [10,11].

Alpha-lactalbumin (α-LA) is a small protein composed of 123 amino acids with a molecular weight of about 14 kDa [12]. The isoelectric point of the protein in the solution is around 4.5 [13]. It is one of the key proteins in human milk and a key nutrient for newborns and infants [14]. In living organisms, in addition to its nutritional properties, it is also part of the lactose synthase enzyme and a key carrier of calcium [15]. Protein has two metal binding sites. The first is a very strong bond of the order 10^4-10^5 M^{-1} and

* Corresponding author.
E-mail address: p.pomastowski@umk.pl (P. Pomastowski).

https://doi.org/10.1016/j.molstruc.2022.133940

the second is a bond of approximately 10^3 M^{-1} [16,17]. Besides calcium, other metals can also be bound by protein through the strongest binding site [18,19]. Binding of different metals to α-LA is associated with conformational rather than structural changes [20]. Therefore, the characterization of metal-α-LA binding requires sensitive and specific test methods such as molecular dynamic. The form of a protein saturated with calcium (holo form) is one of proteins most stable and most resistant to thermal denaturation [21]. It is also one of the most stable proteins in an acidic environment, where it creates the molten globule state [22]. In this state, it can be used as a seed for active substances in, for example, anti-cancer therapies [23].

The selectivity of the interaction of metals with proteins is noted; a number of properties of metals and ligands should be considered in the analysis of this type of interactions leading to the formation of coordination-type compounds [24]. α-LA is a high containing sulphur protein (has eight cysteine residues per 123 amino acids). Coordination bonds between sulphur (methionine, cysteine, cystine), nitrogen rich amino acid (lysine, histidine, proline, arginine) residues and silver and electrostatic attractions (glutamic and aspartamic acids) have been shown as crucial [25]. Additionally, silver has stronger affinity to sulphur than to nitrogen species [26].

The aim of this work is an attempt to explain the mechanism of silver binding to α-LA. The silver- α-LA composite has been synthesized and the process has been characterized by interdisciplinary research. Kinetic and thermodynamic research provide insight into the affinity of a metal for a protein; for this purpose, ICP-MS technique was used for determining silver concentration. Molecular dynamics (MD) simulations and quantum mechanics (QM) calculations using density functional theory (DFT) were used to determine and simulate functional groups from the protein structure particularly affecting the binding with silver. Spectrometric techniques (FT-IR and Raman) were used to characterize the changes in the secondary protein structure after the binding process. After characterization of the process and the composite, the application possibilities of using this type of product for personalized medical therapy were examined; the degree of silver release in simulated human gastric and intestinal fluids was tested (in relation to USP) and the cytotoxicity of the composite was determined for the L927 cell lines. The cytotoxicity of obtained nanoparticles was measured through the MTT dye, lactate dehydrogenase (LDH) assays, determination of the level of reactive oxygen species as well as monitoring of the amount of silver taken by L929 cells.

2. Materials and methods

The commercial standard of α-LA was used in all experiments. The protein was obtained from Sigma Aldrich (Sigma-Aldrich, Steinheim, Germany). Supplier stated that the purity of the material is higher than 85% (SDS-PAGE method).

2.1. Synthesis of α-LA composites with silver. Kinetic study of silver binding to protein by ICP-MS technique

Silver nanoparticles onto α-LA composite were synthesized in an aqueous solution. A solution of silver nitrate (Sigma-Aldrich, Steinheim, Germany) with a silver concentration of 60 mg Ag/L was prepared in 18.2 MΩ water (Merck Millipore, Darmstadt, Germany). A 5 mg/mL α-LA solution was prepared in double-deionized 18.2 MΩ water. The pH of the solutions was adjusted to 4.5 against a pH meter by adding the diluted NaOH or HNO_3 (Merck Suprapure, Darmstadt, Germany) solutions dropwise. Solutions of silver and protein suspension were mixed with each other in a 1:1 volume ratio. The sample was incubated at room temperature while constantly stirring at 900 rpm using Thermomixer comfort (Eppendorf AG, Hamburg, Germany). In order to study the kinetics of the binding process, various solutions were prepared and incubated for a specific time. Incubation times were 2, 5, 10, 30 min, 1, 2, 4, 6, 21, 24, 48 h. Upon incubation, the solutions were transferred to the Amicon Ultracell 3 kDa (Merck, Darmstadt, Germany) membrane and centrifuged for 15 min at 4°C and 14,000 rpm to separate an unbound portion of the silver solution from the composite. The filtrate was diluted 200 times with a 1% HNO_3 (Merck Suprapure, Darmstadt, Germany) solution. Such solutions were analyzed using ICP-MS. The initial concentration of silver was determined as well. Calibration curve method was used to obtain concentration result in samples. Silver standard solution (Sigma-Aldrich, Steinheim, Germany) was diluted to appropriate region of concentrations (from 0.1 µg/L to 100 µg/L). Rhodium was used as an internal standard. Shimadzu ICPMS 2030 (Shimadzu, Kyoto, Japan) spectrometer was used with active Collision Reaction Cell (helium flow was 6 mL/min). The signals at m/z of 107 and 109 were monitored. The binding kinetics was determined as the difference between the initial silver concentration and unbound fraction of silver by the protein. Experimental data were analyzed using pseudo zero (1), zero (2) and Weber-Morris (3) kinetic models [27]. The experimental silver concentration data was fitted to following formulas:

$$q_t = q_0 - kt \quad (1)$$

for pseudo−zero order model

$$C_t = C_0 - kt \quad (2)$$

for zero order model

$$q_t = A + Kip\sqrt{t} \quad (3)$$

for Weber−Morris model

where q_t is the amount of silver sorbed for a certain period of time [mg/g], q_o value of q at equilibria; k- the rate constant of sorption kinetics; t- time of process; C and C_0 are silver concentration for a certain period of time and equilibrium, respectively. A–a constant indicating the thickness of the boundary layer diffusion or external surface adsorption [mg/g], Kip–the diffusion rate constant [mg/g $min^{0.5}$].

The thermodynamic parameters: amount of zinc bounded to protein Q_t, distribution coefficient K_d (4) and Gibbs free energy (5) of adsorption were calculated using kinetic data:

$$K_d = \frac{q_e}{C_e} \quad (4)$$

$$\Delta G^0 = -RTlnK_d \quad (5)$$

2.2. Preparation of complexes for further studies

According to the kinetic study, the complexes sample was incubated for about 5 min. The unbound metal fraction was separated using Amicon Ultracell 3 kDa centrifugal unit. Composites were washed twice with deionized water. The solution was recovered from the membrane. The complexes were lyophilized (FreeZone Labconco, Kansas City, US) and dry mass were stored at -20°C.

2.3. Characterization of α-LA composites with silver by Molecular Dynamics (MD) and Quantum Mechanics (QM) – DFT – calculations

Molecular Dynamics (MD) simulations were carried out according to protocol of Pomastowski et al. [2] and Žuvela et al. [28]. The α-LA was analysed in apo form and their complexes with silver were characterized. Initial structure of α-LA was obtained from the Protein Databank (PDB ID; 1A4V) [29]. It is a structure determined

Table 1
Molecular dynamics and quantum mechanics parameters of analyses.

Summary of unscaled / scaled concentration of the Ag-α-LA systems			
Concentration [mg/L]		Proportion of ions to protein molecule	Scaled
30		1.55	65
MD parameters for Ag^+			
Ion	$R_{min/2}$	epsilon	sigma
Ag	1.341	0.00818431	0.238939

by X-ray diffraction with a resolution of 1.80 Angstrom. Solvation in a TIP3P water box with a variable side length, depending on the size of the system was performed. Due to the limited volume of solvation boxes, the amounts (in moles) of α-LA - Ag solutions were upscaled (Table 1) with constant scaling factors (to fully preserve the concentration ratios for Ag- α-LA).

To account for non-bonded interactions of Ag^+ with α-LA, parameters compatible with the TIP3P water model were obtained from Li et al. [30,31] (Table 1).

Solvation was followed by electrostatic neutralization with Na^+ or Cl^- ions. Such systems were subjected to energy minimization to remove bad contacts and structural clashes. Fast heating to 298.15K was carried out at a constant volume, followed by density equilibration step by subjecting the systems to (1 bar) and temperature (298.15K) – NPT ensemble. Production MD simulations were carried out in the NVT ensemble using the GROMACS 5.1.2 software using the AMBER ff99-SB-ILDN force field [32]. Visual Molecular Dynamics (VMD) 1.9.3 software, and Python 3.9 were used for visualization and data analysis.

2.4. Binding interaction of Ag^+ with aspartate and Glutamate residues by DFT calculations

To shed light on the interaction of silver ion (Ag^+) with and α-LA protein, various possible conformations of 1:1 Ag^+-Asp^- and Ag^+-Glu^- complexes were examined by M06-2X [29] DFT method, using the G16 programs [30]. Geometry optimizations and frequency calculations were performed at M06-2X/BS1 level and binding free energies at M06-2X/BS1 level, based on the M06-2X/BS1 optimized geometries. The BS1 basis set correspond to the smaller 6-31G* basis set for non-silver atoms and Def2-SVPD [31] basis set for silver atoms while the larger BS2 basis set correspond to the 6-311+G(2d,p) basis set for non-silver atoms and Def2-TZVPD [32] for silver atoms. The D2SVP and Def2-TZVPD basis sets for Ag contain an effective core potential (ECP). The solvation effect of aqueous medium ($\varepsilon = 78.4$) was modelled with an implicit solvation model SMD [33] in geometry optimizations and single-point energy calculations.

2.5. Characterization of α-LA composites with silver by spectroscopic techniques (ATR-FTIR, Raman)

The sample was further analyzed using attenuated total reflection Fourier Transform Infrared spectroscopy (ATR-FTIR) using Alpha FTIR Spectrometer (Bruker, Billerica, Massachusetts, USA). Spectra were obtained in the range of 400 – 4000 cm^{-1}. Dried sample was attached to measurement window and analyzed.

Raman spectra were taken using a Raman Spectrometer (Senterra, Bruker Optik). The sample was dissolved in a small volume of water. Tiny droplet of suspension was injected to glass. The spectra were registered in the region 4000–400 cm^{-1} at the wavelength (532 nm) as excitation light, with the power of approximately 2mW and the acquisition time of 20 s. The spectroscopic data were processed using OPUS software (Bruker, Billerica, Massachusetts, USA)).

2.6. Characterization of α-LA composites with silver by microscopic techniques: SEM and SEM-EDX

To obtain information about morphology, topography and semi-quantitative analysis of elements in composite, scanning electron microscopy (SEM) as well as with EDX were carried out. Microscopes were: SEM (Quanta 3D) and SEM-EDX instrument (1430 VP (LEO Electron Microscopy Ltd, UK)). The solution of nanoparticles was applied on the grid.

2.7. Application of α-LA composites with silver. Stability in Synthetic Physiological Fluids

Dissolution of silver from the composite was studied in four model synthetic fluids: gastric and intestinal with and without specific enzymes (pepsin and pancreatin for gastric and intestinal, respectively). The fluid was prepared according to Ref. [27]. 0.2 mg of complexes was weighed on analytical balance and dissolved in dissolution fluid. The solution was transferred to Amicon centrifugal device 3 kDa (Merck, Darmstadt, Germany). After 24 h of incubation time, the released silver solution was separated by applying centrifuge (15 min, 14,000 rpm, 10°C). The filtered solution was diluted (dilution factor 100) in 1 % HNO_3 (Merck Suprapure, Darmstadt, Germany). The quantitative analysis of silver by ICP-MS technique was performed as described as in 2.1. Section.

2.8. Biological activity of α-LA composites

The research was conducted on two cell lines L929 and Caco-2 purchased from ECACC (European Collection of Authenticated Cell Cultures operated by Public Health England). They were cultured in Dulbecco's Modified Eagle Medium (DMEM) supplemented with 10% (v/v) fetal bovine serum, 2 mM glutamine, 100 U/mL penicillin, and 100 μg/mL streptomycin. After reaching 80% confluence cells were passaged by trypsinization with 0.25% trypsin/EDTA. For tests, cells were seeded in 96-well plates at density 2 × 105 cells/mL. After 24 h the medium was replaced with a new one containing tested Ag complexes and incubated for 24 h. A silver nitrate control was performed to differentiate the cell response to various forms of silver compounds. After another 24 h 10% (v/v) of MTT solution (5mg/mL in PBS) was added to each well and incubated for 4 h. Later, medium from wells was removed and the formazan crystals were dissolved in DMSO for 10 min by mixing. Absorbance was measured with microplate reader (Multiskan, ThermoFisher) at 570 nm and 650 nm as background absorbance.

Lactate Dehydrogenase Activity Assay Kit (MAK066, Sigma) was used for LDH (enzyme lactate dehydrogenase) release assay. Cells were prepared in the same way as for MTT assay. Cells were incubated with Ag complexes and silver nitrate to induce cytotoxicity. In this time release of LDH occurs and the medium with released LDH was transferred to a new plate. To this medium LDH 50 μL of the Reaction Mixture was added. Absorbance was measured at 450 nm with microplate reader (Varioskan TM LUX Thermo Fisher Scientific, Waltham, MA, USA). Results are presented as a percent of activity in comparison to control.

Fluorometric Intracellular ROS kit (MAK144, Sigma-Aldrich) was used to evaluate the level of reactive oxygen species. Cells were cultured as for MTT assay and incubated with Ag complexes and silver nitrate for 24 h. After this time the 100 μL of Master Reaction Mix was added to each well. After 30 min fluorescence intensity was measured at λex = 540/λem = 570 nm using microplate reader (Varioskan TM LUX, Thermo Fisher Scientific, Waltham, MA, USA). Results are presented as a percent of activity in comparison to control.

To check the amount of silver ions taken from α-LA composites, L929 cells were incubated for 24 h with Ag_complex and AgNO3

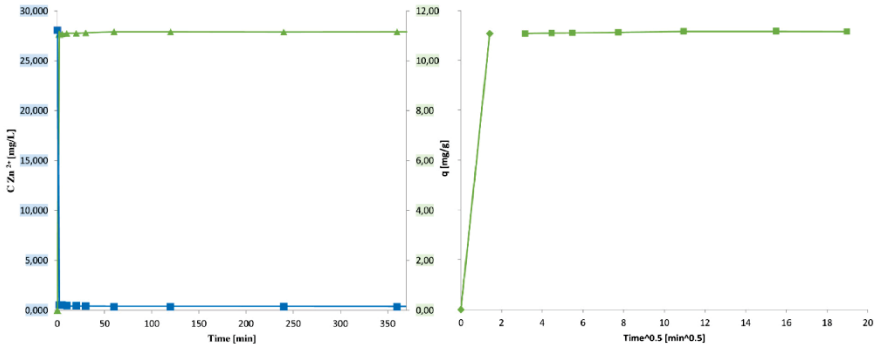

Fig. 1. Kinetics of silver binding onto α-LA. Blue points and line of model is related to zero order, green relationship on left chart is pseudo-zero kinetic and on the right panel the Weber-Morris model is showed.

Table 2
Thermodynamic parameters of binding silver onto α-LA process.

Parameters	Value [units]
C_e	27.6 [mg/L]
Q_e	11.2 [mg/g]
K_D	38037.8
ΔG	-25.85 [kJ/mol]

at concentration 0.05 and 0.5 mM for 24 h. After that time cells were washed 2 times with Dulbecco's PBS, trypsinized with 0.25% trypsin and again washed with Dulbecco's PBS. The obtained cell pellet was mineralized with nitric acid and analyzed by ICP-MS.

3. Results and discussion

3.1. Kinetic study of silver binding to protein using ICP-MS

Fig. 1 shows the dependence of changes in the silver concentration in the solution after the uptake by α-LA. Two linear steps of the process can be distinguished. The first phase is a sharp decrease in the concentration of silver in the solution. During the first 2 min of incubation, the concentration of silver is nearly null. Based on the zero-order kinetic model, the reaction rate constant for this stage was determined to be 13.75 mg min / L. The second step in the process can be described as establishing an equilibrium. During the incubation period between 5 min and 48 h, the concentration of silver in the solution is constant (the reaction rate constant for the zero order is positive with the order of 10^{-4} mg min/L). Such a dependence of the silver concentration changes over time may suggest a fast process taking place on the surface of the protein, where the limiting stage is the diffusion of silver ions to the surface of the protein. Table 2 shows the thermochemical data. The process is thermodynamically preferred and spontaneous because the Gibbs free enthalpy has a negative value (**Table 2**). A negative sign of Gibb's enthalpy is presented also for silver to many different proteins. Pomastowski et al. [2] reported ΔG value about -16 kJ/mol for silver lactoferrin interaction. Complex sorption mechanisms usually lead to an increase in the amount of absorbed metal ions by protein. Pryshchepa et al. studied impact of light on process silver ion interaction to casein and showed more negative Gibb's enthalpy for process conducted with access to light due to an additional mechanism for reducing silver to a metallic form [7]. The ΔG reported in this pair: metal-protein may be the result of a spontaneous (and effective) reduction of silver ions to a reduced form induced by the functional groups of the protein. The Q_e parameter of 11.2 mg/g which describes amount of silver bound per 1 g of protein confirms the strong possibility of binding silver by the protein as well as silver concentration noted at equilibria C_e show the binding efficiency as full and they describe very strong silver binding to α-LA.

3.2. Characterization of α-LA composites with silver via Molecular Dynamics (MD) and Quantum Mechanics (QM) calculations using DFT

Fig. 2A and **2B** depicts modeled structure of protein and complex with silver cations with concentration used in all studies (30 mg Ag/L). These structures were obtained after energy minimization. Production MD simulations were running for roughly 400 ns. Generated trajectories in the range of 50-200 ns (after equilibration and convergence) were used for further MD analysis. Stability, flexibility, and silver binding were analyzed. Root mean square deviation (RMSD) profiles depicted in Fig. 3S were used to sample the conformational space (50-200 ns). For both the APO protein and the α-LA-Ag^+ complexes, the average RMSD is around 1.3 Angstrom.

Interestingly, flexibility (expressed as root mean square of fluctuation – RMSF) of the four key regions is similar with the apo form of α-LA (Fig. 4Si).

Table 1S summarizes percentage of participation of amino acids residues in interaction with silver. Analyzed interactions between Ag cations and GLU, ASP, CYS, HIS, TYR, TRP, PHE, MET, ARG, and LYS with a distance threshold of 0.35 nm were examined. Glu, Asp, TYR, LYS amino acids are dominating with interaction with silver cations. Glutamic and Aspartic acid account for >90% of total interactions with silver. Intriguingly, notably more interactions are observed for silver uptake by α-LA than the uptake of zinc [paper in revision].

3.3. Binding interactions of aspartate and glutamate residues towards Ag^+ (aq)

The interaction of silver ion (Ag^-) with selected amino acid residues, namely Asp , Glu , Tyr, Lys and Met, has been investigated by DFT calculations earlier [41]. We have shown that the negatively charged Asp^- and Glu^- residues are the strongest Ag^+ binders. To further shed light on possible binding modes of Ag^+

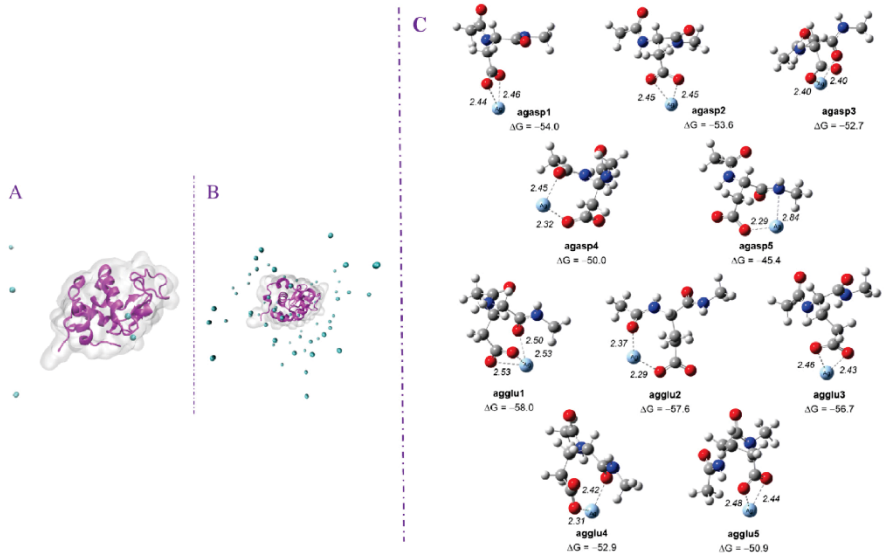

Fig. 2. Molecular structures of α-LA in apo form **(A)** and of the modeled complex with silver cations (with concentration 30 mg Ag/L in reagent mixture) **(B)** and optimized geometries of various conformations of Ag^{-}-Asp^{-} (**agasp1**–**asasp5**) and Ag^{-}- Glu^{-} (**agglu1**–**agglu5**) complexes; interaction distances are in Å and binding free energies (ΔG_{298}) are in kJ/mol **(C)**.

with aspartate and glutamate residues, DFT calculations were performed for various possible conformations of the 1:1 Ag^{+}- Asp^{-} and Ag^{-}- Glu^{-} complexes. In particular, we focused on the possible interaction of Ag^{-} with the protein backbone. To this end, the Asp^{-} and Glu^{-} residues were modelled with two amide units and capped with methyl groups to model the polypeptide backbone. Solvation effect in aqueous environment was modelled using the implicit SMD solvation model. The optimized geometries and binding free energies ($Ag^{+} + AA^{-} \rightarrow Ag^{-}$-$AA^{-}$, ΔG_{298}) of various key conformations of the two complexes, **agasp1**–**asasp5** and **agglu1**–**agglu5** for Ag^{+}-Asp^{-} and Ag^{+}-Glu^{-} complexes, respectively are given in **Fig. 2C**. In all cases, monodentate/bidentate interaction between the Ag^{+} cation and the negatively charged carboxyl group (COO^{-}) represents the key interaction. This is attributed to the strong electrostatic attraction between Ag^{+} cation and carboxyl group (COO^{-}). It is feasible to have additional interaction/coordination of Ag^{+} with the backbone, namely amino nitrogen and carbonyl oxygen. For instance, multiple interactions with COO^{-} and backbone carbonyl oxygen are observed in Ag^{+}-Glu^{-} conformations (**agglu1, agglu2** and **aglu4**). The Ag^{+}•••O interaction distances are comparable for both COO^{-} and carbonyl groups (**Fig. 2C**). For the lowest energy conformation of the Ag^{+}-Glu^{-} complex (**agglu1**), it has a tridentate coordination mode. Due to the additional carbon unit, the side chain of glutamate residue is more flexible than that of aspartate residue. Thus, it is easier for glutamate to adopt multiple interactions with Ag^{+} ion. Second attachment to amino nitrogen (backbone) is seen in the Ag^{+}-Asp^{-} conformation **agasp5**. In general, the amino nitrogen is less accessible than carbonyl oxygen because of the relatively rigid geometry of the backbone. It is worth noting that Ag^{+}•••O interaction distances in Ag^{+}- Asp^{-} and Ag^{+}- Glu^{-} complexes are similar. The calculated binding free energies (ΔG_{298}) of various conformers of both Ag^{+}-AA^{-} complexes are exergonic (**Fig. 2C**), suggesting that the formation of the Ag^{-}-AA^{-} complex is an energetically favorable process. This result readily supports the dominant occurrence of aspartate and glutamate residues in the MD simulations. Since the binding free energies of different conformations of Ag^{+}-AA^{-} complexes are comparable, similar strong Ag^{+} binding affinity on different aspartate and glutamate residues of α-LA protein is expected. In relation to FT-IR spectra, the frequency of stretching vibration of the carbonyl group changed as a result of the interaction of this group with silver.

3.4. Characterization of α-LA composites with silver by spectroscopic techniques (ATR-FTIR, Raman)

Fig. 3A shows the infrared spectra of the Ag- α-LA composite with the reference to the native protein before synthesis. After the binding process, the absorbance almost of all the bands decreased compared to the control. Lower concentration of the substance under analysis (based on the Beer-Lambert law) leads to even and constant change of spectrum. However, in the recorded spectrum for Ag- α-LA a selective enhancements and suppressions in the intensity of individual bands are localized, which proves the influence of silver on the spectrum.

The first band at 3273 cm^{-1} is responsible for the stretching vibration of N-H Amide A. Band at 3057 cm^{-1} can be assign to Amide B due to the Fermi resonance [34]. The next two bands at around 2900 cm^{-1} come from the C-H stretching vibrations. The breakdown of this range (bands at 2959-2871 cm^{-1}) into actually three bands indicates the presence of different groups and the occurrence of hydrogen bonding effects. Then, there is a complex of bands from 2360 cm^{-1} to 1882 cm^{-1}, which has shifted compared to the control. These bands are a result of the presence of overtones and/or combination bands originating mainly from ring vibrations [35]. Region at 1645 cm^{-1} is the Amide I vibration. More-

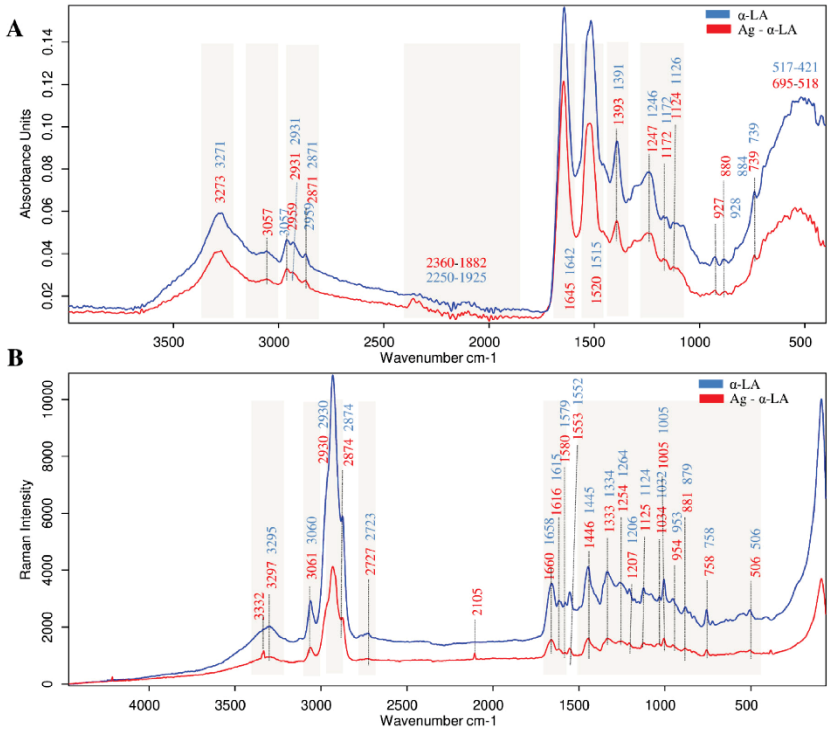

Fig. 3. (A) IR spectra of Ag- α-LA composite (red) with comparison to native α-LA as a control (blue); (B) Raman spectra of Ag- α-LA composite (red) with comparison to native α-LA as a control (blue).

over, the IR technique is sensitive to conformational changes in the C=O vibration, compared to the control the change in frequency of this vibration from 1642 cm^{-1} indicates the effect of a conformational change of this moiety as well as structure of backbone [33]. Another band at 1520 cm^{-1}, which has shifted from 1515 cm^{-1}, is responsible for the vibration of the Amide II. A pair of two bands at 1393 cm^{-1} and 1247 cm^{-1} is responsible for the vibration of the Amide III. This range reveals changes in the relative intensities of the bands after the silver bonding process with comparison to control. The largest relative decrease was recorded for the Amide II band. The next bands can be assigned to the vibration for each amino acid [36]. Zhang et al. studied FT IR spectrum of α-LA after binding with silver and did not register significant changes in spectrum after binding process [25]. The secondary and tertiary structure was unchanged. In our work small change in Amide I frequency (from 1642 to 1645 cm^{-1}) was observed, which points to conformational change of carboxylic residue and environment of acidic residues of protein.

Fig. 3B shows the Raman spectra of the Ag-α-LA composites with respect to the control. The band at 3330 cm^{-1} in the form of a doublet can be attributed to the N-H stretching vibration. Subsequent bands at 3061 cm^{-1}, 2930 cm^{-1} and around 2874 cm^{-1} represent the =C-H and C-H vibration bands, respectively. The band at around 2723 cm^{-1} is due to the S-H vibrations [37]. The band at around 1660 cm^{-1} is due to amide I vibrations. The carbonyl group of glutamic and aspartame amino acids gives the band from the C=O stretching vibration [37] but in Ag- α-LA sample the relative intensity of bands at 1615 cm^{-1} to 1660 cm^{-1} band is higher than in native protein and consequently its higher contribution $Ag-COO^{-}$ in sample. Then, the spectra show a rich set of bands derived from vibrations of individual amino acid groups (fingerprint region) [38,39]. The region from 700-660 cm^{-1} and smaller wavelength are indicator of S-S state in compound [37]. The cysteine residue is involved in interaction with silver by detecting the band at 758 cm^{-1} [37]. In Table 3 a summary of the discussed vibrations for both spectroscopic techniques is presented.

3.5. Characterization of α-LA composites with silver by microscopic techniques: SEM and SEM-EDX

After silver binding process, grouped clusters, randomly arranged spherical particles can be observed (Fig. 1S). Particles are differing in size (Fig. 1C S). This is confirmed by the presence of silver particles on the surface of the α-LA protein. Zhang et al. have shown similar results on Ag- α-LA composites [25] In addition, the photos show blur and lack of sharpness. This effect could not be removed despite washing the complexes several times. It could be consequence of the presence of an organic film on the surface of the protein-derived nanoparticles. Dehvari and Ghahghaei have studied α-LA with AgNPS by TEM microscopy [40]. α-LA forms

Table 3
Analyzed ATR-IR and Raman bands.

ATR-FTIR		RAMAN	
Wavenumber [cm-1]	Assignment's	Wavenumber [cm-1]	Assignment's
3273	N-H streching Amide A	3330	N-H stretching vibration
3057	Amide B	3061, 2930, 2874	=C-H and C-H
2360 - 1882	overtones and/or combination bands	2723	S-H
1645	Amide I	1660	Amide I with Ag
1520	Amide II	1615	Amide I with Ag
1393, 1247	Amide III	758	S from cysteine interacting with Ag

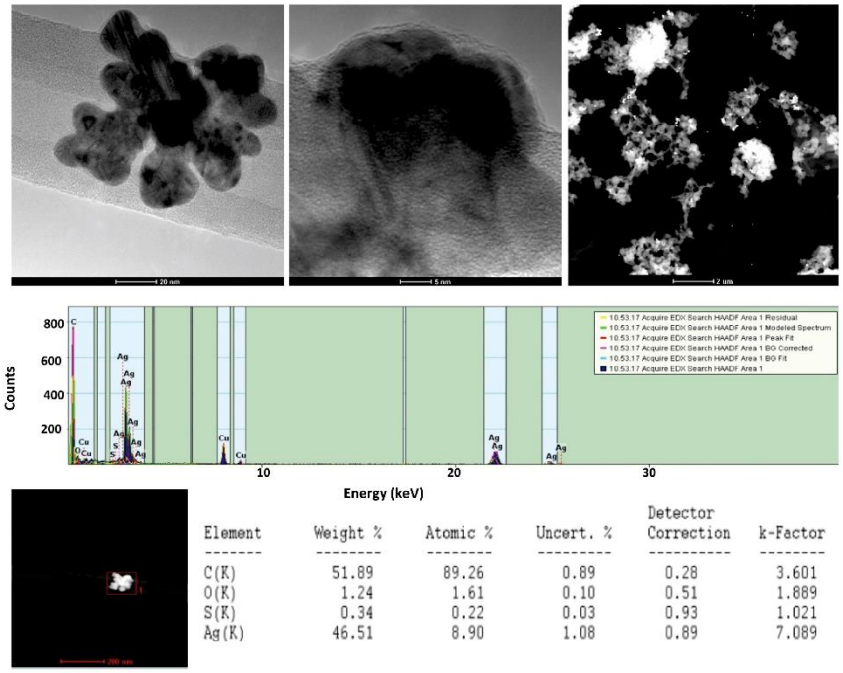

Fig. 4. TEM images of α-LA composites with silver as well as TEM-EDX analysis result.

long, smooth fibrillary aggregates upon a half-hour incubation at 37°C. After binding of Ag at 5 mg Ag/mL, however, there was a reduction in the number and average fibril length. At higher silver concentration (20 mg Ag/L) the fibrillary character of α-LA disappeared and some oligomers along with amorphous aggregates were observed. The obtained results stem from a different nature of the synthesis, where in our research the synthesis and reduction of Ag takes place on the surface of the protein.

SEM-EDX analysis confirmed presence of Ag in obtained Ag-α-LA composites (Fig. 2S). In addition to silver, among others, carbon, oxygen, aluminum, and sulfur were identified which are components of amino acid residues, as well as calcium, which is a co-factor of α-LA. The presence of copper is caused by a grid on which sample is overlaid during the analysis.

Fig. 4 shows TEM images of structures of α-LA composites with silver. The particles are spherical in shape and have tendency to create clusters. The surface is covered by continuous layer of silver. EDX analysis has shown the elements analysis of point at the particle surface, and the most abundant element is carbon (52 % by weight) followed by silver which is the second element (47 %). The very low oxygen amount (1 %) proves the absence of silver oxide nanoparticles and consequently the creation of silver reduced to zero valance step nanoparticles onto α-LA. Pryshchepa et al studied silver binding to casein protein and reported creation of spherical particles covered by silver in the highest amount [7].

3.6. Application of α-LA composites with silver. Stability in synthetic physiological fluids and cytotoxicity

The experiment of silver dissolution from Ag-α-LA composites was performed in the four types of synthetic physiological fluids after 24 h of releasing. In a gastric synthetic environment, a certain amount (13.9 % of initial amount) of silver is released from the complex, in contrast, with the enzyme-pepsin as solvent increasing this release to 29.9 %. The mechanism of the enzyme's action may be based on the digestion of the protein into individual peptides, which, under the conditions of sample preparation,

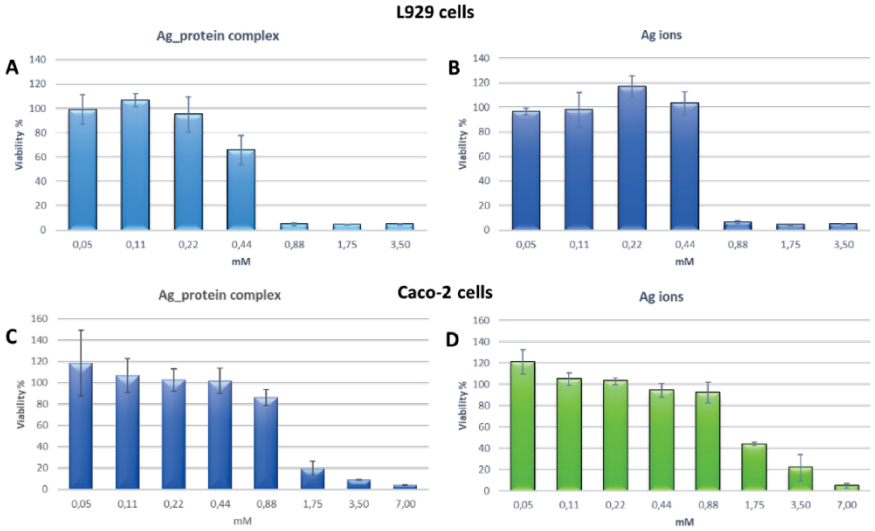

Fig. 5. L929 and Caco-2 cells viability after treatment with Ag protein complex and Ag ions measured by MTT method.

pass into the test solution through the ultrafiltration membrane. On the other hand, in an alkaline environment which are present in intestine, the values of the released silver are rather small and the presence of the enzyme does not change the value of the silver release (4.9 % and 4.7 %, respectively). This may be due to the alkaline durability of the composite and/or the non-dissolving effect of silver under alkaline conditions. Under these conditions, silver is insoluble and does not significantly pass into the test solution.

Cytotoxicity of α-LA composites and Ag ions was determined by MTT method on L929 mouse fibroblast cell line and human epithelial colorectal adenocarcinoma Caco-2 cell line [40–42]. L929 cell line is usually applied for testing the biocompatibility of new materials according to ISO 10993-5 and ISO 10993-12 norms. Moreover, this cell line may represent *in vitro* model for skin treatment formulation. Caco-2 cells display many similarities in terms of their morphology and biochemistry with enterocytes - intestinal absorptive cells. These cells are used as *in vitro* model to study absorption of orally administered drugs. The anti-proliferative effect was tested with two colorimetric assays: 3–(4,5–dimethylthiazol–2–yl)–2,5-diphenyl tetrazolium bromide (MTT) and lactate dehydrogenase (LDH) release from cells. MTT test is based on the ability of mitochondrial enzyme dehydrogenase to transfer yellow tetrazolium dye into formazan crystals. The level of obtained formazan crystals is directly proportional to cells viability. Therefore, the level of formazan crystals in the control, untreated sample is set to 100% viability. In the LDH assay protocol, the level of lactate dehydrogenase, that is released into the culture medium following the loss of membrane integrity is measured. LDH activity is recognized as an indicator of cell membrane integrity.

As shown in (**Fig. 5A** and **5B**) the MTT results demonstrated that in L929 cells, Ag in the form of bound with complex as well free ions shows similar and significant cytotoxicity in the concentration higher than 0.88 mM. In concentration up to 0.44 mM, the viability of cells was higher than 50%. Caco-2 cells were less sensitive to both forms of Ag than L929 cells. At concentration 0.88 mM, their viability was over 80% (Fig. 1 C, D). One of the reasons for the difference may be that L929 cells belong to normal cell line while Caco-2 cells are from malignant tissue, colorectal adenocarcinoma.

To monitor the membrane damage of more susceptible L929 cells LDH test was performed (**Fig. 5A**). The results of this assay show that the lactate dehydrogenase release is mostly very similar for both silver ions and silver complexes. For the lowest concentration (0.05 mM), treatment of cells with silver complex caused the release of enzyme in an amount similar to that of the control cells. On the other hand, silver ions lowered the amount of released enzyme by half. In higher concentrations, the level of released enzyme also decreased for both type of tested silver what can be associated with the fact that the cell number was too small to give the reliable result.

One of the aspect of cytotoxicity is oxidative stress. In order to detect reactive oxygen species after treatment with silver ions and complexes, a fluorometric intracellular ROS Kit that detects in particular superoxide and hydroxyl radicals was performed (Fig. 6B). Studies showed that level of ROS was similar for cells treated with silver ions and silver complexes. Only for higher concentrations (3.5 and 7 mM) the level of oxidative stress was higher than in control cells. α-LA composites at concentration 7 mM generated a higher number of free radicals higher than silver ions (Fig. 11B).

Fig. 7 (A–C) presents changes in L929 cells morphology after treatment with 0.05 and 0.5 mM silver complex for 24 h. Concentration 0.05 mM did not lowered the degree of confluence and the observed morphology is similar to control cells. However, the treatment with 0.5 mM of protein complex significantly reduced the number of cells, but most of them still adhered to the substrate. Their shape was changed to balloon-like and the expanding cytosol was observed. These changes can be related to occurring apoptosis process.

To check the amount of silver ions taken from the protein complexes, L929 cells were incubated for 24 h with silver complexes and for comparison with silver nitrate (**Fig. 7D**). Results showed that for lower applied concentration (0.05 mM) the level of adsorbed silver was two times higher for protein complex than for

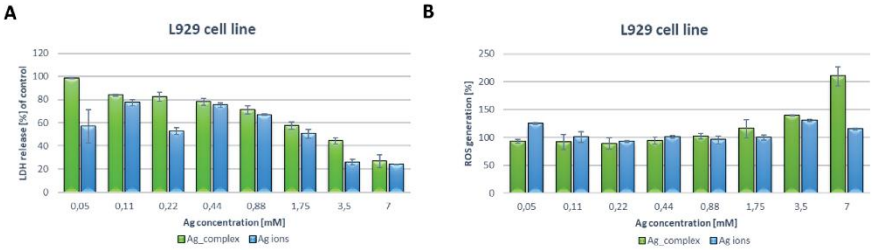

Fig. 6. (A) LDH leakage level of L929 cells treated with Ag ions and Ag complex; (B) Concentration-dependent ROS generation by Ag ions and Ag complex in L929 cells.

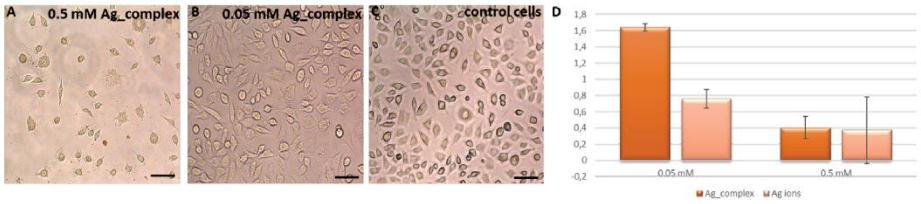

Fig. 7. (A–C) morphology of L929 cells treated with silver complex; (D) % of silver taken up by L929 cells from Ag complex and silver nitrate.

silver ions. For higher concentration (0.5 mM) there was no difference in the bioavailability of the silver ions. This process can be associated with low level of cells under tested concentration. Also, high standard deviation between samples can reflect the different number of cells that can absorb Ag. Observations allowed us to conclude that α-LA composites with silver are characterized by better biocompatibility and can be efficient in lower concentrations than silver nitrate.

4. Conclusions

The process of binding silver to alpha-lactalbumin was studied. Basic multidisciplinary studies have shown the formation of metal and protein. Equilibrium is achieved after 2 min of the binding reaction process, all the silver atoms at the concentration tested are almost fully bound, and the silver is reduced to metallic form- Ag (0). Aspartic and glutamic amino acids are mainly contributing in silver binding. The results of bioavailability tests proved that is not released to more than 50% under the simulated conditions of the human digestive system. Cytotoxicity study showed better biocompatibility of composite and silver can be efficient in lower concentrations than in control.

Declaration of Competing Interest

The authors declare that they have no known competing financial interests or personal relationships that could have appeared to influence the work reported in this paper.

CRediT authorship contribution statement

A. Gołębiowski: Conceptualization, Methodology, Investigation, Writing – original draft, Writing – review & editing, Visualization. **P. Pomastowski:** Conceptualization, Methodology, Project administration, Funding acquisition. **K. Rafińska:** Investigation, Writing – original draft, Formal analysis. **P. Żuvela:** Investigation, Writing – original draft, Formal analysis. **M.W. Wong:** Investigation, Writing – original draft, Formal analysis. **P. Madajski:** Investigation, Writing – original draft. **B. Buszewski:** Supervision.

Data availability

Data will be made available on request.

Acknowledgments

This work was financially supported by the National Science Centre within the framework of Opus 14 project No. 2017/27/B/ST4/02628 (2018-2021).Adrian Gołębiowski, Paweł Pomastowski, Katarzyna Rafinska and Bogusław Buszewski are members of Toruń Center of Excellence "Towards Personalized Medicine" operating under Excellence Initiative-Research University.

Supplementary materials

Supplementary material associated with this article can be found, in the online version, at doi:10.1016/j.molstruc.2022.133940.

References

[1] T. Khampieng, S. Wongkittithavorn, S. Chaiarwut, P. Ekabutr, P. Pavasant, P. Supaphol, Silver nanoparticles-based hydrogel: characterization of material parameters for pressure ulcer dressing applications, J. Drug Deliv. Sci. Technol. 44 (2018) 91–100, doi:10.1016/j.jddst.2017.12.005.
[2] P. Pomastowski, M. Sprynskyy, P. Żuvela, K. Rafińska, M. Milanowski, J.J. Liu, M. Yi, B. Buszewski, Silver-lactoferrin nanocomplexes as a potent antimicrobial agent, J. Am. Chem. Soc. 138 (2016) 7899–7909, doi:10.1021/jacs.6b02699.
[3] I. Chakraborty, N. Feliu, S. Roy, K. Dawson, W.J. Parak, Protein-mediated shape control of silver nanoparticles, Bioconjug. Chem. 29 (2018) 1261–1265, doi:10.1021/acs.bioconjchem.8b00034.
[4] N. Durán, C.P. Silveira, M. Durán, D.S.T. Martinez, Silver nanoparticle protein corona and toxicity: a mini-review, J. Nanobiotechnol. 13 (2015), doi:10.1186/s12951-015-0114-4.
[5] K. Kalantari, E. Mostafavi, A.M. Afifi, Z. Izadiyan, H. Jahangirian, R. Rafiee-Moghaddam, T.J. Webster, Wound dressings functionalized with silver nanoparticles: promises and pitfalls, Nanoscale 12 (2020) 2268–2291, doi:10.1039/c9nr08234d.

[6] I.L. Hsiao, Y.K. Hsieh, C.F. Wang, I.C. Chen, Y.J. Huang, Trojan-horse mechanism in the cellular uptake of silver nanoparticles verified by direct intra- and extracellular silver speciation analysis, Environ. Sci. Technol. 49 (2015) 3813–3821, doi:10.1021/es504705p.
[7] O. Pryshchepa, G.N. Sagandykova, P. Pomastowski, V. Railean-Plugaru, A. Król, A. Rogowska, A. Rodzik, M. Sprynskyy, B. Buszewski, A new approach for spontaneous silver ions immobilization onto casein, Int. J. Mol. Sci. 20 (2019), doi:10.3390/ijms20163864.
[8] R.P. Viorica, P. Pawel, M. Kinga, Z. Michal, R. Katarzyna, B. Boguslaw, Lactococcus lactis as a safe and inexpensive source of bioactive silver composites, Appl. Microbiol. Biotechnol. 101 (2017) 7141–7153, doi:10.1007/s00253-017-8443-x.
[9] O. Pryshchepa, P. Pomastowski, B. Buszewski, Silver nanoparticles: Synthesis, investigation techniques, and properties, Adv. Colloid Interface Sci. 284 (2020), doi:10.1016/j.cis.2020.102246.
[10] O. Pryshchepa, P. Pomastowski, B. Buszewski, Silver nanoparticles: Synthesis, investigation techniques, and properties, Adv. Colloid Interface Sci. 284 (2020) 87–100, doi:10.1016/j.cis.2020.102246.
[11] T.S. Sych, A.A. Buglak, Z.V. Reveguk, V.A. Pomogaev, R.R. Ramazanov, A.I. Kononov, Which amino acids are capable of nucleating fluorescent silver clusters in proteins? J. Phys. Chem. C 122 (2018) 26275–26280, doi:10.1021/acs.jpcc.8b08979.
[12] M. Svensson, H. Sabharwal, A. Håkansson, A.K. Mossberg, P. Lipniunas, H. Leffler, C. Svanborg, S. Linse, Molecular characterization of α-lactalbumin folding variants that induce apoptosis in tumor cells, J. Biol. Chem. 274 (1999) 6388–6396, doi:10.1074/jbc.274.10.6388.
[13] C. Bramaud, P. Aimar, G. Daufin, Thermal isoelectric precipitation of α-lactalbumin from a whey protein concentrate: influence of protein–calcium complexation, Biotechnol. Bioeng. 47 (1995) 121–130, doi:10.1002/bit.260470202.
[14] B Lönnerdal, EL Lien, Nutritional and physiologic significance of alpha-lactalbumin in infants, Nutr Rev 61 (9) (2003 Sep) 295–305, doi:10.1301/nr.2003.sept.295-305.
[15] E.A. Permyakov, α-Lactalbumin, amazing calcium-binding protein, Biomolecules 10 (2020) 1–50, doi:10.3390/biom10091210.
[16] E.A. Permyakov, V.L. Shnyrov, L.P. Kalinichenko, A. Kuchar, L.L. Reyzer, L.J. Berliner, Binding of Zn (II) ions to a-lactalbumin, J. Protein Chem. 10 (1991).
[17] M.S. Atri, A.A. Saboury, A.A. Moosavi-Movahedi, K. Kavousi, S. Ariaeenejad, Effects of zinc binding on the structure and thermal stability of camel alpha-lactalbumin, J. Therm. Anal. Calorim. 120 (2015) 481–488, doi:10.1007/s10973-014-4274-5.
[18] K. Noyelle, H. Van Dael, Kinetics of conformational changes induced by the binding of various metal ions to bovine α-lactalbumin, J. Inorg. Biochem. 88 (2002) 69–76, doi:10.1016/S0162-0134(01)00343-9.
[19] K. Murakami, P.J. Andree, L.J. Berliner, Metal ion binding to α-lactalbumin species, Biochemistry 21 (1982) 5488–5494, doi:10.1021/bi00265a017.
[20] M.J. Kronman, G.D. Fasman, Metal-ion binding and the molecular conformational properties of α lactalbumi, Crit. Rev. Biochem. Mol. Biol. 24 (1989) 565–667, doi:10.3109/10409239809080054.
[21] N.A. Bushmarina, Cofactor effects on the protein folding reaction: Acceleration of -lactalbumin refolding by metal ions, Protein Sci. 15 (2006) 659–671, doi:10.1110/ps.051904206.
[22] H.I. Rösner, C. Redfield, The human α-lactalbumin molten globule: comparison of structural preferences at pH 2 and pH 7, J. Mol. Biol. 394 (2009) 351–362, doi:10.1016/j.jmb.2009.09.025.
[23] D.S. Yarramala, P. Prakash, D.S. Ranade, S. Doshi, P.P. Kulkarni, P. Bhaumik, C.P. Rao, Cytotoxicity of apo bovine α-lactalbumin complexed with La 3– on cancer cells supported by its high resolution crystal structure, Sci. Rep. 9 (2019) 1–11, doi:10.1038/s41598-018-38024-1.
[24] T. Dudev, C. Lim, Competition among metal ions for protein binding sites: determinants of metal ion selectivity in proteins, Chem. Rev. 114 (2014) 538–556, doi:10.1021/cr4004665.
[25] B. Zhang, Y. Luo, Q. Wang, Development of silver/α-lactalbumin nanocomposites: a new approach to reduce silver toxicity, Int. J. Antimicrob. Agents 38 (2011) 502–509, doi:10.1016/j.ijantimicag.2011.07.009.
[26] V. W-M Lee, H. Li, T.-C. Lau, R. Guevremont, K.W. Michael Siu, Relative silver(I) ion binding energies of-amino acids: a determination by means of the kinetic method, 1998.
[27] B. Buszewski, A. Rodzik, V. Railean-Plugaru, M. Sprynskyy, P. Pomastowski, A study of zinc ions immobilization by β-lactoglobulin, Colloids Surf. A 591 (2020) 124443, doi:10.1016/j.colsurfa.2020.124443.
[28] P. Žuvela, J.J. Liu, M. Yi, P.P. Pomastowski, G. Sagandykova, M. Belka, J. David, T. Bączek, K. Szafrański, B. Żołnowska, J. Sławiński, C.T. Supuran, M.W. Wong, B. Buszewski, Target-based drug discovery through inversion of quantitative structure-drug-property relationships and molecular simulation: CA IX-sulphonamide complexes, J. Enzym. Inhib. Med. Chem. 33 (2018) 1430–1443, doi:10.1080/14756366.2018.1511551.
[29] N. Chandra, K. Brew, K.R. Acharya, Structural evidence for the presence of a secondary calcium binding site in human r-lactalbumin †, ‡, 1998.
[30] P. Li, L.F. Song, K.M. Merz, Systematic parameterization of monovalent ions employing the nonbonded model, J. Chem. Theory Comput. 11 (2015) 1645–1657, doi:10.1021/ct500918t.
[31] P. Li, B.P. Roberts, D.K. Chakravorty, K.M. Merz, Rational design of particle mesh ewald compatible lennard-jones parameters for +2 metal cations in explicit solvent, J. Chem. Theory Comput. 9 (2013) 2733–2748, doi:10.1021/ct400146w.
[32] K. Lindorff-Larsen, S. Piana, K. Palmo, P. Maragakis, J.L. Klepeis, R.O. Dror, D.E. Shaw, Improved side-chain torsion potentials for the Amber ff99SB protein force field, Proteins Struct. Funct. Bioinform. 78 (2010) 1950–1958, doi:10.1002/prot.22711.
[33] A. Barth, Infrared spectroscopy of proteins, Biochim. Biophys.Acta (BBA) Bioenerg. 1767 (2007) 1073–1101, doi:10.1016/j.bbabio.2007.06.004.
[34] A.I. Pavlyuchko, E.V. Vasilyev, L.A. Gribov, Calculations of molecular ir spectra in the overtone and combination frequency regions, J. Appl. Spectrosc. 78 (2011) 639–645, doi:10.1007/s10812-011-9511-0.
[35] A. Barth, The infrared absorption of amino acid side chains, Prog. Biophys. Mol. Biol. 74 (2000) 141–173, doi:10.1016/S0079-6107(00)00021-3.
[36] A. Torreggiani, A. Tinti, Raman spectroscopy a promising technique for investigations of metallothioneins, Metallomics 2 (2010) 246–260, doi:10.1039/b922526a.
[37] G. Zhu, X. Zhu, Q. Fan, X. Wan, Raman spectra of amino acids and their aqueous solutions, Spectrochim. Acta Part A Mol. Biomol. Spectrosc. 78 (2011) 1187–1195, doi:10.1016/j.saa.2010.12.079.
[38] A.L. Jenkins, R.A. Larsen, T.B. Williams, Characterization of amino acids using Raman spectroscopy, Spectrochim. Acta Part A Mol. Biomol. Spectrosc. 61 (2005) 1585–1594, doi:10.1016/j.saa.2004.11.055.
[39] M. Dehvari, A. Ghahghaei, The effect of green synthesis silver nanoparticles (AgNPs) from Pulicaria undulata on the amyloid formation in α-lactalbumin and the chaperon action of α-casein, Int. J. Biol. Macromol. 108 (2018) 1128–1139, doi:10.1016/j.ijbiomac.2017.12.040.
[40] S. Rekha, E.I. Anila, *In vitro* cytotoxicity studies of surface modified CaS nanoparticles on L929 cell lines using MTT assay, Mater. Lett. 236 (2019) 637–639, doi:10.1016/j.matlet.2018.11.009.
[41] G. Fotakis, J.A. Timbrell, *In vitro* cytotoxicity assays: Comparison of LDH, neutral red, MTT and protein assay in hepatoma cell lines following exposure to cadmium chloride, Toxicol. Lett. 160 (2006) 171–177, doi:10.1016/j.toxlet.2005.07.001.
[42] J. van Meerloo, G.J.L. Kaspers, J. Cloos, Cell sensitivity assays: the MTT assay, in: I.A. Cree (Ed.), Cancer Cell Culture: Methods and Protocols, Humana Press, Totowa, NJ, 2011, pp. 237–245, doi:10.1007/978-1-61779-080-5_20.

Materiały uzupełniające do publikacji

Binding of silver ions to alpha-lactalbumin

Są również dostępne jako załącznik do publikacji pod adresem:

https://doi.org/10.1016/j.molstruc.2022.133940

UNIWERSYTET MIKOŁAJA KOPERNIKA W TORUNIU
Wydział Chemii

Binding of silver ions to alpha-lactalbumin

A. Gołębiowski[1,2], P. Pomastowski[1*], K. Rafińska[2], P. Žuvela[3], M. W. Wong[3], P. Madajski[4], B. Buszewski[1,2]

[1] Centre for Modern Interdisciplinary Technologies, Nicolaus Copernicus University in Torun, 4 Wileńska St., 87-100 Torun, Poland
[2] Department of Environmental Chemistry and Bioanalytics, Faculty of Chemistry, Nicolaus Copernicus University in Torun, 7 Gagarina St., 87-100 Torun, Poland
[3] Department of Chemistry, National University of Singapore, 3 Science Drive 3, 117543, Singapore
[4] Department of Chemistry of Materials Adsorption and Catalysis, Faculty of Chemistry, Nicolaus Copernicus University in Torun, Gagarina 7, 87-100 Torun, Poland

[*] Correspondence: p.pomastowki@umk.pl

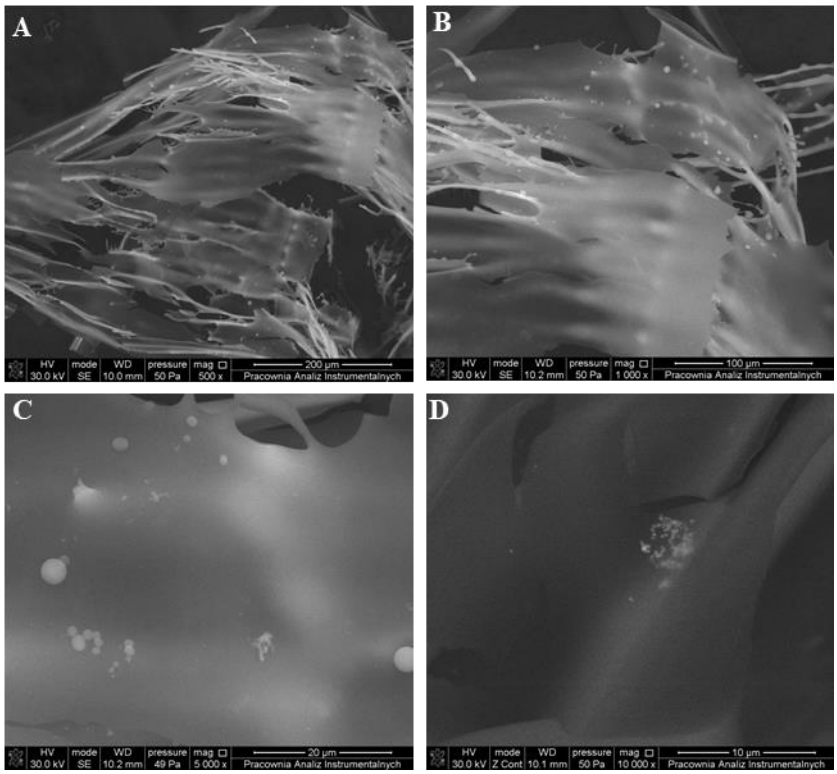

Figure 1S. SEM images of Ag- α-LA composite on others magnificence (A-D).

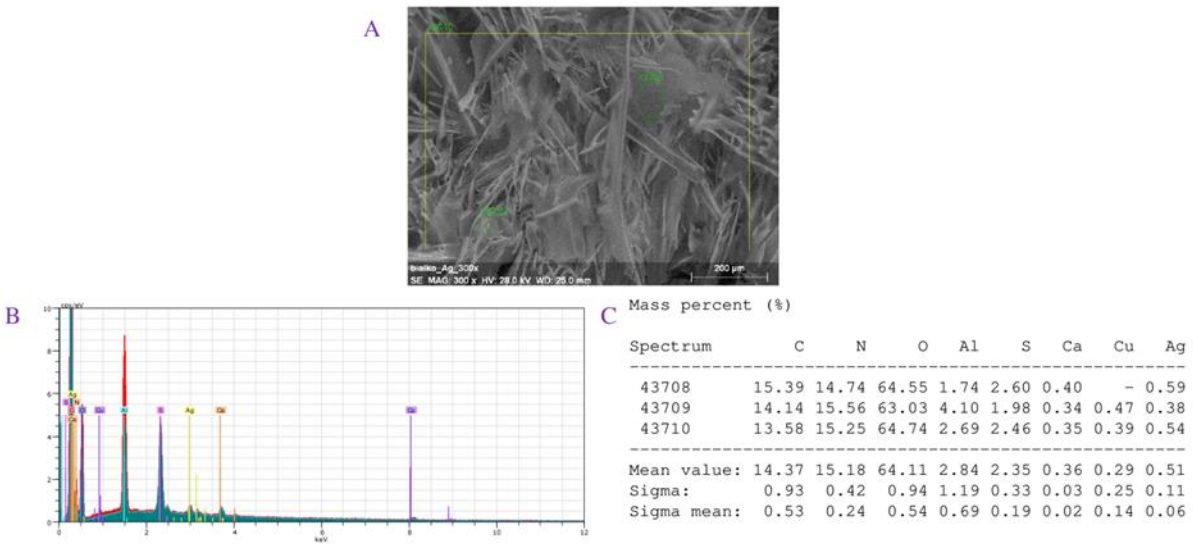

Spectrum	C	N	O	Al	S	Ca	Cu	Ag
43708	15.39	14.74	64.55	1.74	2.60	0.40	-	0.59
43709	14.14	15.56	63.03	4.10	1.98	0.34	0.47	0.38
43710	13.58	15.25	64.74	2.69	2.46	0.35	0.39	0.54
Mean value:	14.37	15.18	64.11	2.84	2.35	0.36	0.29	0.51
Sigma:	0.93	0.42	0.94	1.19	0.33	0.03	0.25	0.11
Sigma mean:	0.53	0.24	0.54	0.69	0.19	0.02	0.14	0.06

Figure 2S. SEM-EDX characterization of Ag- α-LA composite.

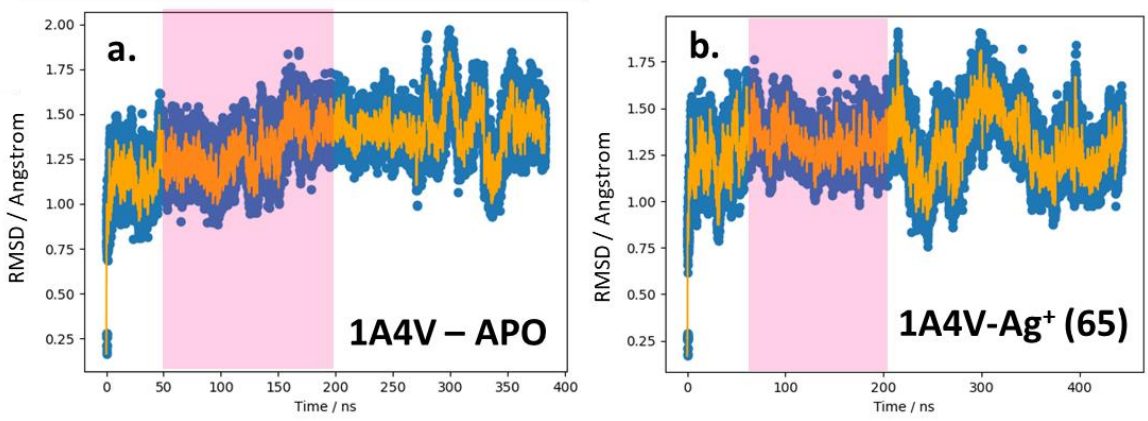

Figure 3S. Stability analysis of **(A)** APO α-LA, and **(B)** α-LA-Ag complexes.

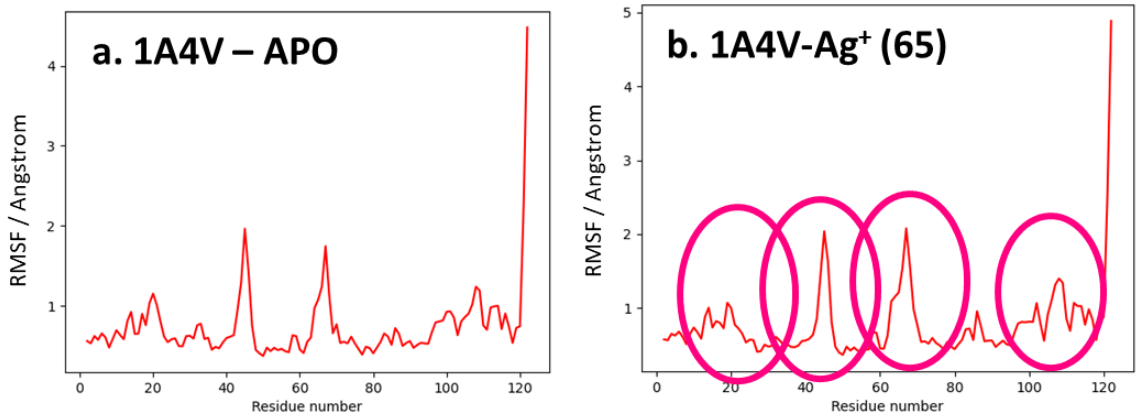

Figure 4S. Flexibility analysis of **(A)** APO α-LA, and **(B)** α-LA-Ag complexes.

Table 1S. Participation of amino acids of α-LA in interaction with silver cations at studied concentration of metal.

Amino-acid	α-LA-Ag^+ number of binding sites	α-LA-Ag^+ percentage of binding sites
GLU	**77609**	**40.078**
ASP	**98452**	**50.842**
CYS	157	0.081
HIS	0	0.000
TYR	**667**	**0.344**
TRP	12	0.006
PHE	795	0.411
MET	188	0.097
ARG	131	0.068
LYS	**15632**	**8.073**
	193643	

UNIWERSYTET MIKOŁAJA KOPERNIKA W TORUNIU
Wydział Chemii

Oświadczenia współautorów

mgr Adrian Gołębiowski

Uniwersytet Mikołaja Kopernika w Toruniu
Wydział Chemii
Katedra Chemii Środowiska i Bioanalityki

Toruń, 17.05.2023

mgr Adrian Gołębiowski
Katedra Chemii Środowiska i Bioanalityki
Wydział Chemii UMK w Toruniu
Interdyscyplinarne Centrum Nowoczesnych Technologii UMK w Toruniu

Oświadczenie

Jako współautor następujących publikacji:

1. Golebiowski, Adrian & Buszewski, Bogusław. (2023). Characterization of colloidal particles of a biological and metallic nature, *Microchemical Journal*, 108864, https://doi.org/10.1016/j.microc.2023.108864.
2. Golebiowski, Adrian & Kowalkowski, Tomasz & Buszewski, Bogusław. (2020). Molecular parameters of low methoxylated pectin affected by gelation with copper and cadmium cations. *Bioactive Carbohydrates and Dietary Fibre*. **21**. 100211. 10.1016/j.bcdf.2020.100211.
3. Golebiowski, Adrian & Pomastowski, Paweł & Rodzik, Agnieszka & Król-Górniak, Anna & Kowalkowski, Tomasz & Górecki, Marcin & Buszewski, Bogusław. (2020). Isolation and Self-Association Studies of Beta-Lactoglobulin. *International Journal of Molecular Sciences*. **21**. 10.3390/ijms21249711.
4. Golebiowski, Adrian & Pomastowski, Paweł & Rafińska, Katarzyna & Žuvela, Petar & Wong, M.W. & Madajski, P. & Buszewski, Bogusław. (2022). Binding of silver ions to alpha-lactalbumin. *Journal of Molecular Structure*. **1270**. 133940. 10.1016/j.molstruc.2022.133940.
5. Golebiowski, Adrian & Pomastowski, Paweł & Rafińska, Katarzyna & Žuvela, Petar & Wong, Ming & Pryshchepa, Oleksandra & Madajski, Piotr & Buszewski, Bogusław. (2022). Functionalization of Alpha-Lactalbumin by Zinc Ions. *ACS Omega*. **7**, 43, 10.1021/acsomega.2c03674.

wchodzących w skład mojej rozprawy doktorskiej pt. *„Układy koloidalne oraz ich oddziaływania z wybranymi metalami ciężkimi"*,

oświadczam, że mój wkład polegał na planowaniu doświadczeń i samodzielnym ich wykonywaniu (większości), zbieraniu danych surowych, analizie i interpretacji uzyskanych wyników, uczestniczeniu w dyskusji na temat ogólnej koncepcji pracy, przygotowywaniu wstępnych wersji manuskryptów oraz ich rewizji.

ul. Gagarina 7, 87-100 Toruń
Tel.: (+48) (56) 61 14 308; 797 329 345 Fax: (+48) (56) 61 14 837; e-mail: rgadz@umk.pl

UNIWERSYTET
MIKOŁAJA KOPERNIKA
W TORUNIU
Wydział Chemii

prof. zw. dr hab. Bogusław Buszewski

UNIWERSYTET
MIKOŁAJA KOPERNIKA
W TORUNIU
Wydział Chemii

**Katedra Chemii Środowiska
i Bioanalityki
ul. Gagarina 7, 87 100 TORUŃ**

UCZELNIA BADAWCZA

Tel.: (+48) (56) 61 14 308 • *Tel/fax:* (+48) (56) 61 14 837 • *e-mail:* bbusz@ umk.pl

prof. zw. dr hab. dr h.c. Bogusław Buszewski, członk. rzecz. PAN & EASA

Toruń, 17.05.2023

Oświadczenie

Jako współautor następujących publikacji:

1. Golebiowski, Adrian & Buszewski, Bogusław. (2023). Characterization of colloidal particles of a biological and metallic nature, *Microchemical Journal*, 108864, https://doi.org/10.1016/j.microc.2023.108864.
2. Golebiowski, Adrian & Kowalkowski, Tomasz & Buszewski, Bogusław. (2020). Molecular parameters of low methoxylated pectin affected by gelation with copper and cadmium cations. *Bioactive Carbohydrates and Dietary Fibre*. **21**. 100211. 10.1016/j.bcdf.2020.100211.
3. Golebiowski, Adrian & Pomastowski, Paweł & Rodzik, Agnieszka & Król-Górniak, Anna & Kowalkowski, Tomasz & Górecki, Marcin & Buszewski, Bogusław. (2020). Isolation and Self-Association Studies of Bcta-Lactoglobulin. *International Journal of Molecular Sciences*. **21**. 10.3390/ijms21249711.
4. Golebiowski, Adrian & Pomastowski, Paweł & Rafińska, Katarzyna & Žuvela, Petar & Wong, M.W. & Madajski, P. & Buszewski, Bogusław. (2022). Binding of silver ions to alpha-lactalbumin. *Journal of Molecular Structure*. **1270**. 133940. 10.1016/j.molstruc.2022.133940.
5. Golebiowski, Adrian & Pomastowski, Paweł & Rafińska, Katarzyna & Žuvela, Petar & Wong, Ming & Pryshchepa, Oleksandra & Madajski, Piotr & Buszewski, Bogusław. (2022). Functionalization of Alpha-Lactalbumin by Zinc Ions. *ACS Omega*. **7**, 43, 10.1021/acsomega.2c03674.

wchodzących w skład rozprawy doktorskiej mgr. Adriana Gołębiowskiego,

oświadczam, że mój wkład polegał na współudziale w opracowaniu koncepcji, planowaniu eksperymentów, dyskusji nad wynikami badań, sprawowaniu merytorycznego nadzoru nad realizacją badań oraz korektach manuskryptów.

prof. zw. dr hab. Bogusław Buszewski, dr h.c. mult.

UNIWERSYTET MIKOŁAJA KOPERNIKA W TORUNIU
Wydział Chemii

Dr hab. Tomasz Kowalkowski, prof. UMK

Uniwersytet Mikołaja Kopernika w Toruniu
Wydział Chemii
Katedra Chemii Środowiska i Bioanalityki

Toruń, 18.05.2023

dr hab. Tomasz Kowalkowski, prof. UMK
Katedra Chemii Środowiska i Bioanalityki
Wydział Chemii UMK w Toruniu
Interdyscyplinarne Centrum Nowoczesnych Technologii UMK w Toruniu

Oświadczenie

Jako współautor następujących publikacji:

1. Golebiowski, Adrian & Kowalkowski, Tomasz & Buszewski, Bogusław. (2020). Molecular parameters of low methoxylated pectin affected by gelation with copper and cadmium cations. Bioactive Carbohydrates and Dietary Fibre. 21. 100211. 10.1016/j.bcdf.2020.100211.
2. Golebiowski, Adrian & Pomastowski, Paweł & Rodzik, Agnieszka & Król-Górniak, Anna & Kowalkowski, Tomasz & Górecki, Marcin & Buszewski, Bogusław. (2020). Isolation and Self-Association Studies of Beta-Lactoglobulin. *International Journal of Molecular Sciences*. **21**. 10.3390/ijms21249711.

wchodzących w skład rozprawy doktorskiej mgr. Adriana Gołębiowskiego,

oświadczam, że mój wkład polegał na współudziale w opracowaniu koncepcji, planowaniu eksperymentów dotyczących techniki AF4 oraz ICP/MS, dyskusji nad uzyskanymi wynikami badań, sprawowaniu nadzoru nad realizacją badań, korektach manuskryptów.

ul. Gagarina 7, 87-100 Toruń
Tel.: (+48) (56) 61 14 308; 797 329 345 Fax: (+48) (56) 61 14 837; e-mail: rgadz@umk.pl

UNIWERSYTET
MIKOŁAJA KOPERNIKA
W TORUNIU
Wydział Chemii

Dr hab. Paweł Pomastowski, prof. UMK

UNIWERSYTET
MIKOŁAJA KOPERNIKA
W TORUNIU
Interdyscyplinarne Centrum
Nowoczesnych Technologii

Toruń, 17.05.2023

dr hab. Paweł Pomastowski, prof. UMK
Interdyscyplinarne Centrum Nowoczesnych Technologii
UMK w Toruniu

Oświadczenie

Jako współautor następujących publikacji:

1. Golebiowski, Adrian & Pomastowski, Paweł & Rodzik, Agnieszka & Król-Górniak, Anna & Kowalkowski, Tomasz & Górecki, Marcin & Buszewski, Bogusław. (2020). Isolation and Self-Association Studies of Beta-Lactoglobulin. *International Journal of Molecular Sciences*. **21**. 10.3390/ijms21249711.
2. Golebiowski, Adrian & Pomastowski, Paweł & Rafińska, Katarzyna & Žuvela, Petar & Wong, M.W. & Madajski, P. & Buszewski, Bogusław. (2022). Binding of silver ions to alpha-lactalbumin. *Journal of Molecular Structure*. **1270**. 133940. 10.1016/j.molstruc.2022.133940.
3. Golebiowski, Adrian & Pomastowski, Paweł & Rafińska, Katarzyna & Žuvela, Petar & Wong, Ming & Pryshchepa, Oleksandra & Madajski, Piotr & Buszewski, Bogusław. (2022). Functionalization of Alpha-Lactalbumin by Zinc Ions. *ACS Omega*. **7**, 43, 10.1021/acsomega.2c03674.

wchodzących w skład rozprawy doktorskiej mgr. Adriana Gołębiowskiego,

oświadczam, że mój wkład polegał na współudziale w opracowaniu koncepcji, planowaniu eksperymentów, dyskusji nad wynikami badań, sprawowaniu nadzoru nad realizacją badań, korektach manuskryptów oraz pozyskaniu środków na realizacje badań.

Uzyskane wyniki stanowią wskaźnik rezultatu bezpośredniego prac badawczych Wykonawcy: Pana mgr Adriana Gołębiowskiego w ramach kierowanego przeze mnie projektu pt. *„Synteza kompleksowych związków srebra i cynku na bazie kazein białek serwatki oraz nanocząstek srebra i tlenku cynku przez probiotyczne bakterie kwasu mlekowego"* finansowanego przez Narodowe Centrum Nauki w ramach programu Opus 14, 2017/27/B/ST4/02628.

KIEROWNIK PROJEKTU

Dr hab. Katarzyna Rafińska, prof. UMK

UNIWERSYTET MIKOŁAJA KOPERNIKA W TORUNIU Wydział Chemii
UCZELNIA BADAWCZA

Uniwersytet Mikołaja Kopernika w Toruniu
Wydział Chemii
Katedra Chemii Środowiska i Bioanalityki

Toruń, 17.05.2023

dr hab. Katarzyna Rafińska, prof. UMK
Interdyscyplinarne Centrum Nowoczesnych Technologii UMK w Toruniu
Katedra Chemii Środowiska i Bioanalityki
Wydział Chemii UMK w Toruniu

Oświadczenie

Jako współautorka następujących publikacji:

1. Golebiowski, Adrian & Pomastowski, Paweł & Rafińska, Katarzyna & Žuvela, Petar & Wong, M.W. & Madajski, P. & Buszewski, Bogusław. (2022). Binding of silver ions to alpha-lactalbumin. *Journal of Molecular Structure*. **1270**. 133940. 10.1016/j.molstruc.2022.133940.
2. Golebiowski, Adrian & Pomastowski, Paweł & Rafińska, Katarzyna & Žuvela, Petar & Wong, Ming & Pryshchepa, Oleksandra & Madajski, Piotr & Buszewski, Bogusław. (2022). Functionalization of Alpha-Lactalbumin by Zinc Ions. *ACS Omega*. **7**, 43, 10.1021/acsomega.2c03674.

wchodzących w skład rozprawy doktorskiej mgr. Adriana Gołębiowskiego,

oświadczam, że mój wkład polegał na samodzielnym zaplanowaniu, wykonaniu eksperymentów, interpretacji wyników dotyczących aktywności biologicznej kompleksów, współudziale przy wykonywaniu eksperymentów techniką ATR-FT-IR, nadzorowaniu wykonania eksperymentów techniką SEM oraz TEM, przygotowaniu wstępnej wersji manuskryptów.

ul. Gagarina 7, 87-100 Toruń
Tel.: (+48) (56) 61 14 308; 797 329 345 Fax: (+48) (56) 61 14 837; e-mail: rgadz@umk.pl

UNIWERSYTET
MIKOŁAJA KOPERNIKA
W TORUNIU
Wydział Chemii

Dr hab. Inż. Marcin Górecki, prof. IChO PAN

Instytut Chemii Organicznej
Polskiej Akademii Nauk

Laboratorium Analizy Substancji Bioaktywnych
Pracownia Spektroskopii Optycznej

dr hab. inż. Marcin Górecki, prof. IChO PAN

+48 22 343 22 12
marcin.gorecki@icho.edu.pl

Warszawa, 18.05.2023

OŚWIADCZENIE

Jako współautor następujących publikacji:

Golebiowski, Adrian & Pomastowski, Paweł & Rodzik, Agnieszka & Król-Górniak, Anna & Kowalkowski, Tomasz & Górecki, Marcin & Buszewski, Bogusław. (2020). Isolation and Self-Association Studies of Beta-Lactoglobulin. *International Journal of Molecular Sciences*. 21. 10.3390/ijms21249711.

wchodzących w skład rozprawy doktorskiej mgr. Adriana Gołębiowskiego,

oświadczam, że mój wkład polegał na planowaniu, samodzielnym wykonywaniu, zbieraniu danych surowych oraz interpretacji wyników eksperymentów zebranych techniką CD jak również przygotowaniu wstępnej wersji manuskryptu.

Marcin
Janusz
Górecki

Elektronicznie podpisany przez Marcin Janusz Górecki
DN: c=PL, sn=Górecki, givenName=Marcin Janusz, cn=Marcin Janusz Górecki, serialNumber=PNOPL-81112112075, o=Instytut Chemii Organicznej Polskiej Akademii Nauk, postalAddress=Kasprzaka 44/52, 01-224, Warszawa
Data: 2023.05.18 11:55:18 +02'00'

UNIWERSYTET MIKOŁAJA KOPERNIKA W TORUNIU
Wydział Chemii

prof. Ming Wah Wong

Uniwersytet Mikołaja Kopernika w Toruniu
Wydział Chemii
Katedra Chemii Środowiska i Bioanalityki

19 May 2023

Prof. Ming Wah Wong
Department of Chemistry
National University of Singapore
Email: chmwmw@nus.edu.sg

Statement

As a co-author of the following publications:

1. Golebiowski, Adrian & Pomastowski, Paweł & Rafińska, Katarzyna & Žuvela, Petar & Wong, M.W. & Madajski, P. & Buszewski, Bogusław. (2022). Binding of silver ions to alpha-lactalbumin. Journal of Molecular Structure. 1270. 133940. 10.1016/j.molstruc.2022.133940.
2. Golebiowski, Adrian & Pomastowski, Paweł & Rafińska, Katarzyna & Žuvela, Petar & Wong, Ming & Pryshchepa, Oleksandra & Madajski, Piotr & Buszewski, Bogusław. (2022). Functionalization of Alpha-Lactalbumin by Zinc Ions. ACS Omega. 7, 43, 10.1021/acsomega.2c03674.

Being a part of doctoral dissertation of MSc Adrian Gołębiowski,

I declare that my involvement in these publications encompassed computational studies only.

Yours sincerely,

M. W. Wong

ul. Gagarina 7, 87-100 Toruń
Tel.: (+48) (56) 61 14 308; 797 329 345 Fax: (+48) (56) 61 14 837; e-mail: rgadz@umk.pl

UNIWERSYTET MIKOŁAJA KOPERNIKA W TORUNIU
Wydział Chemii

Dr Petar Žuvela

Uniwersytet Mikołaja Kopernika w Toruniu
Wydział Chemii

May, 18 2023

dr Petar Žuvela
Department of Chemistry
National University of Singapore
Email: petar@petar-zuvela.com

Statement

As a co-author of the following publications:

1. Golebiowski, Adrian & Pomastowski, Paweł & Rafińska, Katarzyna & Žuvela, Petar & Wong, M.W. & Madajski, P. & Buszewski, Bogusław. (2022). Binding of silver ions to alpha-lactalbumin. Journal of Molecular Structure. 1270. 133940. 10.1016/j.molstruc.2022.133940.
2. Golebiowski, Adrian & Pomastowski, Paweł & Rafińska, Katarzyna & Žuvela, Petar & Wong, Ming & Pryshchepa, Oleksandra & Madajski, Piotr & Buszewski, Bogusław. (2022). Functionalization of Alpha-Lactalbumin by Zinc Ions. ACS Omega. 7, 43, 10.1021/acsomega.2c03674.

Being a part of doctoral dissertation of MSc Adrian Gołębiowski,

I declare that, my contribution was the participation in design, simulations and investigation of DFT calculation, visualization and validation of data as well as writing and editing of the manuscript.

Petar Žuvela

ul. Gagarina 7, 87-100 Toruń
Tel.: (+48) (56) 61 14 308; 797 329 345 Fax: (+48) (56) 61 14 837; e-mail: rgadz@umk.pl

UNIWERSYTET MIKOŁAJA KOPERNIKA W TORUNIU
Wydział Chemii

Dr Anna Król-Górniak

Uniwersytet Mikołaja Kopernika w Toruniu
Wydział Chemii
Katedra Chemii Środowiska i Bioanalityki

Toruń, 23.05.2023

dr Anna Król-Górniak
Katedra Chemii Środowiska i Bioanalityki
Wydział Chemii UMK w Toruniu
Interdyscyplinarne Centrum Nowoczesnych Technologii UMK w Toruniu

Oświadczenie

Jako współautorka następujących publikacji:

1. Golebiowski, Adrian & Pomastowski, Paweł & Rodzik, Agnieszka & Król-Górniak, Anna & Kowalkowski, Tomasz & Górecki, Marcin & Buszewski, Bogusław. (2020). Isolation and Self-Association Studies of Beta-Lactoglobulin. *International Journal of Molecular Sciences*. **21**. 10.3390/ijms21249711.

wchodzących w skład rozprawy doktorskiej mgr. Adriana Gołębiowskiego,

oświadczam, że mój wkład polegał na planowaniu, samodzielnym wykonywaniu, zbieraniu danych surowych oraz analizowania wyników eksperymentów zebranych techniką CE oraz przygotowaniu wstępnej wersji manuskryptu.

Anna Król-Górniak

ul. Gagarina 7, 87-100 Toruń
Tel.: (+48) (56) 61 14 308; 797 329 345 Fax: (+48) (56) 61 14 837; e-mail: rgadz@umk.pl

UNIWERSYTET MIKOŁAJA KOPERNIKA W TORUNIU
Wydział Chemii

Dr Oleksandra Pryshchepa

UNIWERSYTET MIKOŁAJA KOPERNIKA W TORUNIU Wydział Chemii
UCZELNIA BADAWCZA

Uniwersytet Mikołaja Kopernika w Toruniu
Wydział Chemii
Katedra Chemii Środowiska i Bioanalityki

KChŚiB

Toruń, 17.05.2023

dr Oleksandra Pryshchepa
Interdyscyplinarne Centrum Nowoczesnych Technologii UMK w Toruniu

Oświadczenie

Jako współautorka następujących publikacji:

1. Golebiowski, Adrian & Pomastowski, Paweł & Rafińska, Katarzyna & Žuvela, Petar & Wong, Ming & Pryshchepa, Oleksandra & Madajski, Piotr & Buszewski, Bogusław. (2022). Functionalization of Alpha-Lactalbumin by Zinc Ions. *ACS Omega*. **7**, 43, 10.1021/acsomega.2c03674.

wchodzących w skład rozprawy doktorskiej mgr. Adriana Gołębiowskiego,

oświadczam, że mój wkład polegał na zaplanowaniu, samodzielnym wykonaniu oraz interpretacji wyników badań nad enzymatyczną degradacją kompleksów oraz przygotowaniu wstępnej wersji manuskryptu.

17.05.2023 O. Pryshchepa.

ul. Gagarina 7, 87-100 Toruń
Tel.: (+48) (56) 61 14 308; 797 329 345 Fax: (+48) (56) 61 14 837; e-mail: rgadz@umk.pl

Mgr Agnieszka Rodzik

Uniwersytet Mikołaja Kopernika w Toruniu
Wydział Chemii
Katedra Chemii Środowiska i Bioanalityki

Toruń, 18.05.2023

mgr Agnieszka Rodzik
Katedra Chemii Środowiska i Bioanalityki
Wydział Chemii UMK w Toruniu
Interdyscyplinarne Centrum Nowoczesnych Technologii UMK w Toruniu

Oświadczenie

Jako współautorka następujących publikacji:

1. Golebiowski, Adrian & Pomastowski, Paweł & Rodzik, Agnieszka & Król-Górniak, Anna & Kowalkowski, Tomasz & Górecki, Marcin & Buszewski, Bogusław. (2020). Isolation and Self-Association Studies of Beta-Lactoglobulin. *International Journal of Molecular Sciences*. **21**. 10.3390/ijms21249711.

wchodzących w skład rozprawy doktorskiej mgr. Adriana Gołębiowskiego,

oświadczam, że mój wkład polegał na współudziale w planowaniu, wykonywaniu, zbieraniu danych surowych oraz analizowania wyników eksperymentów zebranych techniką MALDI-TOF/MS oraz przygotowaniu wstępnej wersji manuskryptu.

Agnieszka Rodzik

ul. Gagarina 7, 87-100 Toruń
Tel.: (+48) (56) 61 14 308; 797 329 345 Fax: (+48) (56) 61 14 837; e-mail: rgadz@umk.pl

UNIWERSYTET MIKOŁAJA KOPERNIKA W TORUNIU
Wydział Chemii

Mgr Piotr Madajski

UNIWERSYTET MIKOŁAJA KOPERNIKA W TORUNIU Wydział Chemii
UCZELNIA BADAWCZA

Uniwersytet Mikołaja Kopernika w Toruniu
Wydział Chemii
Katedra Chemii Środowiska i Bioanalityki

KCHŚiB

Toruń, 17.05.2023

mgr Piotr Madajski
Katedra Chemii Analitycznej i Spektroskopii Stosowanej
Wydziału Chemii UMK w Toruniu

Oświadczenie

Jako współautor następujących publikacji:

1. Golebiowski, Adrian & Pomastowski, Paweł & Rafińska, Katarzyna & Žuvela, Petar & Wong, M.W. & Madajski, P. & Buszewski, Bogusław. (2022). Binding of silver ions to alpha-lactalbumin. *Journal of Molecular Structure*. **1270**. 133940. 10.1016/j.molstruc.2022.133940.
2. Golebiowski, Adrian & Pomastowski, Paweł & Rafińska, Katarzyna & Žuvela, Petar & Wong, Ming & Pryshchepa, Oleksandra & Madajski, Piotr & Buszewski, Bogusław. (2022). Functionalization of Alpha-Lactalbumin by Zinc Ions. *ACS Omega*. 7, 43, 10.1021/acsomega.2c03674.

wchodzących w skład rozprawy doktorskiej mgr. Adriana Gołębiowskiego,

oświadczam, że mój wkład polegał na planowaniu i samodzielnym wykonaniu eksperymentów techniką TEM.

Madajski

ul. Gagarina 7, 87-100 Toruń
Tel.: (+48) (56) 61 14 308; 797 329 345 Fax: (+48) (56) 61 14 837; e-mail: rgadz@umk.pl